Evaluation of a packed bed tri-medium system for the removal of Iron and Manganese from groundwater

By

Wagiewe July Mngidi

A thesis submitted in fulfilment of the requirements for the degree

Master of Engineering: Chemical Engineering

in the

Faculty of Engineering and the Built Environment

at the

Cape Peninsula University of Technology

Supervisor: **Prof Mujahid Aziz**

February 2023

DECLARATION

I, Wagiewe July Mngidi, hereby declare that the contents of this dissertation/thesis represent my own unaided work, and that the dissertation/thesis has not previously been submitted for academic examination towards any qualification. Furthermore, it represents my own opinions and not necessarily those of the Cape Peninsula University of Technology.

Signed : *Wagiewe July Mngidi* Date : *February 2023*

Abstract

Clean water access is drastically deteriorating globally due to stresses posed by an increase in industrial development, population growth, and expanding economic activities. Industry development escalates water pollution, which has societal impacts on human lively hoods by causing diseases such as diarrhoea, malnutrition and cancer, Africa being one of the continents suffering from this predicament. The expansion of population and economic activities doubles the demand for clean water globally every twenty-one years. This lessens the supply and availability of clean drinking water since the earth comprises 97% saline water; only 3% is deemed freshwater for human consumption. Out of this percentage, a low 0.06% is accessible, while the rest are ice, groundwater, and wastewater.

Groundwater has become the natural alternative source of water that is substantially reliable. However, it consists of heavy metals that significantly impact nature and human health. The contamination of groundwater is a global challenge as this puts pressure on the necessity for filtration before any use. Iron and manganese are abundant elements found in the earth's crust and are primarily found in pollutants in the surface and groundwater; even though they are aesthetic, higher concentrations of these elements have adverse health effects and can damage equipment.

This study takes the treatment of groundwater to remove iron and manganese. These metals are abundantly found in the earth's crust, if not treated, might damage equipment such as pipes and geysers and have health effects on humans if consumed in high concentrations. The previous studies determined that it was complex to remove iron and manganese simultaneously. This study aimed to assess the effect of flow rates, contact time and pH for removing these metals in one system with variously packed media (tri-medium). The experiment was performed in a laboratory-scale treatment process in a packed bed integrated tri-medium (three media system consists of glass, polystyrene beads and ion exchange)for the treatment of iron (Fe) and manganese (Mn) from ground water in line with the City of Cape Town and South African National Standards 241 (SANS241) standards for potable application. This research followed an experimental quantitative approach. The study comprises of two parts, which entail the application of chemical oxidation r and the evaluation of a tri-medium system.

The three medium used in this experiment was characterized using Fourier Transform Infrared Spectroscopy (FTIR) to determine their surface chemical functional group. Design Expert 10 was used to generate a predictive model using the Box-Behnken Design (BBD) approach to describe the effect of operating conditions on Fe and Mn removal. Isotherms models (Langmuir, Freundlich, Temkin and Dubinin-Radushkevich) were used to assess the system adsorption performance and kinetic models (Pseudo-First Order (PFO), Pseudo-Second Order (PSO), Intra-Particle Diffusion (IP) and Elovich) to investigate the rate of mass transfer mechanism on the experimental data collected. Mathematical (Thomas Model, Adams & Bohart and Yoon-Nelson) models were utilized to determine the efficiency and capabilities of the fixed bed column.

The highest average removal percentage of Fe and Mn were found to be 71% and 89%, respectively, after 60 minutes of running time. The best percentage removal after adsorption was 93% at operating conditions of pH: 8.5, flow rate: 0.174l/min and dosage: 1.67ml/min for Fe and pH: 6.5, flow rate: 2.52l/min and dosage: 0.262ml/min for Mn. This was deemed the best operation condition for removing Fe and Mn for the experiment. These results indicate that the treated effluent aligns with national standards for safe disposal or reuse since the concentration of Fe and Mn was found to be 0.15mg/l and 0.2mg/l, respectively.

The FTIR revealed the "media" contained bonds that are advantageous for the adsorption of Fe & Mn. The adsorption kinetic data for Fe was shown to follow pseudo-second-order reaction kinetics the best with linear regression R^2=1 and follow the Freundlich adsorption isotherms the closest with R^2 0.99. The adsorption kinetic data for Mn was directed to follow pseudo-second-order reaction kinetics with high R^2=0.99 compared to other models and follow the Freundlich adsorption isotherms the closest with R^2=0.99. It was observed that the predictive model successfully described the optimal operating conditions for removing Fe and Mn within the design space of the model.

Mathematical models were investigated to determine this fixed bed column's appraisal efficiency and capabilities. Adams & Bohart's Model illustrated high adsorption capacities compared to Yoon Nelson and Thomas's model. According to the results determined from this study, the tri-medium packed bed system indicated a positive outcome for the simultaneous removal of iron and manganese.

Research Outputs

Mngidi WJ & Aziz M; 2022, Assessment of a packed bed tri-medium system for the exclusion of iron and manganese from groundwater, Inter-institutional Postgraduate Symposium, STIAS, Stellenbosch University, Stellenbosch, South Africa, 30 September 2022

Mngidi WJ & Aziz, M; 2023,The elimination of Iron and Manganese from groundwater using a packed bed-tri-medium system. Submitted XX February 2023 [Paper ID.: XX-XX-XX]

Acknowledgements

I'm most grateful to the Almighty for giving me the strength to persevere and succeed with this project, protecting and guiding me when I was at my lowest, and blessing me with an unbeatable support system, my parents, friends, and family.

This research project was conducted in the Chemical Engineering Department between January 2020 and February 2023

I want to express my gratitude to the following people for their contributions towards the completion of this thesis:

My Supervisor, Prof Mujahid Aziz, for his incomparable supervision, persistent guidance, and technical expertise in this research field; I am grateful for his sustained academic and research strategies.

The Environmental Engineering Research Group (EnvERG) in the Department of Chemical Engineering for their support

Research Directorate of the Cape Peninsula University of Technology (CPUT) for their support and student scholarship

My employer WET Technologies for providing me with space to do my experimental work

My deep and sincere gratitude goes to my family for their continuous and exceptional love, help and support.

Dedication

In memory of my late mother, **Martha Nkomozakhe Mngidi**, for always believing in me and giving me all the support I needed

My dad, **Charlie Sobena Mngidi**, and my siblings for their endless love, support, encouragement, and inspiration

My kids, **Sphesihle**, **Prayer**, **Sethu** and **Yabantle Mngidi**, for persevering while I was on this journey to attain this qualification.

This achievement would not be possible without you.

I am forever grateful for your presence in my life.

Table of content

List of tables

List of figures

NOMENCLATURE

Symbol	Definition	unit
b	Temkin adsorption heat constant	J mol^{-2}
B	D-R constant	mol^2 kJ^{-2}
Ce	equilibrium concentration	mol/L
E	sorption free energy	kJ /mol
C_i	initial concentration	mol /L
K_f	Freundlich constant	mol /g
K^l	Langmuir constant	L/mol
K_t	equilibrium binding constant	L/mol
K_{id}	Intraparticle diffusion constant	mg/g.$min^{0.5}$
K_T	Temkin equilibrium binding constant	l/mg
m	mass	g
n	sorption intensity	
n	number of data	
p	number of parameters	
q_e	adsorption capacity	mg/g
$q_{e, calc}$	calculated value	mg/g
q_t	amount of contaminant adsorbed at a time t	mg/g
q_m	maximum adsorption capacity	mg/g
q_s	D-R constant	mg/g
R	universal gas constant 8.314	$JK^{-1}m^{-1}$
R^2	Correlation Coefficient	
R_L	dimensionless constant separation factor	
T	temperature	K
V	volume of solution	L

List of equations

List of photographs

CHAPTER 1

Introduction

CHAPTER 1: Introduction

1.Introduction

1.1 Background

Safe and clean drinking water is essential to all human activity and wildlife. Water availability is drastically deteriorating globally due to stresses posed by an increase in industrial development, population growth, and expanding economic activities. All productive sectors within society require water in one form or another. Managing and allocating these water sources is fundamental to sustainable development and human well-being. The water supply pressure is also driven by climate change and environmental degradation. The current status of water scarcity will only worsen unless steps are taken to reduce water consumption and increase reuse water applications (Roman, 2021).

Since the demand for freshwater has gained the attention of governments and water industries, the development and management of alternative water sources have been explored (Deng et al., 2013), especially in countries where supply exceeds demand, with the African continent and South Africa being among the list(Li et al., 2016; M et al., 2016). Groundwater has become the most used source of water that is substantially reliable (M et al., 2016), as research indicated that 44% of the US population and 30% of Canadians in small communities depend on groundwater as a drinking water source (Diaz-Alarcón et al., 2019), which was also confirmed by the study conducted by the World Bank, indicating that most water supplies to urban areas are from groundwater (Salem et al., 2012).

Groundwater consists of heavy metals that significantly impact nature and human health (Dalai et al., 2015). Groundwater is water from the rain that percolates through space, soil, and fractured rocks to the underground surface, forming a portion of the Earth's water cycle(Sanderson & Frey, 2015). The most common dissolved minerals (parameters) in groundwater are calcium, sodium, chloride, potassium, magnesium, bicarbonate, and sulfate, forming part of naturally occurring elements (Kumar & Raj, 2018).

The contamination of groundwater is a global challenge as this puts pressure on the necessity for filtration before any use (Scher & Caputo, 2014). Iron and manganese are abundant elements in the earth's crust and primarily in pollutants on the surface and groundwater. Even though these elements are aesthetic, higher concentrations have health effects and can damage equipment (Bekri-Abbes et al., 2006; Valerii Orlov et al., 2016). Both these metals are commonly found in high concentrations in groundwater due to the reduced redox reaction (Cheng et al., 2019; Dashtban Kenari & Barbeau, 2016). These parameters in higher concentrations, stains, discolour and affect the taste. The World Health Organization (WHO) has enforced the requirement for water treatment if the iron and manganese concentrations are higher than 0.3 mg/l and 0.1 mg/l, respectively (Indah & Helard, 2017). Tekerlekopoulou et al. 2006stated that these metal ions, even at low concentrations, can cause neurotoxicity in humans and may lead to intellectual impairment in children (Diaz-Alarcón et al., 2019).

Multiple technologies for the removal of iron and manganese from groundwater, such as chemical oxidation, reverse osmosis, manganese coated media, rice husk, activated carbon, micro-organisms and individual adsorptive process of synthetic glass media, expanded polystyrene, and ion exchange resins have been studied and published(Aziz & Kasongo, 2019). However, these methods favour iron removal more effectively than manganese, which is unsatisfactory (Li et al., 2016). Using cost-effective material for treating iron and manganese from groundwater as an adsorbent has been recently emphasized (Kwakye-Awuah et al., 2019) since the treatment method has to accommodate underdeveloped rural communities.

Several studies have been conducted to remove Fe and Mn from groundwater using an adsorption process in recent years. Barloková & Ilavský, 2010, performed an analysis where Activated Sand (Klinopur-Mn) and Birm medium were also used as an adsorbent and found Fe removal of 16% and Mn removal of 23%. Hameed, 2019 performed an integrated treatment process for groundwater where adsorption, Zeolite media, was used. The study showed a max Fe removal of 76 % and Mn of 45%. The simultaneous removal of iron and manganese ions is essential as this is currently facing many water utilities due to the inefficiency of the existing treatment (Roccaro et al., 2007). The emphasis on the improved groundwater treatment system for the simultaneous removal of iron and manganese is essential to meet the water quality standards. The integrated tri-medium method for groundwater treatment is proposed in this study to determine the effect of pH, flow rate and contact time for the simultaneous removal of these metals to mitigate the challenges faced by previous research.

1.2 Problem statement

Iron and Manganese concentrations in groundwater are too high and have become a big problem causing immense antagonistic effects on the ecological biota and human health. Existing conventional treatment favours iron removal and has demonstrated ineffective removal of Manganese. Groundwater has been used in Cape Town since 2017 when the city experienced drought. Iron and manganese are the most significant challenges hindering the direct use of this water without treatment. An enhanced, innovative packed bed integrated tri-medium technology is a potential solution in line with the City of Cape Town (CoCT) and South African National Standards (SANS241) for potential potable application.

1.3 Research questions

- Will chemical oxidation follow by a tri-medium packed bed medium filtration treat groundwater for potential potable application?

- How will the flow rates, contact time and pH affect the Fe and Mn removal during the adsorption process of groundwater?

1.4 Research Aim and objectives

This research aims to improve groundwater quality in a packed bed integrated tri-medium adsorption system for a potential potable application.

The specific objectives were:

1.4.1. To determine the effect of flow rates, contact time and pH on the removal efficiency of Fe and Mn from groundwater during a batch adsorption process.

1.4.2. To investigate kinetic, isotherm and modelling studies on the removal of Fe and Mn

1.5 Significance of the study

The development of new innovative groundwater treatment technology is empirical to address the removal of heavy metals, especially iron and manganese. The developed treatment system needs to be durable, cost-effective and efficient in contaminants removal to treat groundwater to potable standards to mitigate the shortage of drinking water. The effective system may purify groundwater for potable application, which might comply with the City of Cape Town (CoCT) and South African National Standards (SANS241).

1.6 Delineation

During this study, the removal of Fe and Mn from groundwater was observed through a packed bed tri-medium adsorption treatment process with two steps.

1. Chemical oxidation using hydrogen peroxide (H_2O_2)
2. Adsorption using a tri-medium system consists of glass, polystyrene beads and ion exchange.

All other variables were delineated.

1.7 Structure of the Thesis

Chapter 1: Introduction

The chapter introduces the reader to the background of the project and the problem statement that the project addresses. The aims and objectives are included for addressing the issues stated and the delineation.

Chapter 2: Literature Review

The literature review looks at all the studies other researchers conducted within the same or similar field. It may also identify gaps within water treatment research and highlight the literature on this study's focus points.

Chapter 3: Methodology

The chapter contains the materials and methods used for executing the project from the aims and objectives of the project. Also included are the instruments and equipment used.

Chapter 4: Results and Discussion

This section contains the results and a discussion of the findings.

The area is separated into five parts:

- FTIR Analysis
- Iron and Manganese removal efficiencies
- Adsorption Isotherms Models
- Adsorption Kinetic Models
- Fixed bed Mathematical Model

Chapter 5: Optimization using Response Surface Methodology (RSM) This chapter shows the optimisation of the adsorption process using RSM. This includes developing the multilevel factorial design, central composite design and Box Behnken design predictive models. The best-fitted models were optimised to identify the optimum pH, flow rate and contact time conditions for iron and manganese removal in groundwater by evaluation and verification using Design-Expert Software.

Chapter 6: Conclusion and Recommendation

This section concludes the thesis findings and outlines the significance of the results. Recommendations are presented for the improvement of this study and further research.

Appendices

This section includes tables, graphs and calculations that formed part of the methods and discussions in Chapters 3, 4 and 5.

CHAPTER 2

Literature Review

CHAPTER 2: Literature Review

2. Literature Review

This chapter gives a detailed description of the origin, physical and chemical properties, classification, and applications of groundwater in South Africa &globally, its environmental contamination by industrialization. This chapter includes conventional physical and chemical methods used to treat groundwater to remove iron and manganese.

2.1 Fresh Water Availability Globally

Two-thirds of 3% of water is used globally, and the rest is inaccessible for human consumption(Africa, 2018; Roman, 2021a). The availability of freshwater volume is irregularly distributed over continents, determined by various magnitudes of the continents(Cheshire, 2022). The variations that are drastically impacting the accessibility of clean, fresh water is the climate change, the disappearing of numerous springs around the world, and the declining of river flow such as the Yellow River, the Ganges, Rion Grande, Congo and Murray-darling river(Cheshire, 2022; Rivera, 2017). Hanjra & Qureshi's (2010) articulated that 3 billion people in 2025 will have no access to fresh water compared to half the billion currently experiencing the dilemma. Jury & Vaux (2007) has outlined that the increasing costs of developing new water sources and pollution hinder freshwater accessibility worldwide. Liu et al. (2021) concurred with other authors that climate change, underdeveloped communities and unemployment increase the demand for freshwater since the underprivileged cannot buy the state to maintain the existing freshwater-producing facilities. Figure 1 below illustrates the water scarcity based on the countries on a scale of 0-5, where 0 means less scarce as the number goes up means more scarce water accessibility (Africa, 2018; Cheshire, 2022; Liu et al., 2021).

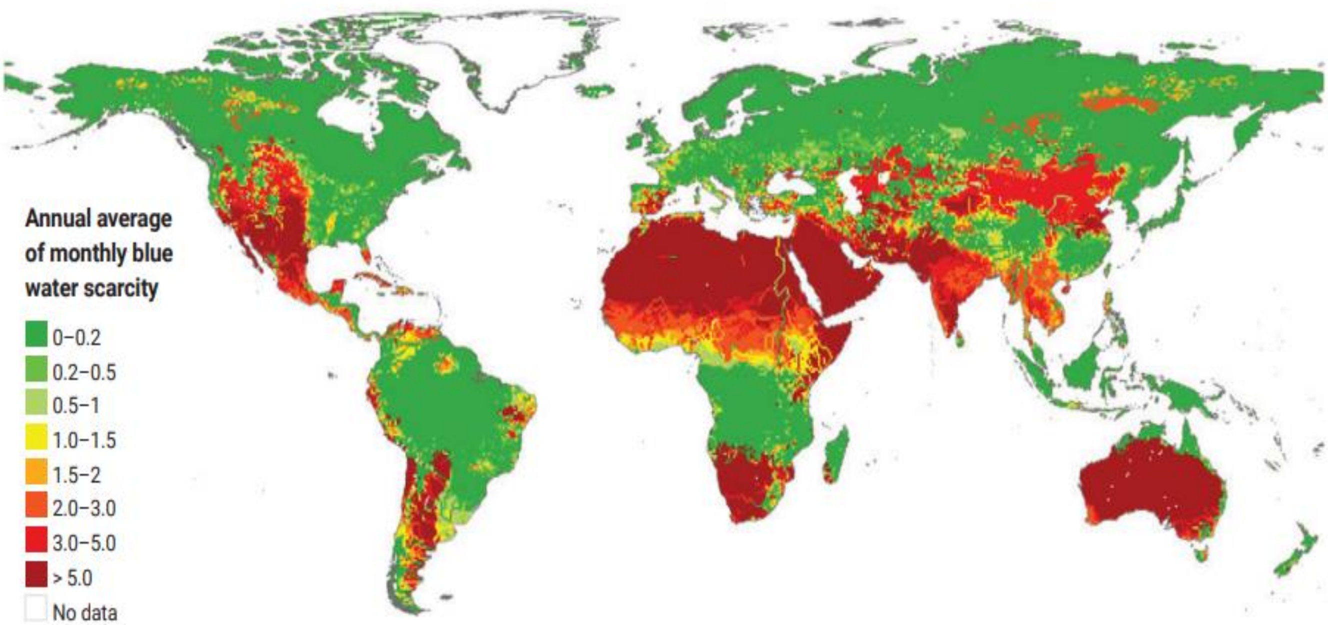

Figure 2-1: Global Water Scarcity (Cheshire, 2022)

As groundwater can be utilized as an alternative source of drinking water (Babu, 2015), it has been discovered that the forecast for reducing the inaccessibility of clean groundwater is to minimise the contamination by adequately managing the landfills, pesticides, de-icing salts and underground installed septic tanks.

2.2 Africa freshwater renewability

The fresh water comparability is contextualized based on the comparison of wet continents, the data presented by(Deng et al., 2013; Rivera, 2017) as illustrated by Figure 2 below. Africa has the lowest freshwater renewal rates, which means access to freshwater is deteriorating significantly since the population growth has increased drastically (Cheshire, 2022).

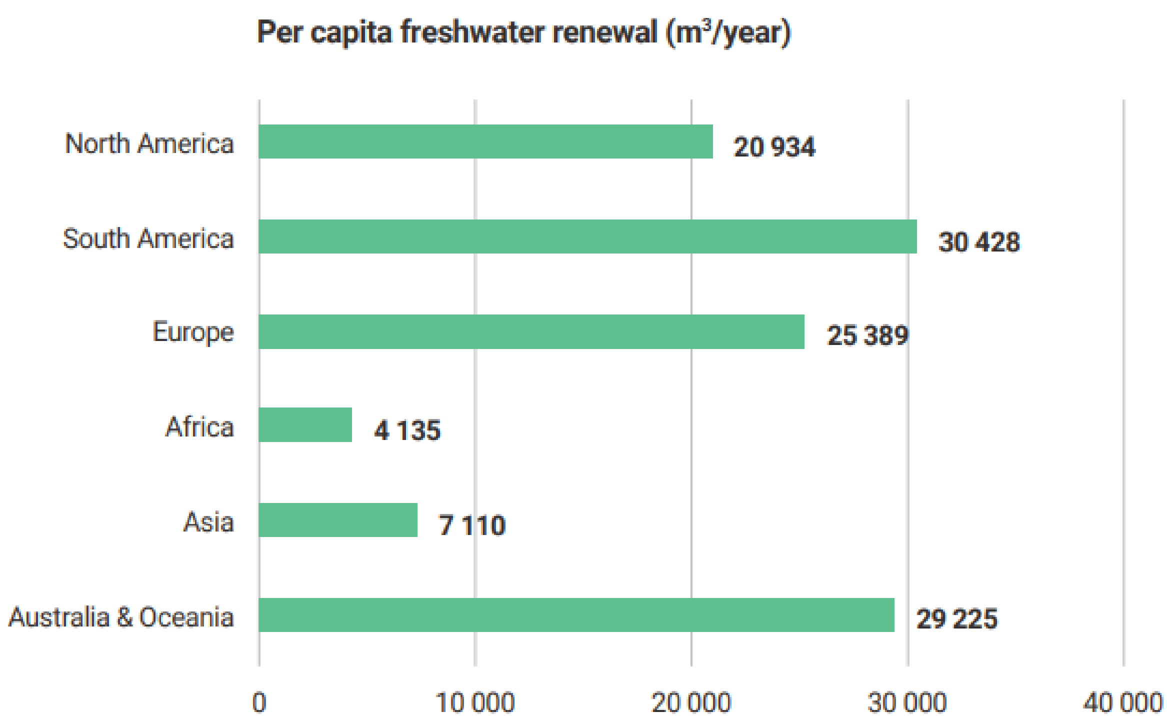

Figure 2-2: Fresh water renewal Africa(Cheshire, 2022)

2.3 Water Supply in South Africa

South Africa is considered semi-arid country since it is mainly affected by climate change and weather variability, which constrains the water resources (Botai et al., 2018). The province of the Western Cape is the reference to this since it was hit by drought in 2017-2019. On the first day of day zero in 2018, there were 22000 privately registered boreholes to serve as an alternative source of water supply during drought in the City of Cape Town (CoCT). Two aquifers were identified to supply the city with approximately 150 million cubic meters. However, later that year, it was discovered that water from these sources could not be directly consumed since it contained parameters like nitrates, fluorides and TDS exceeding the SANS241 drinking water standard (File, 2018). These dissuading parameters were treated to match the effluent standard.

In recent water dryness activities in 2022, Nelson Mandela Bay in Port Elizabeth, renamed Gqeberha, became the first Metro to run out of water; this dryness escalated the acquirement of drilling boreholes in the area for ground water to be an alternative water supply.

In recent water dryness activities in 2022, Nelson Mandela Bay in Port Elizabeth renamed Gqeberha, became the first Metro to run out of water; this dryness escalated the acquirement of drilling boreholes in the area for ground water to be an alternative water supply (Jestinos Mzezewa, 2010). The drying of Nelson Mandela Bay Municipality (NMBM) was noticed in2014 due to low rainfall. Boreholes supplying 357l/min were drilled to provide the community with water. However, this water could not be distributed to the municipality pipe line since it had high iron and manganese content. The bio-filtration plant was erected to treat this water to desired SNS 241 standards to supply the community(Water Resource, 2020).

2.4 Groundwater

Groundwater percolates through the spaces, soil and fractured rocks to the underground surface, forming a portion of the Earth's water cycle, industrial effluent which contains heavy metals and toxic contaminants and find its way to groundwater through this process(Sanderson & Frey, 2015). It contributes to the water supply through wells and surface water through interaction with wetlands, lakes and rivers. In this interacting process, water flow is either from ground to surface or vice versa; the interaction process affects groundwater's hydrology due to surface water pollution from industrial discharge, run-offs from agriculture and waste dumping sites (Boyraz, 2012). Chemical, biological constituents and concentration distribution of groundwater changes due to these effects when surface water percolates to the ground (Sanderson & Frey, 2015).

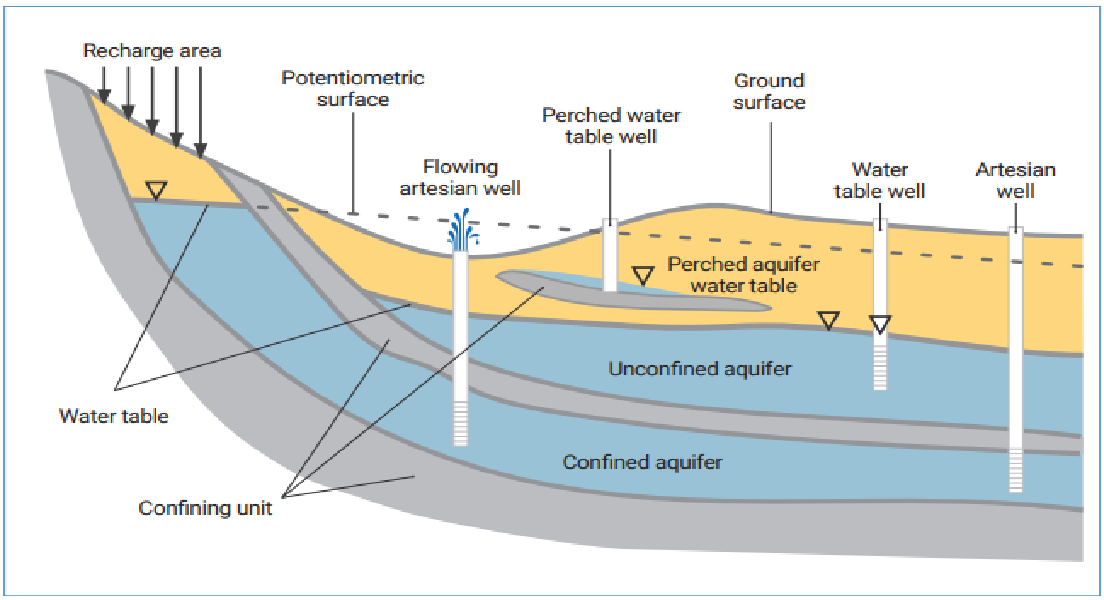

Figure 2-3:Groundwater recharge mechanism(Cheshire, 2022)

Groundwater quality is critical to human health, the economy, and the ecosystem viability of the area it serves (Rivera, 2017). In the preceding years, groundwater was widely used in the agricultural and industrial sectors; however, due to the shortage of fresh water, this water is becoming a primary alternative source for domestic use (Sharifi et al., 2015). However, since groundwater protection is not adequately considered for under the surface water management before domestic use, the heavy metals in groundwater require attention (Rivera, 2017). Figure 2-3 illustrates the groundwater recharge phenomenon.

The recharge area in which groundwater reaches the saturation zone is by surface infiltration. Infiltration flows downward into deeper parts of a water-bearing formation in a recharge area. This recharge phenomenon serves as a transport for contaminants to reach the groundwater. In the case of water table (unconfined) aquifers, usually, the regions occupying higher elevations with deeper water tables constitute the recharge areas, which are the first layers to be reached when drawing groundwater (Prasad, 2011).

2.5 Chemical composition of ground water

Ground water constituents are naturally found beneath the earth's surface (Babu, 2015). Human and industrial activities contribute to uncommon components, as revealed by a Texas study that discovered Trichloroethylene in groundwater due to industrial effluent disposal, which contaminates groundwater during the hydrological cycle (Scher& Caputo, 2014). The most common dissolved minerals in groundwater are calcium, sodium, chloride, potassium, magnesium, bicarbonate, and sulfate, forming part of natural elements (Kumar & Raj, 2018). The contamination of groundwater is a global challenge as this puts pressure on the necessity for filtration before any use (Scher& Caputo, 2014). Iron and manganese are abundant elements in groundwater. High concentrations of these elements have health effects and can damage equipment (Bekri-Abbes et al., 2006; Valeriy Orlov et al., 2016). The World Health Organization has approved that these elements need filtration when their content is 0.3mg/l and manganese 0.1mg/l (Indah & Helard, 2017).

Groundwater chemical composition is vital to pollutant removal because many solutes can inhibit contaminant removal processes. Ionic strengths exceeding 10mM (Arun Yadav et al., 2012), concentrations of dissolved organic matter more significant than 10 mg-C/L (Liu et al., 2015), and pH values below 5.0 can inhibit the adsorption of dissolved metals. A water pH above 5.5 or concentrations of divalent cations or carbonate above 10 mM can slow the oxidation of organic contaminants (Tredoux et al., 2004). According to De Munari & Schäfer (2010), dissolved organic matter concentrations as low as 1 mg/L can diminish the oxidation rate of organic contaminants. These impacts are a concern for protecting water quality across different spatial and temporal settings.

2.6 Iron and Manganese in the environment

The natural existence of iron and manganese in the environment differs from the geology of an area where iron (Fe) and manganese (Mn) naturally occur in groundwater with little or no oxygen.(du Toit et al., 2012)in his study has stipulated that the concentration of iron (Fe) and manganese (Mn) in groundwater can be seasonal due to the amount of rain that can percolate through to the ground water and also, the concentration varies with the depth and location (Baharudin et al., 2018; Mohd Remy Rozainy et al., 2015).

As iron and manganese are not synthetic, their chemical structures are motivated by organic compounds in the subsurface. The limited amount of oxygen in the subsurface results in the complex formation of iron and manganese which appear in the form of $FeCO_3$, FeS_2 $FeTiO_3$for iron and $MnSO_4$, $MnCl_2$, Mn_3O_4, for manganese (Nalbantcilar& Pinarkara, 2015).

The health implications of iron compounds if consumed by humans are linked to the nervous system, liver damage, diabetes mellitus, pigmentation changes and skin cancer (Kumar & Raj, 2018). The study conducted in Bangladesh about the health risk associated with iron and manganese has discovered a positive association between higher manganese concentrations of 0.4 mg/L with the reduced intellectual function of children aged ten years. It also mentioned that infants with increased mortality risk during the first year of life (Ghosh et al., 2020).

2.7 Legislation of iron and manganese in drinking water

South African water legislation, has the health-based threshold of 2mg/land 0.4mg/l as secondary standards for iron and manganese, respectively (Division, 2011; Rivera, 2017; SANS, 2015; World Health Organization, 2011). Water concentrations above the secondary standards will be life-threatening since the primary criteria are 0.3mg/l and 0.1mg/l of iron and manganese, respectively. In particular, for South African legislation, when these two parameters in ground water exceed the secondary standards, the water source is forbidden since the site is considered contaminated(SANS, 2015).

The lack of education and knowledge amongst the people of South Africa about the importance of water, highlighted by the Water Research Commission (WRC) report done in 2012, needs more emphasis due to non-reported water leakages in the communities, which results in water shortages (Roman, 2021). WRC 2021/22 report has highlighted the importance of ground water as an alternative source by publishing a study that enhances groundwater security on the sustainable exploitation of groundwater resources on the West Coast of South Africa. The study's primary outcome constituted an improved understanding of the Langebaan Road Aquifer and Elandsfontein Aquifer inter-relationship to execute a sustainable plan to meet Western Cape Water Supply System demand.

2.8 Chemical properties of iron and manganese

Iron and manganese have similar behaviour in many aspects; however, the colour tainting of the two parameters varies from reddish to brown and black, respectively. When these elements are oxidized become insoluble in water; however have excellent solubility when reduced (Imaging et al., 2016).

2.8.1 Iron

Iron is a metal ranked the 10th most abundant element in the universe. Its multiplication on earth results from nucleosynthesis (the creation centre of protons and neutrons), with no need for supernovas and cataclysmic(EPA, 2007). It is used in steel manufacturing, in engineering for concrete reinforcement, and in making alloys with vanadium, chromium, manganese and tungsten as additives (Iserhien-Emekeme et al., 2017; Schöntag et al., 2015).The physical properties of it being rusted by damp air and dissolving in dilute acids make it aesthetic in groundwater; since water is an ampholyte, it will readily dissolve(Espinoza Márquez et al., 2020).

Iron significantly affects water's colour and taste, resulting in unpleasant sight for drinking (Imaging et al., 2016; Roccaro et al., 2007). As far as the research is concerned, this element possesses no health threats at low concentrations as it is used as a dietary supplement and is mainly found in food. However, high concentrations might produce toxic chelates such as iron pentacarbonyl, resulting in lung diseases. It also promotes the growth of microorganisms that are chlorine tolerant, thus causing odour in water (Palmucci et al., 2016).

2.8.2 Manganese

In ancient history 30,000 years ago, it was used in the Lascaux region situated in France as painted by pre-historic cave writers(World Health Organization, 2011). It's the fifth most abundant metal on Earth. The dominant mineral forms are manganese carbonate and manganese dioxide(Sanderson & Frey, 2015). Manganese is essential for all living organisms since many enzymes contain it. The human body has an average of 12 milligrams of manganese from foods such as wholegrain cereal, nuts, parsley and tea (Chandler, 1989; Dalai et al., 2015).

In water, manganese is found in the most soluble and reduced form (Roccaro et al., 2007). An elevated concentration of this element is considered undesirable because its exposure to air oxidizes Mn(II) to Mn(IV), which results in precipitation that affects the colour of water and imparts bitter, metallic and astringent taste (Kwakye-Awuah et al., 2019).Long term exposure to the high concentration of manganese affects human life. It causes irreversible disease syndrome as Parkinson's disease, including slow speech, muscle pain, headache and insomnia (Kwakye-Awuah et al., 2019; Services, 2002; World Health Organization, 2011).

2.9Chemical treatment of Iron and Manganese

Various methods and techniques had been employed, invented and tested in the removal of Iron and manganese from ground water. Several studies have been published on these treatment processes' efficacy and defects (Vries et al., 2017).

2.9.1Process of Chemical Oxidation followed by Filtration

Oxidation, precipitation and filtration is the most commonly applied method for removing iron and manganese in the water. Chemical oxidation is required to convert these elements from soluble to insoluble (Roccaro et al., 2007). The process involves the application of chemicals and mainly silica sand filtration to adsorb the precipitated form of Fe (III) and manganese (IV) (Naik, 2015).The substances applied for this process are chlorine, ozone, hydrogen peroxide and potassium permanganate.

Because of cost-effectiveness, small-scale filtration mainly uses chlorine or potassium permanganate(Ahmad, 2012).However ,the application of chemicals for the treatment of Iron and manganese is mainly applied where a high concentration of these element is detected (Goher et al., 2015; Naik, 2015). Chemical oxidation is the alteration of soluble iron and manganese to insoluble complexes utilizing electron transfer to the oxidizing agents in the form of chlorine, ozone, potassium permanganate, hydrogen peroxide and chlorine dioxide (Naik, 2015; Talaat et al., 2010).

2.9.2Chlorine (Cl_2)

Chlorine is the abundantly applied oxidant for high concentrations of iron and manganese (Khadse et al., 2015). No significant amount of iron and manganese was removed at lower chlorine doses (5 and 10mg/l). The removal of iron and manganese was notable at 15 mg/L of chlorine dose, however, with a lengthy contact period of 5 hours. The conclusion drawn by this study was that chlorine might not be used on high concentrations of iron and manganese since that will require a higher dosage, which will lead to chlorine byproducts such as chloroform, dichlorobromomethane and bromoforms formed in the water and also the excess chlorine in the effluent (Sharma, 2001*)*

2.9.3Chlorine Dioxide ClO_2

The study performed by (Hoyland et al., 2014) reported that iron and manganese oxidation by chlorine dioxide, a stoichiometric amount of 2.45 mg ClO_2 per mg of both these elements, needs to be followed. However, its oxidation capability was notable in removing manganese at low concentrations, with twice the stoichiometric dose (Vries et al., 2017). It was found that ClO_2 is also effective in water that has TOC compared to other oxidizing agents that are hindered by this parameter (Talaat et al., 2010). The use of chlorine dioxide has a limit due to it yielding the by-products such as chlorite, and chlorate, which results in the limitation of ClO_2 to water. It was deemed inappropriate for treating relatively high amounts of iron and manganese (Hoyland et al., 2014).

2.9.4Ozonation O_3

It is also rated as another oxidant applied in the oxidation of iron and manganese (Talaat et al., 2010). However, its oxidation ratio is 0.87-mg O_3 to 1.0 mg of iron and manganese in water with the absence of other oxidants (Tobiason et al., 2016), the dosing demand increases in the presents of TOC, as reported by the bench scale experiment performed by (Wagh et al., 2007), where O_3 was unsuccessful at oxidizing iron and manganese in water containing less than 5mg/l of TOC. High ozone dosage results in the formation of permanganate in water containing manganese which causes water quality problems (Hoyland et al., 2014; Sharma, 2001).

2.9.5Potassium and sodium permanganate

This oxidant is widely used in manganese-coated sand as a rejuvenator to enhance the oxidation of iron and manganese (Sharma, 2001). Its oxidizing state is pH depended; the stoichiometric dose is between 0.94 to 1.92 $KMnO_4$ per mg of iron and manganese (Vries et al., 2017). The limitation of this oxidant overdosing is that it may increase the dissolve manganese content (Khadse et al., 2015; Robey, 2014).Potassium permanganate is ideally applicable to water with low concentrations of iron and manganese since it causes pink water when dosed in high concentrations and it also forms mud balls precipitants (Goher et al., 2015; Naik, 2015)

Table 2-1:Scientifically proven oxidation and filtration for removal of iron and manganese (Robey, 2014; Sharma, 2001; Vries et al., 2017)

Oxidants	**Amount dosage**	**Oxidation Time**	**pH**	**Scientific Findings**
O_2 Oxygen	0.14mg	10minutes	≥ 7.2	It is ideal for lower concentrations; however, for a pH > 8.5, dual oxidation is necessary for iron and manganese. If the concentration of these parameters is> 5mg/ℓ, oxygen is required to be used as a pre-oxidant to reduce chemical costs.
	0.29mg	1 hour	≥ 9.5	
O_3 Ozone	0.43mg	<1 minute	≥ 5.5	It oxidizers instantly, however on a high chemical dose and low contaminant concentrations
	0.87		≥ 8	
$KMnO_4$ Potassium Permanganate	0.94	<5 minutes	≥ 7.5	In effective in high concentrations of iron and manganese
	1.92		5.5-9.0	
ClO_2 Chlorine Dioxide	0.24	<1 minute	6.8-8.4	It works efficiently in low concentrations, and it is more expensive.
	2.45		5.5-9.0	
HOCl Hypochlorite	0.47	<1 minute	≥ 8.0	Rapid oxidation, ideal for manganese. However, complexes with iron. It doesn't need water with high organics
	0.96	2 to 3 hours	≥ 8.5	
H_2O_2 Hydrogen peroxide	0.30	<1 minute	5.5-9.0	Rapid oxidation with Ions, however, is complex with manganese.
	0.62	> 5 hours	≥ 8.5	

2.10 Physical removal behaviour of Iron and Manganese by different methods

2.10.1 Sequestering

This application involves agents such as sodium silicate, phosphate or polyphosphate for complexifying Iron and manganese in polymeric colloidal structure to prevent them from forming colour. However, the disadvantage of this process is that water is heated to a temperature above 70 ^{O}C, which leads to the precipitation of the bonded elements (Indah & Helard, 2017; Naik, 2015).

2.10.2 Photos-Electrochemical Method

It is the electrode method required to increase the oxidation potential of an element to overcome its activation energy for the formation of manganese oxide (Molari et al., 2020). Talaat et al., 2010 , performed a study of photo-electrochemical to remove iron and manganese in water by using the potential energy of the metals to reach their oxidation state. The study observed that manganese had a high oxidation potential of (1.05 V) and iron (0.77 V); the results showed that iron was removed from 5 to 0.1ppm in 10 minutes while manganese was 5 to 2.2ppm in 20minutes. The conclusion was drawn that iron was successfully oxidized first based on its oxidation potential formation compared to manganese. It was also discovered that this method could be applied in lower concentrations.

2.10.3 Aeration

Aeration is the process in which air is added to the water for the cupellation of gases or oxygenation. It is the chemical reaction between substances in the water and oxygen where the transformation of substances to heavier particles is formed to precipitate (Isaeva & Castro, 2011). Water with dissolved iron and manganese become cloudy and turbid when exposed to air or oxygen due to the oxidation of these two metals to Fe (III) and Mn (IV). However, other studies reported that aeration is less effective due to the persistence of reduced forms of iron and manganese in aerated (Khadse et al., 2015).

2.10.4 Biological Treatment

The utilization of iron and manganese bacteria is a recent innovation discovered for the oxidation of Iron and manganese. Auto-trophic iron and manganese filters are used as oxidizing bacteria. However, the study stated that the physicochemical properties of Iron made bacteria are less effective in removing l manganese and for manganese bacteria on iron (Mota et al., 2020).

2.10.5 Removal of oxidized iron and Manganese by Membrane Technology

The particulate removal is the filtration stage that precedes the oxidation process. Iron and manganese are altered from soluble to insoluble solid particles, which need to be separated from the solution using conventional water purification either by microfiltration or media filtration(Goodwill, 2015).

2.10.6 Microfiltration (MF) / Ultra-filtration (UF) Membranes

This membrane technology has taken a rise recently in the water treatment industry. The application of micro-ultra-filtration membranes has been reported to be able to overcome operational problems faced by conventional technology in treating water (Kasim et al., 2017)**.** The membrane's advantage is the high retention of divalent ions with low energy consumption and operational pressure (Hoyland et al., 2014; Kasim et al., 2017)**.** However, the study by (Fakhfekh et al., 2017) reported that the micro/ultra-filtration membranes could not remove iron and manganese without being destabilized to the filtration form of particles.

Kasim et al., 201, study reported that membrane filtration does remove iron and manganese. However, it was also noticed that the more these elements were being filtered, the product water flow rate decreased drastically due to the fouling, which was also visually observed on the surface of the membrane by morphology analysis, brownish cake for iron fouling and blackish cake for manganese fouling (Bora et al., 2016). In addition, these membranes proved to be effective from direct oxidation (De Munari & Schäfer, 2010). However, its effectiveness depends on the size exclusion of the membrane pores. The more the reduced pore size, the higher the fouling of the surface of the membrane (Fakhfekh et al., 2017; Sousa et al., 2020)**,** which will increase the operational costs.

Table 2-2: Represent the summary of previous technologies for removal of iron and manganese before and after treatment

Reference	Process	pH	Iron (Fe) mg/L		Manganese (Mn) mg/L	
			In (before)	**Out (After)**	**In (before)**	**Out (After)**
(Roccaro et al., 2007)	Potassium permanganate Oxidation, Flocculation settling and Membrane Filtration	6.84	–	–	1.81	1.6
(Barloková & Ilavský, 2010)	Activated Sand (Klinopur-Mn) and Birm	8.3	0.68	0.57	0.56	0.41
(HAMEED, 2019)	Chlorination	7.92	1.93	1.43	0.96	0.71
	Zeolite	7.92	1.93	0.46	0.96	0.52
	Greensand	7.92	1.93	0.32	0.96	0.16
	Birm	7.92	1.93	0.25	0.96	0.07
(Indah & Helard, 2017)	Coated Pumice	7	15	2.4	5	1.3
(Dalai et al., 2015)	Rice Husk Activated Carbon	12	11.10	3.37	10.28	1.48
	Sugarcane Activated Carbon	12	14.10	3.05	13.28	2.72
(Mota et al., 2020)	Cladosporiumhalotolerans and Hypocreajecorina Bacteria	7	-	-	50	2
(Osuagwu et al., 2018)	Expanded Polystyrene	9.9	5.5	3.5	-	-

2.11 Synthetic Filtration Medium for Iron and Manganese removal

2.11.1 Catalytic Oxidation Medium

Catalytic oxidation media is a metal oxide granular medium developed from naturally occurring minerals such as silica sand. These mediums are technically synthesized by being coated with manganese/iron oxide to enhance the oxidation of iron and manganese in the water (Indah & Helard, 2017). The recently developed media are trading as Greensand, DMI65 and Birm (Michel et al., 2020). Dissolved iron and manganese are then removed by sorption from the solution to a solid surface with a pH ranging between 6 and 9 (Lewis, 2011).

2.11.2 Operating conditions of catalytic oxidation medium

The operating conditions of these synthesized mediums may be affected on several occasions. Other work also indicates that from the coating process, the media might not be entirely covered with manganese oxide (Charbonnet, 2018). A study by (Michel et al., 2020) emphasized the importance of ensuring that the coating is done when producing metal oxide media since the layer might break off during transportation.

Charbonnet, 2018, stated that two processes were followed for coating of synthetic media: thermal and chemical coating. However, chemical-coated media yielded better results than thermal in the water treatment field. The research carried out in the column test indicated better performance of manganese oxide than manganese dioxide coated (Michel et al., 2020; Nalbantcilar & Pinarkara, 2015). The main parameters to be monitored when applying this medium in water treatment are pH, temperature and reaction time since they might affect the water quality. After the redox reaction occurs when sorbed iron and manganese are oxidized, the coated media removal capacity gets exhausted, and the coating is reduced (Tobiason et al., 2016).

2.11.3 Adsorption of Iron and Manganese on catalytic oxidation mediums

The surfaces of these metal oxides have Mn (III) oxidation state for iron and manganese removal. Iron Fe (II) and manganese Mn (II) are removed from water through adsorption (Camargo et al., n.d.). The study by (Lewis, 2011) reported that the adsorption of the metals to the medium surface is rapid since it is accompanied by the Hydrogen ion (H+) release, as the cations to oxide adsorption occur on the surface of the media (Camargo et al., n.d.; Michel et al., 2020). However, the adsorption efficiency of these systems depends on the consistent and frequent regeneration of the mediums by sodium hypochlorite and potassium permanganate to oxidize the adsorbed iron and manganese. Then backwash is applied to the media to remove the adsorbed precipitated particulates, which results in high operational costs; also ideal for use on a large scale (Indah & Helard, 2017). Manganese and Iron oxide mediums can oxidise and adsorb these elements; however, they lose their reactivity sites due to the accumulation of reaction products on the surfaces (Hoyland et al., 2014). However, their activity can be rejuvenated by constant chemical dosing that results in high costs, which limits these mediums for being used in tertiary water treatment (Goonetilleke et al., 2016).

2.12 Treatment technologies used in this study

2.12.1 Tri-Medium Integrated System

The selection of filter media is of extraordinary significance for filter performance. This system's design consists of combining three various filtration mediums in one vessel. This study will focus on evaluating this system for the removal of Iron and manganese from groundwater. Different media types can be used alone or in combination with one another in dual or multi-media parallel filters. However, the Tri-Medium System containing Expanded Polystyrene Beads, Virgin Glass Media and Ion Exchange Resin is a foreign study. Even though the media size distribution, density, shape, and porosity are among the critical properties in establishing filter performance characteristics were not taken into high consideration in this study.

2.12.2 Ion Exchange Media

This media hold ions electrostatically on an immobile solids phase surface where a molecule or an atom is exchanged from the solution with a similar charge (Ahmed Mohamed Atta, 2007). These resins are synthetically produced polyelectrolytes with tailored characteristics of exchanging ions. The individual application of this media in Iron and manganese has been studied before; however, it resulted in high fouling, which lessened its effectiveness because the study was carried with water containing a high amount of dissolved oxygen, and this media is dissolved oxygen intolerant (Naik, 2015).

2.12.3 Polystyrene Beads

It is a small, spherically shaped, lightweight cellular plastic containing 98% air. Its composition is exclusive of hydrogen and carbon derived from styrene, a petroleum-derived material. The material is environmentally friendly, cost-effective, and widely used in food packaging (Osuagwu et al., 2018). Its high resistance to mould, fungi, bacteria growth, strong mineral acids and strong alkalis resulted in it as one of the media that can be applied in water treatment (Bekri-Abbes et al., 2006). The study that used this media in water treatment revealed that its efficiency depends on the contact time and the amount of media used (Osuagwu et al., 2018). However, the previous study used polystyrene beads for removal of iron without oxidation.

2.12.4 Virgin Glass Media

The media is developed from a raw glass material (S. D. Sheet, 2018); it has a sub-angular shape, increasing its sphericity and advantage of contact in its water treatment application (Nalbantcilar & Pinarkara, 2015). This media is tailored to cater for any water and is extensively used as pre-filtration in water treatment to support the Medium that does the separation (Uddin et al., 2019). No study or publication was done using virgin glass media for iron and manganese treatment. To the places where it is being currently applied, it yielded positive filtration results in terms of particles removal in less contact as compared to synthetic glass media's

2.14 Adsorption

Adsorption is a separation process employing the transfer of fluid phase mass to the surface of a solid adsorbent (Al Shaarani& Al Wazi, 2006). The adsorbent is mainly tiny particles held in a fixed bed, allowing the fluid to pass through continuously. This process is more favourable than the chemical methods since it is more straightforward and flexible (Roman, 2021a; Tobiason et al., 2016). It does not generate any sludge as in the biological process except for the adsorbent that becomes saturated by the adsorbate particles (Osuagwu et al., 2018). These being stated this separation methodology is the most frequently utilized process. Various media used in this process include activated carbon, glass media, sand, ion exchange resins, etc.(Saleh et al., 2019).

Parameters with a direct adsorption process are contact time, pH and concentration of adsorbate (Saleh et al., 2019). The relation between each factor and the adsorption process should be predicted. In the past, the effect of each element was studied individually at the time as contact time was determined to be an essential parameter for the determination of equilibration point; pH plays a crucial role in determining the nature of adsorption and the mechanism involved, adsorbate concentration to determine the solid-liquid equilibria on mass transfer rate (Al Shaarani&Al Wazi, 2006).

2.14.1 Adsorbent Characterization

Adsorption primarily occurs on the adsorbent surface or the walls of the adsorbent pores (Al Shaarani& Al Wazi, 2006). The experimental design and analysis tool called Response Surface Method (RSM) was developed to determine the response of the adsorbent surface in the separation process. Other methodologies for determining the surface behaviour such as Scanning electron microns (SEM) which is the morphological testing technique to determine unevenness of the media surface in terms of occasional pits & fracture, and Fourier Transformation Infrared (FTIR), which is utilized to characterize the functional groups on the media surface (Kumari et al., 2020). The RSMl method solves the problem by creating a model predicting the relationship between the surface of the adsorbent and the adsorbate (Saleh et al., 2019).

Ozturk & Silah, (2020) stated that the adsorption depends on the adsorbent morphology, which is the porosity and the functional group on the medium surface. On the contrary (Kumar & Raj, 2018) state that the oxidized iron(III) and manganese (IV) oxide form a new surface on the medium for adsorbing iron (II) and manganese (II), and the process becomes adsorption-oxidation. The positive effect of this process is the reduction of oxidant concentration and the time for oxidation reaction (Kumari et al., 2020).

2.15 Models for adsorption of Iron (Fe) and Manganese (Mn) metals

2.15.1 Adsorption Isotherms Models

2.15.2 Introduction

Adsorption isotherms are mainly interpreted in a curve as the phenomenon that explains the involvement of liquid or substance retention in a medium or aqueous solution on a solid particle (Said et al., 2018). According to Ioannou et al. (1994), it is the interaction between adsorbent and adsorbate when the equilibrium state is established on ions adsorbed and ions in the solution.

Freundlich and Langmuir mainly apply the isotherms to characterize the medium adsorption for removing iron and manganese adsorption. According to (Ozturk & Silah, 2020), the adsorption affinity of the medium depends on the electro-negativity and the atomic radius of the adsorbate. The study performed by (bin Jusoh et al., 2005) using GAC (Granular Activated Carbon) for the removal of iron and manganese has observed that since Iron has high electro negativity and low atomic radius compared to manganese has shown positive adsorptive results with Langmuir because this isotherm is also valid for monolayer sorption onto the medium surface of limited identical sites.

2.15.3 Adsorption equilibrium capacity

Adsorption equilibrium is when the supernatant solution particles are adsorbed on the adsorbent. The adsorbate concentration remains unaltered after a certain period, corresponding to interface concentration and adsorbate concentration in bulk solution (Ferreira et al., 2019; Roman, 2021a). The relationship between the adsorbent adsorbed and adsorption isotherms describe the adsorbate amount in a solution (Ferreira et al., 2019; Ioannou et al., 1994). The types of adsorption that mainly occur are physical adsorption, an interaction of weak Van der Waals forces between an adsorbate and the adsorbent and chemisorption adsorption, which is the strong chemical bond interaction using electron transfer among the particles and the adsorbent (Ioannou et al., 1994). The amount adsorbed is calculated by the equation below.

Equation 2-1: Represent adsorption equilibrium capacity

$$q_e = \left(\frac{C_o - C_e}{m}\right) \times V$$

Where $q_e$is the total amount of contaminant adsorbed at equilibrium (mg/g), C_o is the initial concentration of contaminant in solution (mg/L), C_e is the equilibrium concentration of contaminant in solution (mg/L), V is the volume of contaminant solution (L) and m is the mass of adsorbent (mg) (Said et al., 2018).

2.15.4Adsorption Isotherms shapes

The isotherms shapes indicated on the graphs above explain the relationship between the adsorbate and the adsorbent; it also describes if the desorption can be applied to the saturated adsorbent (McCabe et al., 1993).

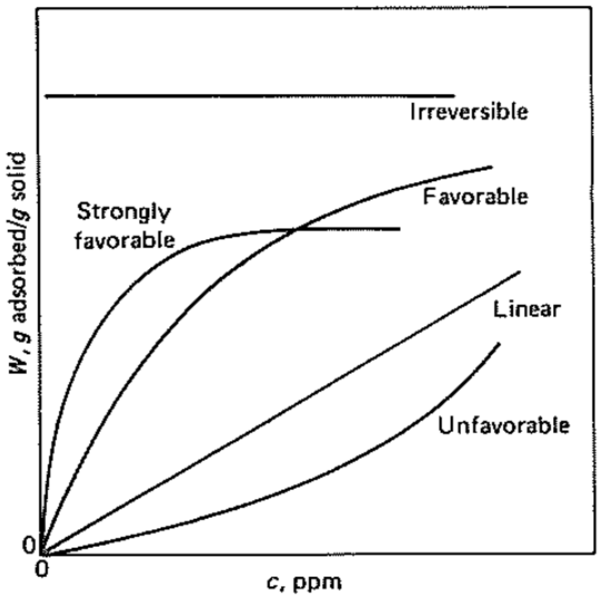

Figure 2-4: Various shapes of the isotherms (McCabe et al., 1993).

If the linear isotherm goes through the origin, the amount adsorbed is proportional to the concentration in the fluid (McCabe et al., 1993). The favourable (convex upwards) isotherms are those with high solid loading. However, they are obtained at low fluid concentrations and regarded as irreversible. Irreversible adsorption characteristics in the figure above represent adsorbents with tiny pores (Serge, 2014). The concave upwards isotherm is viewed as unfavourable since it has poor solid loading and it requires ample time for mass transfer in the bed (McCabe et al., 1993); it also represents nonporous and uniform surface adsorbent (Serge., 2014)

2.15.5Langmuir Isotherm

Langmuir's theory assumes no interaction exists between adsorbed molecules; adsorption occurs only at specific homogeneous sites inside the adsorbent. Once the adsorbent is saturated, no further adsorption appears (M. Hamzaoui, B. Bestani, 2018).

Kumari et al. (2020) stated that this Isotherm predicts monolayer adsorption on the adsorbent's homogeneous, motionless surface. The isotherm is more favourable if constant *b* is large and $bCe>1$ is strongly favoured, and when $bCe<1$, the isotherm is nearly linear (Piccin et al., 2011).

Equation 2-2: Represent Langmuir equation

$$\frac{1}{q_e} = \frac{1}{Q_m} + \frac{1}{bQ_mC_e}$$

Where Q_m is the maximum monolayer adsorption capacity (mg/g), *b* is the Langmuir constant and q_e and C_e are the adsorption capacity (mg/g) and equilibrium concentration (mg/l), respectively (Piccin et al., 2011).

Plotting C_e/q_e versus C_e results in a straight line of slope $1/Q_m$ and intercepts $1/bQ_m$

Equation 2- 3: Langmuir separation factor

$$R_L = \frac{1}{1 + bC_o}$$

2.15.6Freundlich Isotherm

The Freundlich isotherm model describes the heterogeneous multilayer adsorption and the correlation between adsorbate and adsorbent (M. Hamzaoui, B. Bestani, 2018). Freundlich isotherm-associated constants models are sorption capacity (KF) and sorption intensity (1/n).

Equation 2-4: Freundlich Equation

$$\ln q_e = \ln K_F + \frac{1}{n}\ln C_e$$

The value of n describes the affinity. The process is either chemisorption ($n < 1$) or physisorption ($n > 1$) (Piccin et al., 2011). Plot: ln qe versus ln C_e

2.15.7Temkin Isotherm

Temkin Isotherm model pertains to the molecules' heat that decreases linearly when the adsorbent surface is increasingly covered by the adsorbate (Ferreira et al., 2019).

Equation 2-5: Temkin Equation

$$q_e = \frac{RT}{b} lnK_T + \frac{RT}{b} lnC_e$$

Where B_T represents:

Equation 2- 6: Freundlich Adsorption heat constant

$$B_T = \frac{RT}{b}$$

Where K_T is the equilibrium binding constant ($L\ mol^{-1}$) corresponding to the maximum binding energy, b_T is related to the adsorption heat. R is the universal gas constant (8.314 $J\ K^{-1}\ mol^{-1}$) and T is the temperature (K). Plotting $q_e$vs ln(C_e) results in a straight line of slope RT/b_T and intercept (RT ln K_T)/b_T(Piccin et al., 2011).

2.15.8The Dubinin–Radushkevich Isotherm

This model was utilized to envisage the nature of the adsorption process as physical or chemical by calculating sorption energy. The Dubinin–Radushkevich isotherm relates to the heterogeneity of energies close to the adsorbent surface (Saeidi & Parvini, 2015).

The equilibrium correlation of adsorbate-adsorbent can be determined using the adsorption potential (ε).

Equation 2-7: Dubinin_Radushkevich Isotherm

$$\varepsilon = RTln\left(1 + \frac{1}{C_e}\right)$$

The linear form of the model is described as:

Equation 2- 8: Dubinin Linear equation

$$Lnq_e = Lnq_m - \beta\varepsilon^2$$

The mean sorption energy, E ($Jmol^{-1}$), is evaluated by:

Equation 2- 9: Dubinin Sorption energy

$$E = \frac{1}{\sqrt{2\beta}}$$

Values of q_m and β can be determined by linearizing the D-R isotherm. Plotting ln qe versus ε^2, will results in a straight line of slope β and intercept ln (q_e) (Saeidi & Parvini, 2015)**.**

E (J/mol) is the mean free energy of adsorption per molecule adsorbate. If E<8 kJ/mol, the adsorption process is physical and i ranges from 8 to 16 kJ/mol, it is chemical in nature(Saeidi & Parvini, 2015; Said et al., 2018).

2.16 Adsorption Kinetic Models

2.16.1 Introduction

Adsorption Kinetics is an empirical factor in the adsorption process to understand before applying any adsorbent. The kinetics are implicated in determining the reaction rate concerning the adsorption of an adsorbate to an adsorbent in a separation process. The adsorption kinetics are presented in a curve illustrating the retention rate or solute release in a solution at a given pH, flow rate, adsorbent dosage and contact time (Turp et al., 2022).

2.16.2Pseudo-First Order (PFO)

According to (Kumari et al., 2020), PFO adsorption kinetic is more applicable to the adsorption rate that explores vacant active sides of the adsorbent surface. The linearized equation for PFO:

Equation 2- 10: Linearized pseudo first order

$$\ln(q_e - q_t) = lnq_e - k_1 t$$

qt- represent the amount of adsorbate in mg/g at a time, qe – represent the amount of adsorbate in mg/g at equilibrium. The linear graph of ln ($qe - qt$) vs t gives the Pseudo first-order rate kinetic k1.

2.16.3Pseudo Second Order (PSO)

The assumption made on a PSO is that it is depended on the vacant site and the capability of utilizing the adsorbed side, which might be due to the potential electrostatic force on the charged surface of an absorbent in a separation process of adsorbent-adsorbate (Ioannou et al., 1994; Saeidi & Parvini, 2015).

Equation 2-11: Linearized PSO equation

$$\frac{t}{q_t} = \frac{1}{k_2 q_e^2} + \frac{t}{q_e}$$

The amount of adsorbent is determined by the below equation:

Equation 2- 12: Adsorbate amount

$$q_t = \frac{t}{\frac{1}{k_s q_e^2 + \frac{t}{q_t}}}$$

q_t- represent the amount of adsorbate in mg/g at a time, and qe – represent the amount of adsorbate

The interception of plot $\left(\frac{t}{q_t}\right) vs\ t$, will aid in determining the Pseudo Second Order rate constant k_2

2.16.4 Intra particle diffusion model (IP)

The IP model forms part of the surface adsorption mechanism by being widely applied to determine the rate-limiting step during adsorption. The adsorption of the solutes under this mechanism follows three categories: the diffusion of metal ions through the boundary layer, intra-particle diffusion and adsorption of the metal ions on the sorbent surface (Ferreira et al., 2019; Roman, 2021b).The below form presents the equation:

The below form presents the equation:

Equation 2-13: Represent Intra particles diffusion equation

$$q_t = k_d t^{0.5} + C$$

K_d is the intra-particle diffusion rate constant (mg/g min1/2), and C is the boundary layer thickness. The plot of q_t vs t1/2 gives a linear function. The plot structure and the linearity of the IP graph are the main fundamental assessment criteria in determining whether the IP controls the diffusion process in the system. If the plot line is through the origin, it means IP affects the process; if it does not pass through the source, other mechanisms are in charge of the adsorption process (Roman, 2021b). Those mechanisms involve the mass solute transfer after the adsorbent is placed in the solution. This film diffusion is the slow movement of solutes from the boundary layer and the penetration of the solute to the adsorbent pores. These mechanisms are not considered in the engineering design of the kinetics models since this process takes place rapidly (Ferreira et al., 2019).

2.16.5The Elovich Kinetic model

The Elovich Model is assumed to be utilized to further evaluate the chemisorption in the adsorption process (Said et al., 2018). These models are applied to predict the surface interaction of the adsorbent and the adsorbate in terms of mass, surface diffusion, and energy activation to deactivation (Roman, 2021b). It also assumes that the adsorbent surface is energetically heterogeneous and its kinetics are unaffected by desorption or adsorbed species interaction (Saeidi & Parvini, 2015).

Equation 2- 14: Elovich Differential equation

$$\frac{dq_t}{d_t} = a\ \exp^{\beta\ q_t}$$

As $q_t \approx 0$, $dqt/dt \approx \alpha$ which is the initial adsorption rate, and β is the desorption constant.

Equation 2-15: Elovich equation

$$q_t = \frac{1}{\beta} ln\left(t + \frac{1}{\alpha\beta}\right) - \frac{1}{\beta} ln(\alpha\beta)$$

t >> $1\alpha\beta$ as the system reaches equilibrium

Equation 2- 16: Elovich adsorption capacity equation

$$q_t = \frac{1}{\beta} ln(\alpha\beta) + \frac{1}{\beta} ln(t)$$

The plot of q_t vs t determines the adsorption nature whether chemisorption or not

2.17 Error Analysis

Error analysis determines the experimental dataset's most suitable isotherm (A.O, 2012). Even though the correlation coefficient (R^2) is a mainly utilized parameter to specify the best-fit isotherm through analysis, its deficiency presents only linear models (Piccin et al., 2011). The logic behind the error function is to determine the isotherm that shows less error function. Therefore, other models are incorporated to determine isotherms' best fit properly.

Equation 2- 17: SSE equation (Piccin et al., 2011)

$$SSE = \sum_{i=1}^{n} \left(q_{e,calc} - q_{e,meas}\right)_i^2$$

The Sum of Squared Errors (SSE) is the most commonly utilized error function.

Equation 2-18: SAE equation (Piccin et al., 2011)

$$SAE = \sum_{i=1}^{n} \left|q_{e,calc} - q_{e,meas}\right|_i$$

The sum of absolute errors (SAE) tends to be applied for better adjustments in higher concentrations (Piccin et al., 2011).

Equation 2-19: ARE equation (Piccin et al., 2011)

$$ARE = \frac{100}{n} \sum_{i=1}^{n} \left|\frac{q_{e,calc} - q_{e,meas}}{q_{e,meas}}\right|_i$$

The average relative error (ARE) is utilized across various concentration ranges.
Where $q_{e,\ calc}$ is the calculated value, $q_{e,\ meas}$ is the measured value and n is the number of data points.

2.18 Mathematical Models for Fixed-Bed column studies

2.18.1 Introduction

Since the inception of the adsorption process by Bois Reymond and Kayser, it has been the technique applied to remove the contaminants from liquid-solid using adsorbate (a substance from a bulk solution attached to a solid surface) and adsorbent (the solid substance clinging contaminant from a solution) mechanism (H. Patel, 2021)**.** The adsorbate-adsorbent interaction is depicted by various adsorption system techniques, namely Batch, continuous moving bed, continuous fixed bed (up-flow or down-flow), continuous fluidized bed and pulsed bed adsorption (Himanshu Patel, 2019)**.** According to(Dima et al., 2020; Mani & Bhandari, 2022)**,** these adsorption processes have merits and demerits; however, the continuous fixed bed system has a significant advantage since it caters small to large volumes and is mainly applicable in industrial effluent treatment. Also, a gift of these techniques over others mentioned by (Malik et al., 2018) is that fixed-bed columns give admittance of being operated in single, series, and parallel arrangements. The study stated that fixed bed column operations and efficient contaminant removal depend on parameters like flow rate and breakthrough curves (Malik et al., 2018).

2.18.2 Breakthrough curves

A breakthrough curve is a tool utilized to assess the performance of a fixed bed by graphically illustrating the pollutant effluent concentration versus the time profile in the column. This adsorption technique employs various phenomena such as film diffusion resistance, intra-particle diffusion (pore and surface diffusion), axial dispersion and equilibrium sorption of the sorbent (Dima et al., 2020; Malik et al., 2018). The compatibility of the breakthrough curve and fixed bed column is satisfactorily expressed by applying mass transfer zone (MTZ) or primary sorption zone (PSZ) techniques. MTZ or PSZ describes the effectiveness of the initial adsorption stage when the adsorbate enters the upper strata of the column; at that moment, most of the adsorbate is rapidly adsorbed due to less amount of adsorbate entering the adsorbent with most actives sites open for adsorption. Before the upper layers column saturation, the effluent concentration is zero; thus, the influent to effluent concentration ratio is zero C/C_0 is zero. However, as the MTZ becomes saturated, the adsorbate gradually fills the fixed bed with the pollutant to the column exiting point. Further adsorbate exiting the system, the concentration on the effluent changes per point on the fixed bed as C_1/C_0, C_2/C_0, C_3/C_0 and C_4/C_0. After a particular time, the adsorbent will be saturated, reaching its exhaustion point with no more adsorption; thus, the influent and effluent ratio C/C0 will be 1. At this point, the breakthrough point should exhibit the “S” shape (Himanshu Patel, 2019). The figure below illustrates the MTZ hierarchy.

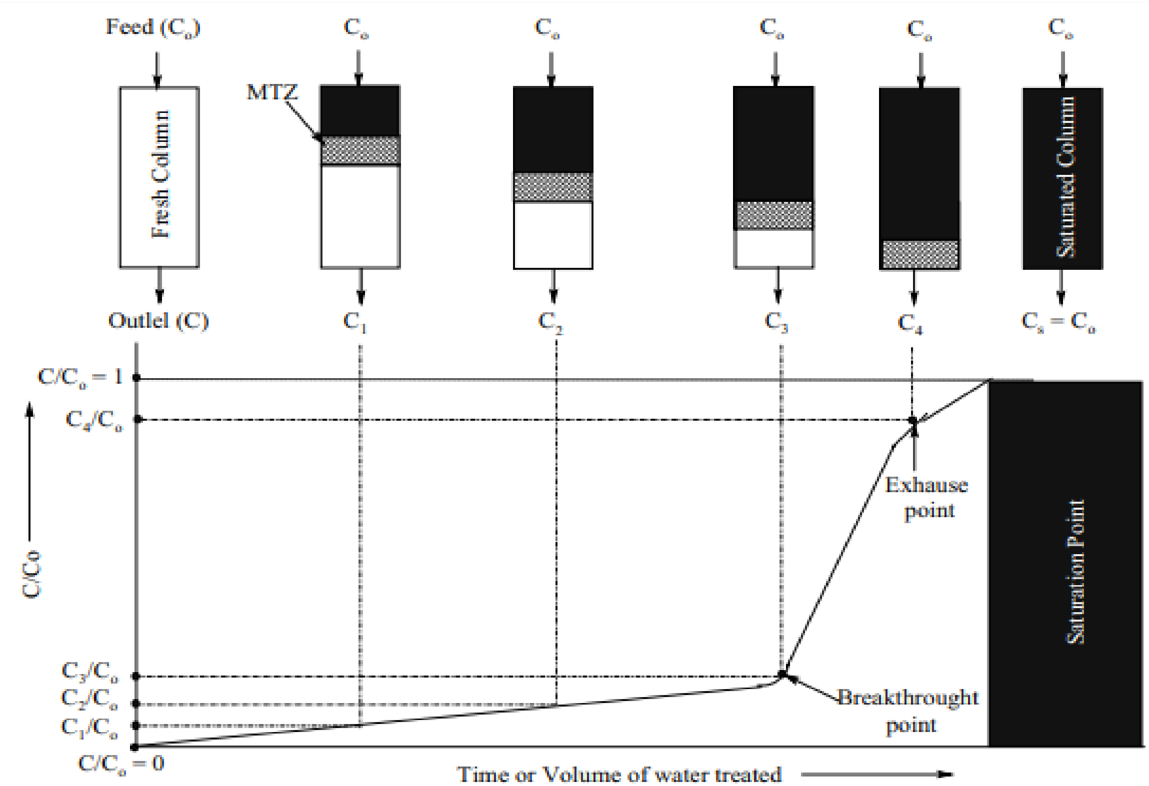

Figure 2-5:Representing breakthrough curve by movement of mass transfer zone (MTZ) (Himanshu Patel, 2019)

.

2.18.3 Mathematical Models for fixed bed columns

Fixed bed mathematical modelling is vital in determining the adsorption dynamic acquaintances such as column operation life, regeneration time and sorbent capacity (Mani & Bhandari, 2022). Multiple mathematical models were developed to investigate the appraisal efficiency and capabilities for a fixed bed column operation. However, the commonly deployed models are Thomas, bed depth service time (BDST), and the Adams and Bohart and Yoon-Nelson Model (Dima et al., 2020; Inglezakis & Fyrillas, 2017).

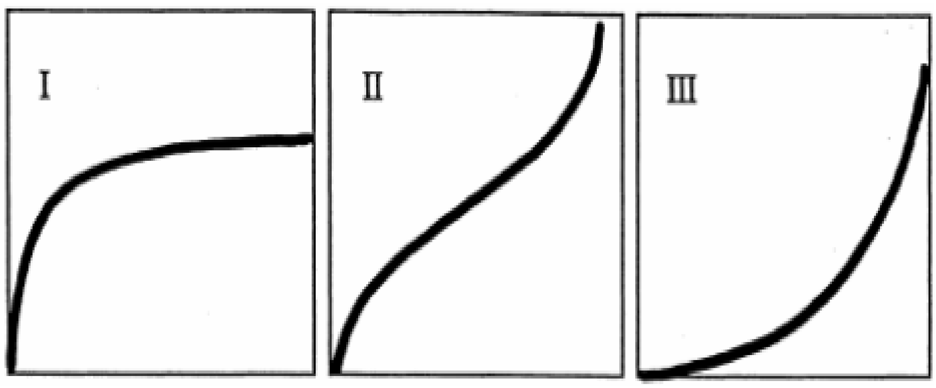

Figure 2-6: Represent classification description of shape by models (Inglezakis & Fyrillas, 2017)

Type (I) mean saturation point of the adsorption column by metal iron or pollutants, type (II) metal or pollutant adsorption through the pores and weak van der Waals forces and Type (III) initial stage adsorbent has high adsorption sites, including electrostatic bonding between adsorbent – adsorbate (Inglezakis& Fyrillas, 2017).

2.18.4Thomas model

This model's originality was developed to describe a liquid phase ion exchange in a fixed bed column (Apiratikul & Chu, 2021). The proposition of Thomas model assumptions is said to follow adsorption-desorption with no axial dispersion like Langmuir isotherm. This model also depicts the early stage of the adsorption process, where the adsorption forces are more active (Malik et al., 2018). The modelling equation for the sizing of fixed bed reads:

Equation 2-20: Thomas's equation

$$\frac{C}{C_0} = \frac{1}{1 + exp\left(\frac{K_{TH}\, q_{eq} m}{Q} - K_{TH} C_0 t\right)}$$

The linear form of this model is:

Equation 2- 21: Linearized Thomas equation

$$ln\left(\frac{C_t}{C_0} - 1\right) = \left(\frac{K_{TH} q_{eq} m}{Q} - K_{TH} C_0 t\right)$$

Where C0 and Ct are initial and final pollutant concentrations (mg L^{-1}), KTH is the Thomas rate constant (mLmin^{-1}mg^{-1}), qeq the theoretical equilibrium pollutant adsorbed per gram of the adsorbent (mg g^{-1}), m the amount of the adsorbent in the column (g), and Q the flow rate of the bulk solution through the column (mLmin^{-1}). KT and q can be determined from a plot of ln(Ct/C0–1) versus t.

2.18.5 Adams and Bohart Model

According to (Apiratikul& Chu, 2021), the initial development of this model was for gas phase adsorption; however, its reparameterization constituted it to be applied as a design tool for other liquid phase substances for sizing the fixed bed column based on breakthrough data from the pilot test. Adams-Bohart model is deployed to illustrate the relationship between concentration ratios (C/C_0) versus time in the fixed bed continuous system. It is also used on the assumption of the initial stage of the breakthrough curve. The model also stresses that the adsorption rate is more dependent on the exposed & available sides of the adsorbent and adsorbate concentration (Apiratikul & Chu, 2021; Himanshu Patel, 2019)**.** The model is expressed as follows: The model is described as follows:

Equation 2-22: Adam and Bohart's equation

$$\frac{C}{C_0} = \frac{1}{1 + exp\left(\frac{K_{AB} N_0 L}{v} - K_{AB} C_0 t\right)}$$

The linearized version is as follows:

Equation 2- 23: Linearized Adam equation

$$ln\left(\frac{C_t}{C_0}\right) = \frac{K_{AB} C_0 t - K_{AB} N_0 L}{v}$$

C_0 and C_t are the feed concentration and the effluent concentration-time t (mg L^{-1}), KAB the Adams-Bohart rate constant (L $min^{-1}mg^{-1}$), t the time (min), v the linear velocity (cm min^{-1}), L the bed depth of the fixed packed bed column (cm), and N0 the maximum adsorption capacity (mg g^{-1}). The values of KAB and N0 were determined from the slope and intercept of the linear plot of $ln(C_t/C_0)$ against time t

2.18.6 Yoon-Nelson Model

The model is based on the assumption that the probable rate of decrease in the adsorption of each adsorbate is proportional to the probability of the adsorbate adsorption and the adsorbate breakthrough on the adsorbent (Apiratikul & Chu, 2021; Malik et al., 2018)The model equation is expressed below:

Equation 2-24: Yoon-Nelson equation

$$\frac{C}{C_0} = \frac{1}{1 + exp(K_{YN}\tau - K_{YN}t)}$$

The linear form of the model can be written as:

Equation 2-25: Yoon Nelson Linear equation

$$n\left(\frac{C_t}{C_0 - C_t}\right) = K_{YN}t - K_{YN}\tau$$

K_{YN} is the rate constant (min–1) and τ the time required for 50 % adsorbate breakthrough (min). The parameter value K_{YN} and τ can be determined from the linear plot of ln ($C_t/C_0–C_t$) against t.

2.19 FTIR Spectroscopy material analysis

“Fourier transform infrared” is abbreviated as FTIR spectroscopy. It’s applied to identify various functional groups in a sample as organic or inorganic material. It is deemed the universal form of infrared spectroscopy since its sample’s surface species determination accommodates species in complex mixtures and the geometrical structures of the isomers, not excluding the polymer's molecular orientation and solutions (Kumari et al., 2020; Roman, 2021b)**.** The versatility of FTIR analysis has escalated its application to spread analytical situations as it is utilized in forensic science and material science; its usage attraction is fuelled by the accuracy and the sensitiveness of its MCT small element detectors that are mainly found in the microscopes (Rintoul et al., 1998)**.**

The review articles published by (Rintoul et al., 1998) have outlined the versatile usage of FTIR for functional group determination, which includes: Mineral composition of Bauxitic Pistol, an ore found mainly in Australia FTIR was applied to determine the composition that made this mineral shiny and radiant like a diamond; The determination of chemometric in human hair; To assess the degradation of polymer insulator.

2.19.1 Analyzing the FTIR

In brief, The IR spectrum is separated into three compartments wavelength regions: Far IR Spectrum (<400cm-1), mid-IR spectrum (400-4000cm-1), and near-IR spectrum (400-13000cm-1); however, this experiment explores the midsection of the spectrum since it is the widely used area in the analysis of the sample (Kumari et al., 2020; Nandiyanto et al., 2019)**.**

Mid Compartments division is divided into:

- o 2500-4000cm-1 represents a single bond region
- o 2000-2500cm-1 represents a triple bond region
- o 1500-2000cm-1 represents a double bond region
- o 500-1500cm-1 represents the fingerprint region

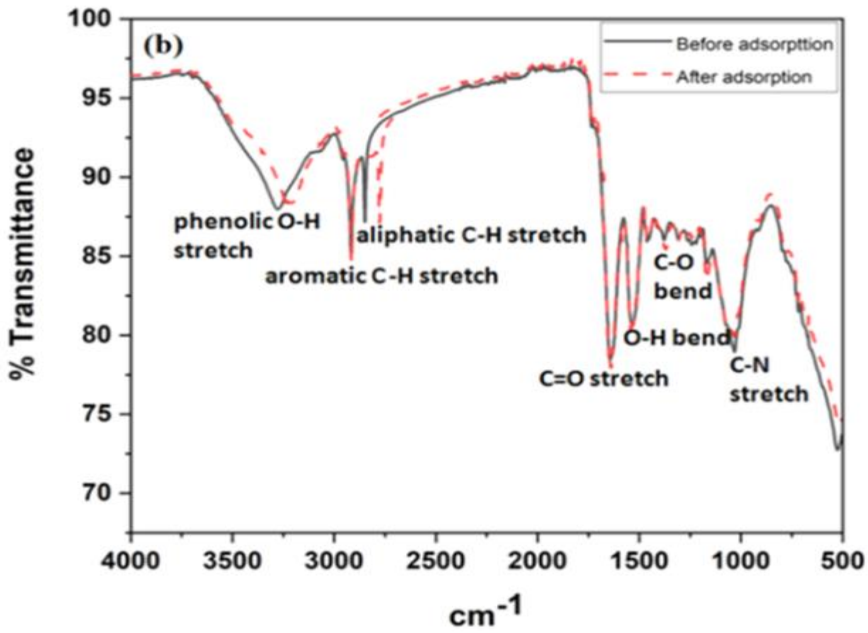

Figure 2-7: Mid-IR Spectrum Region representation (Kumari et al., 2020)

Table 2-3: Functional group and its quantified frequencies (Nandiyanto et al., 2019)

Range (cm-1)	Relative Intensity	Relative Intensity	Species
3700 - 3250	s	-OH	Alcohols, phenols
3520 - 3320	m-s	-NH2	Primary/aromatic amines, amides
3360 - 3340	m	-NH2	Primary amides
3320 - 3250	m	-OH	Oximes
3300 - 3250	m-s	≡CH	Acetylenes
3300 - 3280	s	-NH	Secondary amides
3200 - 3180	s	=-NH2	Primary amides
3100 - 2400	vbr	-OH	Carboxylic acids
3100 - 3000	m	=CH	Aromatic, unsaturated
2990 - 2850	m-s	-CH3, -CH2	Aliphatics
2750 - 2650	w-m	=-CHO	Aldehydes
2285 - 2250	s	-N=C=O	Isocyanates
2260 - 2200	m-s	-C≡N	Nitriles
1870 - 1790	vs	-C=O	Anhydrides

1780 - 1760	s	-C=O	Lactones
1750 - 1740	vs	-C=O	Esters
1740 -1720	s	-C=O	Aldehydes
1720 - 1700	s	-C=O	Ketones
1710 - 1690	s	-C=O	Carboxylic acids
1670 - 1650	vs	-C=O	Primary amides
1550 - 1490	s	-NO2	Aromatic nitro
1400 - 1310	s	-COO-	Carboxylic acids
1000 - 950	s	=-CH=CH2	Vinyl
980 - 960	vs	-CH=CH-	Trans alkenes
950 - 900	vs	-CH=CH2	Vinyl

2.19.2 FTIR sample testing principle

The mapping of surfaces using FTIR is increasingly becoming common. It is achieved by placing a sample on the diamond-shaped glass and applying pressure using FTIR spectroscopy's grinding/ pressing arm. The sample should be flat and horizontal, or the results will be inaccurate. Alternatively, the MCT focal-plane array detectors are used, which determine the images of the spectroscopy (Rintoul et al., 1998).

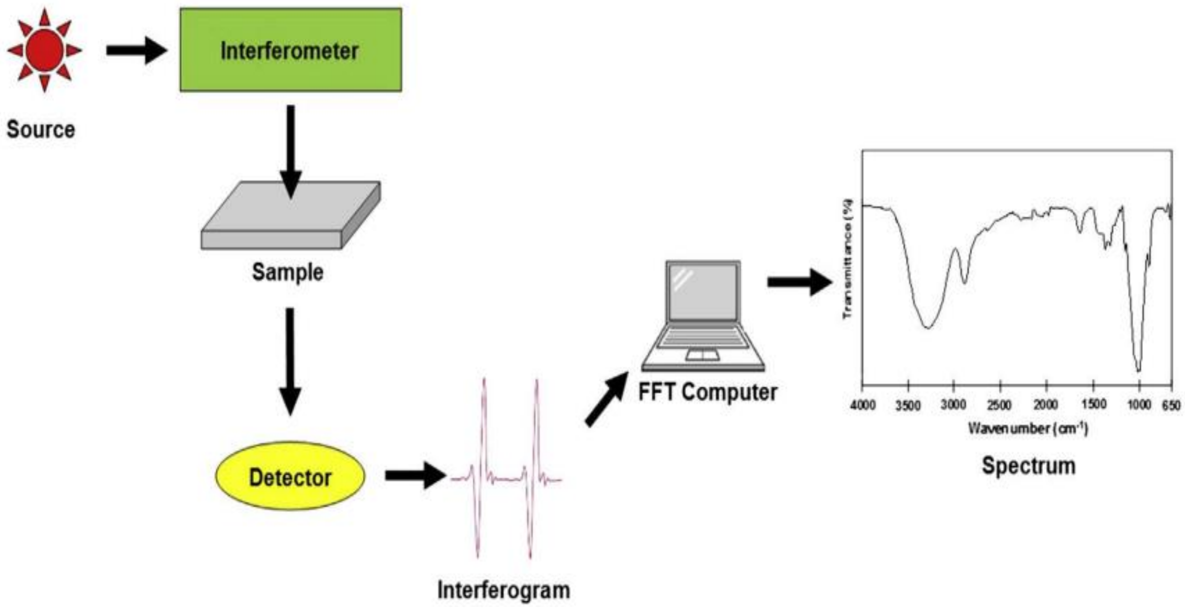

Figure 2-8: Figure illustrates the primary mechanism of FTIR testing (Roman, 2021b)

The sensitiveness and preciseness of the FTIR made it the preferred method of infrared spectroscopy, with the advantage of being rapid compared to older techniques. Its testing mechanism passes the radiation through the sample where the adsorbed radiation is neglected, and the radiation that passes through the sample is recorded. Since molecules consist of various spectra, their spectra are utilized to differentiate between them (Nandiyanto et al., 2019; Roman, 2021a).

As stipulated in the figure above, the chronological method followed by the FTIR spectrometer shows that the infrared source is the interferometer, which is speedy and the Fourier transform. The waves are separated, and the frequency is sent back based on time by the Fourier transform mathematical function. After that, the output of an interferometer is an interferogram graph; however, this graph cannot be used to identify the functional groups of the samples.

Then follows the conversion of the interferogram by Fourier transform to the chart that can be used for analyzing the sample surface functional groups (Nandiyanto et al., 2019; Rintoul et al., 1998; Roman, 2021a).

The determination of functional groups through wavelengths resurrects from the absorption of a specific wavelength that selectively matches a molecule covalent bond, in which the vibrational energy is converted to a bond. The vibration is either stretching or bending, depending on the atoms in the bond induced by infrared radiation. Pattern transmittance differs for every molecule because the functional groups absorb different frequencies. On the FTIR graph, the X-Axis represent the Wavelength, which is the molecular bond's vibration energy, and the Y-Axis is the Transmittance (Yıldırım & Bayrak, 2021).

2.20 Design of Experiment

2.20.1 Introduction

Design of Experiments (DOE) is the mathematical tool employed for conducting and executing experiments to analyse and interpret data obtained from the experimental runs by determining the effects of the variables. It is applied as a portion of the statistical method that is used for performing scientific studies of a product, system or process where the input variable (independent variable) (X) is manipulated to evaluate its effect on the measured response (dependent variable) (Y). Since its inception more than two decades ago, it has prevailed as a tool that traditionally improves product quality and reliability in the scientific world.DOE fundamentals analyse data collected from an experiment by giving the magnitude and direction of the specific measured response from the effects of experimental variables. This method is not only applicable in engineering. It has been used in the food industry, pharmaceutical, marketing and hospitals, and it has been improved over the years by introducing Response Surface Methodology (RSM) to study the input factor and the output factor relationship of any process (Durakovic, 2017; Roman, 2021a)

2.20.2 One Factor Design (OFAT)

OFAT is a single-factor experiment; its approach is to change one variable simultaneously, keeping others constant and investigating the process effects. This optimization method can also be applied to either quantitative factor levels (e.g. flow rate, temperature, concentration etc.) or qualitative factors (materials like sand, glass medium etc.) (Krishnaiah & Shahabudeen, 2012)**.** The optimization technique of OFAT is when the level changes in a factor and generates a change in response, with no interactional effect on other components. Since OFAT has a limitation of not being able to simultaneously involve varying multiple variables for the detection of main effect and the interaction of the response, it gains poor ratings compared to DOE (Dangat et al., 2021; Roman, 2021b).

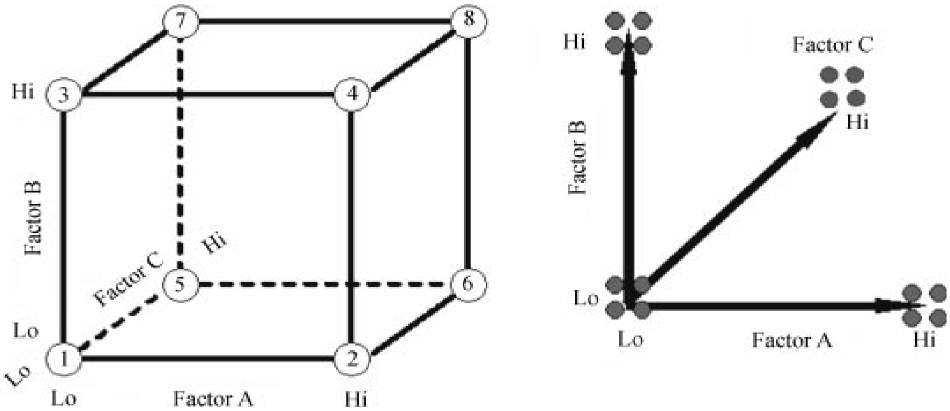

Figure 2-9: Comparison of three factors and one factor at a time (Roman, 2021b)

Figure 2-9 illustrate the comparison between three-factor two-level designs and a one-factor-at-a-time. The less experimental run is notable on the two-level factorial as compared to 16 runs of the one-factor-at-time factorial design; the factorial design carries an advantage over the OFAT design since the variable interaction can be easily noticeable with the measured response (Roman, 2021b).

2.20.3 Factorial design

Factorial design is the method involved in experimental designs; it has a huge footprint in the scientific sphere for conducting experiments. It consists of input variables known as factors, this predetermined matrix of factors is used to alter process parameters simultaneously and deliberately (Dangat et al., 2021; Durakovic, 2017). The factorial design is eminent from a mixed design by its ability to change each aspect separately. This design has two methods under it, named full and fractional factorial designs. According to (Krishnaiah &Shahabudeen, 2012), the widely used methodologies in manufacturing companies are full and fractional designs at 2-levels and 3-levels. The main limitation of full factorial designs is that the size of the experiment is a function of the number of factors to be considered and studied for the investigation. The rule of thumb, therefore, is to use a full factorial design when the number of factors or process parameters is less than or equal to 4. When factors exceed 4, one may look into fractional factorial designs (Antoy, 2014)**.**

2.20.4 Response surface methodology (RSM)

In a nutshell, experimentation is the investigation studied to determine the relationship between the input variable and the response to any process or system output. The RSM method follows a similar technique; however, it’s more specific since the RSM's purpose is to optimize by maximizing the output variable (response) or to understand the system. This response method can be deployed for quantitative parameters to study the relationship. Suppose the relationship to be assessed is to determine the levels of flow rate ($X1$) and time ($X2$) that maximize the yield (Y) of a process (Krishnaiah &Shahabudeen, 2012). RSM consists of two experimental design:
Central Composite Design (CDD) and Box-Behnken Design.

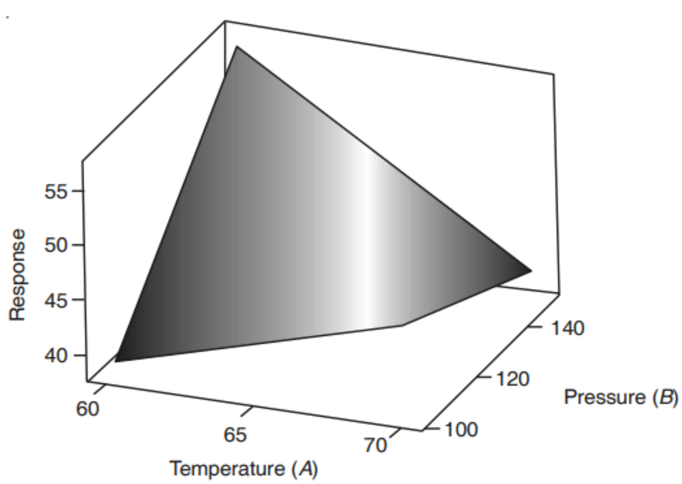

Figure 2-10: Example of response surface (Antoy, 2014)

2.20.4 Central composite Design

The CCD needs the specification of two parameters before implementation; this method design explores the relationship between the response and the input variable. It's also deemed capable of determining an optimum level for the factorial experiment of a given response (Roman, 2021a).

In selecting a CCD, the following three issues are to be addressed:

1. Choosing the factorial portion of the design
2. Number of centre points
3. Determining the α value for the axial point(Antoy, 2014)

2.20.5 Box Behnken Design

Box and Behnken were developed in 1960 as three-level second-order response surface designs. For the development of this design the two-level factorial designs were implicated. The design is formulated as illustrated below.

Block	*Treatments*		
	1	2	3
1	X	X	
2	X		X
3		X	X

Figure 2-11: Box Behnken example (Krishnaiah & Shahabudeen, 2012)

A, B, and C are regarded as three experimental factors; the main advantage of this design is that each factor requires only three levels. In addition, this design is entirely rotatable, so all its equidistant sites from the design centre will display the same prediction variance (Roman, 2021b)..

2.20.6 Evaluation of design models

Predicted vs actual value plot

Figure 2-12: Predicted vs actual this plot evaluates the model's effectiveness. This is done by observing how close the data points are to the straight line the closer the points are, the better the model (Antony, 2014)

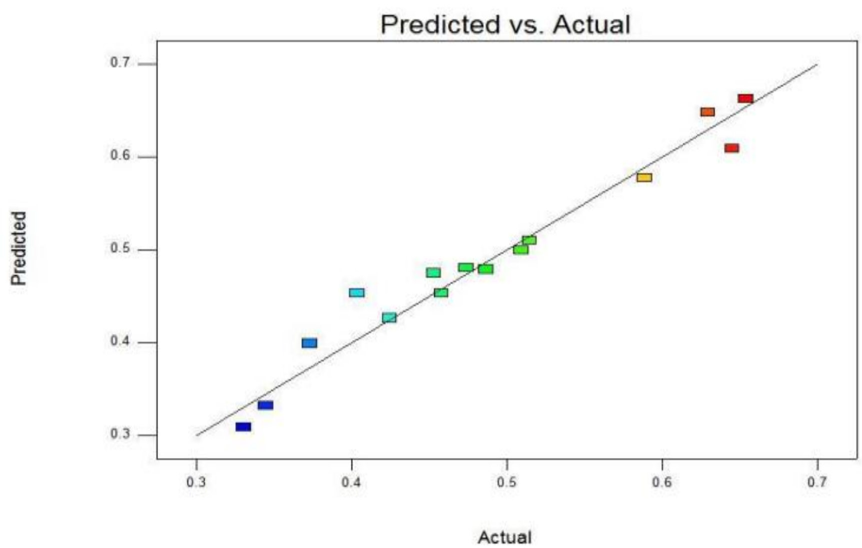

Figure 2-12: Predicted Vs Actual

Residual vs predicted value plot

A plot of residuals vs predicted is illustrated in the figure below. The evaluation of this model is by observing the scatted data point around the line, the model to be feasible the data point should have no specific shape for this model to be valid as shown below (Roman, 2021a).

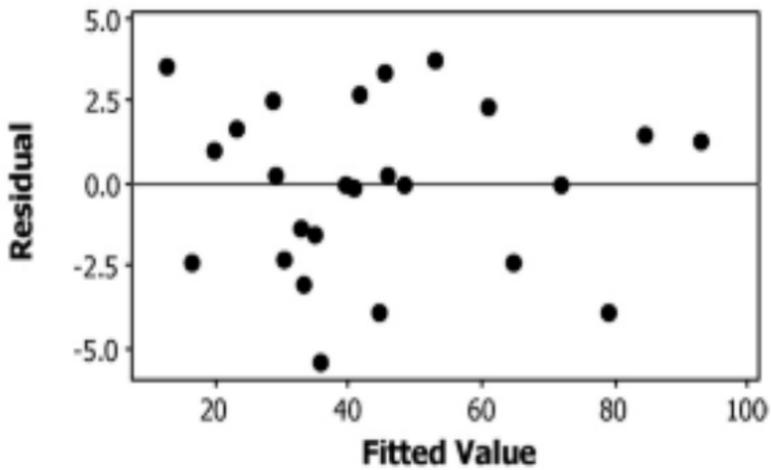

Figure 2-13: Residual vs Predicted

Normal probabilities vs residual

It can be seen in the Figure illustrating that all the points on the normal plot come close to forming a straight line. This implies that the data are fairly normal (Krishnaiah &Shahabudeen, 2012).

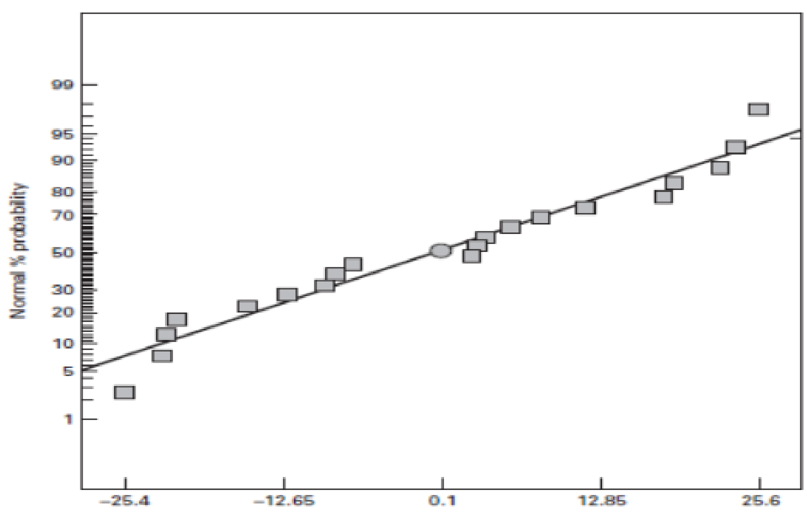

Figure 2-14: Normal probability vs residual

3D and contour plot

In 3D and Contour plots, the interaction between the variable is noticeable, and also the visibility of maximum response is notable (Roman, 2021b)

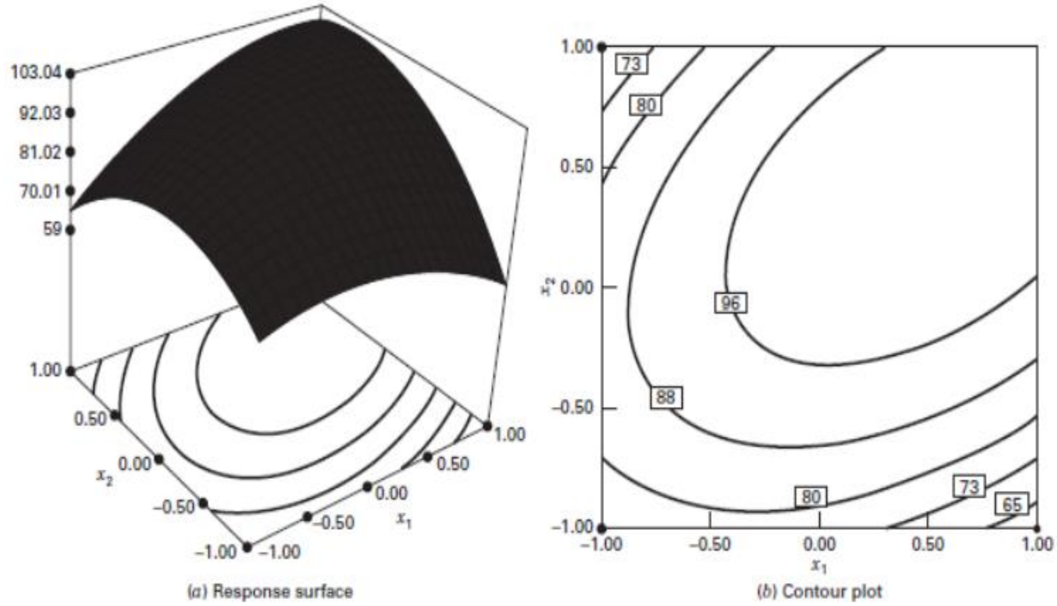

Figure 2-15: Response surface and contour plot

CHAPTER 3

Methodology

CHAPTER 3: Methodology

3. Methodology

Introduction

This section details the use of equipment and materials as well as experimental conditions and procedures to be followed during the investigated experimental runs. A description of instruments is also included.

3.1 Research Design

This research followed an experimental quantitative approach. The study comprises two parts, which entail the application of chemical oxidation in groundwater for iron and manganese and, secondly, the evaluation of various mediums packed in a single column for the removal of iron and manganese.

3.2 Groundwater Collection

Iron and manganese groundwater samples were collected on-site in the City of Cape Town (CoCT), Western Cape. Borehole water was pumped from the ground using a submersible pump. The water was purged for 1 hour to clear it from any settle-abilities to recharge the borehole with fresh groundwater. The groundwater was collected in two batches to be stored in 100 litres, tightly sealed to keep the water composition uniform and prevent any contact of atmospheric oxygen with water, which would have caused iron and manganese oxidation for the entire experimental runs. This water was transported to a student's working place, where the batch experiment was carried out.
The water used for this experiment was original feed, not synthetic. This borehole selection was based on the initial concentration of iron (2.1 mg/l) and manganese (2.7 mg/l) obtained while searching for the source for this experiment. The concentration of these metals became the determining factor for selecting this groundwater since iron and manganese concentrations were above the SANS 241 drinking water standard.

3.3 Groundwater treatment process

3.3.1 Experimental treatment process

The conditions investigated in this experiment are in Table 3-1 below.

Table 3.1: Experimental Conditions

Experimental Conditions		
pH	Flow rate (l/min)	Contact Time (min)
6,5	0,174	10
7,5	0,262	30
8,5	0,523	60

Groundwater treatment aims to reduce iron and manganese from high concentrations to acceptable standards for human use. This study removed these metals by combining chemical oxidation and the tri-medium fixed-packed bed system. The variation conditions include three flow rates, three pH variations, and three contact times to determine the optimum conditions for removing the contaminants in question, as Table 3-1 above stipulated. The conditions selected were 0.174l/min, 0.262l/min & 0.562l/ min and 60 min, 50min, 40min, 30min, 20min & 10 min contact time at pH of 6.5, 7.5 & 8.5. The manual valves controlled the input and output flow rates; samples were collected on the outlet to be analyzed. Figure 3-1 below shows the schematic process flow diagram for removing iron and manganese in the laboratory scale where the experiment was performed. Chemical oxidation employed in this study was used to enhance the removal of iron and manganese by converting it to an insoluble state to be filtered by a tri-medium system.

3.4 Process description

Feed water: Feed water was contained in a 100l tank, pumped by a 24V pump through a 6mm diameter pipe. Then sodium hypochlorite as a pH stabilizer was gravity fed with hydrogen peroxide, an oxidising agent. Water flow continues to a stationary packed bed medium vessel, where insoluble iron and manganese are removed by adsorbing on the media. The initial iron and manganese concentrated water can be seen in Photographs 3-1, while Photographs 3-2 show water after treatment.

3.5 Filtration medium

The preparation of the tri-medium packed bed system in this study consists of The Crushed Glass 2mm Filter Media, Polymex 2mm Ion Exchange Resin and Expanded Polystyrene Beads (EPS) 2mm, which were bought from Ultra Water, Purozone and Isowall Group companies respectively.

3.5.1 Physical properties of the medium

The characteristics of Crushed Glass Filter Media, Polymex Ion Exchange Resin and Expanded Polystyrene Beads (EPS) are shown in Tables 2-3, 2-4 and 2-5, respectively.

Table 3 -2: Crushed virgin glass media specification (S. D. Sheet, 2018)

Crushed Virgin Glass Filter Media	
Composition	Soda Lime Glass
Appearance	White Glass
pH range	9.6-10
Specific Gravity	2.5-2.6
Melting Point	>800ºC
Solubility in water	Insoluble
Decomposition temperature	2000ºC
Particle size	0.25-0.8mm
Contact time	30 minutes

Table 3 -3: Ion exchange resin specification (ROHM & HASS, 2008; P. D. Sheet & Properties, 2019)

Polymex C180 (Iron Exchange Resin) Specification	
Polymer structure	Styrene
Functional Group	HSO^{-}_3
Appearance	Light brown bead
Total Exchange	≥4.5mmol/g
Moisture Content	46-50%
Density	1.25-1.29g/ml
Shipping weight	0.77-0.87g/ml
Particle size	0.135-1.25mm
Effective Particle Size	0.4-0.6mm
Rate	≥90%
Operating temp, Maximum	120ºC
Contact time	30min

The ion exchange resin is quantified as polystyrene crossed linked with divinylbenzene and contains some sulphonic functional groups (By & Ahmed Mohamed Atta, 2007). Its application is mainly in removing total hardness. In this process, sodium ions in an ion exchange resin are exchanged by calcium (II) and magnesium (II), entering a water solution and being retained on the medium surface, whereas the solution gains sodium.

Table 3-4: Expanded polystyrene specification (Aidan, 2016)

Expanded Polystyrene Specifications	
Density	15kg/m3
Thermal Conductivity	0.04W/m.k
Compression strength	80kpa
Shear Strength	190kpa
Water absorption after 1 year	5% (fully submerged)
Minimum Temp (ºC)	-1,57
Maximum Temp(ºC)	110

3.5.2 Filtration Column Design

The 5.23Litre column consists of three compartments for various media of similar sizes, starting with expanded polystyrene beads on top occupying 1.74 litres of the column, followed by 2mm virgin crushed glass with 2.3kg (1.74 litres), and the bottom has 2mm ion exchange resin of 2.2 kilograms (1.75 litres). A carbon fibre-reinforced plastic separated the medium with nine holes of 1mm each that permitted water to pass through. The filtration column can be seen in the below photograph 3-1.

Photograph 3.1: Filtration Column

3.5.3 Schematic representation of laboratory scale process

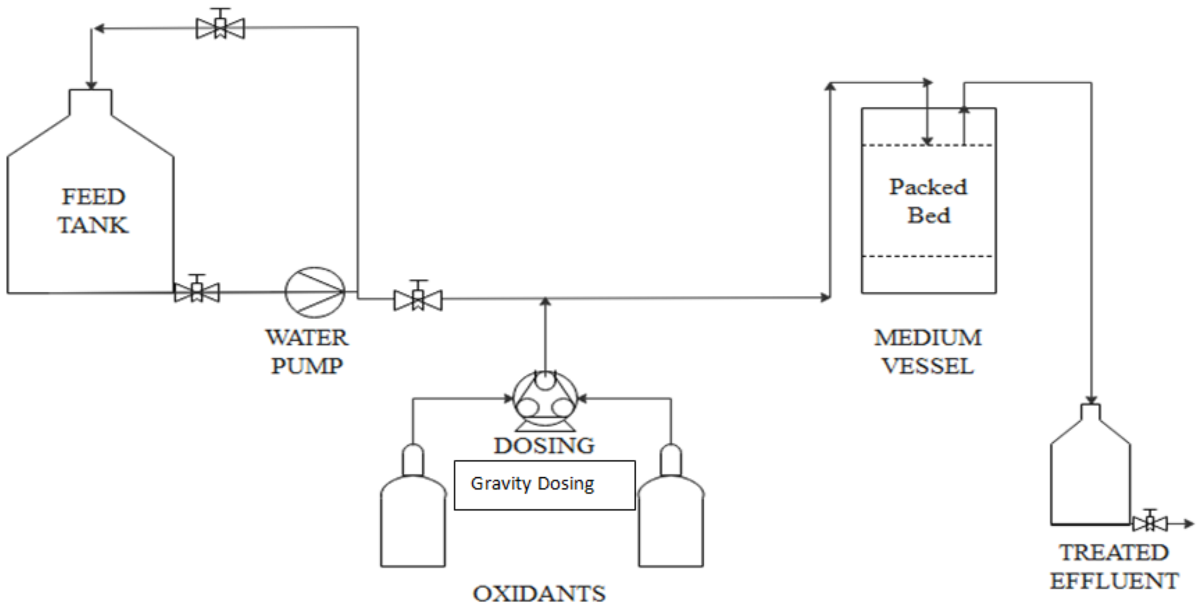

Figure 3:1Schematic filtration process

A  B 

Photograph3.2: Initial groundwater before treatment in A and after treatment B

3.6 Groundwater Analysis

3.6.1 HI97721C (Iron) and HI97709C (Manganese)

HI97721C photograph 3.3A and HI97709C photograph 3-3Bare type of auto diagnostic portable photometers capable of measuring iron and manganese in the range of 0.00-5.0 mg/l (ppm) concentration detection. These meters are a product of Hanna Instruments Inc, Woonsocket, Rhode Island, USA. In this project, groundwater was tested by these meters to detect the concentration of iron and manganese in the groundwater sample. Before testing, the Zero reading sample was utilized to calibrate the testing equipment for the iron and manganese content accuracy in the water. The HI97721C (Iron) has a reaction time of 3 minutes after the sample is inserted in a canvas for reaction time before the reading can be recorded, and the HI97709C (Manganese) has 1 minute 30 seconds reaction time. An ATC-pH meter handheld pen analyzed this water's pH to control the water's pH to the desired stabilizer dosage.

3.7 Equipment

3.7.1 Research Apparatus

The following apparatus was utilised to test iron and manganese in this experiment.

A.


B


Photograph3.3A: H197721C Iron testing and Photograph 3-3B H197709C Manganese High range testing meter,

ATC-pH hand-held pH meter to stabilize the water's pH content for oxidation of iron and manganese was purchased from Take a Lot.

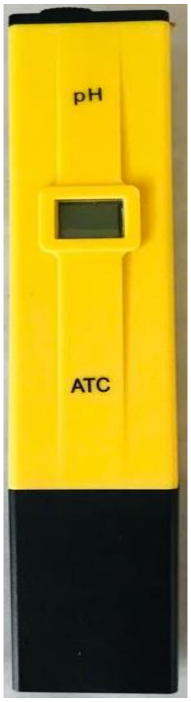

Photograph 3.4:pH meter

3.8 Design of Experiments

Design expert software was utilized to develop the runs performed in this experiment. The response surface Method was selected for this purpose, specifically the Box-Behnken design. The software applied was a 10.0 version from (Stat-Ease Inc., Minneapolis, USA) and generated 27 runs. Table 3-2 below presents the factorial range and levels.

Table 3. 5: Factorial Design Experiment

	Name	**Units**	**Low**	**Middle**	**High**
A	pH		6,5	7,5	8,5
B	Flow rate	l/min	0,174	0,262	0,523
C	Contact Time	min	10	30	60

The 27 random data runs can be seen in the below table. Experimental runs Table 3-6

Table 3.6: Experimental Runs of adsorption runs using design expert

	Factor 1	Factor 2	Response 3
Run	A:pH	B:Flow Rate	C:Contact Time
		l/min	min
1	8.5	0,523	10
2	6.5	0,523	10
3	8.5	0,523	60
4	8.5	0,174	60
5	8.5	0,174	10
6	6.5	0,262	10
7	7.5	0,262	30
8	7.5	0,262	60
9	7.5	0,523	30
10	8.5	0,262	30
11	6.5	0,174	60

12	8.5	0,262	10
13	7.5	0,523	60
14	7.5	0,523	10
15	6.5	0,262	30
16	8.5	0,174	30
17	7.5	0,174	30
18	6.5	0,174	30
19	7.5	0,262	10
20	6.5	0,523	60
21	6.5	0,174	10
22	6.5	0,262	60
23	7.5	0,174	10
24	7.5	0,174	60
25	8.5	0,262	60
26	6.5	0,523	30
27	8.5	0,523	30

3.8.2 Chemical Reagents and oxidation

Oxidation is the alteration of a metal ion from a dissolved state to an insoluble format using a chemical reaction (Naik, 2015). In this experiment, two chemicals were applied to enhance the conversion of soluble Fe (II) to insoluble Fe (III) and dissolved Mn (II) to undissolved Mn (IV) as a preliminary stage before the solution enters the filtration system. The chemicals used were Sodium Hypochlorite (NaOCl) 5% and Hydrogen Peroxide (H_2O_2) 10%, purchased from Protea Chemicals in Cape Town. Sodium Hypochlorite was incorporated to optimize the pH of the solution at 6.5, 7.5 and 8.5. Hydrogen Peroxide was used as an oxidizing agent measured by flow rate from 1.67 ml/min, 2.52 ml/min and 5.0 ml/min. These chemical conditions were applied in various solution flow rates containing Fe (II) and Mn (II) of 0.174 l/min, 0.262 l/min and 0.523 l/min, respectively. Collectively these parameters were the independent variables of this experiment.

It was also determined that the varying oxidation dosing rate of Hydrogen Peroxide on various solution flow rates of 0.174 l/min, 0.262 l/min & 0.523 l/min does not have a significant effect since the dosing rate factor between 1.67ml/min, 2.52ml/min and 5ml/min was found to be 0.95. See below sample calculation.

$$\text{oxidation dosing rate (ORD)} = \frac{\text{oxidation flow rate (l/min)}}{\text{oxidation flow rate } \left(\frac{\text{l}}{\text{min}}\right) + \text{solutionflow rate (l/min)}}$$

$$\text{ODR} = \frac{0.00167}{0.00167 + 0.174}$$

$$\text{ODR} = 0.95$$

3.9 Cleaning of Medium and System

The medium in the vessel was flushed with de-ionized or reverse osmosis water before the start-up and after the experimental run.

After every experimental run, the system was flushed with de-ionized or reverse osmosis water to remove the particles that might have settled during the experimental run.

3.10 Filtration medium Characterization

FTIR characterized the filtration medium used in the experiment to determine the functional groups associated with a specific media. The chemical and weak forces of the surface bonding on the glass medium were investigated by using FTIR spectroscopy. The wavelength was noticed, illustrating the bonds' strength on the graphs' peaks. The FTIR test was performed off-site at the Cape Peninsula University of Technology, in Bellville Campus.

3.11 Adsorption column testing methods

3.11.1 Adsorption isotherms

Four isotherms were applied to verify the affinity of a tri-medium system comprising glass media, polystyrene beads and ion exchange resin to remove Iron (Fe) and Manganese (Mn). The initial concentrations of the metal ions were 2.1 mg/l (Fe), and 2.7mg/l (Mn), the conditions of the experimental runs were 6.5, 7.5 and 8.5 pH, the flow rate of 0.174l/min, 0.262 l/min and 0.523 l/min and 10-60 minutes contact time. After the adsorption process, the data were fitted in Langmuir, Freundlich, Temkin and Dubinin-Radushkevich Isotherm to determine the suitable fit, in which the shape of an isotherm was used to provide the information for the best-fit model and the adsorption affinity of the adsorbate molecule.

CHAPTER 4

Results

&

Discussion

Chapter4: Results & Discussion

This chapter presents the results of removing Fe and Mn from groundwater using the packed bed tri-medium adsorption treatment process. The Fe and Mn levels before and after adsorption were used to evaluate how efficient the integrated approach was. All experimental runs were conducted in randomized order and were repeated twice.

4. FTIR Analysis

4.1 FTIR results for glass media

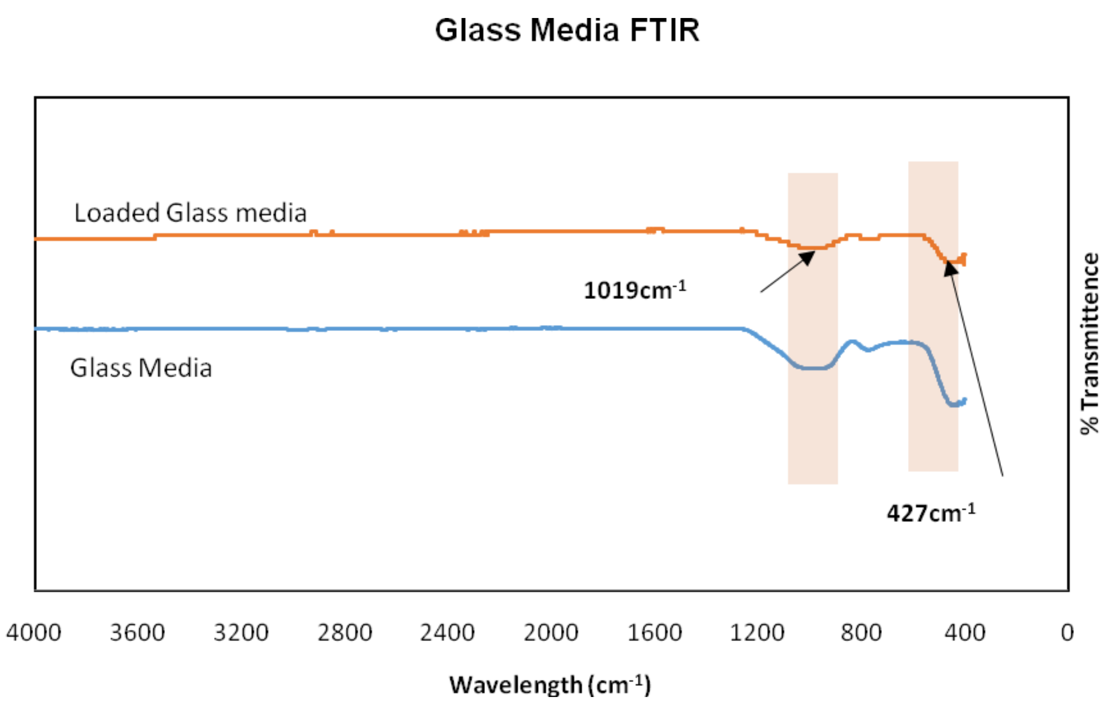

Figure 4:1FTIR Analysis of Glass Medium

The presence of the organic and inorganic functional groups on the glass media surface is shown in Figure 4:1. The FTIR spectrum of virgin glass medium consisted of a broad peak around 1200 cm^{-1} to 800 cm^{-1}, a peak at 800 cm^{-1} to 400cm^{-1} corresponding to common inorganic ions (phosphate and silicate ions), aliphatic chloro-compounds (C-Cl) stretching and aryl disulphide's (S-S) stretch respectively. The broad peak at 1019 cm^{-1} exhibits the silicate and phosphates negatively charged ions utilized when the glass media was activated in an incineration process to increase the negative charge on the spherical glass surface (Sheet, 2018). This charge enhanced the electrostatic force of attraction of iron Fe (III) and manganese Mn (III) to the glass surface, as in loaded glass media, the peak had reduced compared to unloaded glass. The bands assigned to (C-Cl) and (S-S) stretching at peak 427cm^{-1} are associated with weak electrostatic forces and a weak redox state on the surface of the glass at this wavelength (Ojovan & Lee, 2005).

4.2 FTIR results for polystyrene beads

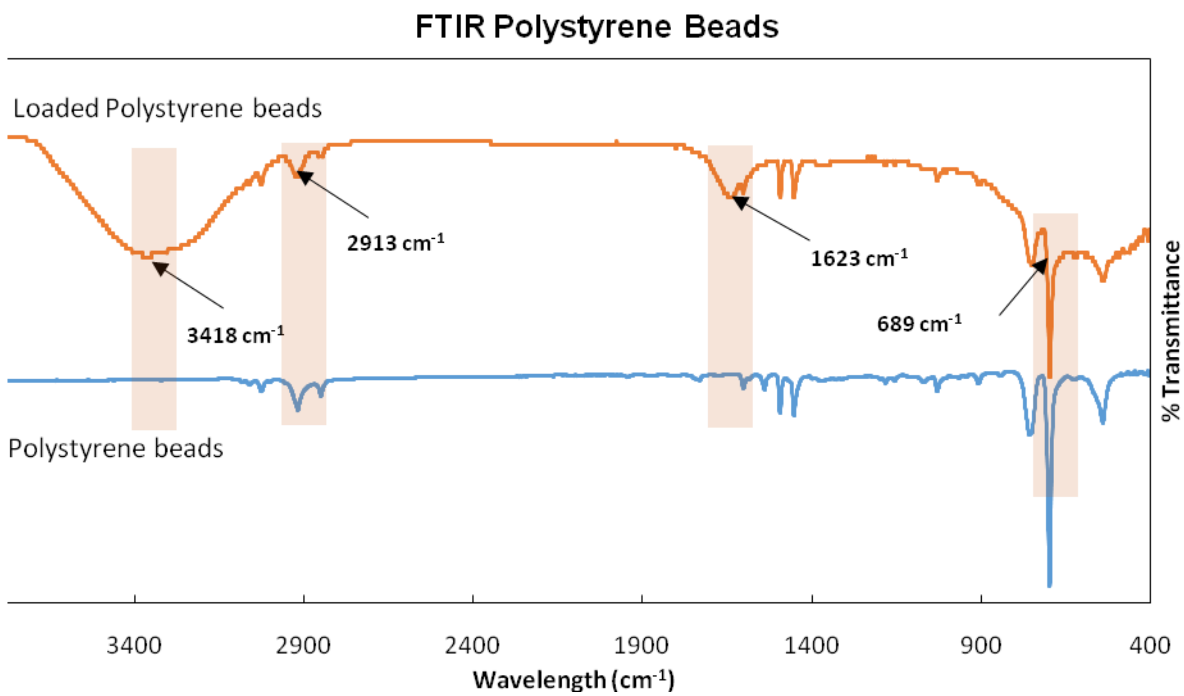

Figure 4.2 FTIR Polystyrene Beads Characteristics

Polystyrene beads are a readily available material, a petroleum by-product that can be infused in the water treatment (Osuagwu et al., 2018). Its main properties include electrostatic charge, which is regarded as a lightweight spherical bead with 98% air. The FTIR of polystyrene beads is notably presented in Figure 4.2; the unloaded polystyrene shows no broad peak between 2500 cm^{-1}- 4000cm^{-1}, whereas the loaded inscribe broadly implies an increased electrostatic attraction charge of the medium when contacting the solution. However, it's not a strong attraction since the peak at 3418 cm^{-1}, defining the olefinic (alkenes) medial, cis- or – trans-C-H stretch existing in wavelength 2900 cm^{-1}- 3418 cm^{-1}, it still confirms less bond attraction between the molecules and the surface. The shallow peak 2872cm^{-1} in the 3390cm^{-1}- 2500cm^{-1} indicates bonded O-H stretch. The band at 1490cm^{-1}- 1410cm^{-1} attributes to carbonate ions, which might positively impact the adsorbate adsorption by increasing the alkalinity in the solution, which will proportionally contribute to the pH and enhance the oxidation and adsorption process (Flintsch, 2012). The sharp, high-intensity peaks in the 700cm^{-1}-600cm^{-1} indicate a strong bonded aliphatic Bromo compound C-Br, supported by other organo-halogens C-I, C-Cl on band 600cm^{-1}- 500cm^{-1}, the halogen is considered as oxidizing agents in water treatment due to their high electron affinity. In this instance, due to high electronegativity, they accelerate the oxidation and attraction of iron and manganese to an insoluble state.

4.3 FTIR Ion Exchange Characteristics

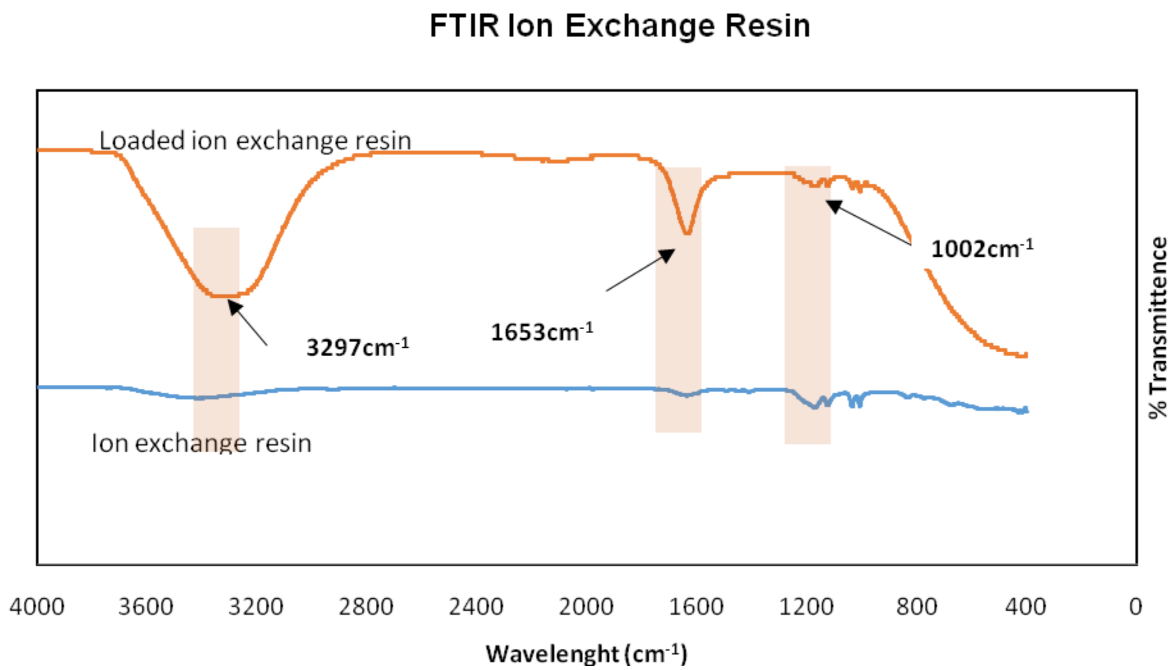

Figure 4.3FTIR analysis of ion Exchange Resin

The FTIR analysis in Figure 4.3 outlines this medium's functional groups and chemical bonds. The broad and intense peak observed at 3297cm^{-1} laments the O-H bond in the structure, which results from hydration water and indicates the presence of sulphonic groups in this medium (Lazar et al., 2014). The 1653cm^{-1} peak describes and confirms the C-C bond of the styrene ring. The bend between 1165cm^{-1} has presented the sulphonic group SO^{-3} and 1007cm$^{-1,}$ showing the stretching and asymmetric vibration. Ion exchange resin has the potential and capabilities to be utilized in removing iron and manganese; however, it needs to be paired with other mediums that will remove particles before reaching this medium to prevent fouling (Naik, 2015). The loaded ion exchange seemed to have more peaks than the unloaded due to it being reactivated by sodium hypochlorite used for pH stabilization since it increases its capability for ion exchange.

4.4 Iron and Manganese removal efficiencies

4.4.1 Introduction

The results in this section are in summarised subsections which include groundwater characteristics, preliminary treatment (oxidation stage), and Iron & Manganese removal efficiencies based on the effects of process variables such as pH, oxidation rate and the flow rate in 60 minutes time interval. This part of the report lucidly presents the data concisely.

4.4.2 Groundwater Characteristics

The groundwater used during this study was original feed to the system, and the specific parameters to be investigated were tested. Iron (Fe) and Manganese (Mn) values were analyzed to be much higher than what is required under the South African National Standards (SANS241) act of 2015 for the potential potable application. The characteristics of the raw groundwater and national drinking water standards are tabulated below, as seen in Table 4.1.

Table 4:1 Raw Groundwater characteristics

Parameters	**Unit**	**Tested value**	**SANS 241:2015**
Iron (Fe)	mg/l	2.1	<0.3
Manganese (Mn)	mg/l	2.7	<0.1
pH	-	6.5	≥5.5 or ≤ 9.5

In particular, for South African legislation, when iron and manganese concentrations in groundwater exceed the secondary standards, the water source is forbidden for drinking since the site is considered contaminated (SANS, 2015).

4.4.3 Chemical oxidation

Vries et al., 2017, discovered that oxidation by sodium hypochlorite complexifies the oxidation of Fe (II) by prolonging its oxidation contact time to two hours, and Robey, 2014 found that hydrogen peroxide complexes with Mn(II), while more favourable to Fe (II). However, a study conducted by Sarkar et al. (2018), discovered that the reaction between sodium hypochlorite and hydrogen peroxide generates an oxygen atom that enhances the oxidation of both Fe (II) and Mn (II) simultaneously, as shown by Equation 4-1. These findings are concurrent to this study results because the high removal of iron and manganese was noticed at the pH of 7.5 after the dosage of hypochlorite as a pH stabilizer, which reacted with hydrogen peroxide, an oxidizer used for this experiment.

Equation 4-1: Reaction of sodium hypochlorite and hydrogen peroxide

$$H_2O_2 + NaOCl \rightarrow O_2 + NaCl + H_2O$$

Sarkar et al. (2018) findings confirm that the generated oxygen atom plays a vital role in hydroxylation (conversion of soluble metal ion to insoluble) by attacking the Fe (II) and Mn (II), oxidizing them to Fe(III) and Mn (IV) for better adsorption on the adsorbent surface..

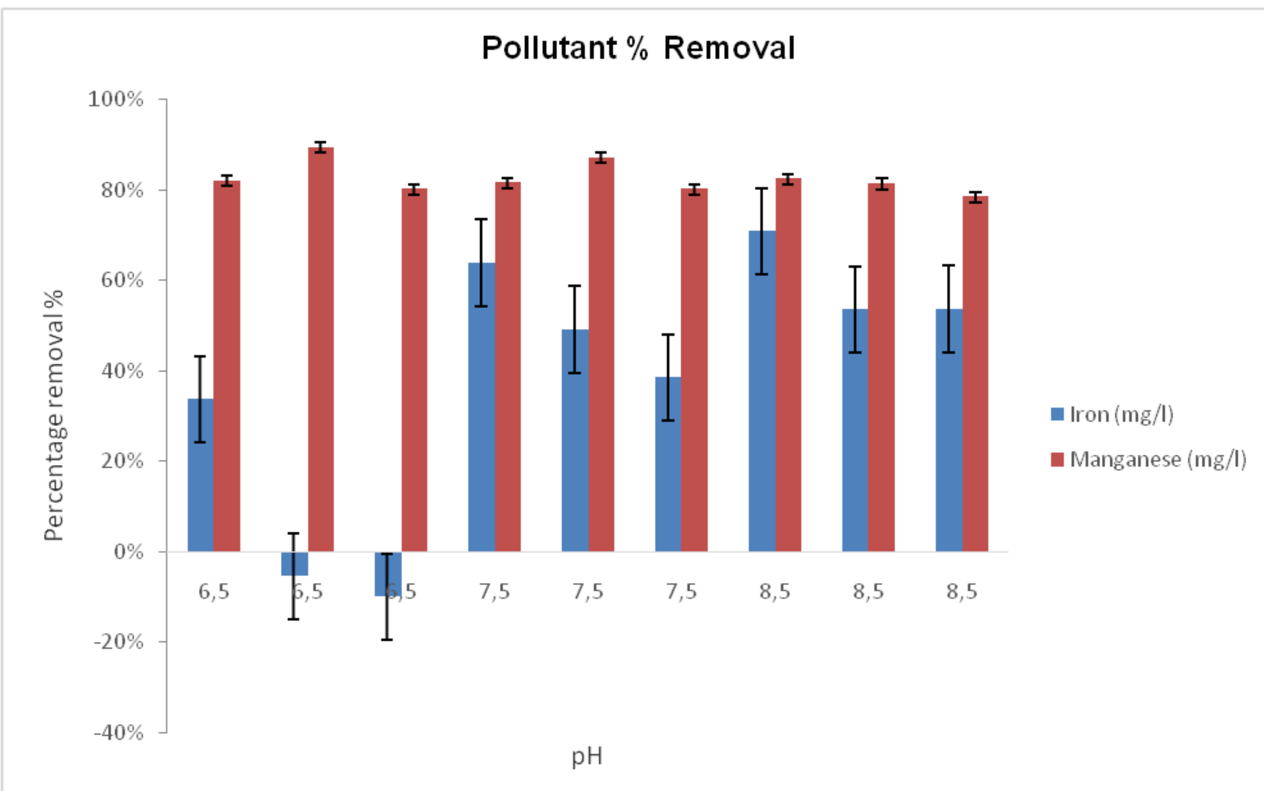

Figure 4.4 Average Fe and Mn removal at various pH

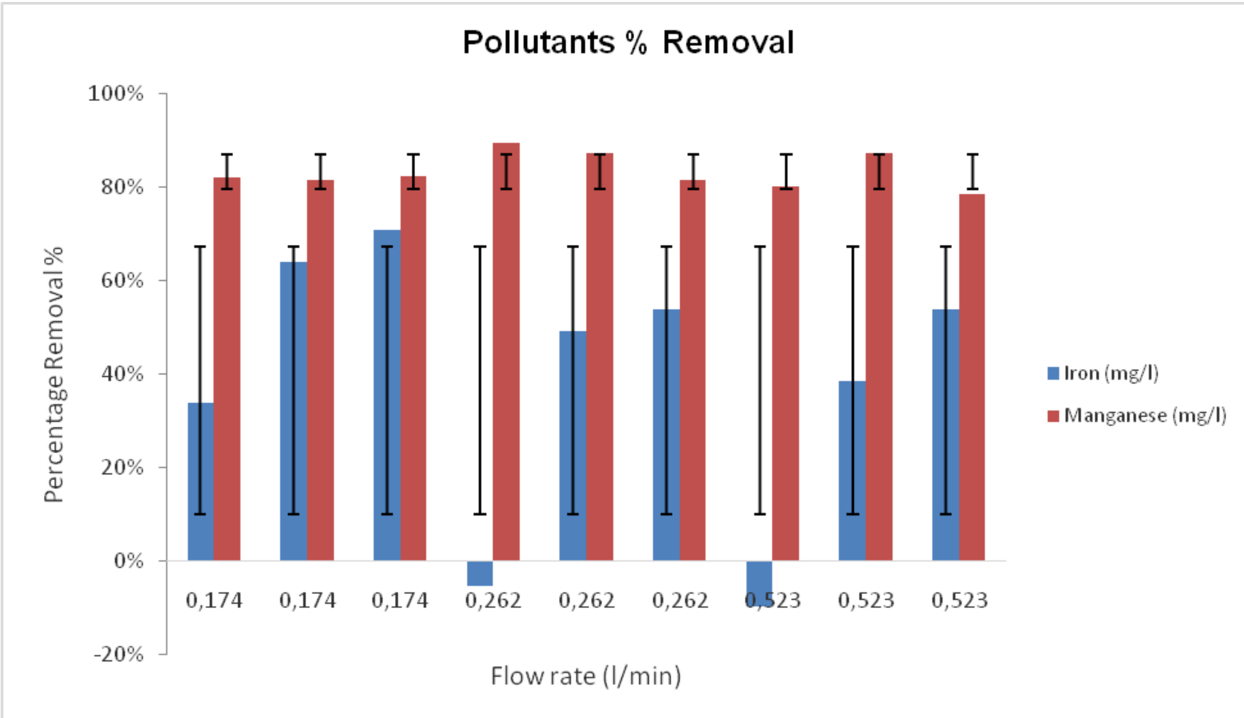

Figure 4.5 Average Fe and Mn removal at various flow rates

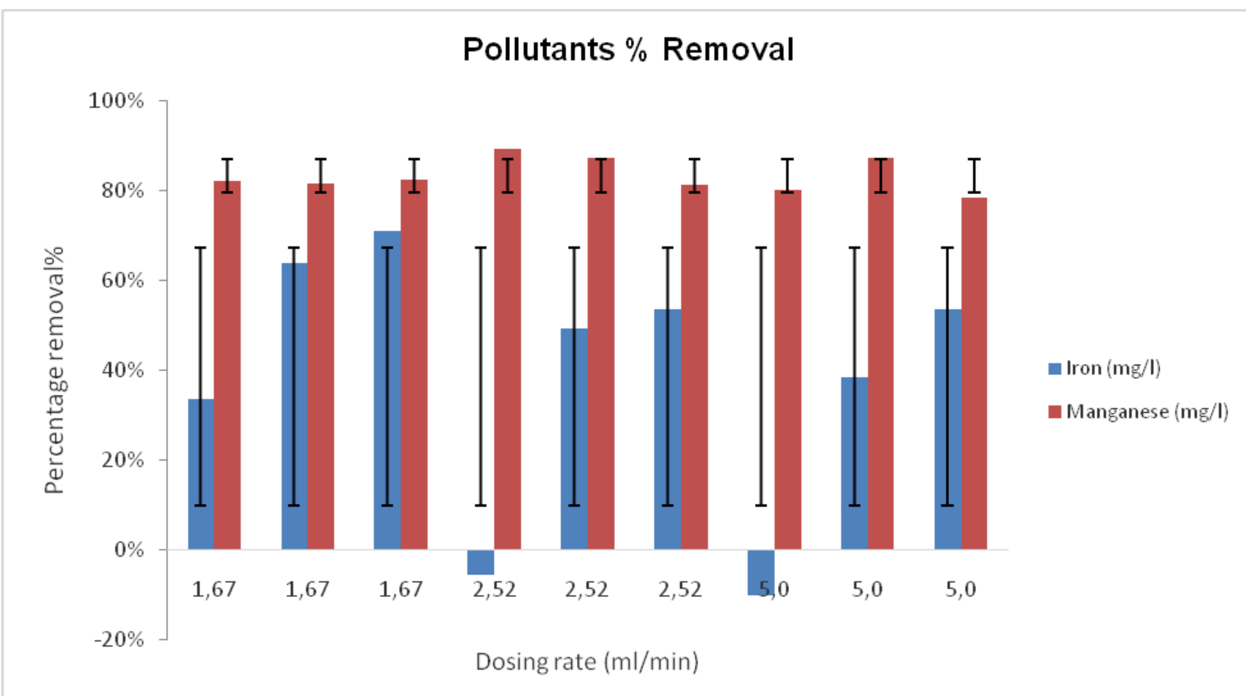

Figure 4.6 Average Fe and Mn removal at various dosing rates

4.4.5 Average removal of Iron Fe (II) by oxidation

Nalbantcilar & Pinarkara, 2015 through the study determined that groundwater iron compound appears as $FeCO_3$, FeS_2 & $FeTiO_3$. Such Fe (II) forms are in suspended solids in borehole water; however, any other format available should be in a complex structure that needs oxidation). This study did not focus on a specific state of iron in groundwater; it evaluated the removal of total iron found in groundwater. The application of oxidation was vital in converting Fe (II) to Fe (III) to be removed in a filtration system. According to (Camargo et al., n.d.), iron readily loses an ion to become acidic in low water pH, resulting in it being complex to be oxidized due to the force of repulsion between the acidic iron and the hydrogen activities in the water as Figure 4.4 shows that at pH 6.5, Fe (II) was not oxidized; instead, the removal percentage decreased to -5% & -10%;the negative removal results indicates that iron was in a dissolved state. Less removal was noticed in Figure 4.6 at dosing rate 2.52 ml/min and 5.0 ml/min, this is relatively due to the hydronium ions and Fe (II) ions which detriment the oxidation of this parameter at low pH and high oxidation rate.

The permissible Fe (II) content in drinking water is 0.3 mg/l, according to SANS241:2015. The amount above the water standard is deemed unsafe to drink (Division, 2011; Rivera, 2017). Consumption of high concentrations of this parameter might result in lung disease (Inglezakis & Fyrillas, 2017). Although oxygen and hydrogen peroxide is the most effective oxidizing agents for Fe (II), according to Sharma (2001), this experiment indicated poor results for low pH. These results concluded that this oxidizing agent is ineffective for iron at low pH, see figure 4.4. Other possibilities for inactive oxidation may be due to the oxidation percentage strength used was not sufficient enough to convert Fe (II) to Fe(III), the reaction time was insufficient for Fe(II) oxidation, and also it might be that the adsorption sites of the medium were saturated.

4.4.6 Manganese Mn (II) Oxidation

Manganese groundwater forms appear as $MnSO_4$, $MnCl_2$ and Mn_3O_4. The excellent performance of manganese removal from the water in this experiment was noticed as shown in figure 4.4-4.6. Based on the manganese groundwater compound structures reported by (Camargo et al., n.d.) that these Mn forms coat the mediums and increase the attraction of un-oxidized manganese, and this coating is reactivated by oxidizing agents such as chlorine and oxygen, which enhances the oxidation and removal of Mn (II). Although Sodium hypochlorite was used to optimize the system's pH, it positively contributed to Mn (II) oxidation to Mn (IV) by acting as a regenerator for manganese uptake onto the media. Sarkar et al. (2018) have discovered that modifying these medium surfaces by adsorbing manganese and being coated surface of the medium offers a negatively charged surface area, which enables more attraction of incoming Mn (II) to be adsorbed.

4.5 Iron Fe (II) and Manganese Mn (II) percentage removal

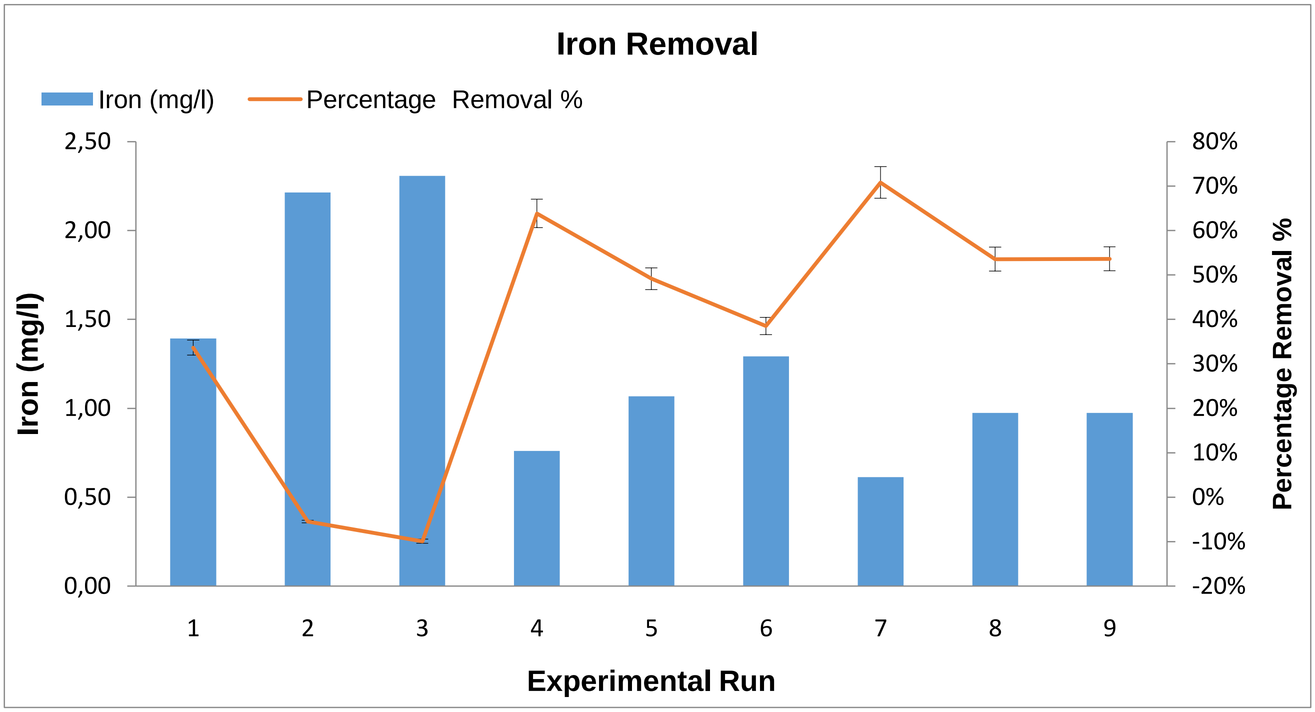

Figure 4.7 Adsorption average Fe (II) percentage removal

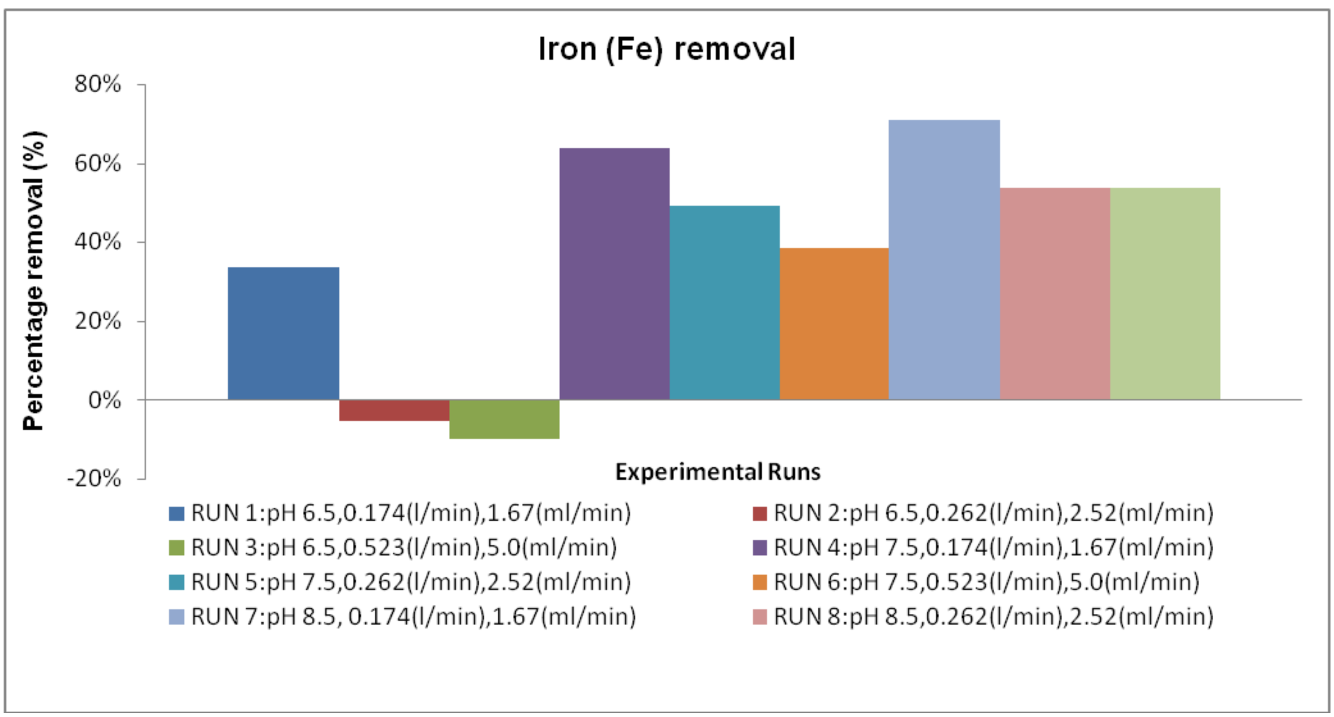

Figure 4.8 Iron Fe (II) removal after adsorption

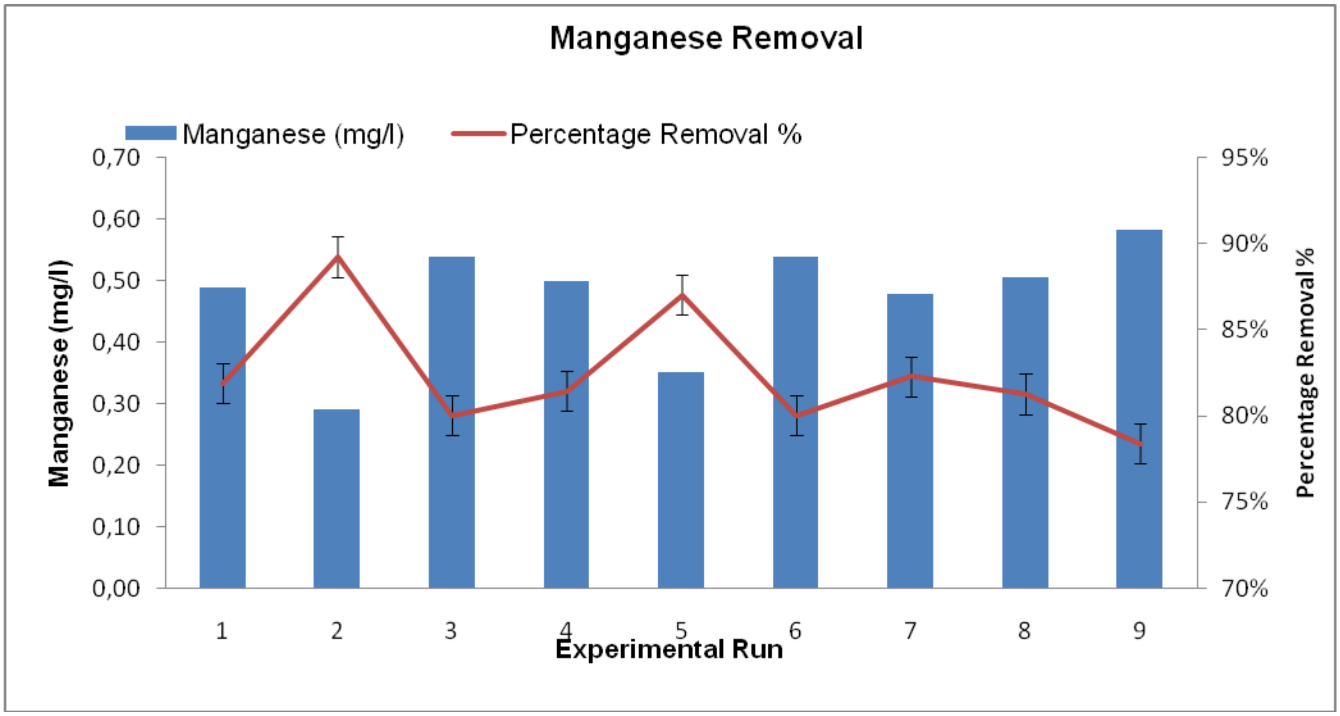

Figure 4.9 Adsorption average Mn (II) percentage removal

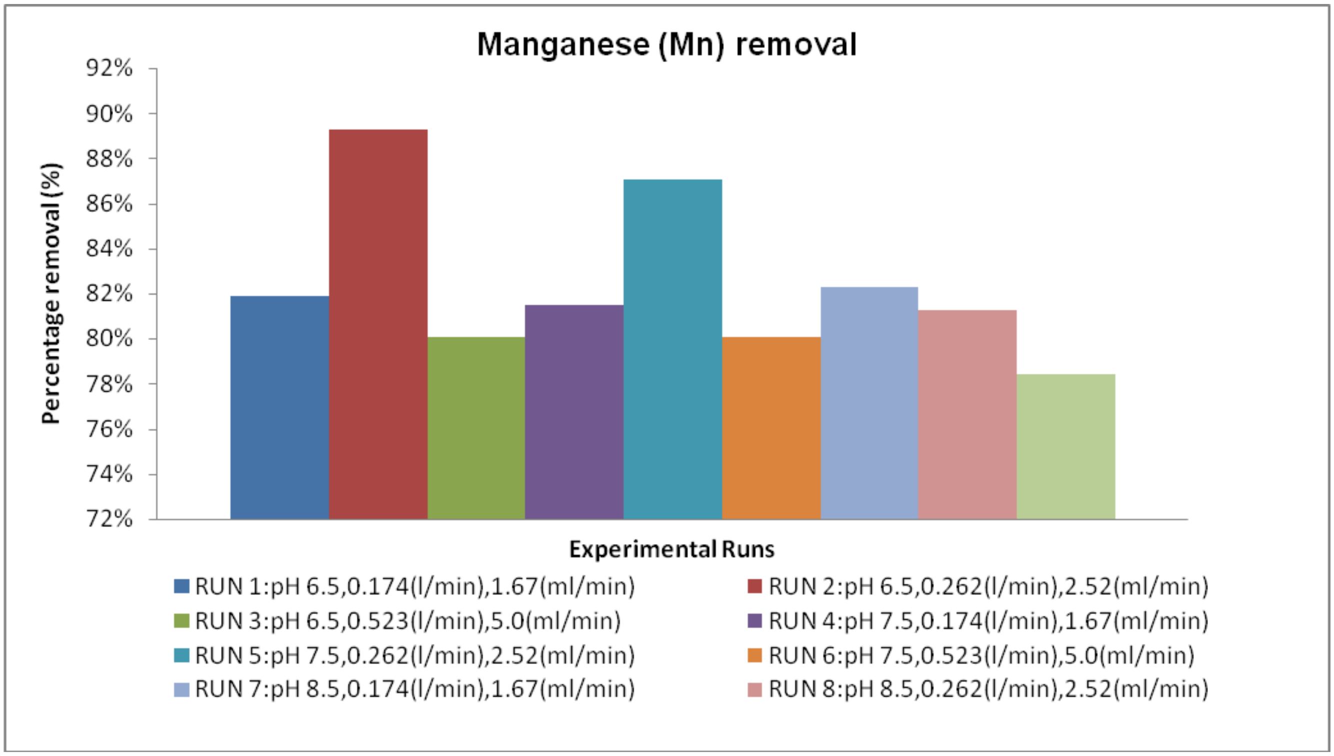

Figure 4.10Manganese Mn (II) removal after adsorption

4.5.1 Effect of pH

The pH of a solution has a significant role in determining the adsorption nature of the medium and the mechanism involved between adsorbent-adsorbate. Polystyrene Beads, Glass Media and Ion exchange resin used for this experiment have various functional moieties; the pH content affects the surface charge of this medium either by attraction or repulsion. The effects of varying pH profiles can be seen in Figures 4-5, representing the concentration and iron removal efficiency (H. Patel, 2021). Experimental run 1,2 & 3 on pH 6.5 presented in figure 4-8 indicates less adsorption of iron (34 %, -5% & -10%), respectively; this is due to the positively charged medium surface as a result of abundant hydronium ion (H^+) activities which increases the electrostatic repulsion between adsorbent and adsorbate. The positive effect of pH can be seen from run four at pH 7.5 in Figure 4D-9. Such an increase in iron removal efficiency of 64%-71% is attributed to the surface charge of the medium altered by the alkaline tendencies of the pH above 7 with a negative charge. However, iron adsorption is notably constant on experimental runs 8 & 9 at pH 8.5 because the iron adsorbed a saturation of medium vacant sites. Osuagwu et al., 2018, discovered that an increase in pH decreased iron adsorption, the reason being less empty site in the medium to absorb all the insoluble Fedue to medium early saturation.

Mn adsorption efficiency presented in Figures 4.9 & 4.10 shows an expected outcome of the manganese adsorption from the system. Figure 4.9 shows experimental run 1 and pH 6.5 supported by percentage removal efficiency shown in figure 4.10, Mn removal was 82%. The effective removal of manganese is advantageous due to the manganese compounds that form part of an oxidizing agent when reacting with an oxidant (Sarkar et al., 2018). The decrease in manganese removal shown in figure 4.10 from run 6-9 resulted from the saturation of vacant adsorbent sites.

4.5.2 Effect of flow rate

Iron (Fe) and Manganese (Mn) removal were assessed over various ranges of flow rates 0.174 l/min, 0.262l/min and 0.523 l/min, respectively. Figures 4.5 clearly show that increasing the solution flow rate decreases the Fe and Mn removal. As can be seen from experimental runs 3 (pH:6.5 and flow rate:0.523l/min), 6 (pH 7.5 & flow rate: 0.523l/min)and 9 (pH:8.5, flow rate: 0.523 l/min) run 3,6 & 9 on Fe removal achieved -5%, 38% & 54% removal while for Mn gained 80%, 80% & 78% respectively, which is the lowest removal percentages in both parameters efficiencies due to flow rate. These percentage removals show a 33% decrease for Fe and a 2% decrease for Mn compared to other flow rates. This observation indicates that the system achieves higher Fe and Mn adsorption rates at flow rates between 0.174 l/min and 0.262 l/min than 0.523l/min. It is confirmed by the 93% Fe removal at 0.174 l/min flow rate and 93% Mn removal at 0.262l/min flow rate presented in Table 7B.1 in the appendix section. Due to chemisorption, these results might show an interaction between the medium surface and the adsorbate. However, 0.523l/min is considered as the high flow rate to the system detriments adsorption of these parameters. The study by (Osuagwu et al., 2018) concurs that a high flow rate does hinder the maximum adsorption of iron or manganese, where they discovered that iron removal efficiency decreased from 23% to 3.6% due to increasing flow rate.

4.5.3 Effect of Contact Time

Contact time is an empirical parameter for determining the equilibrium saturation point. All the Figures above represent a 60 minutes time interval for the run of an experiment. Fe removal in experimental run 7 is 71%, and Mn is 89% in experimental run 2, presented in Figures 4.8 and 4.10, respectively. At 60 min in both instances, the system indicated no more adsorbate uptake on the adsorbent surface. The rapidness of adsorption that was noticed at the beginning of the experiment gradually decreased due to the vacant site of medium saturation. It was confirmed in a study by (Govorova et al., 2019), where they experimented with various system sizes for removing iron and manganese; their findings were that the system with high capacity had to adsorb more contaminants due to extended contact time.

4.6 Adsorption Isotherm

Adsorption isotherms are usually applied in linear and nonlinear forms to determine pollutant quantity adsorbed by the adsorbent at equilibrium. In this research, the comparability of these two states of the isotherms was to determine the best fitting isotherm for linear application, and nonlinear was used to minimize the errors found during linearity (M. Hamzaoui, B. Bestani, 2018).

According to (Piccin et al., 2011), the interaction of pollutants with adsorbent material is the fundamental technique of the isotherms to critically optimize the adsorbents functionality in the industrial adsorption system design. The frequently used isotherms are Langmuir, which assumes no interaction between adsorbed molecules, and Freundlich models describing the heterogeneous multilayer adsorption and correlation between adsorbate-adsorbent (M. Hamzaoui, B. Bestani, 2018). However, in this study edition of Temkin that pertains to the heat of the molecules that decrease linearly due to coverage and Dubinin-Radushkevich isotherms utilized to envisage the nature of the adsorption process as physical or chemical by calculating sorption energy, were imperative to be investigated to determine the relevant information about adsorption spontaneity, mechanism and the stability of the adsorbent-adsorbate relationship (Ferreira et al., 2019).

Previous studies using expanded polystyrene beads (EPS) to remove iron from groundwater found the best isotherm to be that of Freundlich (Osuagwu et al., 2018). However, only Langmuir and Freundlich's adsorption isotherm models were covered. Adsorption thermodynamic parameter plays a vital role in the adsorption system design and selection of adsorbents, such as the Gibbs free energy, enthalpy, and entropy (Piccin et al., 2011). However, this research did not explore thermodynamics since the temperature remained constant throughout the experiment.

4.6.1 Langmuir Isotherm

The Langmuir isotherm model is assumed for good monolayer adsorption onto vacant sites on the adsorbent surface containing a limited number of similar sites. Once the adsorbent is saturated, no further adsorption occurs (Kumari et al., 2020).

The linear form of the model is described in equation 2.2 in the literature. The adsorption parameters for all isotherms are listed in Table 4.2(Fe) & 4D-3 (Mn)

$$\frac{1}{q_e} = \frac{1}{Q_m} + \frac{1}{bQ_mC_e}$$

Where Q_m is the maximum monolayer adsorption capacity (mg/g), *b* is the Langmuir constant related to the affinity of metal ion to be adsorbed, qe and Ce are the adsorption capacity (mg/g) and equilibrium concentration (mg/l), respectively (Piccin et al., 2011).

Plotting Ce/qe versus Ce results in a straight line of slope 1/Qm and intercepts $1/bQ_m$. These plots are illustrated by Figure 4.11 to 4.13 (Fe) and Figure 4.14 to 4.16 (Mn)

4.6.2 Iron Langmuir Linear

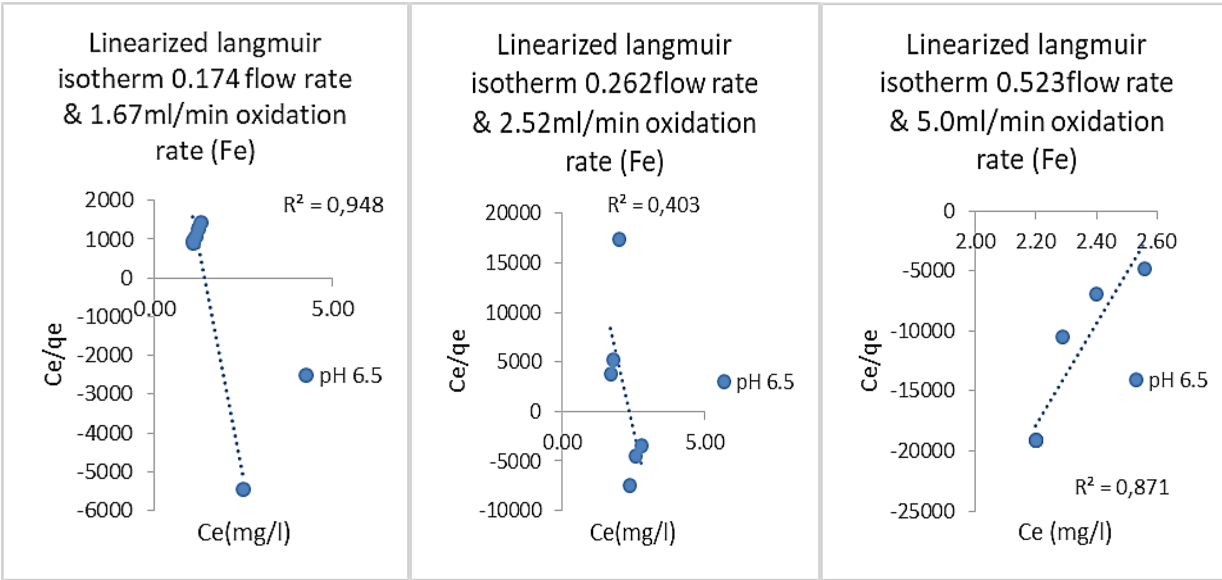

Figure 4.11Linearised Langmuir isotherm pH 6.5 (Fe)

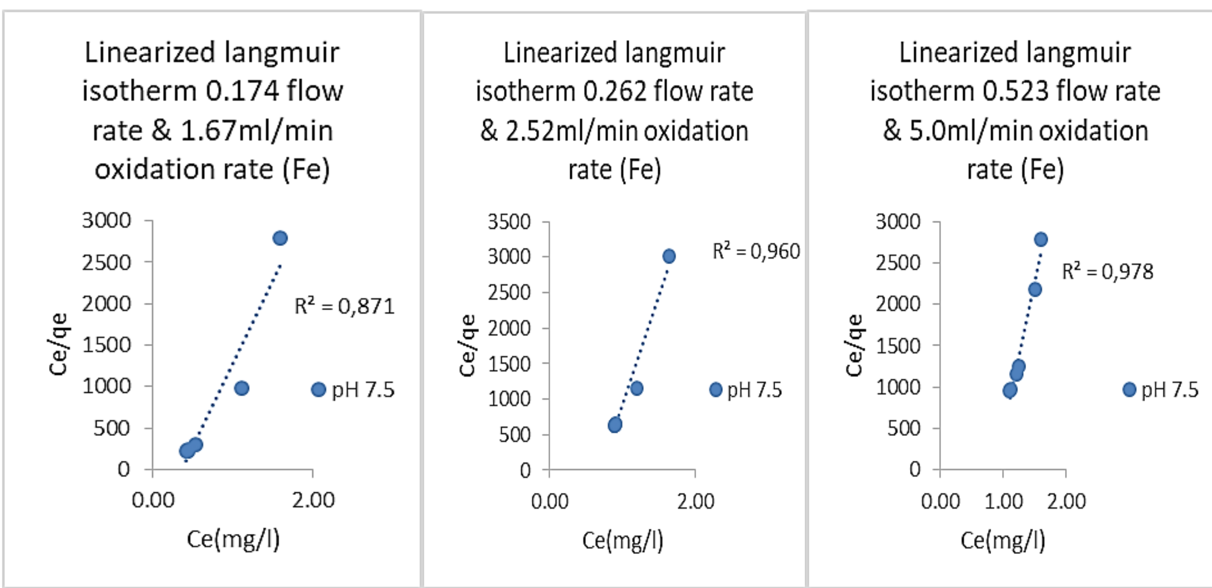

Figure 4.12Linearised Langmuir isotherm 7.5 (Fe)

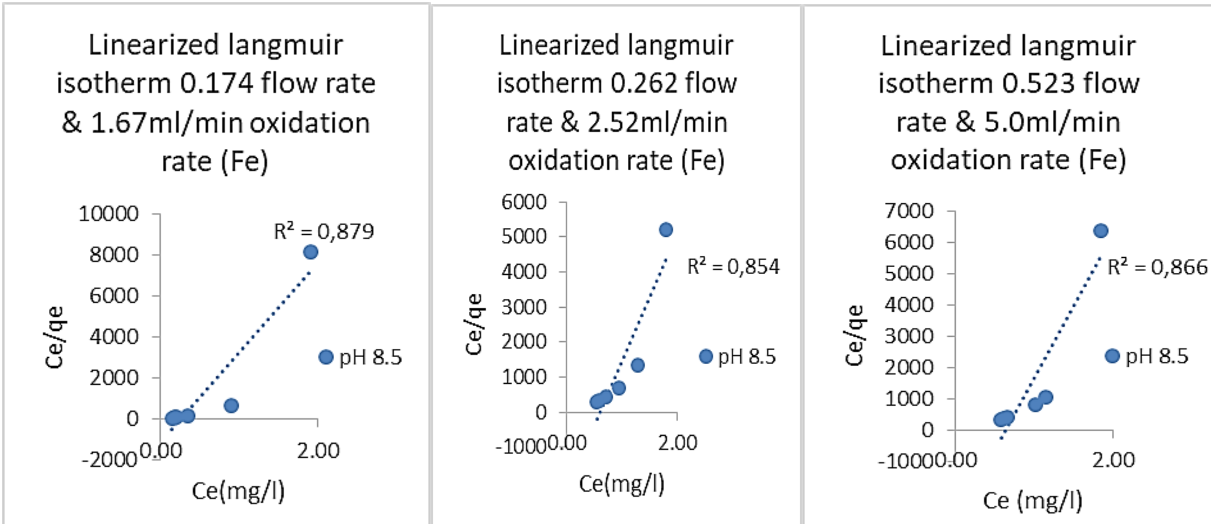

Figure 4.13inearised Langmuir isotherm pH 8.5 (Fe)

4.6.3 Manganese Langmuir Linear

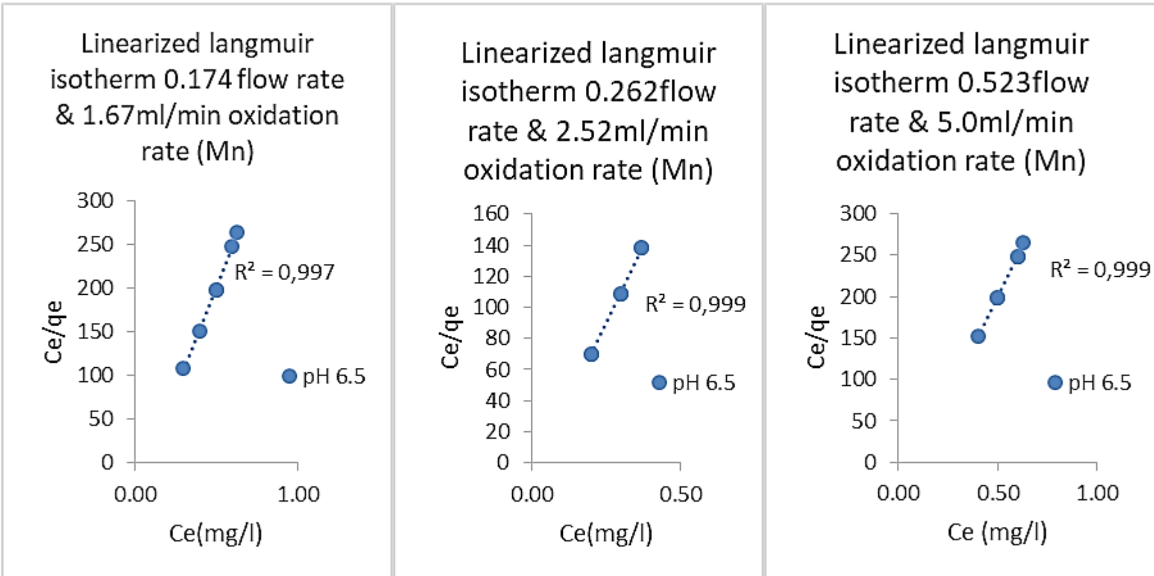

Figure 4.14Linearised Langmuir isotherm pH 6.5 (Mn)

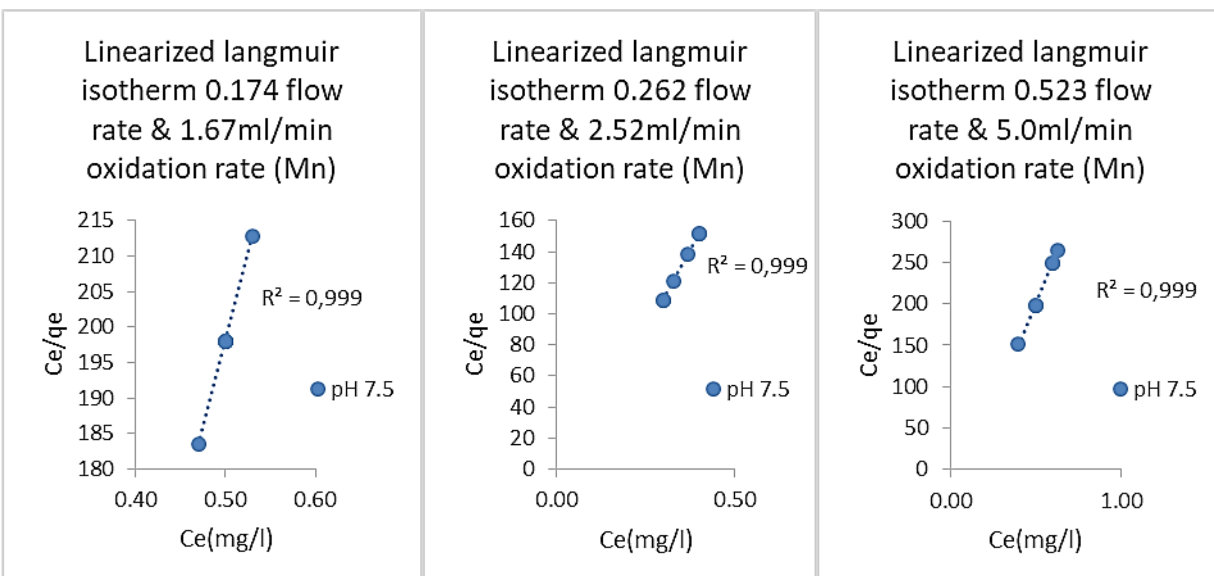

Figure 4.15Linearised Langmuir isotherm pH 7.5 (Mn)

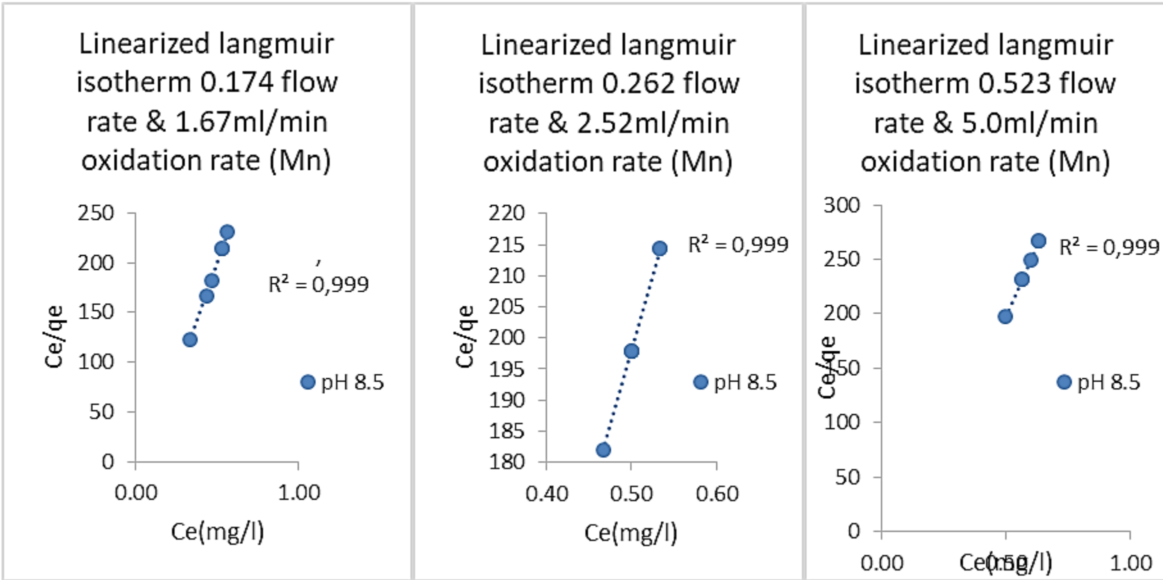

Figure 4.16Linearised Langmuir isotherm pH 8.5 (Mn)

$$R_L = \frac{1}{1 + bC_o}$$

The feasibility and favourability of Langmuir isotherm are determined by assessing the dimensionless constant RL, called the separation factor, as illustrated by the above equation and its values shown in table 4.2 (Fe) and table 4.3 (Mn). Suppose the range of this parameter falls between 0<RL<1, it's then deemed that the experiment and its conditions fit the model (Roman, 2021a). However, this isotherm does not fit the data since the RL for both metal ions is out of the required range.

4.7 Freundlich Isotherm

The Freundlich isotherm model describes the heterogeneous multilayer adsorption and correlation between adsorbate and adsorbent (M. Hamzaoui, B. Bestani, 2018). Freundlich isotherm-associated constants models are sorption capacity (KF) and sorption intensity (1/n).

The equilibrium data were fitted to the Freundlich isotherm below given in equation 2.3 on literature:

$$\ln q_e = \ln K_F + \frac{1}{n} \ln C_e$$

The linear plot lnq_e vs Ce can be seen in Figure 4D.18 & 19 (Fe) and Figure 4.19 to 4.21. The calculation of K_F and n given in tables 4.1 (Fe) & 4.2 (Mn) were determined in these plots.

4.7.1 Iron Freundlich Linear

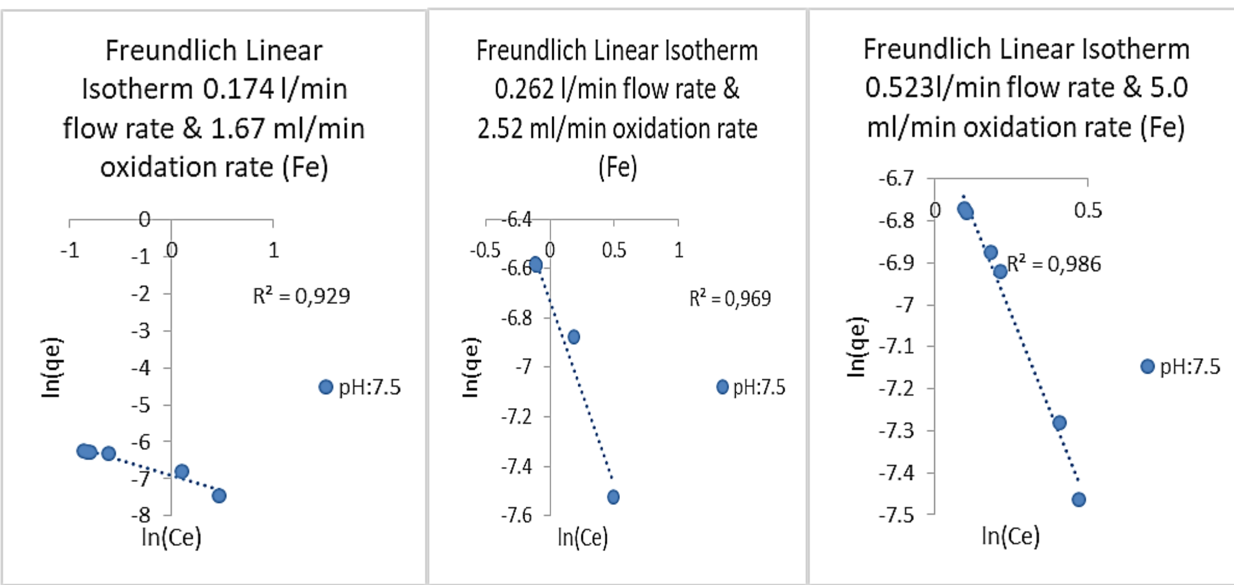

Figure 4.17Linearised Freundlich isothem pH 6.5 (Fe)

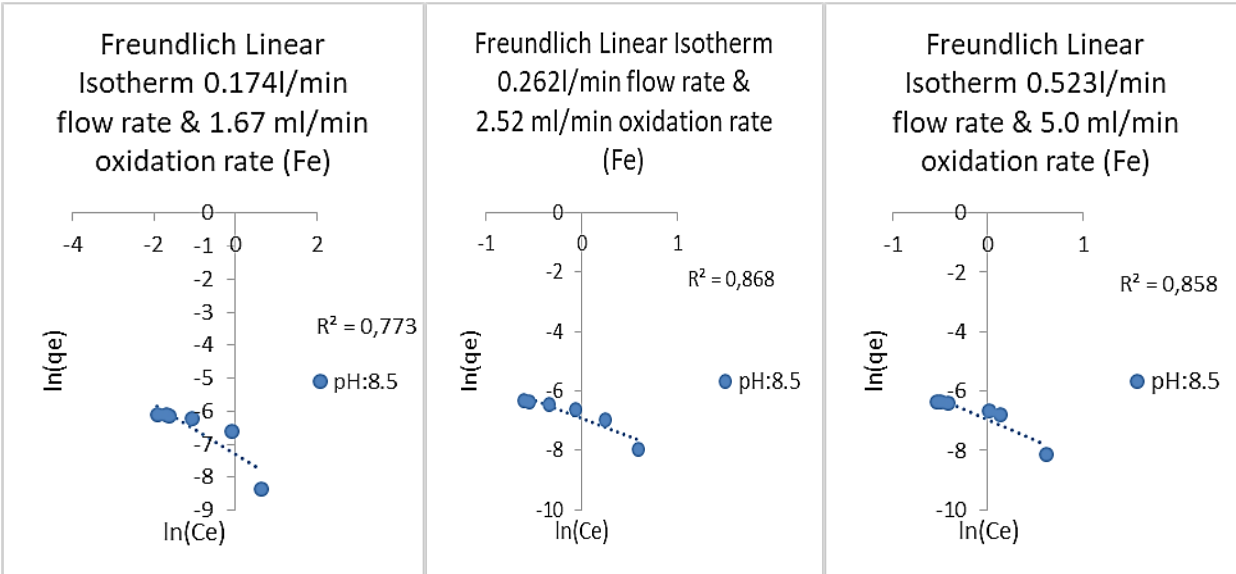

Figure 4.18Linearised Freundlich isothem pH 7.5 (Fe)

4.7.2 Manganese Freundlich Linear

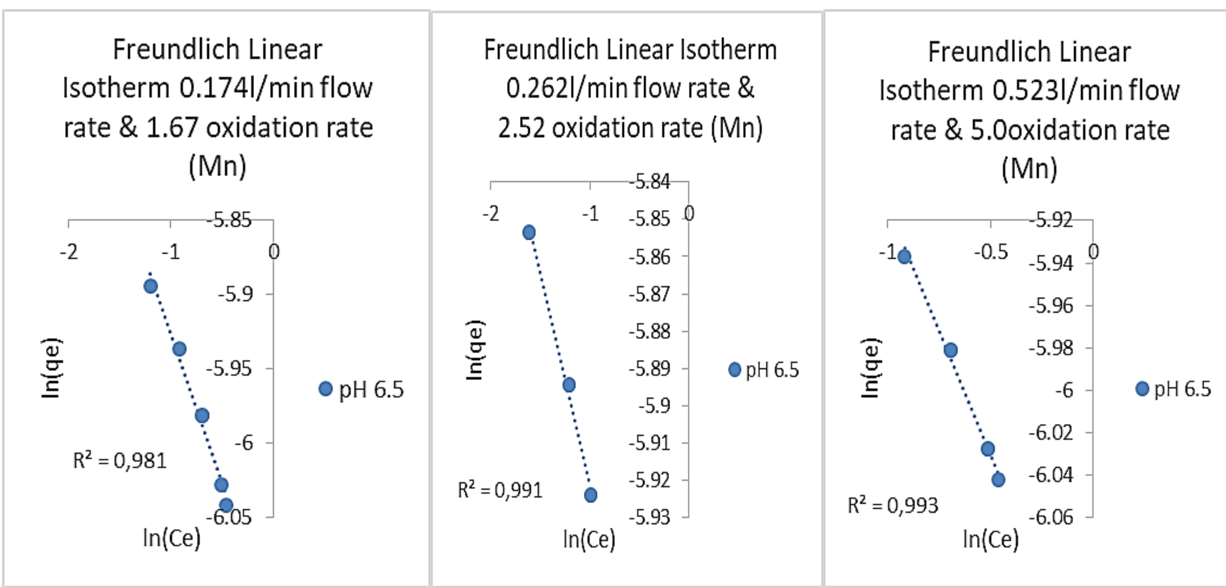

Figure 4.19 Linearised Freundlich isothem pH 6.5 (Mn)

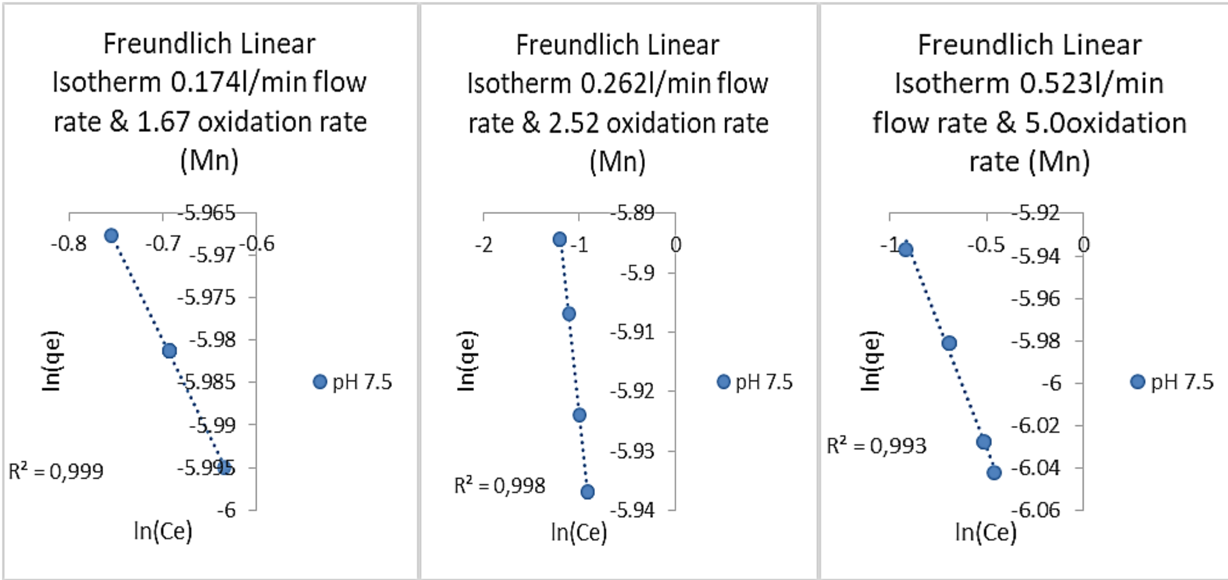

Figure 4.20 Linearised Freundlich isothem pH 7.5 (Mn)

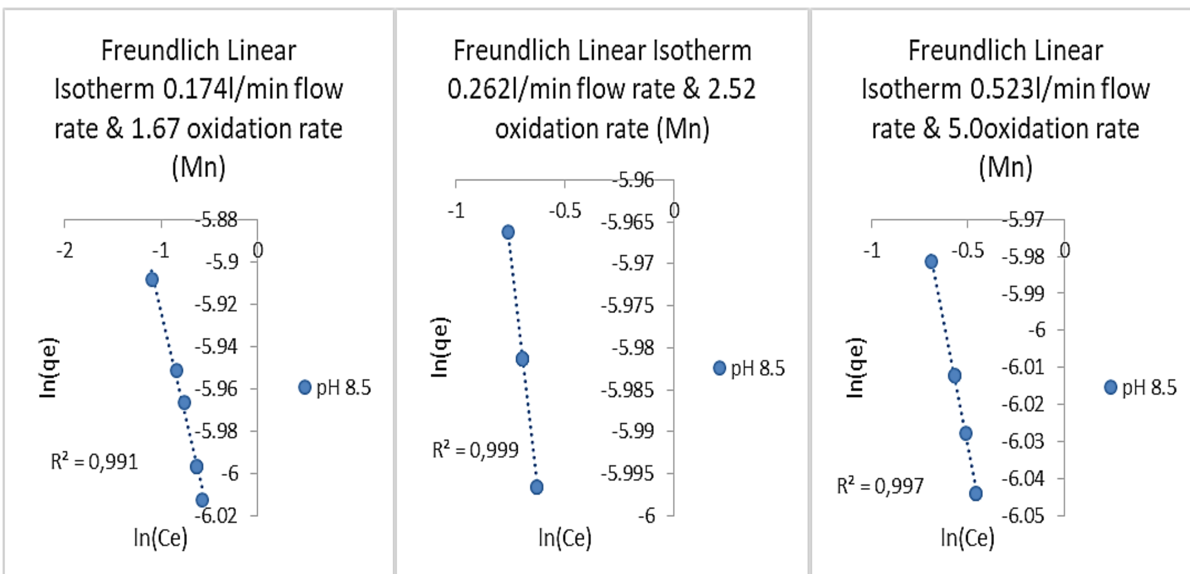

Figure 4.21 Linearised Freundlich isothem pH 8.5 (Mn)

The affinity of the process, whether favours chemisorption or physio-sorption, is measured by the n value where chemisorption ($n < 1$) or physio-sorption ($n > 1$) (Said et al., 2018). As shown in table 4.2 (Fe) & 4.3 (Mn), the existence of interaction between adsorbent and adsorbate is chemisorption since the values of sorption intensity $n<1$. This indicates a chemical bond between adsorbate and adsorbent; this is concurrent to the FTIR results found that the filtration medium used has charges that enhance the removal of these metal ions from groundwater. The chemisorption also supports multilayer adsorption since the adsorbed molecules will attract the influent adsorbate (Piccin et al., 2011).

4.8Temkin Isotherm

The Temkin Isotherm model pertains to the molecules' heat that decreases linearly when the adsorbent surface is increasingly covered by the adsorbate (Ferreira et al., 2019).

The literature presents the Temkin linear equation below as equation 2-4. The figures representing this isotherm are Figure 4.22 to 4.24 and figure 4.25 to 4.27

$$q_e = \frac{RT}{b} lnK_T + \frac{RT}{b} lnC_e$$

Where B_T represents:

$$B_T = \frac{RT}{b}$$

Where K_T is the equilibrium binding constant (L g^{-1}) corresponding to the maximum binding energy, b_T is related to the adsorption heat. R is the universal gas constant (8.314 J K^{-1} mol^{-1}), and T is the temperature (K). Plotting $q_e$vs $\ln(C_e)$ results in a straight line of slope RT/b_T and intercept $(RT \ln K_T)/b_T$(Piccin et al., 2011).

4.8.1 Iron Temkin Linear

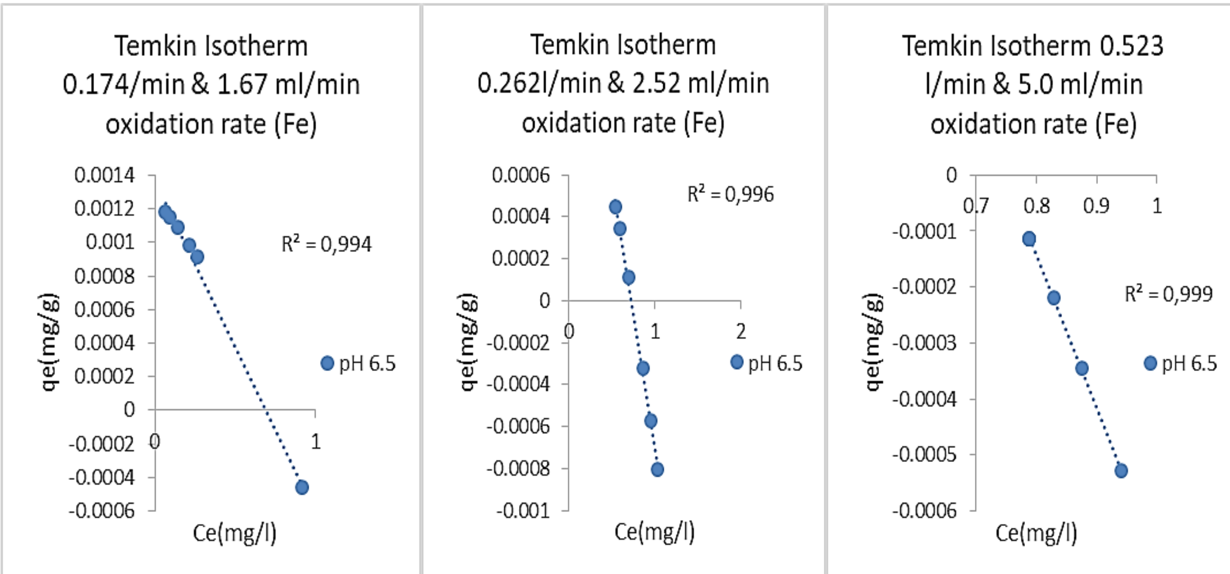

Figure 4.22Linearised Temkin isotherm pH 6.5 (Fe)

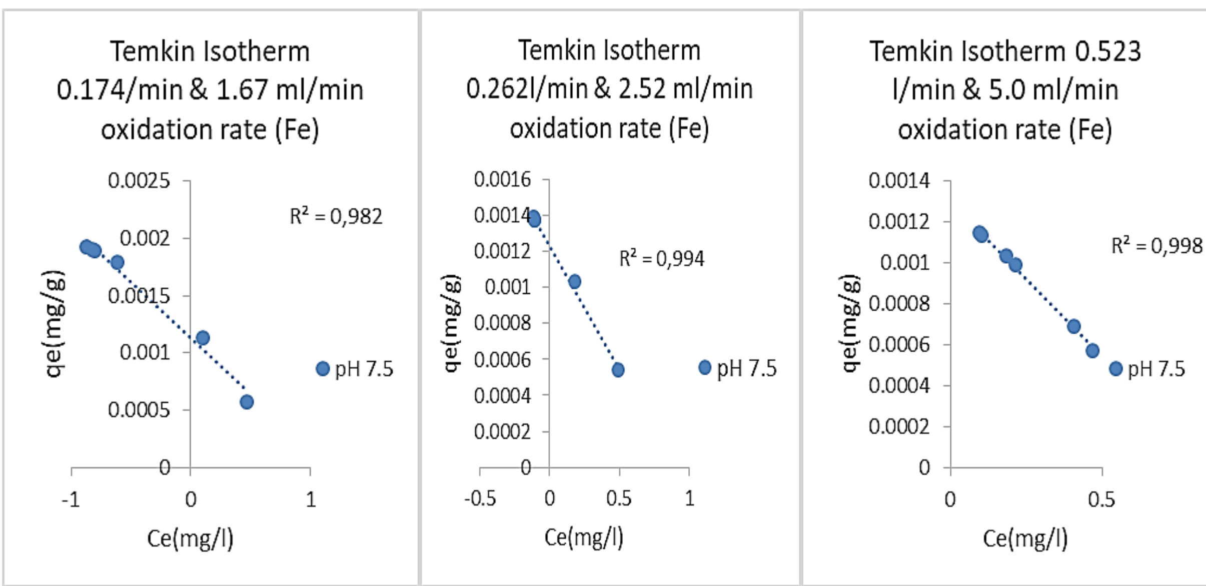

Figure 4.23Linearised Temkin isotherm pH 7.5 (Fe)

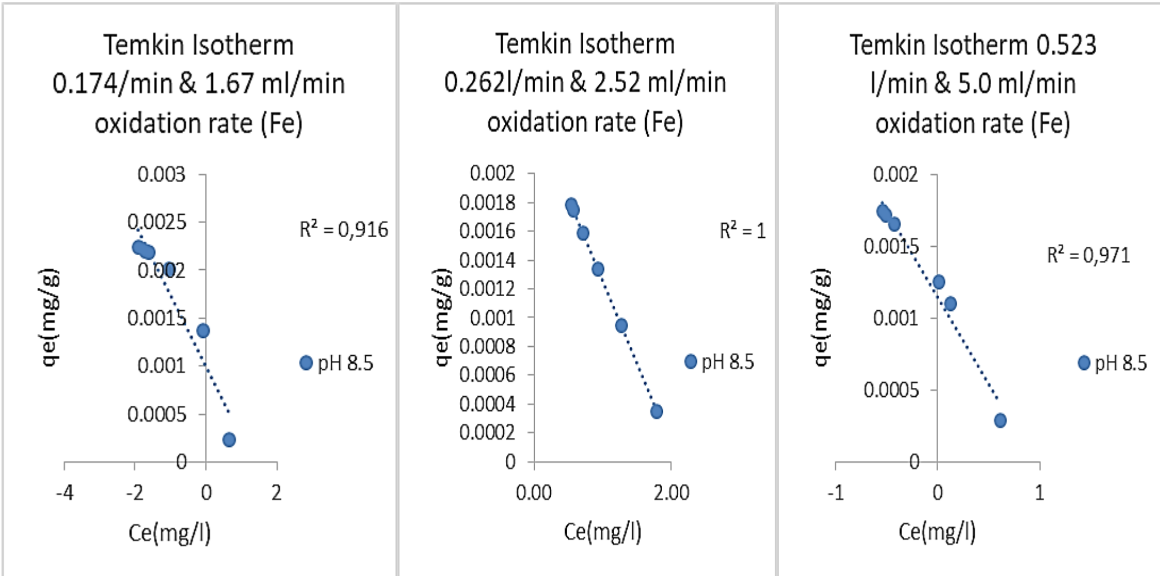

Figure 4.24 Linearised Temkin isotherm pH 8.5 (Fe)

4.8.2 Manganese Temkin Linear

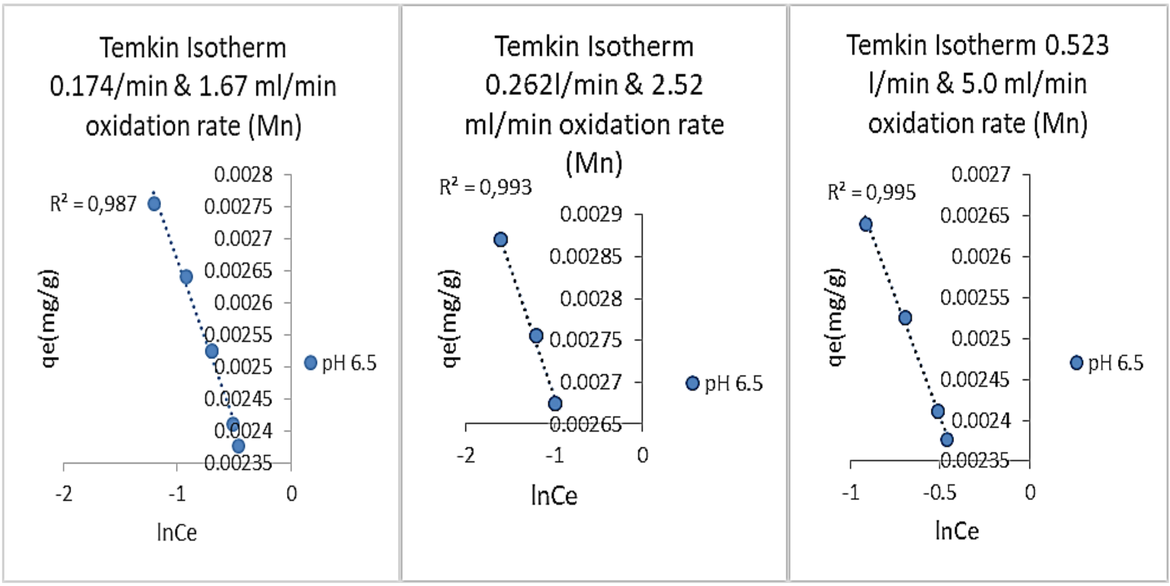

Figure 4.25Linearised Temkin isotherm pH 6.5 (Mn)

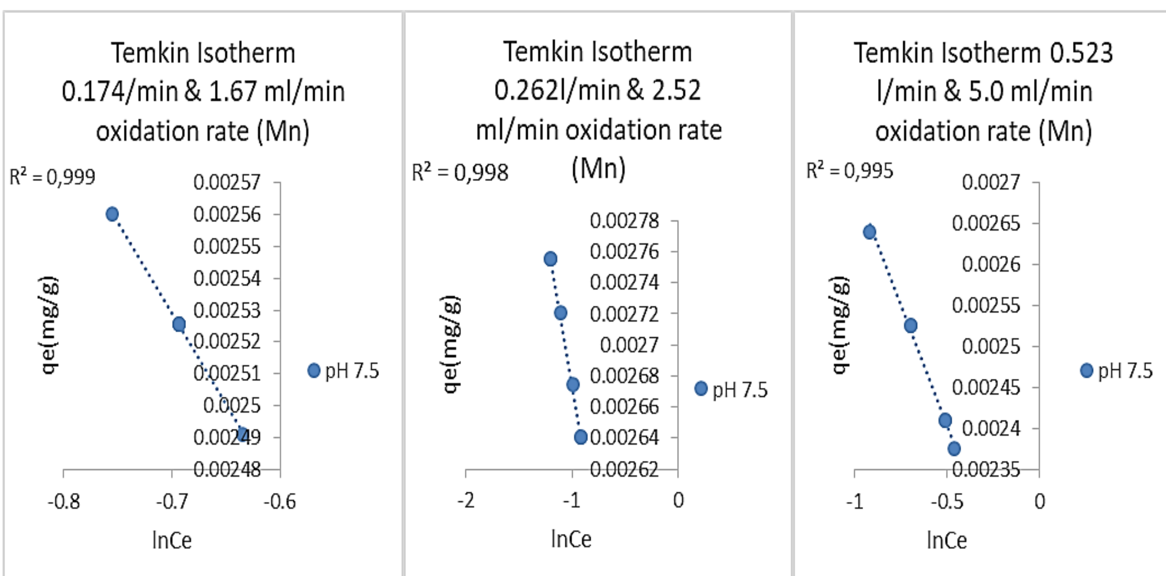

Figure 4.26 Linearised Temkin isotherm pH 7.5 (Mn)

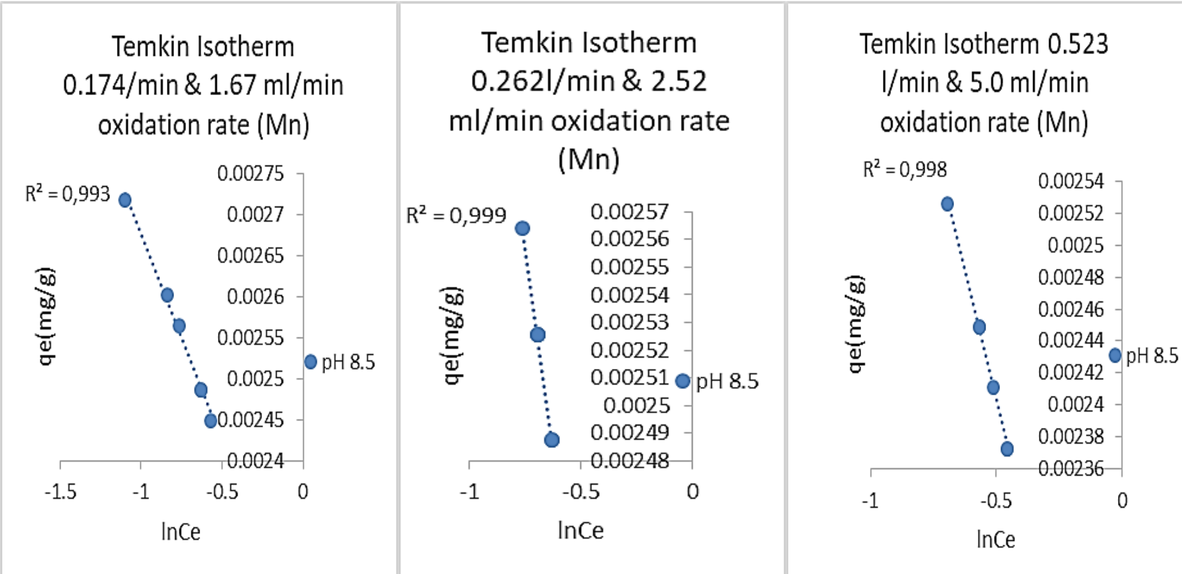

Figure 4.27 Linearised Temkin isotherm pH 8.5 (Mn)

On the data shown in table 4.2 (Fe) and 4.3 (Mn), it can be seen that the is high binding energy between the adsorbent and adsorbate, which is confirmed by the K_T values and the R^2 that is closer to 1, as compared to all other adsorption isotherms in this study. Also, the decrease in equilibrium binding constant is noticed in table 4.2 (Fe) from 0.499 l/g run 1 to 0.267 l/g run 7, which proves this isotherm that the equilibrium binding decrease with the adsorption coverage (Hameed, 2019)

4.9Dubinin-Radushkevich (D-R) Isotherm

This model was utilized to envisage the nature of the adsorption process as physical or chemical by calculating sorption energy. The Dubinin–Radushkevich isotherm relates to the heterogeneity of energies close to the adsorbent surface (Saeidi & Parvini, 2015).

The equilibrium correlation of adsorbate-adsorbent can be determined using the adsorption potential (ε).

$$\varepsilon = RTln\left(1 + \frac{1}{C_e}\right)$$

The linear form of the model is described by equation 2.5 in the literature as

$$Lnq_e = Lnq_m - \beta\varepsilon^2$$

The mean sorption energy, E (Jmol-1), is evaluated by:

$$E = \frac{1}{\sqrt{2\beta}}$$

Values of q_m and β shown in table 4.2 (Fe) and 4.3 (Mn) were determined by linearising the D-R isotherm. Plotting ln qe versus ε2, will result in a straight line of slope β and intercept ln (q_e) (Saeidi & Parvini, 2015).

4.9.1 Iron D-R Linear

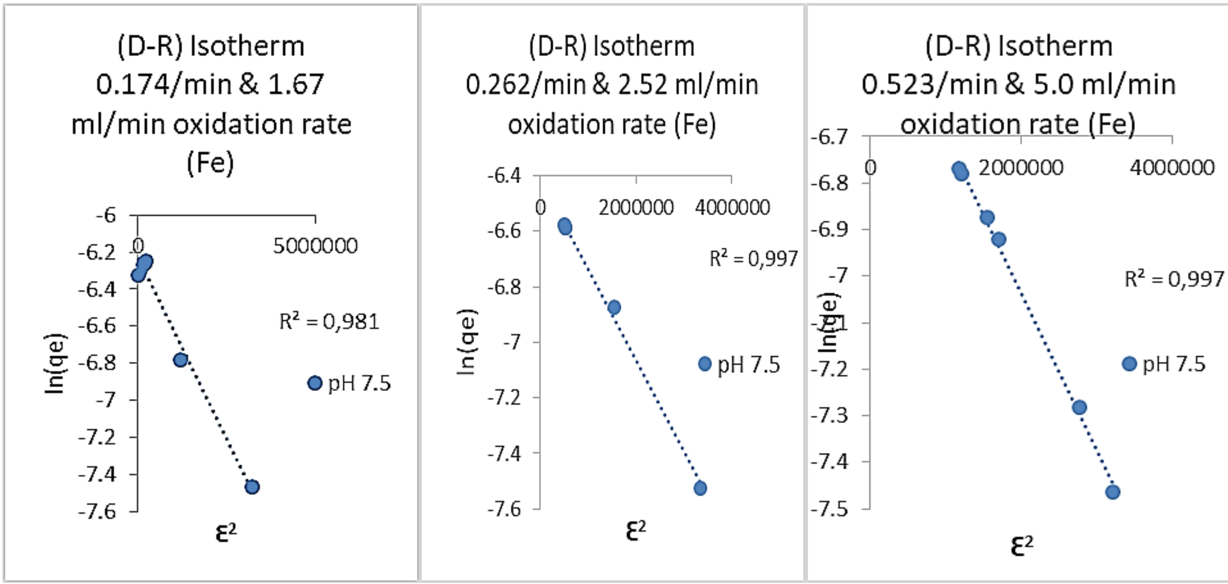

Figure 4.28Linearised D-R isotherm pH 7.5 (Fe)

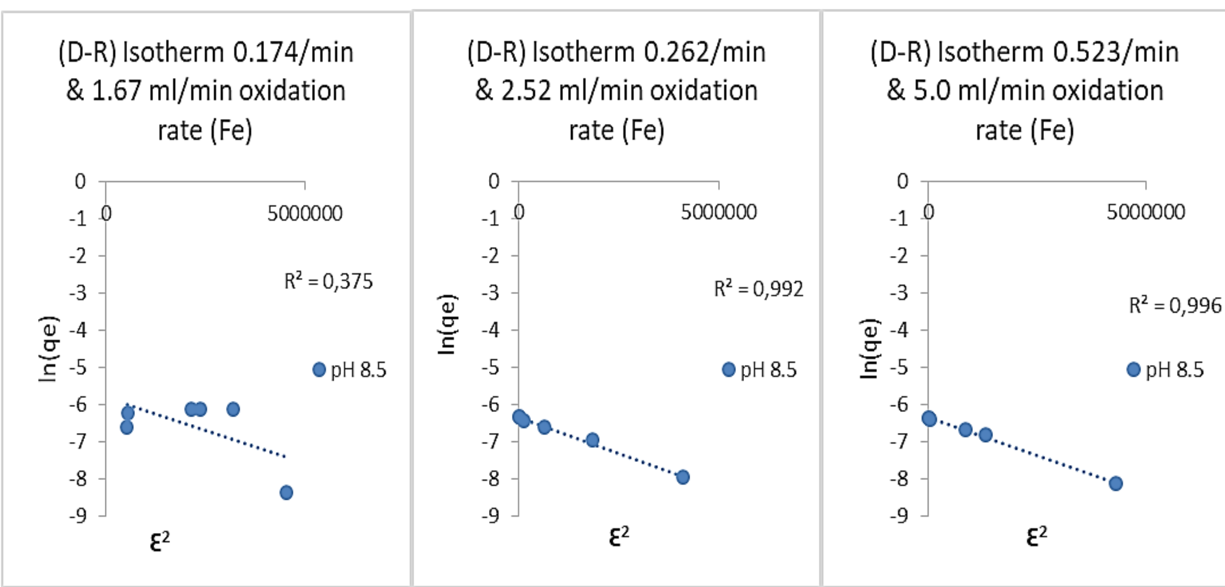

Figure 4.29Linearised D-R isotherm pH 8.5 (Fe)

4.9.2 Manganese D-R linear

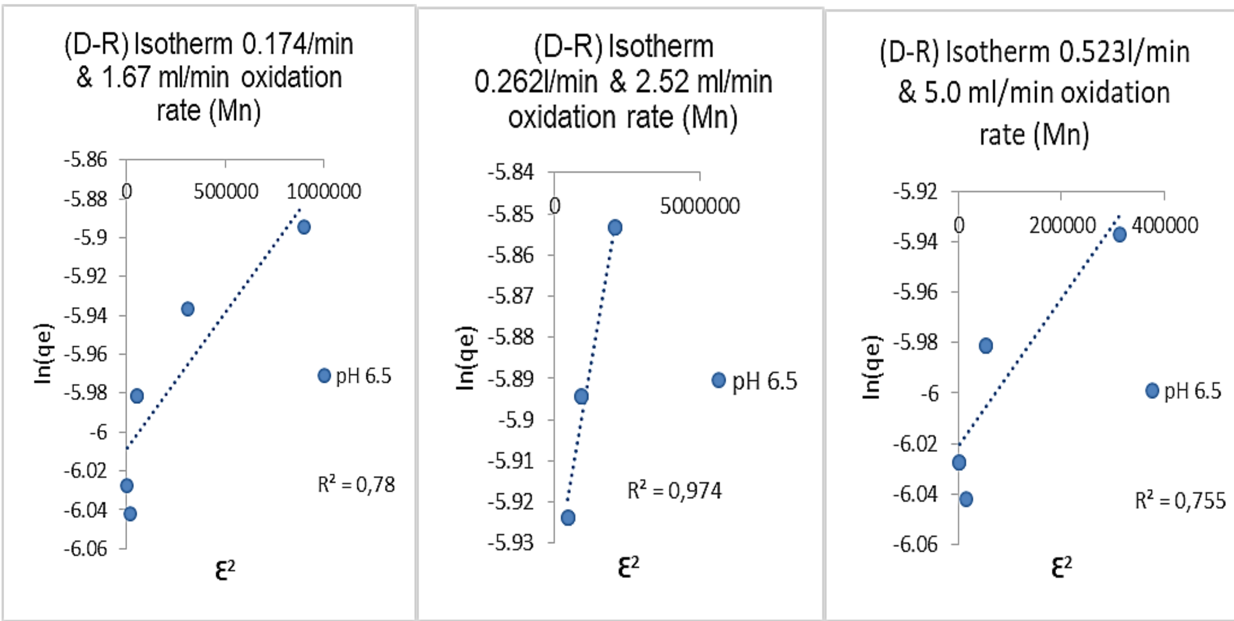

Figure 4.30Linearised D-R isotherm pH 8.5 (Mn)

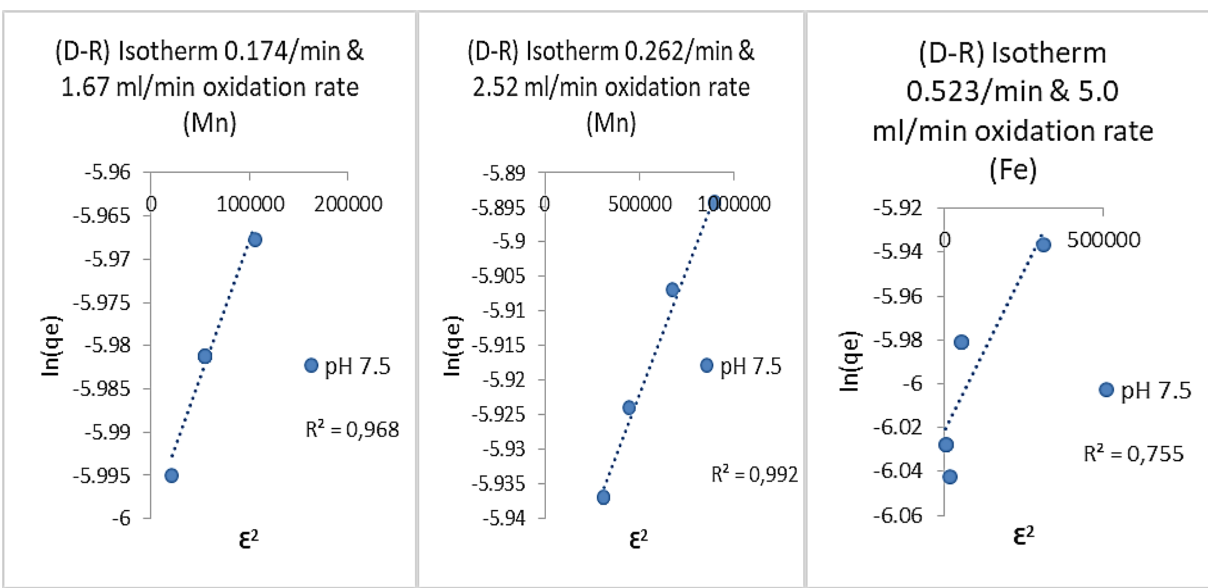

Figure 4.31Linearised D-R isotherm pH 7.5 (Mn)

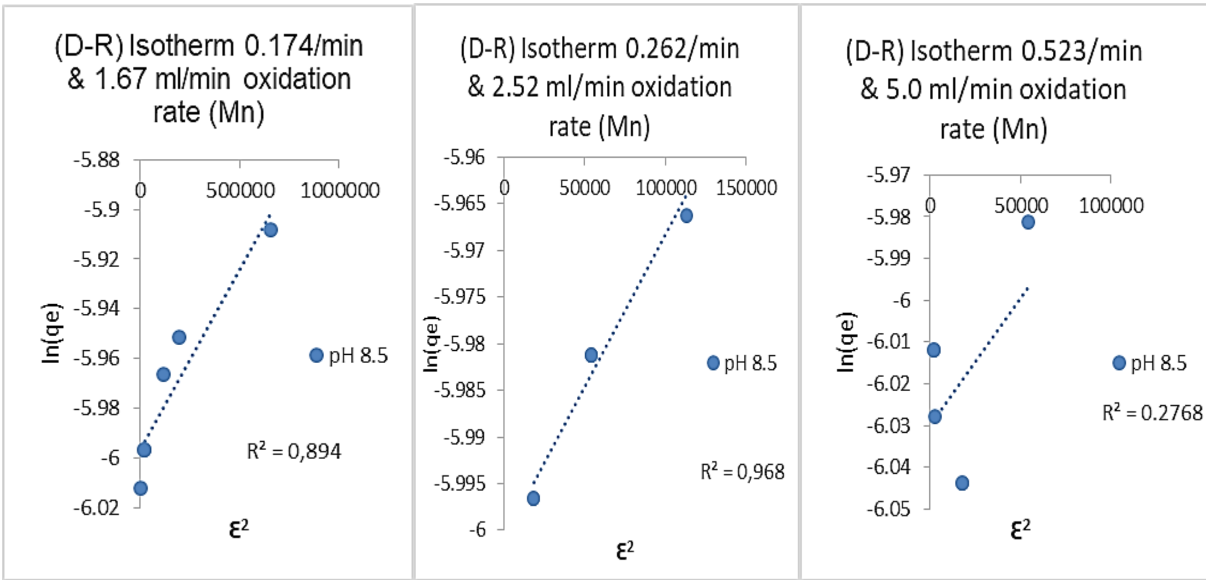

Figure 4.32 Linearised D-R isotherm pH 8.5 (Mn)

E (J/mol) is the mean free energy of adsorption per molecule adsorbate. If E<8 kJ/mol, the adsorption process is physical and ranges from 8 to 16 kJ/mol; it is chemical (Saeidi & Parvini, 2015; Said et al., 2018). The energy for this isotherm was undeterminable due to the negative slope observed when calculating the isotherm constants. This led to –β, which hinders the calculation of E (J/mol) in both Fe and Mn results. However, the figure for linear functions is shown in Figure 4.28 and29 (Fe) and 4.30 to 32(Mn)

Table 4:2 Iron linear adsorption isotherms constants

Iron (Fe)									
RUNS	**1**	**2**	**3**	**4**	**5**	**6**	**7**	**8**	**9**
pH	**6.5**			**7.5**			**8.5**		
Flow rate (l/min)	**0,174 (l/min)**	**0,262 (l/min)**	**0,523 (l/min)**	**0,174 (l/min)**	**0,262 (l/min)**	**0,523 (l/min)**	**0,174 (l/min)**	**0,262 (l/min)**	**0,523 (l/min)**
Langmuir Isotherm									
q_{max} (mg/g)	-2.10E-04	-7.71E-05	2.35E-05	4.97E-04	3.23E-04	2.81E-04	2.27E-04	2.75E-04	2.20E-04
b(L/g)	-0.715	-0.424	-0.382	-2.730	-1.422	-1.169	-3.773	-1.688	-1.578
R_L	-1.993	-0.504	5.030	-0.211	-0.504	5.030	-0.144	-0.393	-0.432
R^2	0.949	0.404	0.872	0.925	0.961	0.978	0.880	0.855	0.866
Freundlich Isotherm									
K_F (mg/g)	1.30E-03			1.00E-03	1.19E-03	1.41E-03	6.62E-04	9.77E-04	9.51E-04
n	-7.72E-01			-1.21	-0.67	-0.55	-5.14	-0.80	-0.71
R^2	0.997			0.99	0.99	0.99	0.77	0.87	0.86
Temkin Isotherm									
B_T (J/mol)	-5.10E-04	-2.52E-03	-2.71E-03	-9.78E-04	-1.38E-03	-1.53E-03	-7.42E-04	-1.17E-03	-1.21E-03
K_T(L/g)	0.499	0.484	0.027	0.316	0.408	0.426	0.261	0.375	0.387
R^2	0.994	0.996	0.999	0.982	0.994	0.998	0.916	1.000	0.971
D-R Isotherm									
q_m (mg/g)				1.96E-03	1.65E-03	1.72E-03	3.03E-03	1.75E-03	1.75E-03
$\beta(mol^2/K^2/J^2)$				3.89E-07	3.29E-07	3.36E-07	3.53E-07	3.87E-07	4.11E-07
R^2				0.982	0.997	0.997	0.375	0.992	0.996

Table 4:3 Manganese linear adsorption isotherms constants

Manganese (Mn)									
RUNS	**1**	**2**	**3**	**4**	**5**	**6**	**7**	**8**	**9**
pH	**6.5**			**7.5**			**8.5**		
Flow rate (l/min)	**0,174 (l/min)**	**0,262 (l/min)**	**0,523 (l/min)**	**0,174 (l/min)**	**0,262 (l/min)**	**0,523 (l/min)**	**0,174 (l/min)**	**0,262 (l/min)**	**0,523 (l/min)**
Langmuir Isotherm									
q_{max} (mg/g)	2.11E-03	2.48E-03	2.02E-03	2.06E-03	2.35E-03	2.02E-03	2.15E-03	2.05E-03	1.93E-03
b(L/g)	-12.984	-35.899	-10.265	-10.807	-22.354	-10.265	-13.735	-10.691	-8.347
R_L	-0.029	-0.010	-0.037	-0.035	-0.017	-0.037	-0.028	-0.036	-0.046
R^2	0.998	1.000	0.999	1.000	1.000	0.999	0.999	1.000	1.000
Freundlich Isotherm									
K_F (mg/g)	2.14E-03	2.40E-03	2.14E-03	2.16E-03	2.31E-03	2.14E-03	2.20E-03	2.16E-03	2.10E-03
n	-4.30	-8.88	-4.29	-4.41	-6.77	-4.29	-5.14	-4.38	-3.76
R^2	0.992	0.992	0.993	0.999	0.999	0.993	0.991	0.999	0.998
Temkin Isotherm									
B_T (J/mol)	-5.10E-04	-3.13E-04	-5.84E-04	-5.73E-04	-3.99E-04	-5.84E-04	-5.03E-04	-5.76E-04	-6.51E-04
K_T(L/g)	0.015	0.001	0.027	0.024	0.003	0.027	0.013	0.025	0.041
R^2	0.987	0.993	0.995	0.999	0.998	0.995	0.993	0.999	0.998
D-R Isotherm									
q_m (mg/g)	0.002458081	2.64E-03	2.43E-03	2.48E-03	2.59E-03	2.43E-03	2.49E-03	2.48E-03	2.41E-03
β($mol^2/K^2/J^2$)	-1.39E-07	-4.11E-08	-2.92E-07	-3.11E-07	-7.19E-08	-2.92E-07	-1.44E-07	-3.25E-07	-6.14E-07
R^2	7.80E-01	9.74E-01	7.55E-01	0.969	0.992	0.755	0.894	0.969	0.277

Table 4-2 and 4-3 shows the adsorption isotherms constants for Langmuir, Freundlich, Temkin and Dubinin-Radushkevich. It can be seen that R^2 for Freundlich isotherm is higher than all other isotherms for Iron (Fe), and Langmuir isotherm R^2 favours Manganese (Mn). Whereas Temkin and Dubinin-Radushkevich, It can be noticed that the isotherm model simulation gives a less acceptable regression coefficient R^2.

It was observed that Langmuir isotherm represented the equilibrium sorption best in removing manganese; this observation means monolayer coverage of the surface Glass, Polystyrene and Ion exchange since the Langmuir isotherm assumes that the surface is homogeneous. A similar isotherm fit for sorption has been discovered by (Osuagwu et al., 2018).

Interaction between adsorbed molecules was observed on the Freundlich Isotherm to remove Iron (Fe) since the isotherm model applies to heterogeneous surfaces and the interaction between adsorbed molecules (Bestani, 2018).

This interaction was noticed more when the pH was adjusted between 7.5-8.5, which increased the interaction between the adsorbate and adsorbent; this observation proves the adsorption of Iron (Fe) is controlled by chemisorption and since adsorption intensity (n) values of the Freundlich isotherm model demonstrate ($n < 1$) (Piccin et al., 2011).

4.10 Adsorption Kinetic Modelling

The adsorption kinetics are presented in a curve illustrating the retention rate or solute release in a solution at a given pH, flow rate, adsorbent dosage and contact time (Turp et al., 2022).Evaluating the adsorbent removal rate in the adsorption process is essential for adequately designing the water treatment system. Exploring the sorption rate in this experiment was vital to assess the removal of Iron (Fe) and Manganese (Mn) with an effect of contact time. To further understand the effects adsorption rate mechanism of Fe and Mn on Glass Media, Polystyrene Beads and Ion exchange, sorption kinetic model studies were conducted (Ferreira et al., 2019). The kinetic models used to evaluate the system were pseudo-first-order, pseudo-second-order, intra-particle diffusion and Elovich. The regression coefficients and information are presented in this section.

4.10.1 Pseudo First Order (PFO) Model

PFO adsorption kinetic is more applicable to the adsorption rate that explores vacant active sides of the adsorbent surface (Kumari et al., 2020).

Data was fitted on the linearized equation for PFO presented by the equation in the literature.

$$\ln(q_e - q_t) = ln q_e - k_1 t$$

4.10.1 (i) Iron PFO linear

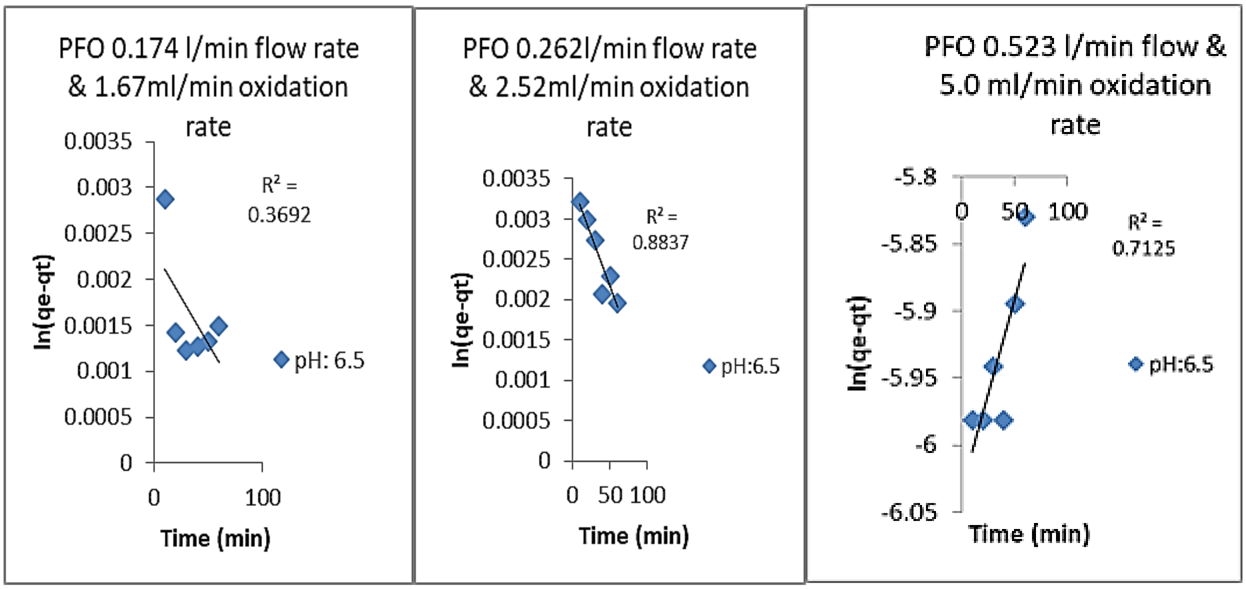

Figure 4.33 PFO linear iron at pH 6.5

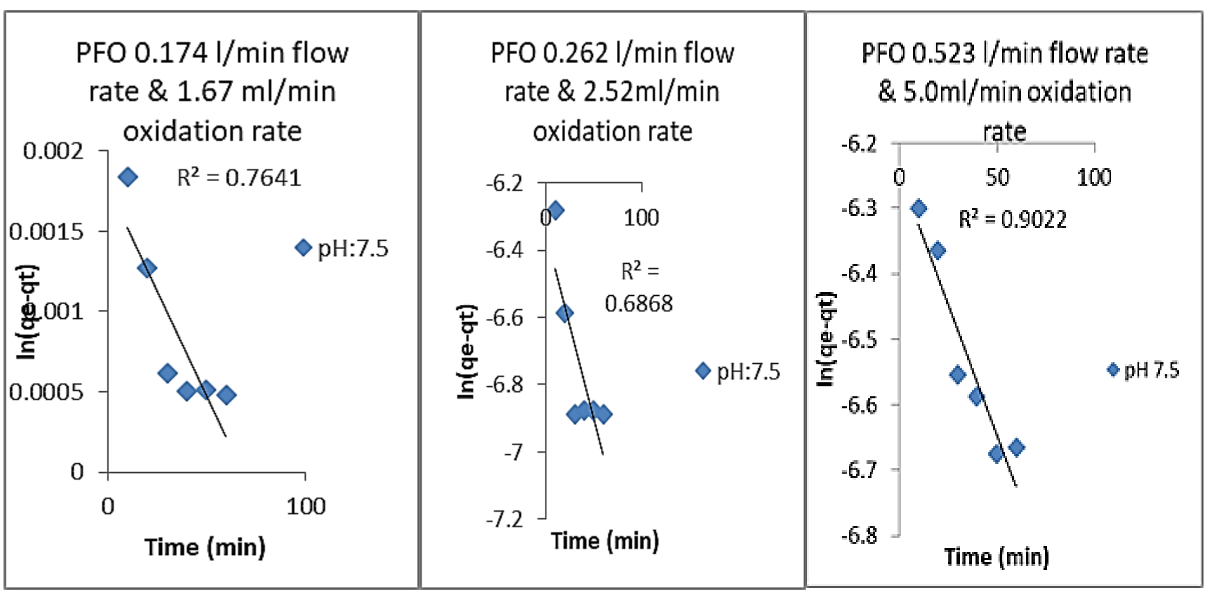

Figure 4.34 PFO linear iron at pH 7.5

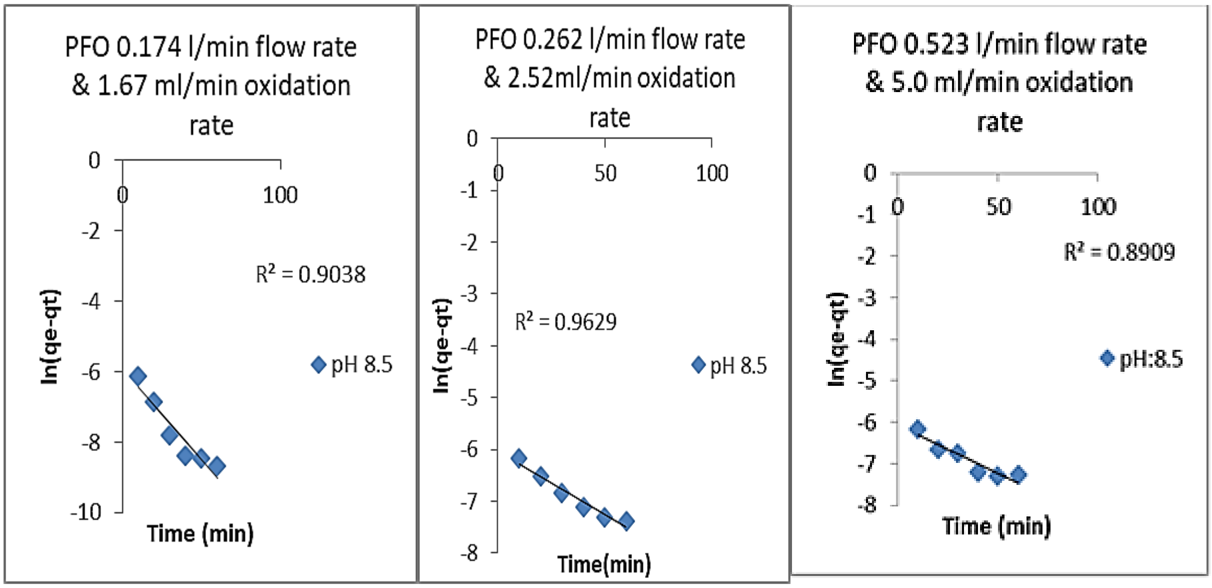

Figure 4.35 PFO linear iron at pH 8.5

4.10.1 (ii) Manganese PFO linear

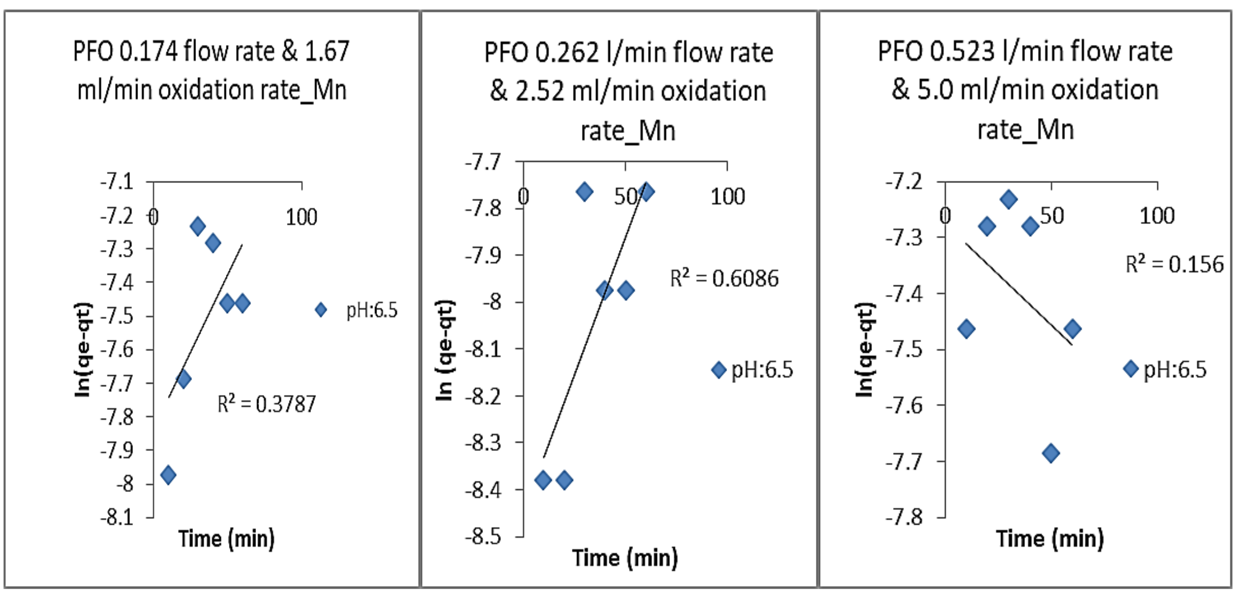

Figure 4.36 PFO linear manganese at pH 6.5

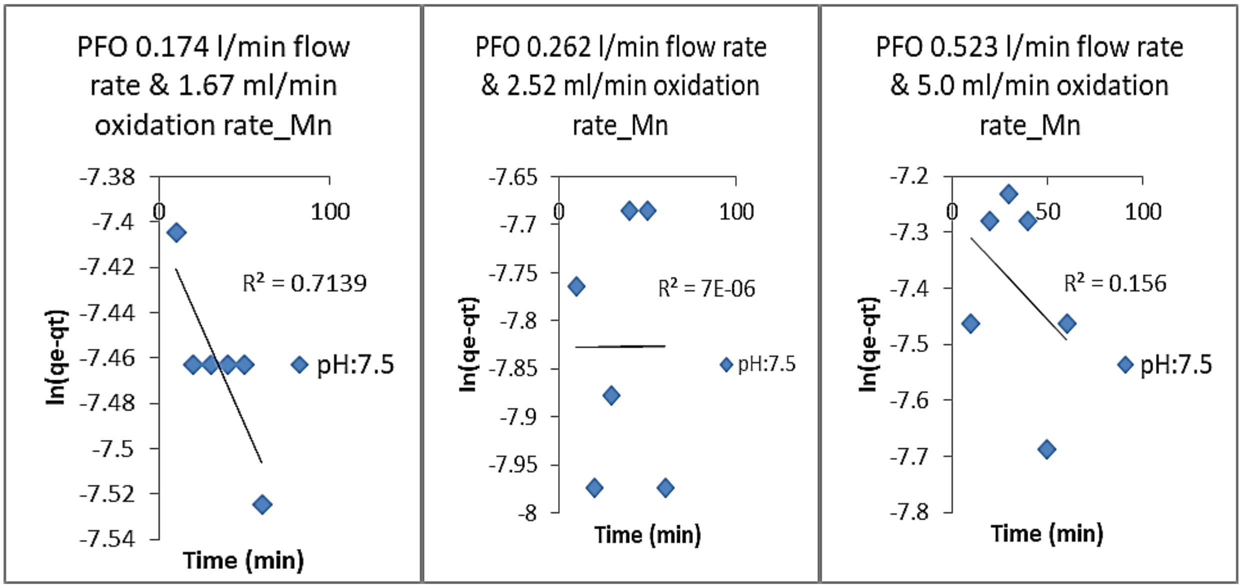

Figure 4.37 PFO linear manganese at pH 7.5

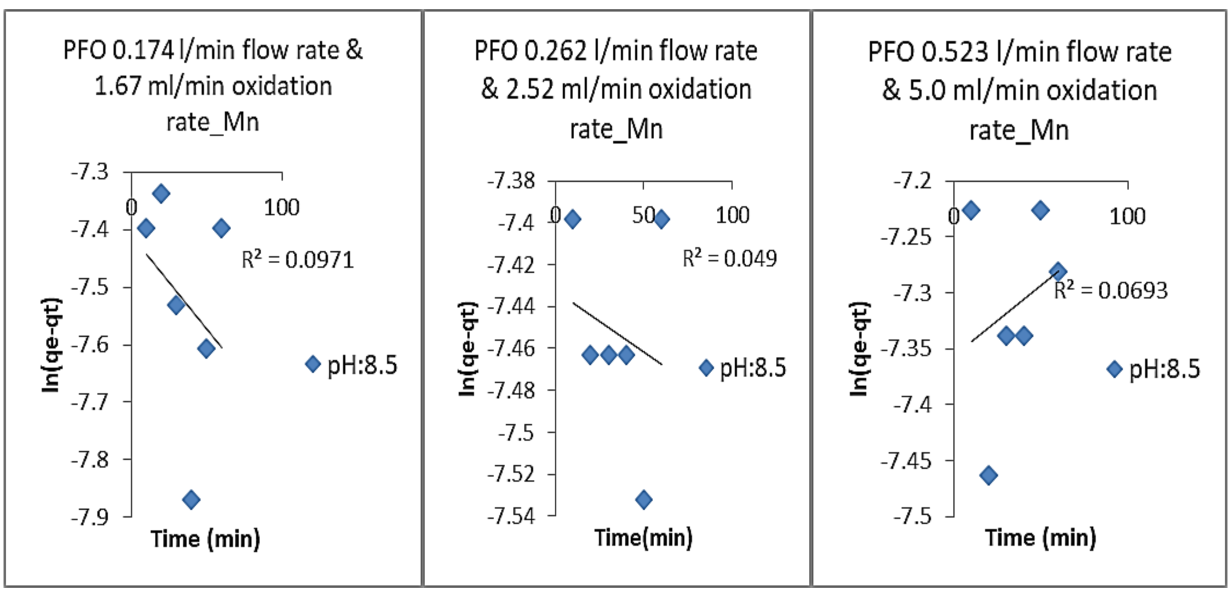

Figure 4.38 PFO linear manganese at pH 8.5

The linear graph of versus t gives the Pseudo first-order rate kinetic constant k1 and qe – the amount of adsorbate in mg/g at equilibrium, the values of the parameters are presented in table 4.4 (Iron) and 4.5 (Manganese), and the values of experimental and calculated equilibrium capacity are in disagreement. The correlation coefficients R^2 are more negligible. The observed adsorption kinetic data describes pseudo first order not fitting the data in this experiment.

4.11 Pseudo Second Order (PSO) Model

The assumption made on a PSO is that it is dependable on the vacant site and the capability of utilizing the adsorbed side (Ioannou et al., 1994).

The linearized equation presented by equation 2.7 in the literature

$$\frac{t}{q_t} = \frac{1}{k_2 q_e^2} + \frac{t}{q_e}$$

The below equation calculated the equilibrium adsorption:

$$q_t = \frac{t}{\frac{1}{k_S q_e^2 + \frac{t}{q_t}}}$$

The interception of plot t/qt vs time will aid in determining the Pseudo Second Order rate constant k_2

4.11.1 Iron PSO linear

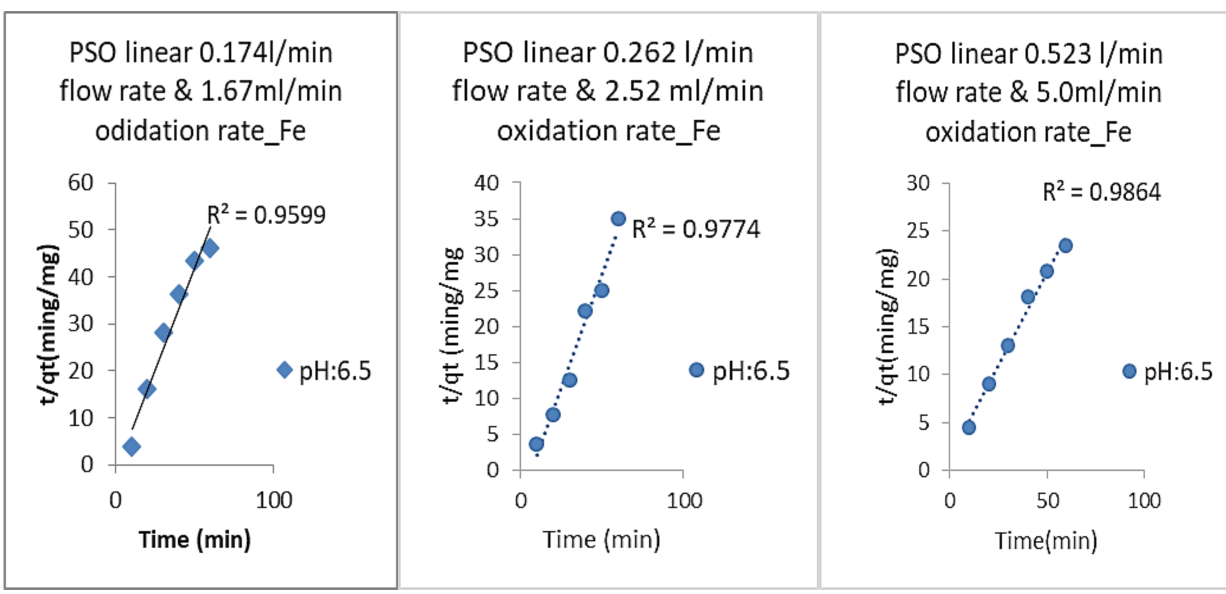

Figure 4.39 PSO linear iron at pH 6.5

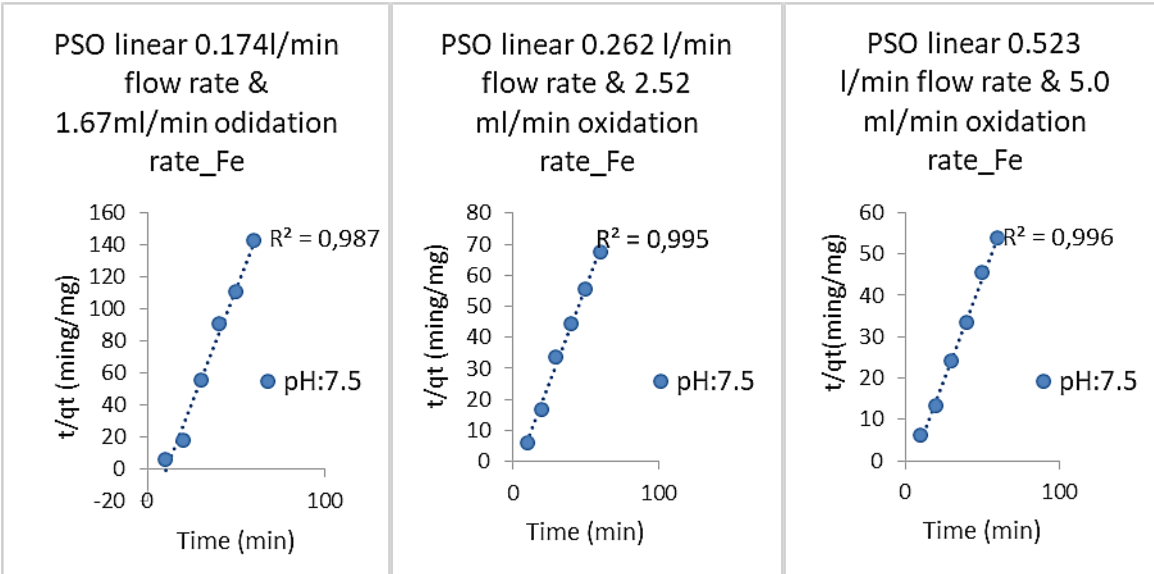

Figure 4.40 PSO linear iron at pH 7.5

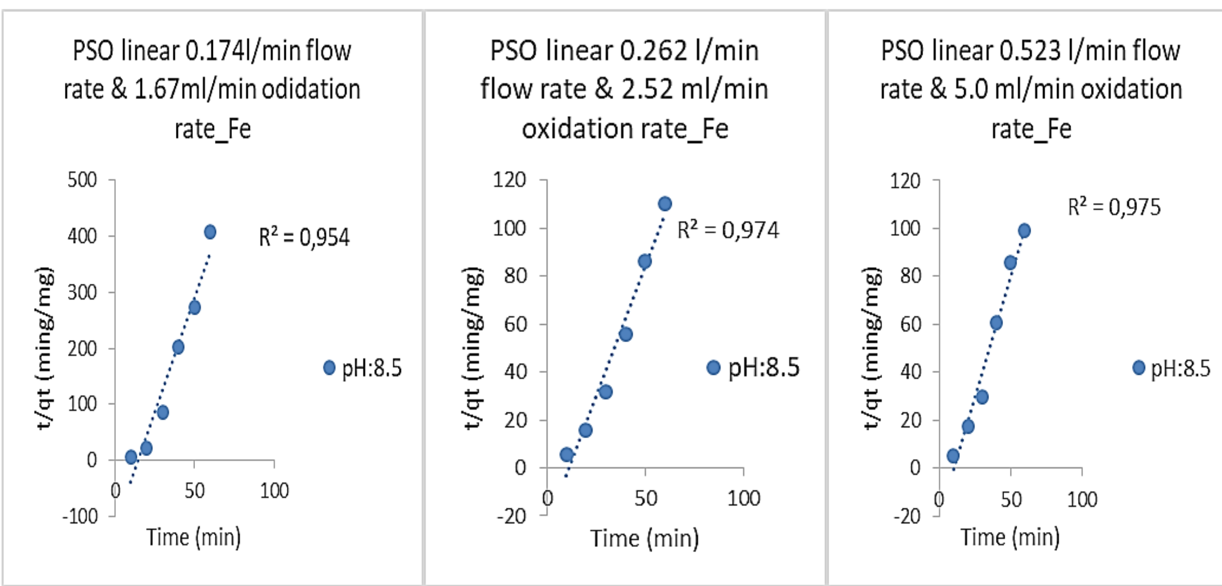

Figure 4.41 PSO linear iron at pH 8.5

4.11.2 Manganese PSO linear

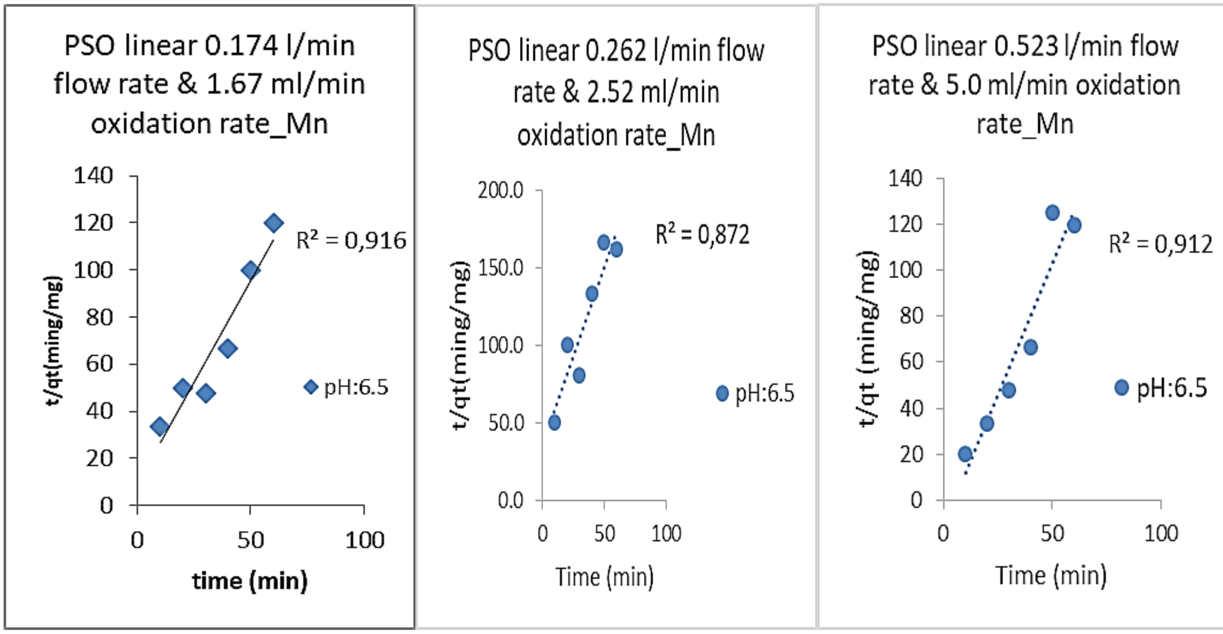

Figure 4.42 PSO linear Manganese at pH 6.5

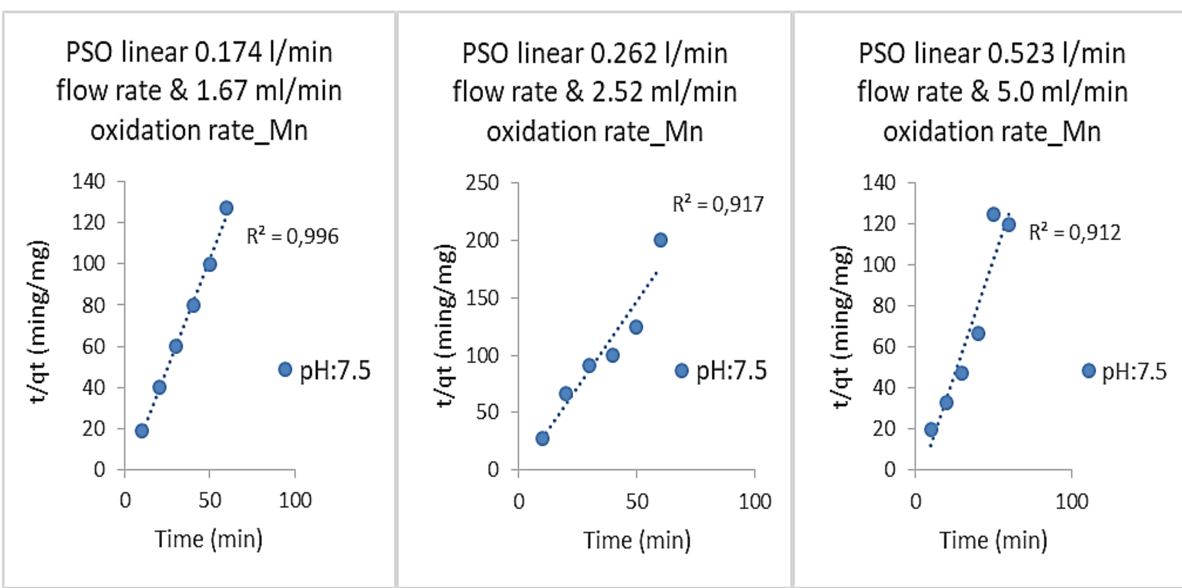

Figure 4.43 PSO linear Manganese at pH 7.5

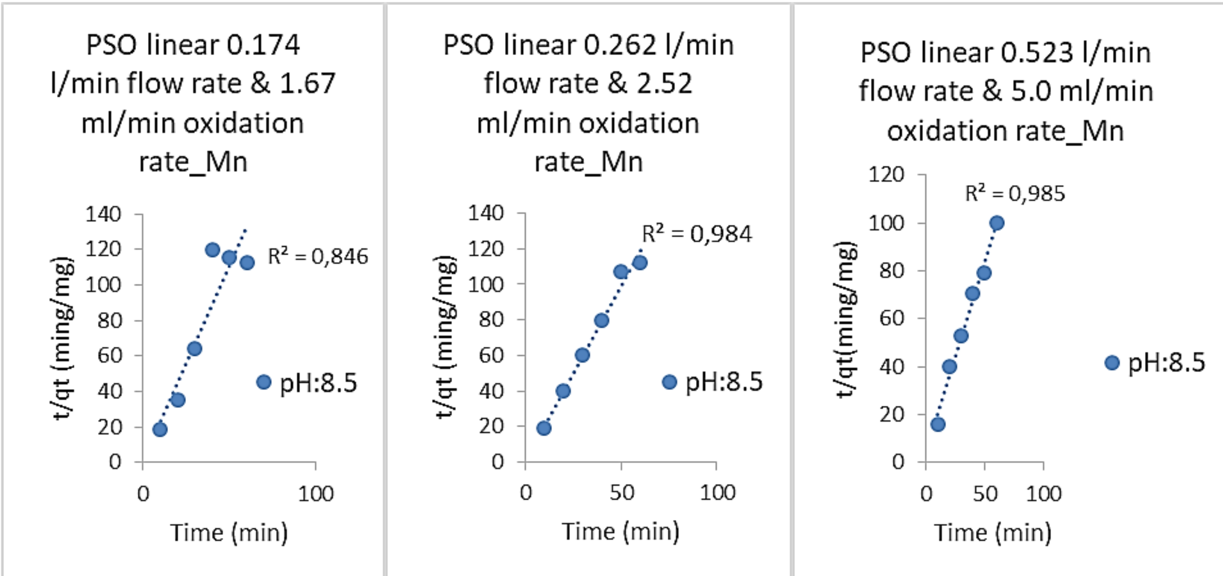

Figure 4.44 PSO linear Manganese at pH 8.5

The linear graph of t/q_t versus time gives the Pseudo second order rate kinetic constant $k_2$and q_e the amount of adsorbate in mg/g at equilibrium. The values of the parameters are presented in Table 4.4 (Iron) and 4.5 (Manganese), and the experimental and calculated equilibrium capacities are in agreement. The correlation coefficient R^2 is closer to 1 in all the runs. The observed adsorption kinetic data describes pseudo-second order more approximated in fitting the data in this experiment.

4.12 Elovich Model

The Elovich Model is assumed to be utilized to further evaluate the chemisorption in the adsorption process (Said et al., 2018).

Equation 2-9: Elovich kinetic model

$$\frac{dq_t}{d_t} = a\ exp^{\beta q_t}$$

The plot of q_t vs t determines the adsorption nature, whether chemisorption or not.

4.12.1 Iron Elovich linear

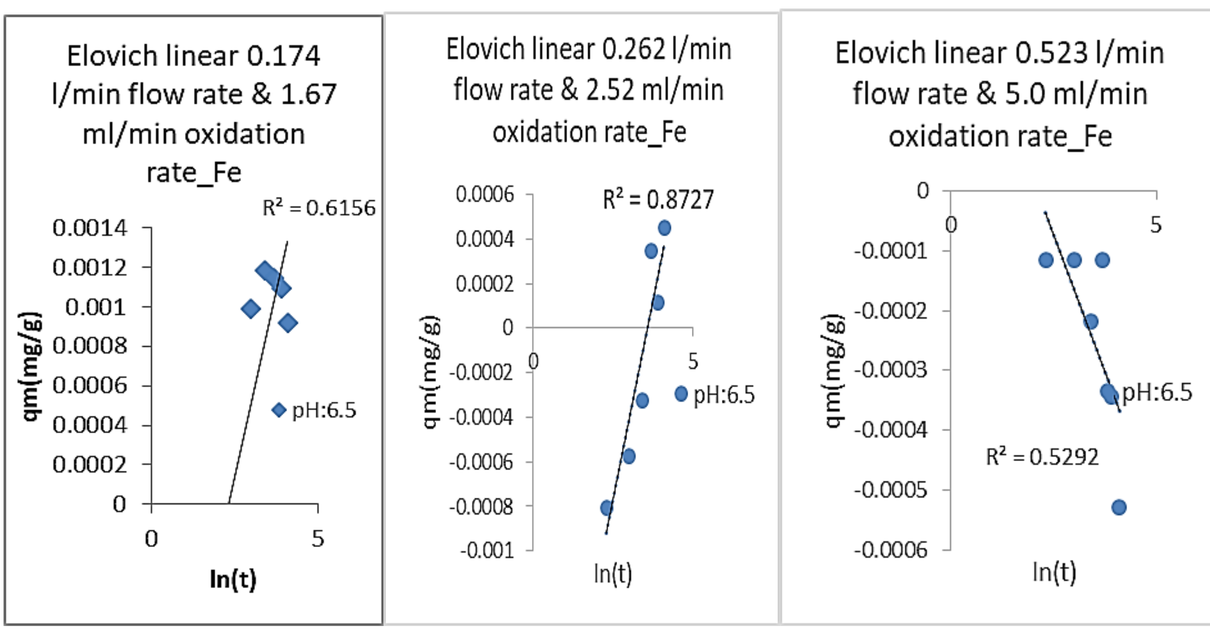

Figure 4.45Elovich linear iron at pH 6.5

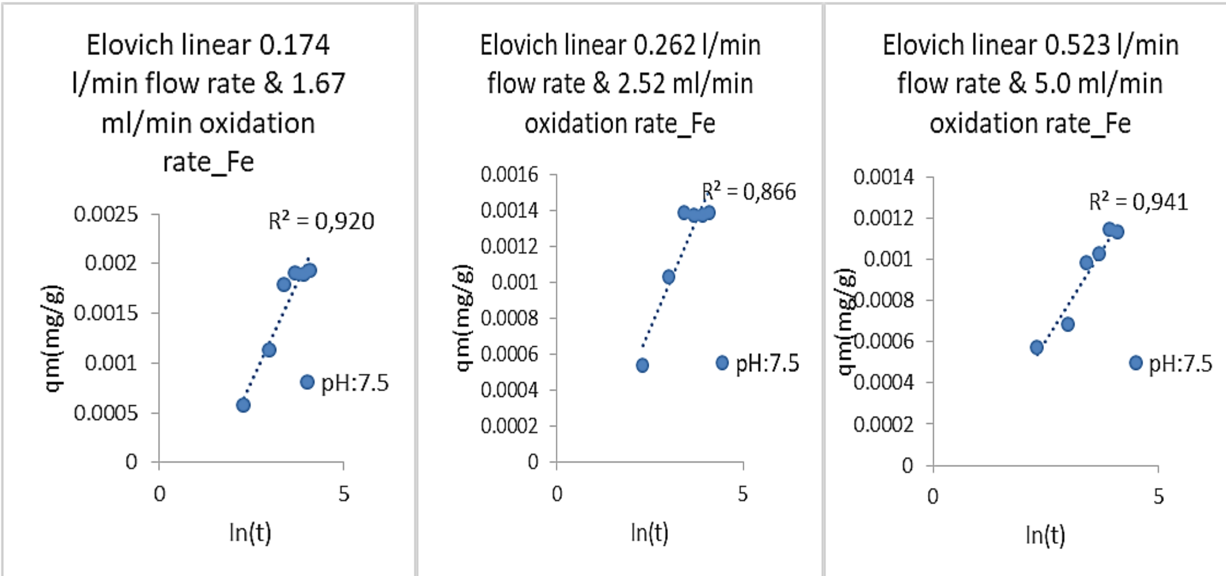

Figure 4.46Elovich linear iron at pH 7.5

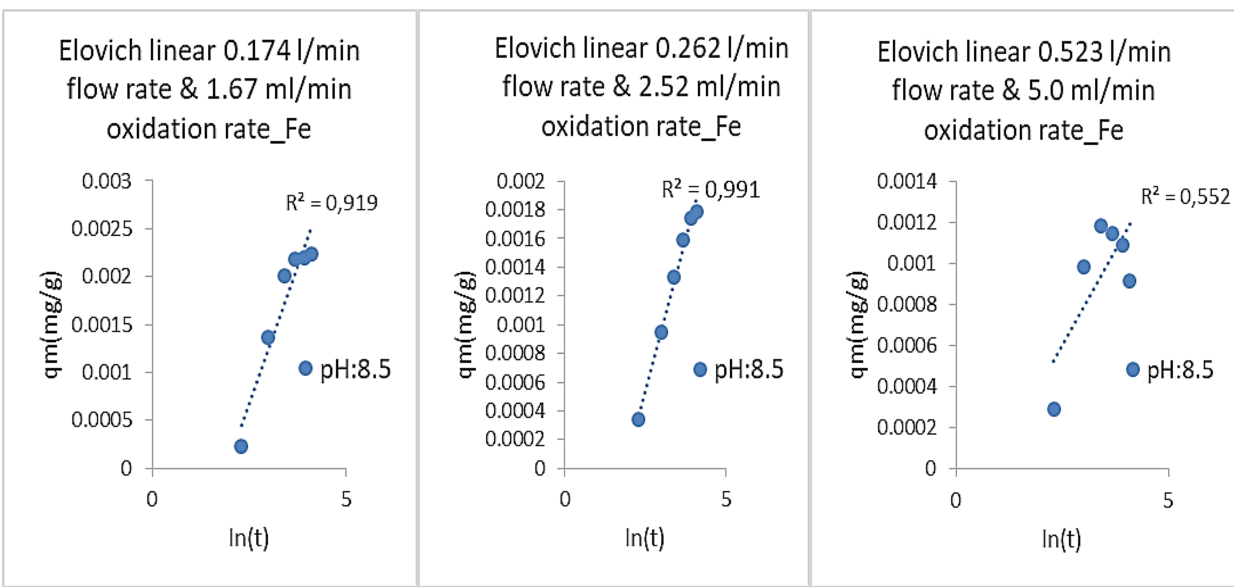

Figure 4.47Elovich linear iron at pH 8.5

4.12.2 Manganese Elovich linear

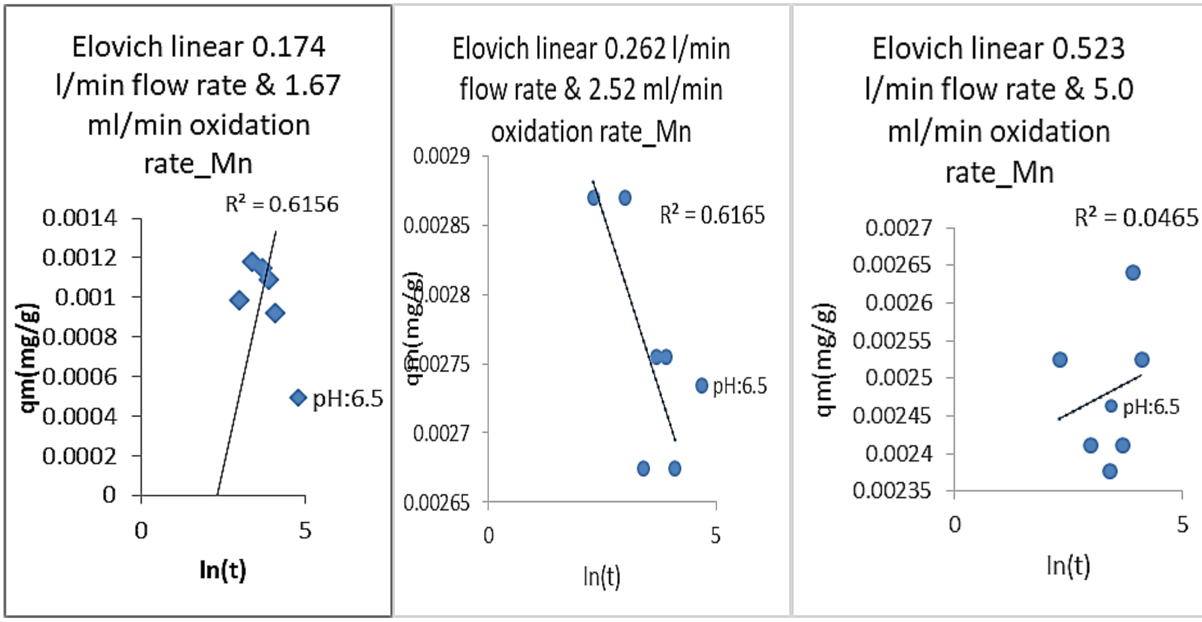

Figure 4.48Elovich linear manganese at pH 6.5

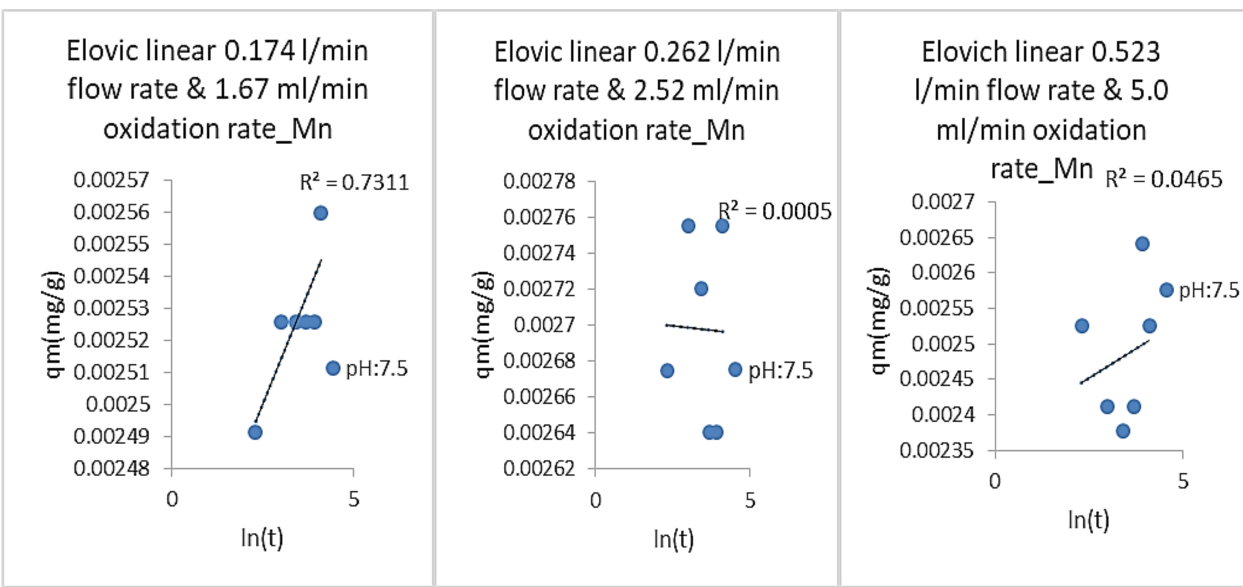

Figure 4.49 Elovich linear manganese at pH 7.5

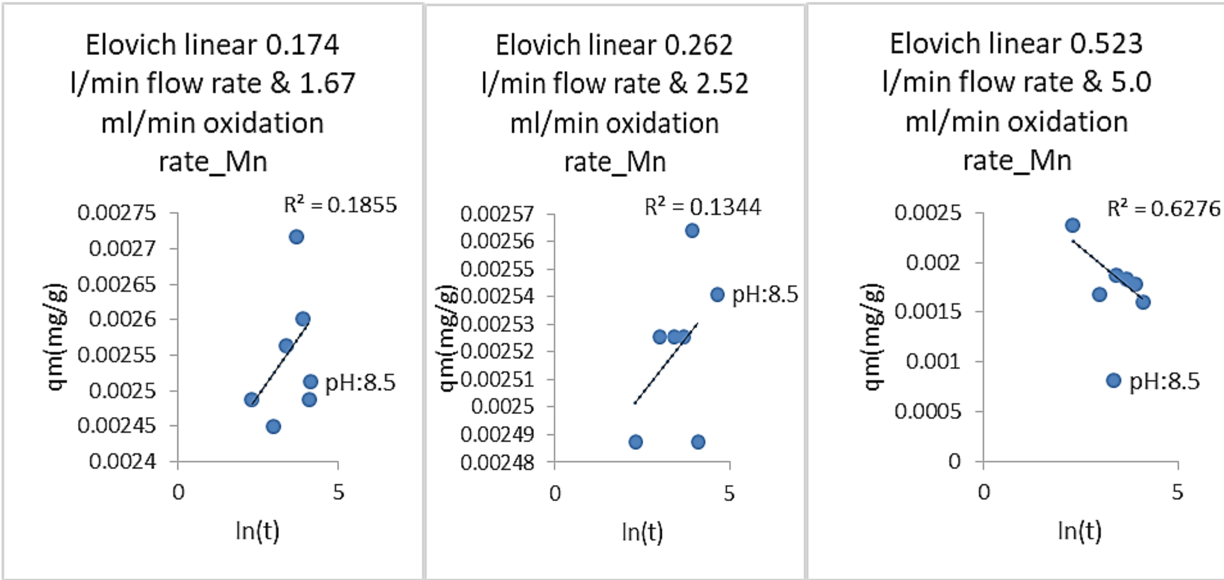

Figure 4.50 Elovich linear manganese at pH 8.5

The Elovich kinetic model considers the solid surface of the adsorbent to be energetically heterogeneous, and the influence of the desorption process and interactions between adsorbed species on adsorption kinetics are not significant (Saeidi & Parvini, 2015). The α parameter is related to the initial adsorption rate. Tables 4.4 and 4.5 show that the high values of α agree with the kinetic data indication equilibrium in 30 minutes for all experiments. The β value parameter was observed to be very low, related to low desorption between an adsorbent and the adsorbate. This observation proves the chemical bond attributed to chemisorptions under this kinetic since the desorption coefficient is very low; it shows more interaction of Fe and Mn with the Glass, Polystyrene and Ion exchange resin(Ferreira et al., 2019).

4.13 Intra-Particles Diffusion (IPD) Model

The IP model forms part of the surface adsorption mechanism by being widely applied to determine the rate-limiting step during adsorption (Ferreira et al., 2019; Roman, 2021b)**.**The below form presents the equation:

Equation 2-8: IPD equation

$$q_t = k_d t^{0.5} + C$$

4.13.1 Iron IP linear

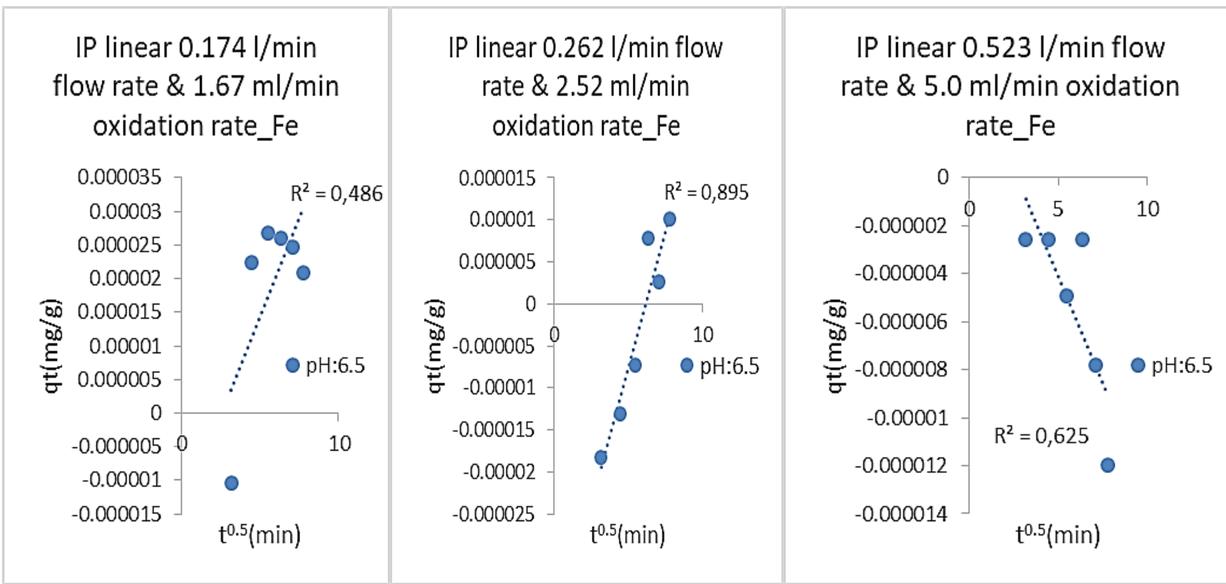

Figure 4.51 IP linear iron at pH 6.5

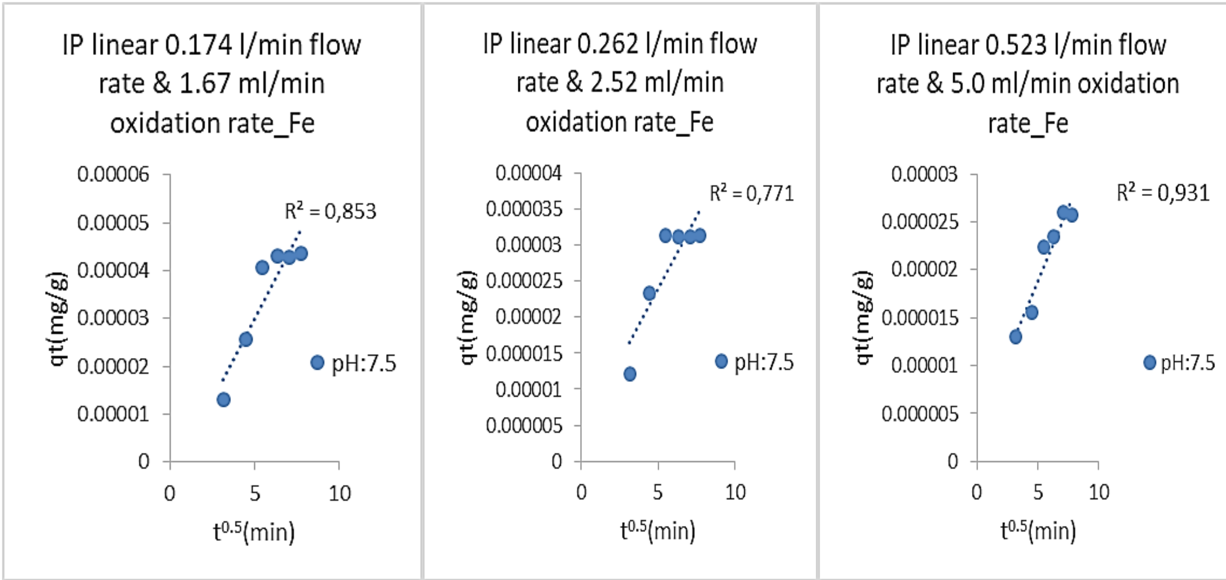

Figure 4.52 IP linear ironat pH 7.5

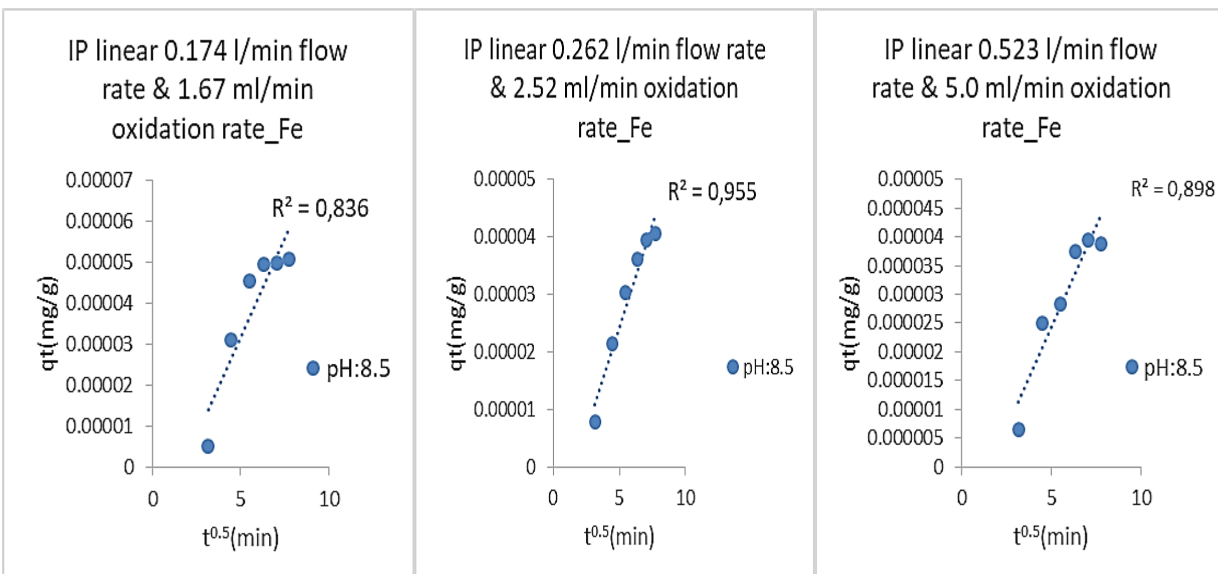

Figure 4.53 IP linear iron at pH 8.5

4.13.2 Manganese IP linear

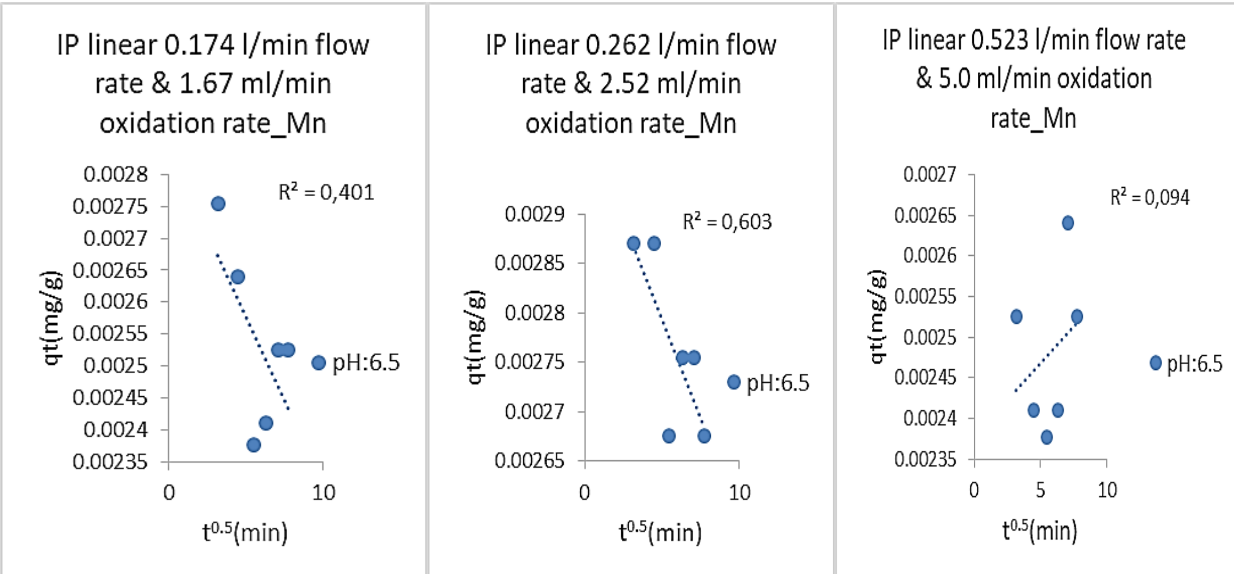

Figure 4.54 IP linear manganese at pH 6.5

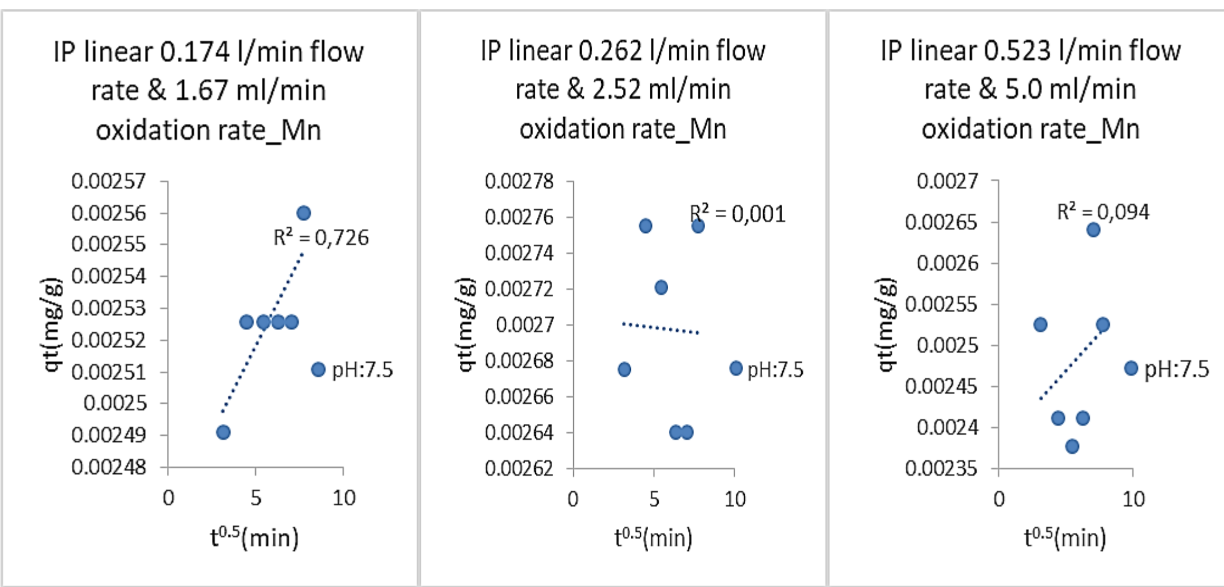

Figure 4.55 IP linear manganese at pH 7.5

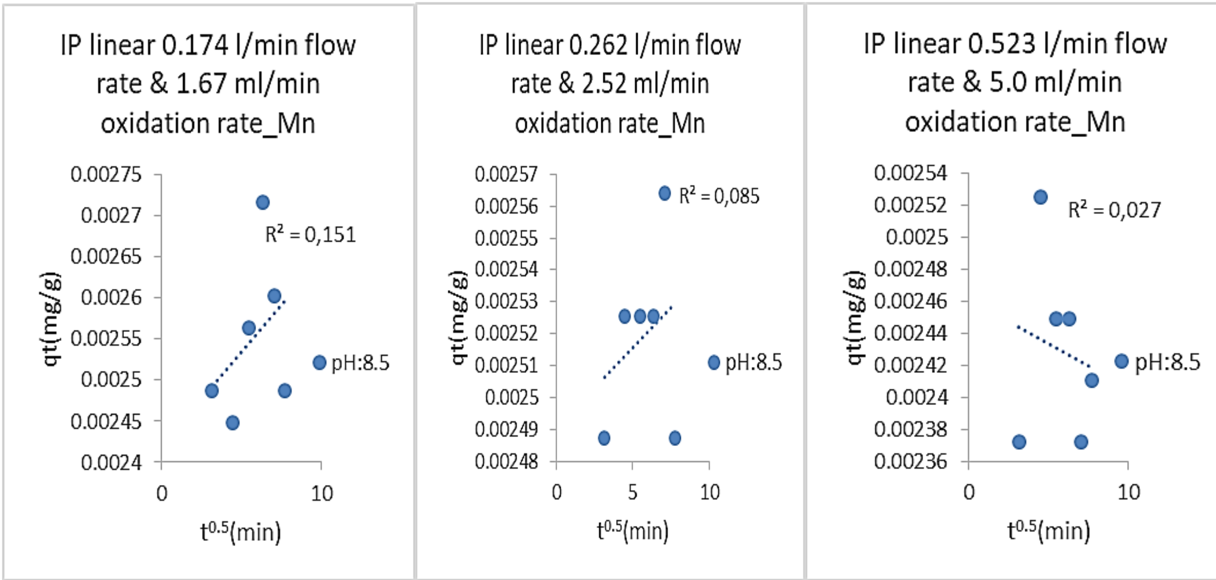

Figure 4.56 IP linear manganese at pH 8.5

K_{diff} is the intra-particle diffusion rate constant (mg/g min$^{1/2}$), and C is the boundary layer thickness. The plot of q_t vs $t^{1/2}$ gives a linear function. Stated in the literature that the plot structure and the linearity of the IP graph are the main fundamental assessment criteria in determining whether the IP controls the diffusion process or not in the system; if the plot line is through the origin, it means IP is in the effect of the process, if it does not pass through the origin it means other mechanisms are in charge of the adsorption process (Roman, 2021b). Observing the IP plots above and the R^2 presented by table 4.4 (Fe) and 4.4 (Mn) for both metal ion diffusion, it's noted that intra-particle diffusion is not the rate-limiting step. This might fall to another mechanism; those mechanisms involve the mass solute transfer after the adsorbent is placed in the solution. This film diffusion is the slow movement of solutes from the boundary layer and the penetration of the solute to the adsorbent pores.

Table 4:4 Iron linear adsorption kinetics constants

Iron (Fe)									
RUNS	1	2	3	4	5	6	7	8	9
pH	6.5			7.5			8.5		
Flow rate (l/min)	0,174 (l/min)	0,262 (l/min)	0,523 (l/min)	0,174 (l/min)	0,262 (l/min)	0,523 (l/min)	0,174 (l/min)	0,262 (l/min)	0,523 (l/min)
PFO									
qe exp (mg/g)	8.11E-04	-1.32E-04	-2.39E-04	1.54E-03	1.18E-03	9.28E-04	1.71E-03	1.29E-03	1.29E-03
qe cal (mg/g)	0.990	0.990	1.003	0.973	0.989	0.992	0.949	0.976	0.977
b (min^{-1})	-0.0002	-0.0002	0.00005	-0.0005	-0.0002	-0.0001	-0.0009	-0.0004	-0.0004
R^2	0.338	0.687	0.713	0.818	0.687	0.902	0.904	0.963	0.891
PSO									
qe exp (mg/g)	2.10	1.60	2.60	0.35	0.81	1.02	0.12	0.46	0.50
qe cal (mg/g)	1.16	2.49	2.28	0.52	1.05	2.30	0.16	0.10	0.74
ks (g/mg min)	-0.68	-0.09	0.11	-0.28	-0.25	-0.19	-0.56	-0.19	-0.20
R^2	0.96	0.98	0.99	0.99	1.00	1.00	0.95	0.97	0.98
IPD									
K_{diff}(mg/g.min$^{0.5}$)	5.86E-06	6.44E-06	-1.77E-06	6.90E-06	4.05E-06	3.09E-06	9.65E-06	7.28E-06	7.04E-06
C (mg/g)	-0.0000151	-0.0000398	0.0000047	-0.0000045	0.0000037	0.0000034	-0.0000164	-0.0000123	-0.0000109
R^2	0.487	0.895	0.626	0.854	0.772	0.932	0.837	0.956	0.898
Elovich									
α (mg/g.min)	1340.155206	1.39E+03	-5.42E+03	1.23E+03	2.06E+03	2.84E+03	8.73E+02	1.19E+03	2.69E+03
β(g/mg)	7.39E-05	2.00E-05	-	1.81E-04	1.86E-04	1.64E-04	1.70E-04	1.31E-04	1.54E-04
R^2	6.16E-01	8.73E-01	5.29E-01	0.920	0.867	0.942	0.920	0.991	0.552

The kinetic models explored for testing experimental data were Pseudo-first order (PFO), pseudo-second-order (PSO), intra-particles diffusion (IPD) and Elovich model; their parameters and constants for both metal ions Fe (II) and Mn (II) are presented in Table 4.2& 4.3 respectively. The kinetics models were investigated in linear forms, as seen in tables 4.4 (Fe) & 4.5 (Mn). Assessing all the kinetic models, PSO indicated best fitted the data, observed by the proximity of the experimental and calculated adsorption capacity, also the R^2 values equal to 1 in most runs, as compared to all other kinetics tested in this experiment (Ioannou et al., 1994; Saeidi & Parvini, 2015). This finding describes the chemisorption that's taking place in the process and confirms that the tri-medium used can be a multilayer. Elovich's model supports the chemisorption, which is seen by the β value parameter observed to be very low, which is related to low desorption between an adsorbent and the adsorbate. The PFO kinetics rejected the data by showing very low experimental and calculated adsorption capacity and R^2 values.

Intra-particle diffusion is assumed to be used to determine the rate-controlling step, and it's said to be judged by the plot between qt vs $t^{1/2}$ passing through the origin to deem this model as an effect on the process. However, as seen in the plots, the various data point on the graphs illustrate that the IPD has no impact on limiting the rate of adsorption of Fe and Mn(Said et al., 2018).

Table 4:5Manganese linear adsorption constants

Manganese (Mn)									
RUNS	1	2	3	4	5	6	7	8	9
pH	6.5			7.5			8.5		
Flow rate (l/min)	0,174 (l/min)	0,262 (l/min)	0,523 (l/min)	0,174 (l/min)	0,262 (l/min)	0,523 (l/min)	0,174 (l/min)	0,262 (l/min)	0,523 (l/min)
PFO									
qe_{exp} (mg/g)	2.54E-03	2.77E-03	2.48E-03	2.53E-03	2.70E-03	2.48E-03	2.55E-03	2.52E-03	2.43E-03
qe_{cal} (mg/g)	3.96E-04	2.15E-04	6.93E-04	6.09E-04	3.99E-04	6.93E-04	6.06E-04	5.92E-04	2.09E-05
b (min^{-1})	0.0002	1.94E-04	-6.02E-05	-2.86E-05	3.25E-07	-6.02E-05	-5.43E-05	-9.86E-06	2.09E-05
R^2	0.379	0.609	0.156	0.714	7.42E-06	0.156	0.097	0.049	0.069
PSO									
qe_{exp} (mg/g)	0.5810	0.4305	0.4408	0.4705	0.3337	0.4408	0.4577	0.5071	0.6300
qe_{cal} (mg/g)	0.4822	0.2839	0.5354	0.4740	0.3339	0.5354	0.4475	0.4998	0.5716
k_s (g/mg min)	0.3163	0.1576	-0.4840	-1.3659	-2.7259	-0.4840	3.8850	5.4440	0.6061
R^2	0.9166	0.8721	0.9124	0.9968	0.9177	0.9124	0.8461	0.9845	0.9852
IPD									
K_{diff}(mg/g.min$^{0.5}$)	-5.28E-05	-4.01E-05	1.81E-05	1.09E-05	-9.99E-07	1.81E-05	2.26E-05	4.96E-06	-5.67E-06
C (mg/g)	0.0028403	0.0029956	0.0023780	0.0024633	0.0027035	0.0023780	0.0024218	0.0024910	0.0024623
R^2	0.401	0.604	0.095	0.727	0.001	0.095	0.716	0.086	0.028
Elovich									
α (mg/g.min)	- 6619.809885	-9.62E+03	3.07E+04	3.56E+04	-5.36E+05	3.07E+04	1.56E+04	6.28E+04	-3.09E+03
β(g/mg)		0.00E+00	1.19E+27	9.93E+32		1.19E+27	3.82E+11	2.44E+62	
R^2	5.00E-01	6.17E-01	4.65E-02	0.731	0.001	0.047	0.186	0.134	0.628

4.14 Non-linear Adsorption Isotherms

The use of non-linear analysis avoids errors raised by different estimates resulting from simple linear regression of the linearised forms of Langmuir, Freundlich, Temkin and D-R equation, which can affect R^2 values significantly. The non-linear analysis is an acceptable method used. It is a fascinating way to describe adsorption isotherms used for many applications, such as water treatment (M. Hamzaoui, B. Bestani, 2018).

4.14.1 Iron non-linear adsorption isotherms

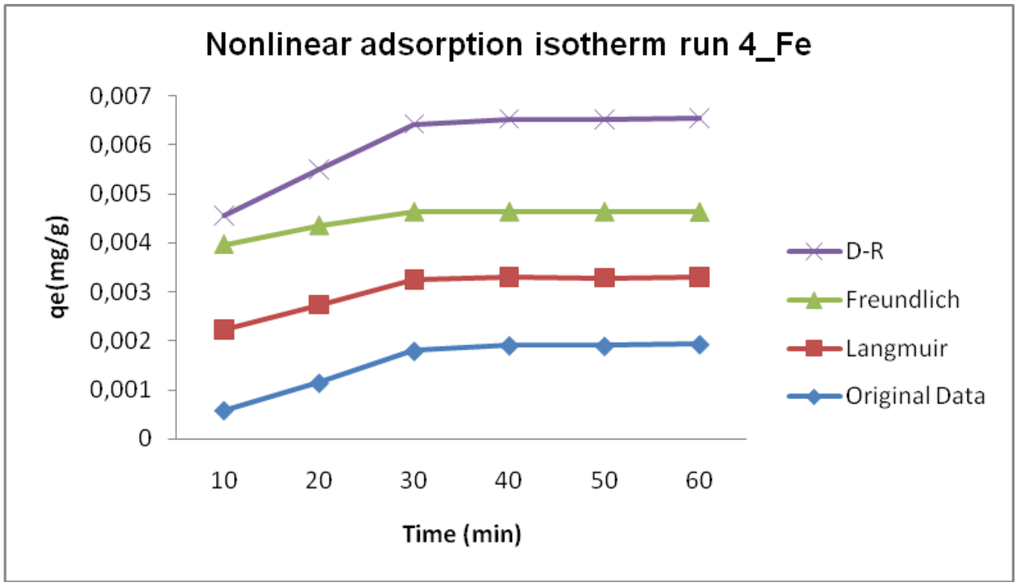

Figure 4.57Non-linear adsorption isotherm run 4_pH 7.5

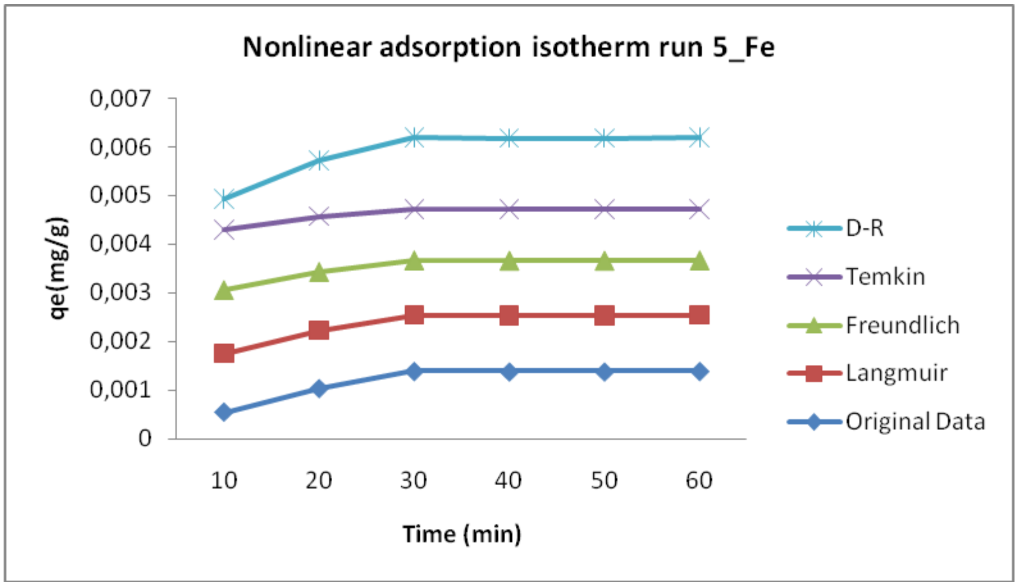

Figure 4.58Non-linear adsorption isotherm run 5_pH 7.5

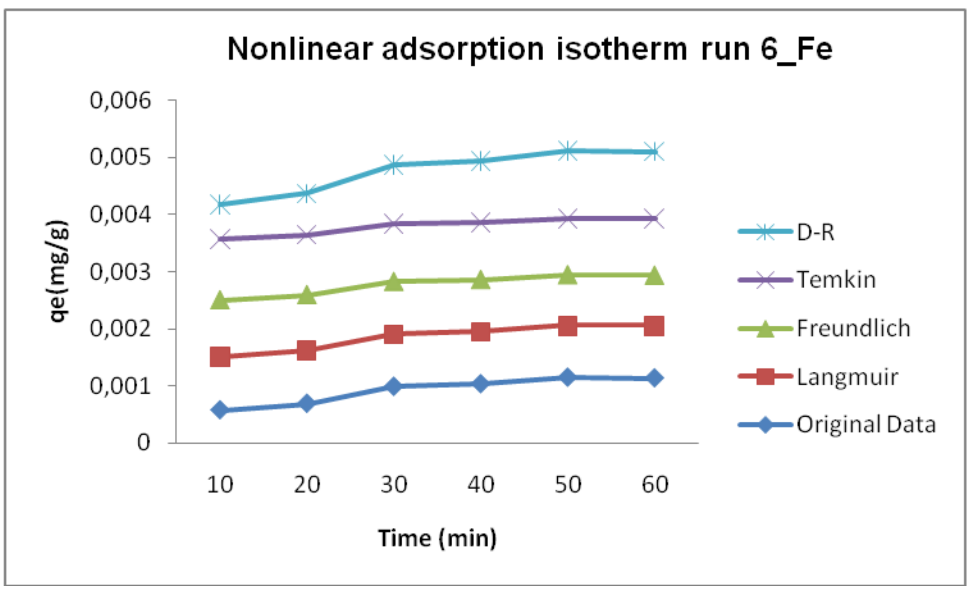

Figure 4.59Non-linear adsorption isotherm run 6_pH 7.5

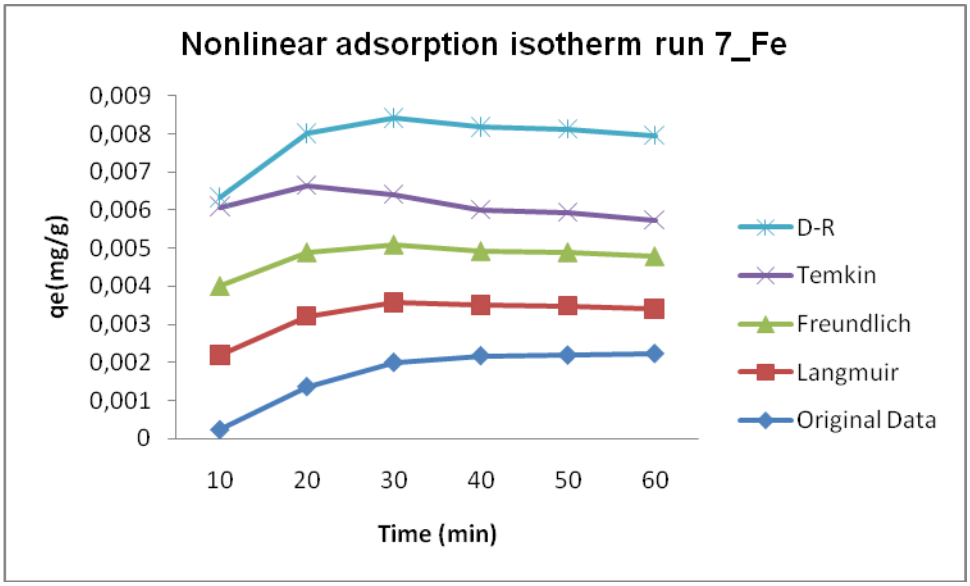

Figure 4.60Non-linear adsorption isotherm run 4_pH 8.5

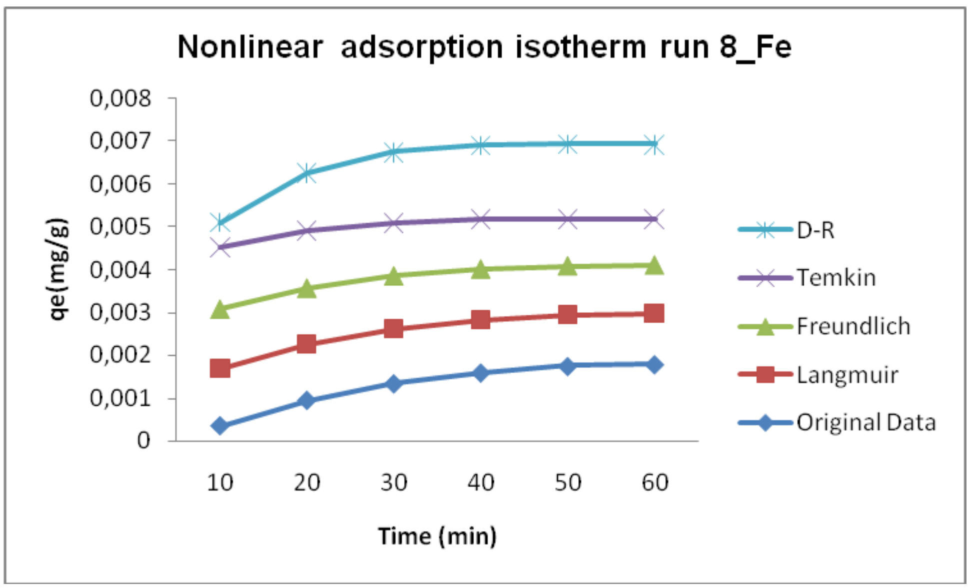

Figure 4.61Non-linear adsorption isotherm run 8_pH 8.5

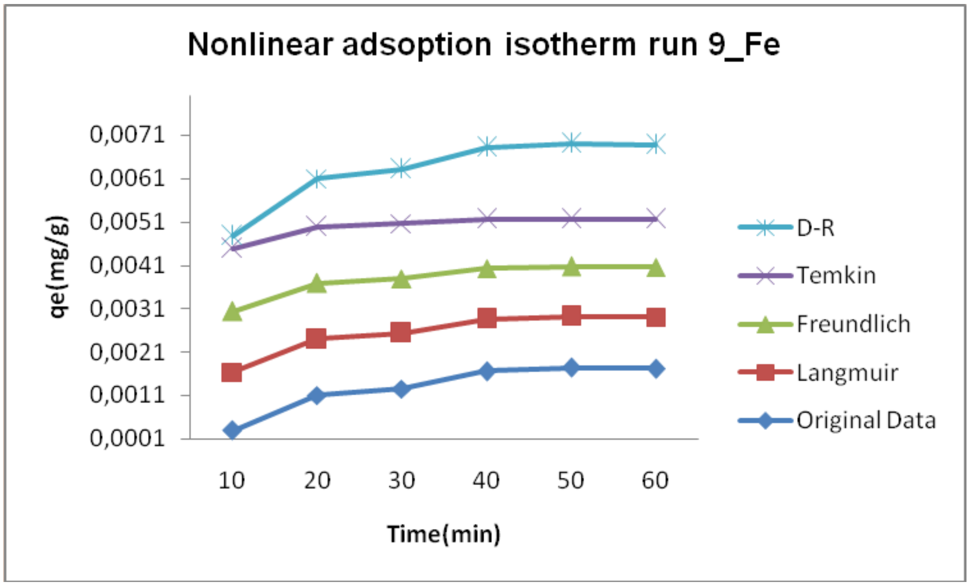

Figure 4.62Non-linear adsorption isotherm run 4_pH 8.5

4.14.2 Manganese non-linear adsorption isotherms

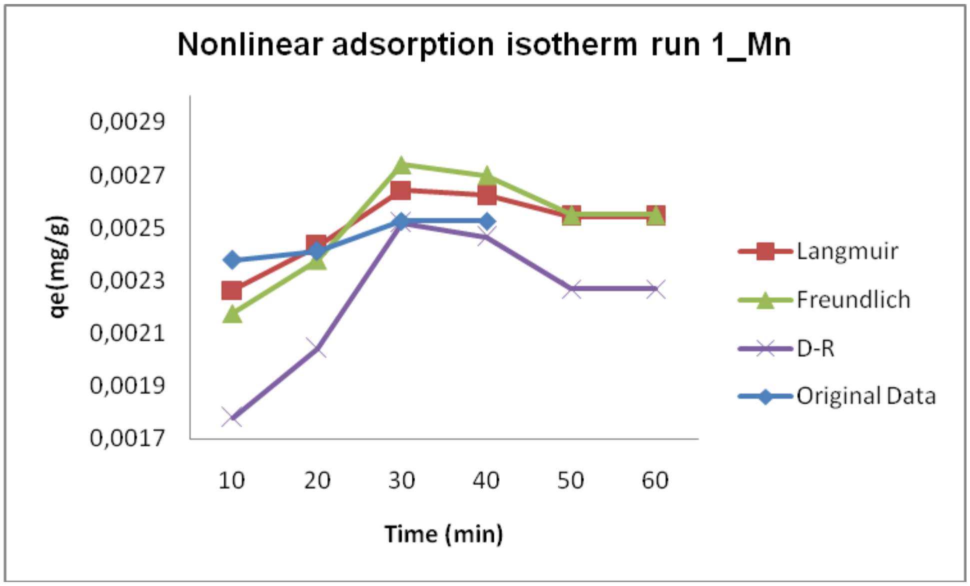

Figure 4.63Non-linear adsorption isotherm run 1_pH 6.5

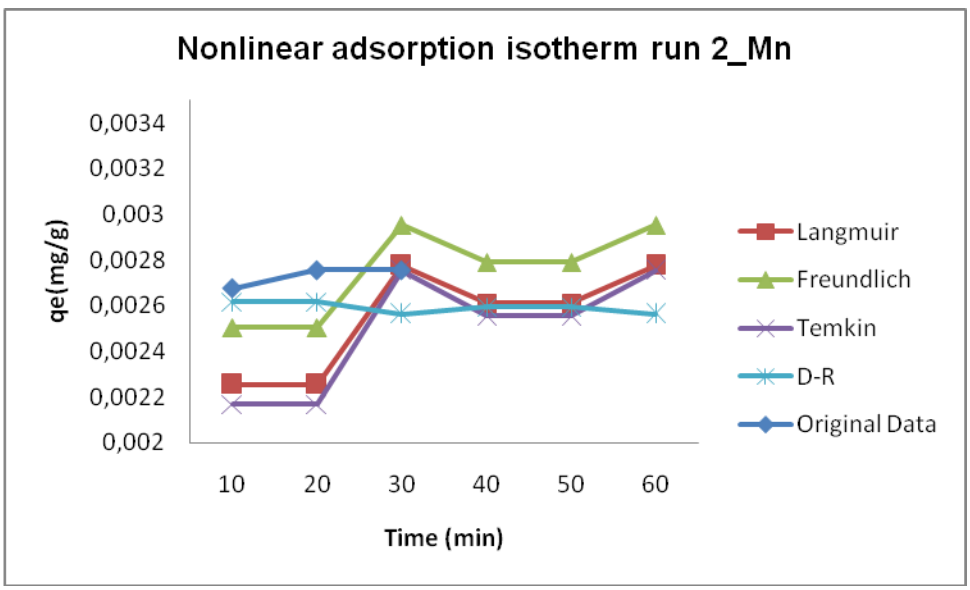

Figure 4.64Non-linear adsorption isotherm run 2_pH 6.5

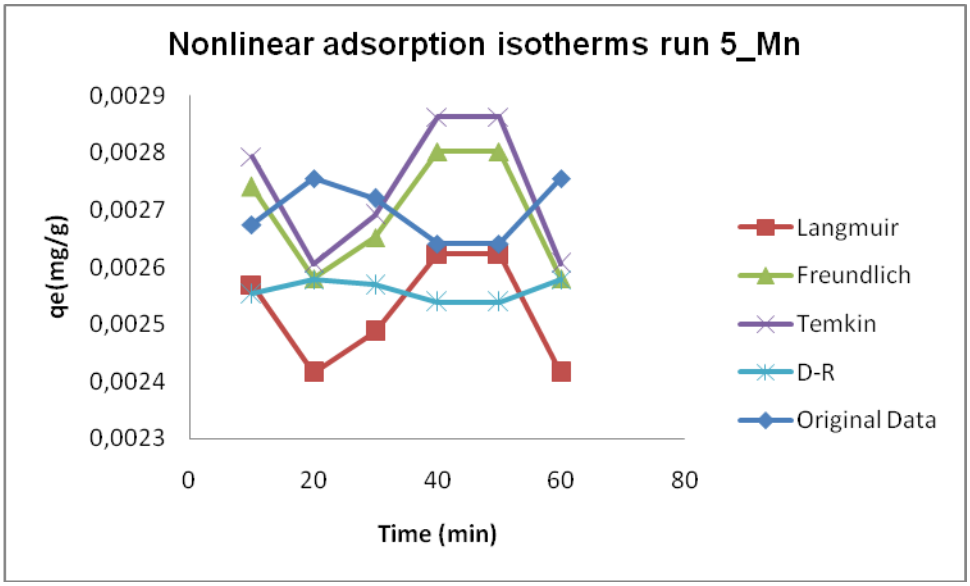

Figure 4.65Non-linear adsorption isotherm run 5_pH 7.5

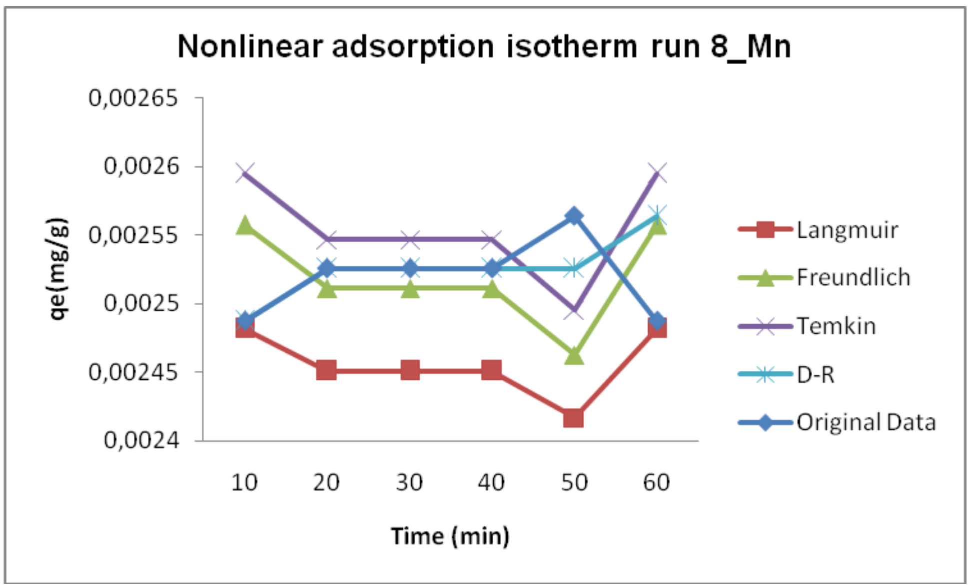

Figure 4.66Non-linear adsorption isotherm run 8_pH 8.5

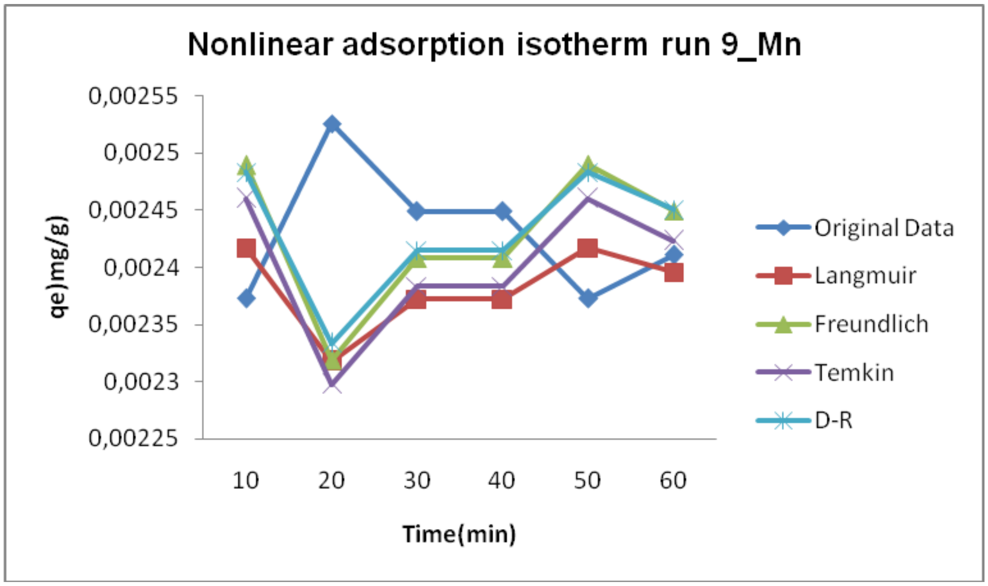

Figure 4.67Non-linear adsorption isotherm run 9_pH 8.5

Table 4:6 Non-linear adsorption constants

Iron (Fe)									
RUNS	1	2	3	4	5	6	7	8	9
pH	6,5			7,5			8,5		
Flow rate (l/min)	0,174 (l/min)	0,262 (l/min)	0,523 (l/min)	0,174 (l/min)	0,262 (l/min)	0,523 (l/min)	0,174 (l/min)	0,262 (l/min)	0,523 (l/min)
Langmuir Isotherm									
q_{max} (mg/g)	8,68E-04	-1,43E-04	-2,51E-04	1,77E-03	1,30E-03	1,00E-03	2,07E-03	1,43E-03	1,43E-03
b(L/g)	6,270	7,260	7,850	8,110	8,580	8,720	8,730	8,980	7,980
R_L	0,071	0,062	0,057	0,055	0,053	0,052	0,052	0,050	0,056
R^2	0,721	0,985	0,574	0,076	0,491	0,625	0,630	0,174	0,198
Freundlich Isotherm									
KF (mg/g)	7,15E-04	-1,26E-04	-1,98E-04	1,59E-03	1,15E-03	8,67E-04	1,71E-03	1,26E-03	1,26E-03
n	4,280	3,950	3,220	4,880	4,010	3,480	9,280	6,250	5,680
R2	0,756	0,981	0,507	0,217	0,346	0,539	0,500	0,291	0,300
Temkin Isotherm									
BT (J/mol)	-3,42E+01	5,82E+01	5,82E+01	1,22E+01	4,90E+01	9,20E+01	3,82E+01	4,21E+01	3,33E+01
AT(L/g)	-5,37E+07	-3,09E-05	4,01E-06	2,22E+03	2,84E-04	2,13E-04	4,43E-04	4,01E-06	4,01E-06
R2	0,835	0,982	0,570	-	0,279	0,591	0,771	0,402	0,387
D-R Isotherm									
qm (mg/g)	2,68E-08	1,95E-08	5,85E-08	1,10E-06	3,74E-07	1,37E-07	1,10E-06	4,81E-07	4,81E-07
β (mol2/K2/J2)	1,65E-05	1,40E-06	3,12E-05	3,20E-06	4,21E-05	1,31E-05	1,70E-06	1,32E-04	1,70E-06
R2	0,993	1,000	0,805	1,000	0,974	0,974	1,000	0,996	1,000

The adsorption isotherms used to assess the tri-medium system for removing iron and manganese were Langmuir, Freundlich, Temkin and D-R. The parameter constants and the error functions were determined individually for each metal ion to choose the model suitable to describe the system when iron or manganese is treated. These metal ions behaved differently under the set conditions of 0.174, 0.262 & 0.523l/min flow rate, with pH of 6.5, 7.5 & 8.5 and 10-60 minutes contact time. The findings from Figures4.57 to 4.62 represent the system's adsorption isotherms for iron removal behaviour; under the above conditions, Freundlich seemed to be the best-fit isotherm. The D-R isotherms follow closely on the Freundlich isotherm for iron removal, while Langmuir and Temkin's isotherms did not fit the data well. This can be seen in tables 4.6 (Fe) & 4.7 (Mn), where Freundlich and D-R isotherms have R^2 values closest to 1 across all conditions. While manganese is presented in Figures4.63 to 4.67, across all the set requirements, this metal ion data favoured Freundlich and Temkin isotherms, observed from R^2 values of 0.99. Still, the Langmuir and D-R seemed to lose a grip under these conditions for removing manganese by a tri-medium system. Another methodology applied to evaluate the best isotherms was the error analysis; Tables 4.10, 4.11 & 4.12 present SSE, SAE & ARE for iron data. The Langmuir isotherm was observed to have fewer errors than other isotherms, and Tables 4.13, 4.14 & 4.15 presented the error analysis for manganese. It was noticed that the SSE, SAE & ARE Freundlich isotherm was observed to be the best fit by having minimum errors compared to other isotherms. A study performed by (Osuagwu et al., 2018), where the removal of iron from aqueous solutions using expanded polystyrene beads was studied, found that the data fitted the Freundlich isotherm better than Langmuir and a study performed by (Bekri-Abbes et al. 2006), optimization of reaction parameters and properties. The study found the data best fitted to the Freundlich isotherm, which agrees with the findings of this study. However, the analysis performed by (Ozturk & Silah, 2020) investigated the adsorption of iron, ammonia and manganese by macroporous and found the data to fit the Langmuir isotherm best. From these observations, Freundlich seemed to be the most favourable, which means that the tri-medium has a multilayer capability supported by n values greater than 1 ($n>1$), which confirms the physical attraction of the solutes.

Table 4:7 Non-linear adsorption constants (Mn)

Manganese (Mn)									
RUNS	1	2	3	4	5	6	7	8	9
pH	6,5			7,5			8,5		
Flow rate (l/min)	0,174 (l/min)	0,262 (l/min)	0,523 (l/min)	0,174 (l/min)	0,262 (l/min)	0,523 (l/min)	0,174 (l/min)	0,262 (l/min)	0,523 (l/min)
Langmuir Isotherm									
q_{max} (mg/g)	3,11E-03	3,82E-03	2,98E-03	3,07E-03	3,53E-03	2,98E-03	3,13E-03	3,06E-03	2,88E-03
b(L/g)	8,890	7,220	9,262	7,250	7,190	8,590	9,210	8,080	8,230
R_L	0,040	0,049	0,038	0,049	0,049	0,041	0,039	0,044	0,043
R^2	0,936	0,874	0,975	0,984	0,953	0,972	0,970	0,994	0,990
Freundlich Isotherm									
K_F (mg/g)	3,16E-03	3,85E-03	3,05E-03	3,05E-03	3,64E-03	2,95E-03	3,09E-03	3,06E-03	2,86E-03
n	3,220	3,740	2,990	3,660	3,490	3,570	3,860	3,520	3,330
R2	0,902	0,944	0,953	0,998	0,983	0,961	0,961	0,997	0,987
Temkin Isotherm									
B_T (J/mol)	-5,10E-04	-3,13E-04	-5,84E-04	-5,73E-04	-3,99E-04	-5,84E-04	-5,03E-04	-5,76E-04	-6,51E-04
AT(L/g)	-34,22	49,00	59,20	0,15	61,20	58,16	57,60	61,00	56,00
R2	-	0,826	0,960	1,000	0,979	0,959	0,951	0,996	0,987
D-R Isotherm									
qm (mg/g)	2,03325E-09	1,43426E-08	3,5242E-09	6,77601E-10	5,10195E-09	3,5242E-09	2,24235E-09	1,37707E-09	2,33258E-08
β (mol2/K2/J2)	0,00023	0,000032	0,0000025	0,0000321	0,000035	0,00037	0,000014	1,02E-09	0,00017
R2	0,896	0,990	1,000	0,999	0,984	0,984	0,999	1,000	0,991

4.15. Non-linear Adsorption Kinetic Models

The experimental data was plotted using excel software. The analysis results are found in Figures 4.67 to 4.80 for both Fe and Mn and Tables 4.8& 4.9. The data were fitted to pseudo-first-order (PFO), pseudo-second-order (PSO), intra-particle diffusion (IP) and Elovich kinetic to determine the best fit kinetic and compare the findings to that of linear regression.

4.15.1 Iron non-linear adsorption kinetics

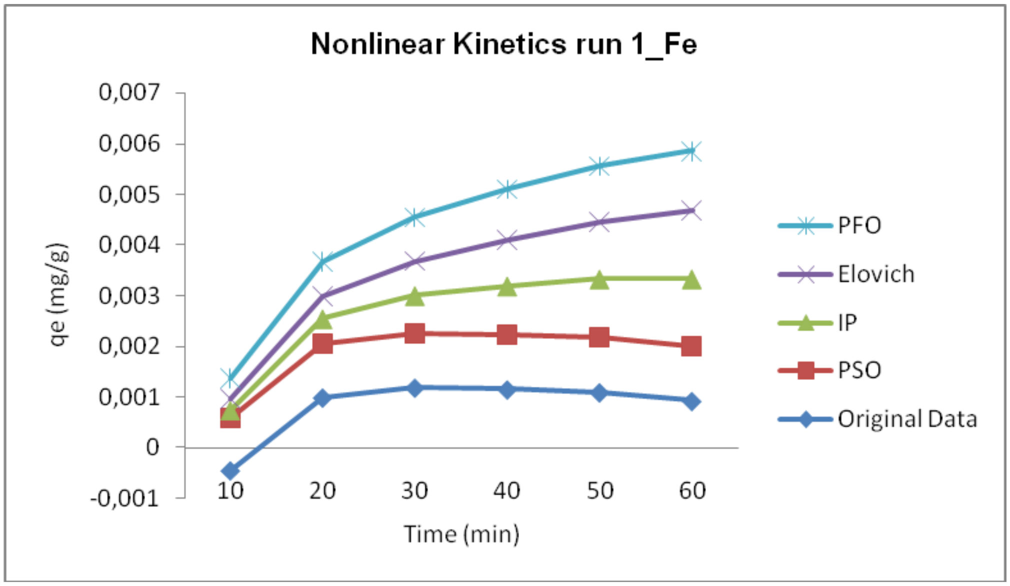

Figure 4.68Non-linear adsorption kinetics (Fe) run 1_pH 6.5

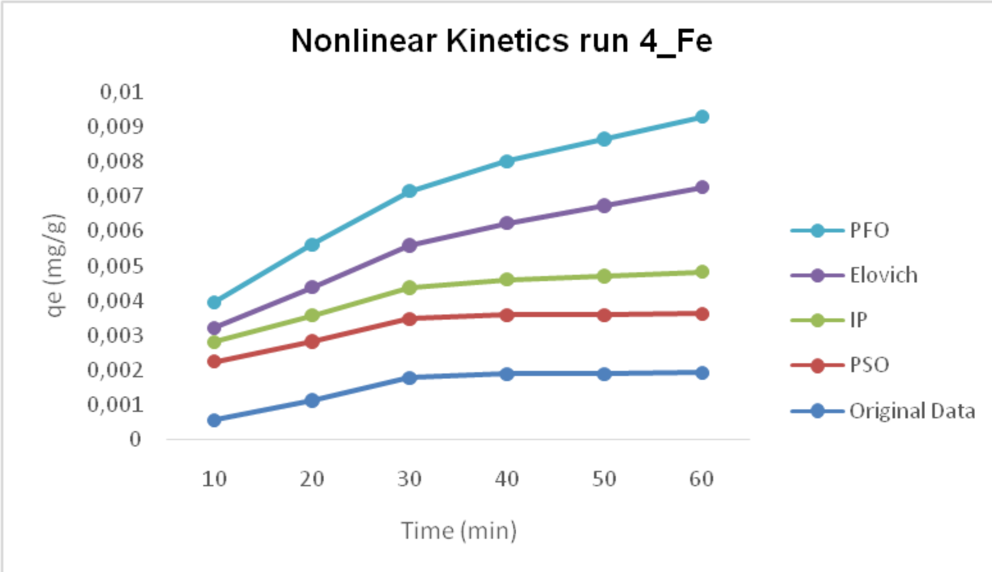

Figure 4.69Non-linear adsorption kinetics (Fe) run 4_pH 7.5

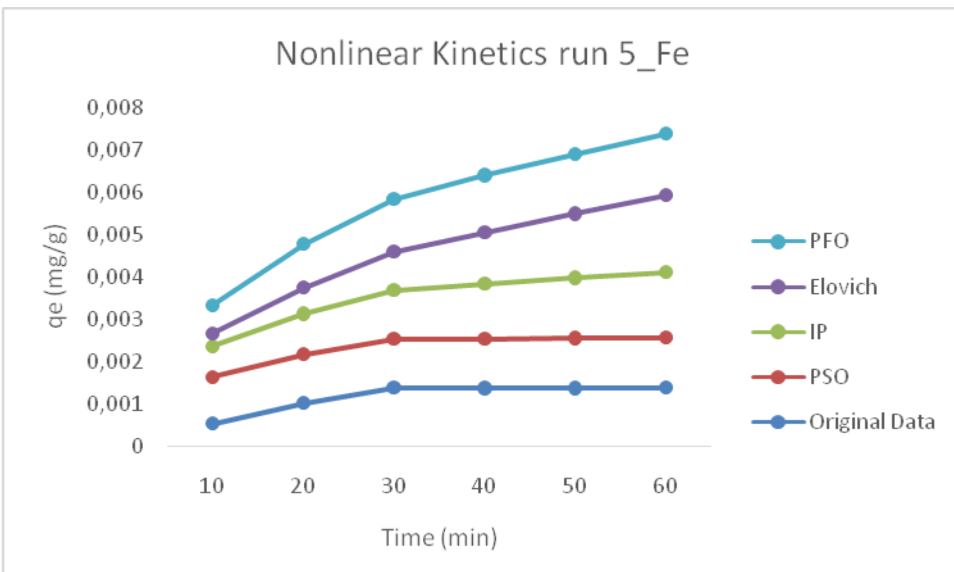

Figure 4.70Non-linear adsorption kinetics (Fe) run 5_pH 7.5

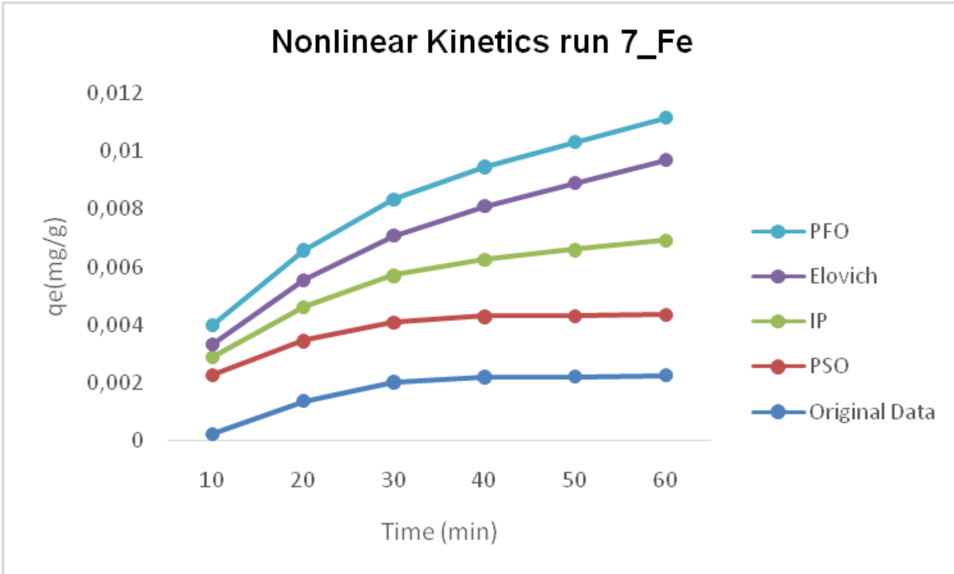

Figure 4.71Non-linear adsorption kinetics (Fe) run 7_pH 8.5

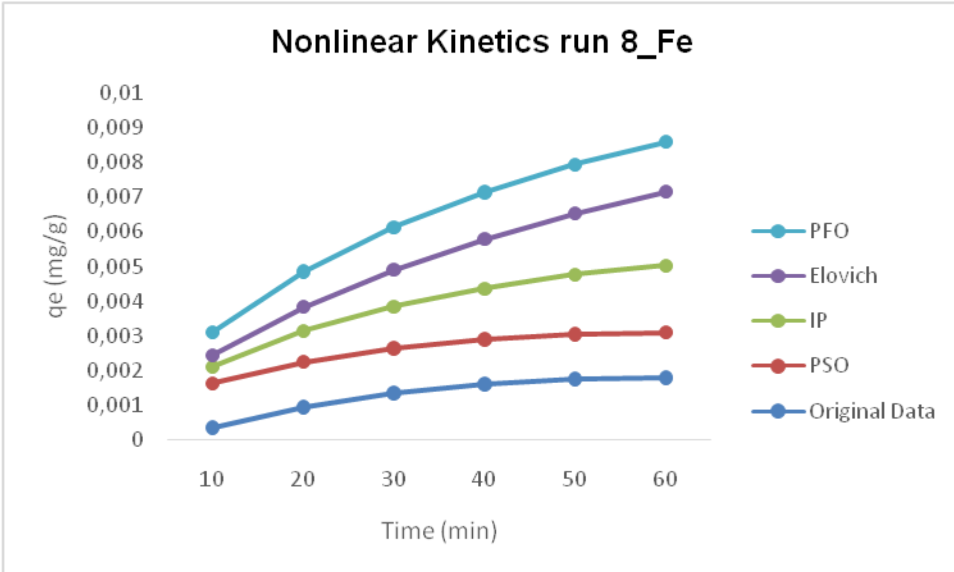

Figure 4.72Non-linear adsorption kinetics (Fe) run 8_pH 8.5

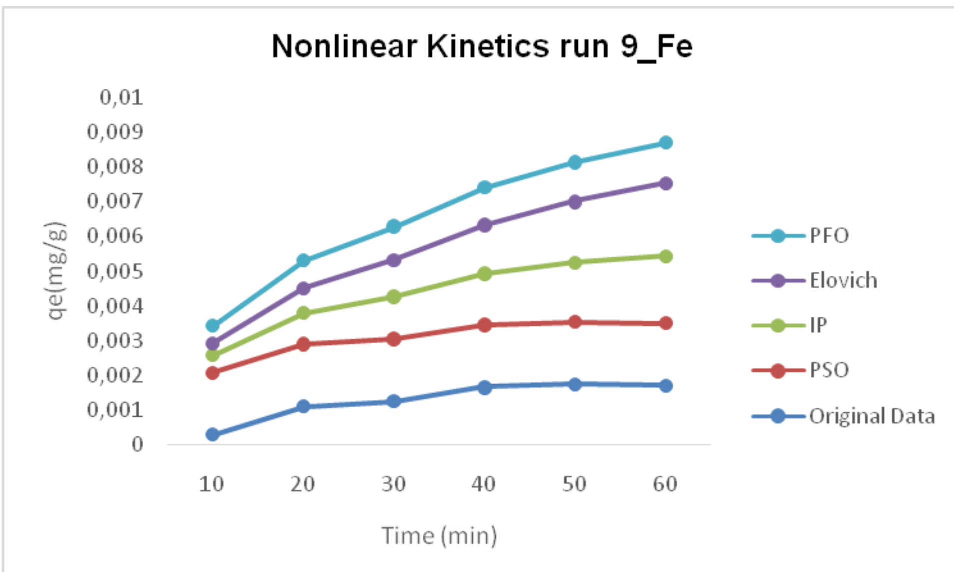

Figure 4.73Non-linear adsorption kinetics (Fe) run 9_pH 8.5

4.15.2 Manganese non-linear adsorption kinetics

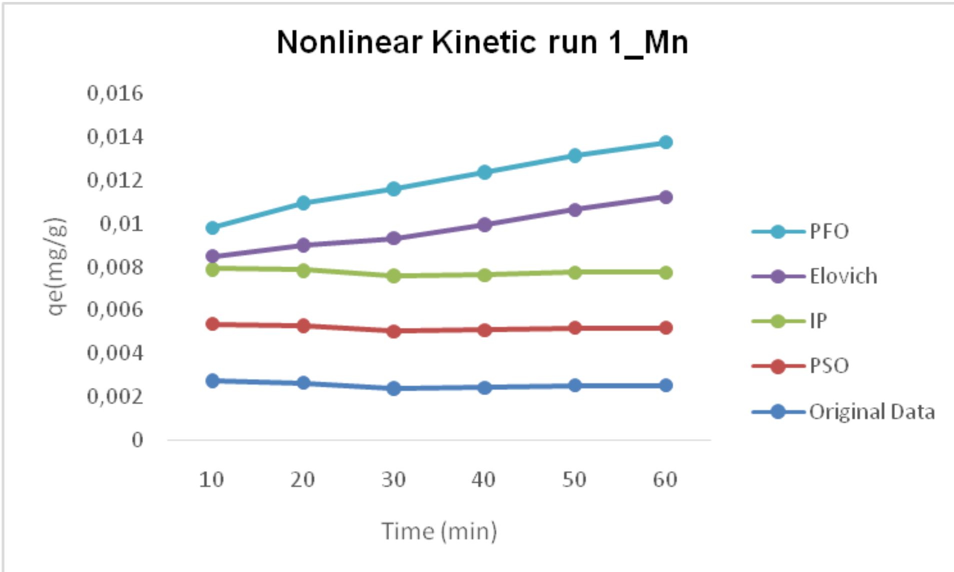

Figure 4.74Non-linear adsorption kinetics (Mn) run 1_pH 6.5

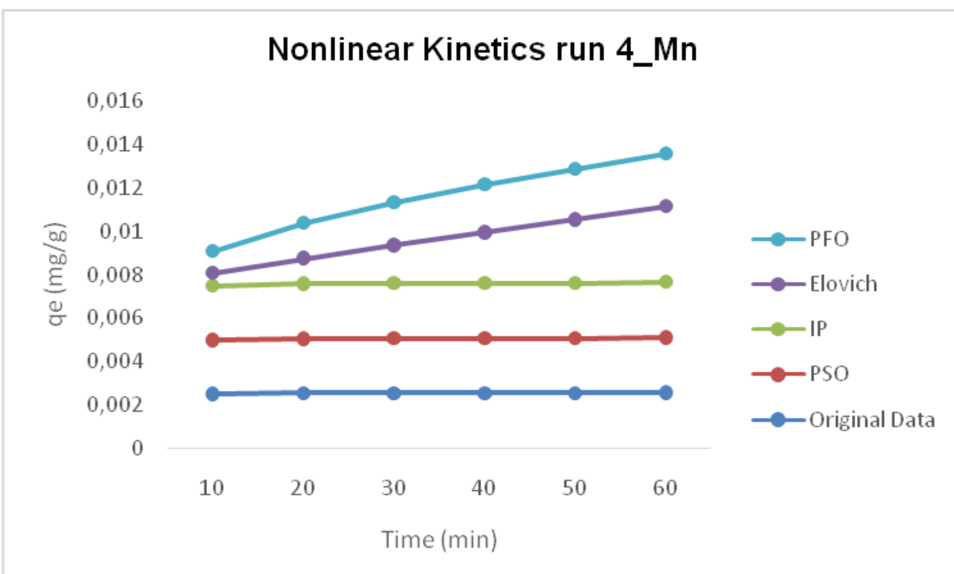

Figure 4.75Non-linear adsorption kinetics (Mn) run 4_pH 7.5

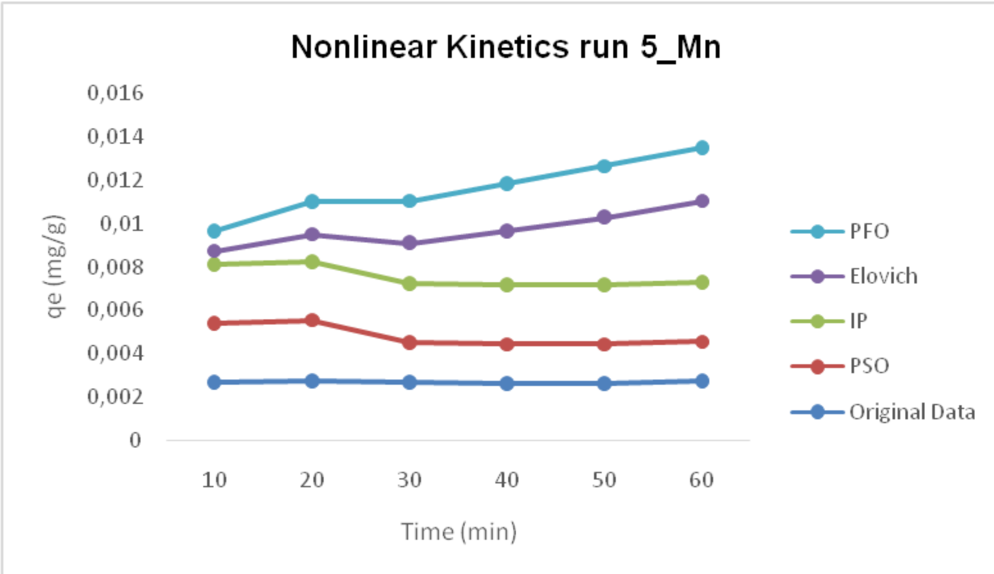

Figure 4.76Non-linear adsorption kinetics (Mn) run 5_pH 7.5

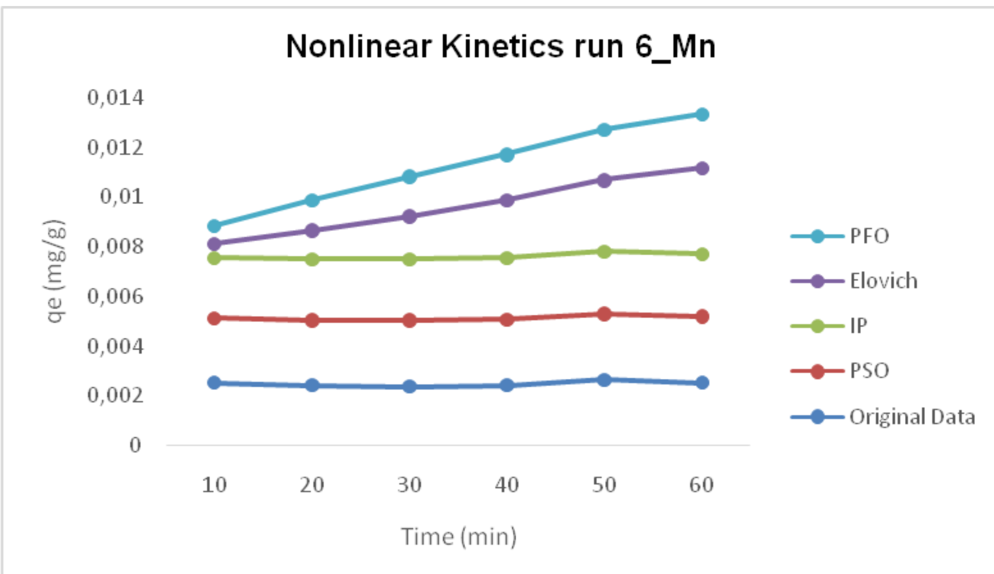

Figure 4.77Non-linear adsorption kinetics (Mn) run 6_pH 7.5

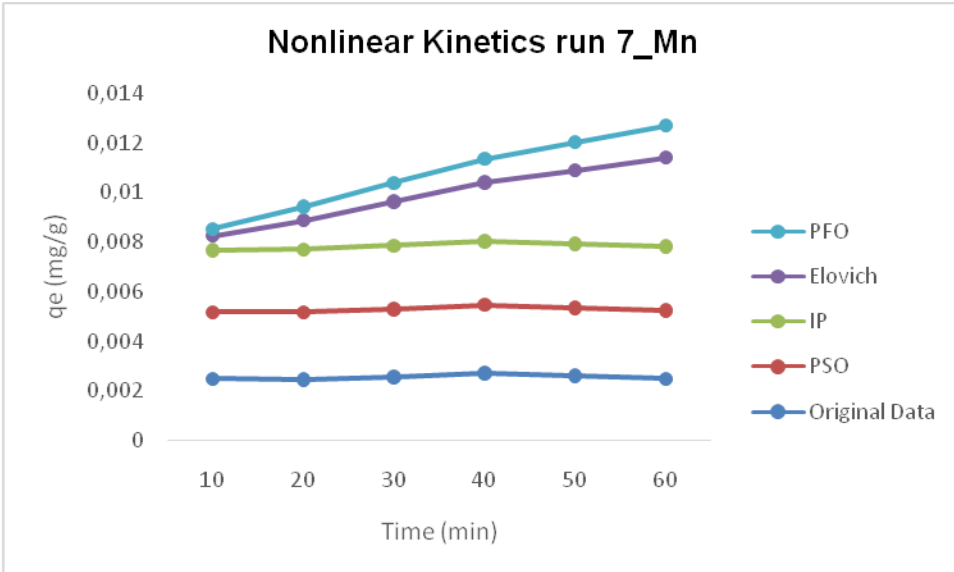

Figure 4.78: Non-linear adsorption kinetics (Mn) run 7_pH 8.5

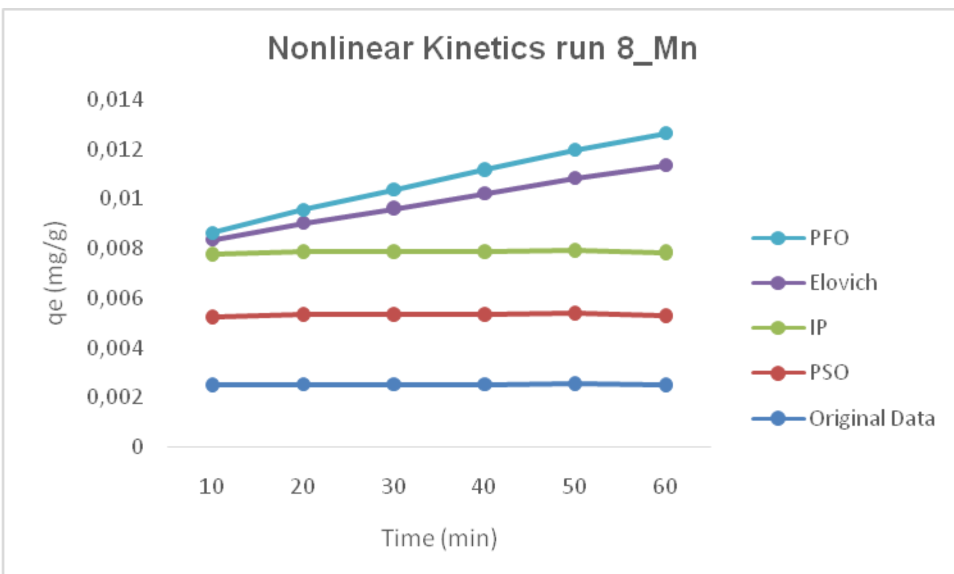

Figure 4.79Non-linear adsorption kinetics (Mn) run 8_pH 8.5

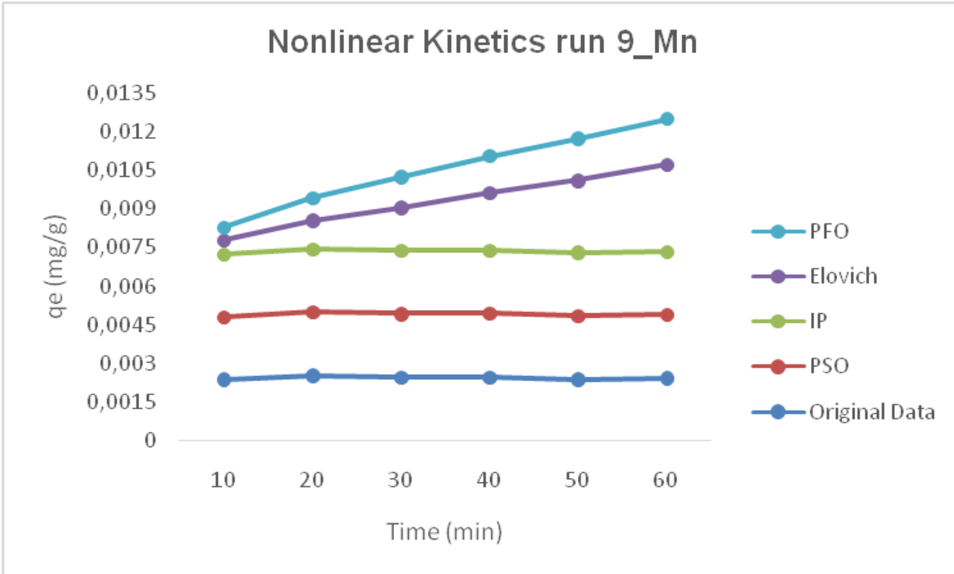

Figure 4.80Non-linear adsorption kinetics (Mn) run 9_pH 8.5

Table 4:8 Non-linear adsorption constants (Fe)

Iron (Fe)									
RUNS	1	2	3	4	5	6	7	8	9
pH	6,5			7,5			8,5		
Flow rate (l/min)	0,174 (l/min)	0,262 (l/min)	0,523 (l/min)	0,174 (l/min)	0,262 (l/min)	0,523 (l/min)	0,174 (l/min)	0,262 (l/min)	0,523 (l/min)
PFO									
qe_{exp} (mg/g)	1,07E-03	2,30E-06	-2,39E-04	1,73E-03	1,31E-03	9,99E-04	2,00E-03	1,48E-03	1,29E-03
qe_{ca}l (mg/g)	8,7E-04	6,46E-05	-2,46E-04	1,55E-03	0,001	9,25E-04	1,75E-03	1,31E-03	1,31E-03
b (min^{-1})	0,0354	0,0004	0,00661	0,0405	0,0586	0,0534	0,0309	0,0256	0,0288
R^2	0,961	0,997	0,999	0,721	0,662	0,702	0,842	0,433	0,997
PSO									
qe_{exp} (mg/g)	1,07E-03	-1,32E-04	-2,64E-04	1,73E-03	1,31E-03	9,99E-04	2,00E-03	1,48E-03	1,49E-03
qe_{cal} (mg/g)	1,07E-03	2,28E-03	7,56E-01	1,69E-03	1,16E-03	9,69E-03	2,08E-03	1,30E-03	1,80E-03
b (min-1)	2184	1976	3438,57205	3312	1009	3225	1036	8760	9681
R2	1,000	0,839	0,833	0,999	0,955	0,836	0,998	0,978	0,970
IPD									
K_{diff}(mg/g.min0.5)	2,58E-04	2,84E-04	-7,88E-05	1,36E-04	1,78E-04	1,36E-04	4,25E-04	3,20E-04	3,10E-04
C (mg/g)	-6,64E-04	-1,76E-03	2,08E-04	1,48E-04	1,65E-04	1,48E-04	-7,24E-04	-5,41E-04	-4,80E-04
R2	1,000	1,000	1,000	1,000	1,000	1,000	1,000	1,000	1,000
Elovich									
α (mg/g.min)	2,27147E-05	97,35631206	97,35637418	4,66011E-05	3,03289E-05	2,38041E-05	4,66011E-05	3,53569E-05	3,51509E-05
β (g/mg)	4,02	0,000115	0,00024	4,01	3,33	3,56	4,7	3,82	2,79
R2	1,000	0,846	0,856	0,983	0,977	0,971	0,993	0,988	0,990

The effects of contact time on Fe and Mn by the tri-medium system are shown in Figures 4.68-4.80 above for both Fe and Mn. The amount of Fe and Mn increased with the contact time, and equilibrium was reached after 30 min. Figure (above) shows the effect of contact time. The adsorption amount sharply increases with time in the initial stage (0–30 min range), then gradually increases to reach an equilibrium value in approximately 30 min. A further increase in contact time had a negligible effect on the amount of adsorption. The rapid adsorption of the metal ions in the first minutes 30 minutes can be attributed to the availability of many vacant surface sites on the adsorbent. The adsorption rate gradually decreases during the adsorption process until the equilibrium is reached. The decreasing Fe and Mn adsorption rate is perhaps due to surface diffusion.

The data was shown to follow PSO kinetics making it the best model to describe the data for both metal ions, Iron and Manganese. The PSO model was shown to have the highest R^2 values across all the runs and the lowest SSE, SAE and ARE across all the runs. The values of q_{exp} and q_{cal} were well within agreement for the PSO kinetic model more than the PFO model. The PSO model also exhibits significantly lower rate constants than the PFO, further supporting the agreement between the experimental and calculated qe values.

Table 4:9 Non-linear adsorption kinetics constants (Mn)

Manganese (Mn)									
RUNS	1	2	3	4	5	6	7	8	9
pH	6,5			7,5			8,5		
Flow rate (l/min)	0,174 (l/min)	0,262 (l/min)	0,523 (l/min)	0,174 (l/min)	0,262 (l/min)	0,523 (l/min)	0,174 (l/min)	0,262 (l/min)	0,523 (l/min)
PFO									
qe_{exp} (mg/g)	2,50E-03	2,75E-03	2,48E-03	2,53E-03	2,70E-03	2,47E-03	2,56E-03	2,53E-03	2,44E-03
qe_{cal} (mg/g)	2,2E-03	2,29E-03	1,86E-03	1,92E-03	0,002	1,59E-03	8,74E-05	8,29E-04	1,22E-03
b (min^{-1})	0,0752	0,0670	0,04900	0,0510	0,0420	0,0340	0,0010	0,0120	0,0220
R^2	0,956	0,934	0,895	0,894	0,885	0,874	0,832	0,839	0,851
PSO									
qe_{exp} (mg/g)	2,50E-03	2,75E-03	2,47E-03	2,53E-03	2,70E-03	2,56E-03	2,56E-03	2,53E-03	2,44E-03
qe_{cal} (mg/g)	2,66E-03	2,87E-03	2,43E-03	2,52E-03	2,78E-03	2,65E-03	2,73E-03	2,81E-03	2,47E-03
b (min-1)	1231	978	1087	1099	1185	1194	1276	1341	1332
R2	0,878	0,880	0,977	0,930	0,899	0,928	0,882	0,842	0,970
IPD									
K_{diff}(mg/g.$min^{0.5}$)	2,50E-06	1,90E-07	1,81E-05	1,45E-06	2,30E-06	1,81E-05	2,26E-05	1,90E-06	3,30E-06
C (mg/g)	2,54E-03	2,77E-03	2,38E-03	2,52E-03	2,70E-03	2,38E-03	2,42E-03	2,52E-03	2,43E-03
R2	0,998	1,000	1,000	0,992	0,989	1,000	1,000	0,975	0,982
Elovich									
α (mg/g.min)	5,81853E-05	97,35653551	97,35650876	5,96246E-05	6,27039E-05	5,80554E-05	5,96246E-05	5,86015E-05	5,63014E-05
β (g/mg)	4,03	7,62E-05	6,83E-05	4,03	4,02	3,81	3,02	2,92	3,62
R2	0,969	0,976	0,976	0,968	0,968	0,969	0,969	0,969	0,968

4.16.1 Error analysis

Error analysis is employed to determine the experimental dataset's most suitable isotherm (AO, 2012). The validation of adsorption models and kinetic models was performed using three different statistical error functions, namely, the sum of square error (SSE) and the sum of absolute error (SAE) and average relative error (ARE). The best fit model will be the model with the lowest values of SSE, SAE and ARE. The equations used are as follows:

$$SSE = \sum_{i=1}^{n} \left(q_{e,calc} - q_{e,meas}\right)_i^2$$

$$SAE = \sum_{i=1}^{n} \left|q_{e,calc} - q_{e,meas}\right|_i$$

$$ARE = \frac{100}{n} \sum_{i=1}^{n} \left|\frac{q_{e,calc} - q_{e,meas}}{q_{e,meas}}\right|_i$$

4.16.2 Error analysis adsorption isotherms

Table 4:10 SSE adsorption isotherms_ Fe

SSE (Fe)				
Run	**Langmuir**	**Freundlich**	**Temkin**	**D-R**
1	5,51E-08	7,61E-08	-	2,85E-08
2	1,89E-10	1,76E-08	1,11E-08	7,03E-11
3	8,5E-11	1,12E-08	1,09E-10	6,42E-08
4	1,77E-07	1,88E-07	-	6,69E-12
5	8,58E-09	1,47E-08	1,75E-07	2,98E-07
6	1,75E-09	4,4E-10	2,89E-07	3,72E-08
7	1,36E-06	9,13E-07	3,96E-06	1,29E-09
8	3,04E-08	1,19E-07	1,73E-07	1,11E-06
9	7,43E-08	1,17E-07	1,57E-07	1,39E-10

Table 4:11 SSE adsorption Isotherm_Mn

SSE (Mn)				
Run	**Langmuir**	**Freundlich**	**Temkin**	**D-R**
1	3,70323E-08	2,141E-08	-	3,58E-06
2	1,7266E-06	1,148E-08	2,73E-06	1,11E-06
3	6,797E-10	4,52E-09	4,35E-10	1,12E-10
4	5,09078E-07	6,201E-12	-	5,11E-08
5	1,11462E-06	8,953E-10	5,53E-08	6,91E-07
6	4,85311E-08	2,626E-09	3,1E-09	1,66E-06
7	2,91498E-09	3,116E-09	1,4E-08	8,21E-08
8	1,45955E-07	2,088E-11	4,33E-08	1,46E-09
9	8,27042E-08	2,639E-10	2,95E-08	2,24E-13

Table 4:12 SAE adsorption isotherms_Fe

SAE (Fe)				
Run	**Langmuir**	**Freundlich**	**Temkin**	**D-R**
1	2,35E-04	2,76E-04	-	-1,69E-04
2	1,37E-05	1,33E-04	1,05E-04	8,38E-06
3	-9,22E-06	1,06E-04	1,04E-05	2,53E-04
4	4,21E-04	4,34E-04	-	2,59E-06
5	9,26E-05	1,21E-04	4,18E-04	-5,46E-04
6	4,19E-05	-2,10E-05	-5,38E-04	-1,93E-04
7	1,17E-03	9,55E-04	1,99E-03	3,59E-05
8	1,74E-04	3,44E-04	4,15E-04	-1,05E-03
9	2,73E-04	3,42E-04	3,97E-04	-1,18E-05

Table 4:13 SAE adsorption isotherm_Mn

SAE (Mn)				
Run	Langmuir	Freundlich	Temkin	D-R
1	1,92E-04	1,46E-04	-	1,89E-03
2	1,31E-03	1,07E-04	1,65E-03	1,06E-03
3	2,61E-05	6,72E-05	-2,09E-05	1,06E-05
4	7,13E-04	2,49E-06	-	2,26E-04
5	1,06E-03	2,99E-05	-2,35E-04	8,31E-04
6	2,20E-04	5,12E-05	5,57E-05	1,29E-03
7	5,40E-05	5,58E-05	1,18E-04	2,87E-04
8	3,82E-04	4,57E-06	-2,08E-04	-3,83E-05
9	2,88E-04	1,62E-05	1,72E-04	4,73E-07

Table 4:14: ARE adsorption isotherms_Fe

ARE (Fe)				
Run	Langmuir	Freundlich	Temkin	D-R
1	0,844	1,002	-	-0,559
2	-0,284	-2,390	-1,955	-0,175
3	0,108	-1,144	-0,120	-2,502
4	0,796	0,821	-	0,005
5	0,220	0,289	1,043	-1,189
6	0,126	-0,063	-1,468	-0,558
7	2,146	1,715	4,023	0,059
8	0,384	0,775	0,944	-1,994
9	0,607	0,768	0,898	-0,025

Table 4:15: ARE adsorption isotherm_Mn

ARE (Mn)				
Run	**Langmuir**	**Freundlich**	**Temkin**	**D-R**
1	0,213	0,162	-	2,363
2	1,433	0,108	1,841	1,132
3	0,029	0,076	-0,023	0,012
4	0,824	0,003	-	0,252
5	1,163	0,031	-0,239	0,902
6	0,250	0,058	0,063	1,579
7	0,059	0,061	0,130	0,318
8	0,432	0,005	-0,226	-0,042
9	0,335	0,019	0,199	0,001

Table 4:16: Experimental vs theoretical qe values for adsorption Isotherms_Fe

Iron (Fe)					
Run	q_{exp}	**Langmuir**	**Freundlich**	**Temkin**	**D-R**
1	0,001391	0,001324	0,001312	-	0,001439
2	-0,000226	-0,000230	-0,000264	-0,000256	-0,000229
3	-0,000410	-0,000407	-0,000440	-0,000413	-0,000482
4	0,002637	0,002517	0,002513	-	0,002636
5	0,002030	0,002004	0,001996	0,001911	0,002186
6	0,001591	0,001579	0,001597	0,001744	0,001646
7	0,002926	0,002592	0,002653	0,002357	0,002916
8	0,002214	0,002164	0,002116	0,002095	0,002515
9	0,002216	0,002138	0,002119	0,002103	0,002220

Table 4:17: Experimental vs theoretical qe values for adsorption Isotherm_Mn

Manganese (Mn)					
Run	**q_{exp}**	**Langmuir**	**Freundlich**	**Temkin**	**D-R**
1	0,004353	0,004298	0,004311	-	0,003812
2	0,004743	0,004368	0,004712	0,004271	0,004441
3	0,004254	0,004247	0,004235	0,004260	0,004251
4	0,004330	0,004126	0,004329	0,002525	0,004265
5	0,004625	0,004323	0,004616	0,004692	0,004387
6	0,004254	0,004191	0,004240	0,004238	0,003886
7	0,004373	0,004358	0,004357	0,004340	0,004292
8	0,004319	0,004210	0,004317	0,004378	0,004330
9	0,004166	0,004083	0,004161	0,004117	0,004166

4.16.3 Error Analysis Adsorption Kinetics

Table 4:18 SSE adsorption kinetics_Fe

SSE (Fe)				
Run	**PFO**	**PSO**	**IP**	**Elovich**
1	1,08E-07	2,44E-06	4,51E-10	1,14E-08
2	1,39E-06	0,000209	6,89E-11	0,001225
3	1,87E-09	20,58767	3,18E-10	0,001348
4	6,89E-09	8,04E-07	1,35E-05	5,05E-07
5	1,64E-09	1,89E-08	2,65E-10	5,64E-07
6	3,55E-10	0,002762	2,56E-10	3,34E-07
7	8,6E-07	5,06E-06	4,46E-10	2,5E-07
8	3,63E-07	5,32E-10	4,58E-10	1,2E-07
9	4,87E-06	9,11E-06	4,63E-10	1,53E-07

Table 4:19 SSE adsorption kinetics_Mn

SSE (Mn)				
Run	**PFO**	**PSO**	**IP**	**Elovich**
1	5,02E-06	5,05E-07	7,33E-09	9,47E-06
2	8,1E-06	3,77E-07	1,19E-08	7,21E-06
3	1,38E-05	8,42E-08	2,76E-17	5,14E-06
4	1,31E-05	1,46E-10	5,75E-10	8,25E-06
5	2,26E-05	1,23E-05	5,83E-09	9,55E-06
6	2,84E-05	9,78E-07	2,76E-17	7,6E-06
7	0,000219	1,13E-06	3,37E-17	8,03E-06
8	0,000103	3,04E-06	4,24E-09	8,15E-06
9	5,24E-05	5,74E-08	1,28E-08	7,89E-06

Table 4:20 SAE adsorption kinetics_Fe

SAE (Fe)				
Run	**PFO**	**PSO**	**IP**	**Elovich**
1	-3,28E-04	-1,56E-03	2,12E-05	1,07E-04
2	-1,18E-03	-1,45E-02	8,30E-06	-3,50E-02
3	4,33E-05	-4,54E+00	1,78E-05	-3,67E-02
4	-8,30E-05	-8,97E-04	3,68E-03	7,11E-04
5	-4,05E-05	1,38E-04	1,63E-05	7,51E-04
6	1,88E-05	-5,26E-02	1,60E-05	5,78E-04
7	9,27E-04	-2,25E-03	2,11E-05	5,00E-04
8	6,02E-04	-2,31E-05	2,14E-05	3,46E-04
9	2,21E-03	-3,02E-03	2,15E-05	3,91E-04

Table 4:21 SAE adsorption kinetics_Mn

SAE (Mn)				
Run	**PFO**	**PSO**	**IP**	**Elovich**
1	2,24E-03	-7,10E-04	-8,56E-05	3,08E-03
2	2,85E-03	-6,14E-04	-1,09E-04	2,68E-03
3	3,72E-03	2,90E-04	-5,25E-09	2,27E-03
4	3,62E-03	1,21E-05	-2,40E-05	2,87E-03
5	4,75E-03	3,50E-03	-7,63E-05	3,09E-03
6	5,33E-03	-9,89E-04	-5,25E-09	2,76E-03
7	1,48E-02	-1,06E-03	-5,81E-09	2,83E-03
8	1,01E-02	-1,74E-03	-6,51E-05	2,85E-03
9	7,24E-03	-2,40E-04	-1,13E-04	2,81E-03

Table 4:22 ARE adsorption kinetics_Fe

ARE (Fe)				
Run	**PFO**	**PSO**	**IP**	**Elovich**
1	-1,052	-4,051	0,073	0,374
2	-50,738	-17,632	-0,173	-17,053
3	-0,488	-16,672	-0,205	-17,345
4	-0,149	-1,476	11,042	1,390
5	-0,094	0,329	0,038	1,970
6	0,057	-15,070	0,048	1,931
7	1,659	-3,002	0,034	0,856
8	1,405	-0,049	0,046	0,778
9	6,631	-4,668	0,046	0,884

Table 4:23 ARE adsorption kinetics_Mn

ARE (Mn)				
Run	**PFO**	**PSO**	**IP**	**Elovich**
1	2,873	-0,743	-0,093	4,218
2	3,449	-0,595	-0,109	3,215
3	5,545	0,331	0,000	2,992
4	5,228	0,013	-0,026	3,899
5	6,928	4,598	-0,078	3,933
6	9,296	-1,038	0,000	3,786
7	469,898	-1,084	0,000	3,787
8	33,981	-1,725	-0,071	3,880
9	16,426	-0,269	-0,128	3,976

Table 4:24 Experimental vs theoretical qe values for adsorption kinetics_Fe

Iron (Fe)					
Run	q_{exp}	PFO	PSO	IP	Elovich
1	0,001391	0,001484	0,001837	0,001385	0,001360
2	-0,000226	0,000111	0,003908	-0,000229	0,009775
3	-0,000410	-0,000422	1,295980	-0,000415	0,010080
4	0,002637	0,002661	0,002893	0,001586	0,002434
5	0,002030	0,002042	0,001991	0,002026	0,001816
6	0,001591	0,001585	0,016607	0,001586	0,001426
7	0,002926	0,002661	0,003569	0,002920	0,002783
8	0,002214	0,002042	0,002221	0,002208	0,002115
9	0,002216	0,001585	0,003079	0,002210	0,002105

Table 4:25 Experimental vs theoretical qe values for adsorption kinetics_Mn

Manganese (Mn)					
Run	q_{exp}	PFO	PSO	IP	Elovich
1	0,004353	0,003713	0,004556	0,004377	0,003474
2	0,004743	0,003930	0,004918	0,004774	0,003976
3	0,004254	0,003192	0,004171	0,004254	0,003607
4	0,004330	0,003296	0,004326	0,004337	0,003509
5	0,004625	0,003267	0,003625	0,004647	0,003742
6	0,004254	0,002731	0,004537	0,004254	0,003467
7	0,004373	0,000150	0,004677	0,004373	0,003564
8	0,004319	0,001421	0,004817	0,004337	0,003503
9	0,004166	0,002098	0,004234	0,004198	0,003363

4.17 Linear and non-linear comparison

The application of linearized kinetics models is mainly to find the best fit for the data to evaluate the functionality of the filtration medium used. However, based on the assumptions made on the linearized functions, the plots and interpretation of data might be inaccurate. Thus, crucial to perform the non-linear functions to minimize the errors that can result from linearized versions of the models. The accuracy of the non-linear kinetic models is observed from the proximity of q_{exp} and q_{cal} adsorption capacity and the difference between the parameter constants of PFO, PSO, IP and Elovich kinetic models. For metal ion Fe (II) and Mn (II), when evaluating pseudo first order data in linear and non-linear form, show comparable values of R^2. However, the calculated adsorption capacities are different to the experimental ones. At the same time, the q_{cal} computed values for the non-linear regression are much closer to that of the experimental values. In the linear regression, the values are not in agreement. The kinetics parameter constants are equally crucial since they are used to measure the affinity of the system to be modelled; observing from b (PFO), Ks (PSO), C (IP), β (Elovich), the linear regression showed a difference between the values of these parameters. However, the non-linear regression showed a minimal difference in these parameters, with PSO being the most kinetic model to fit the data. The PSO describes that the tri-medium system doesn't only depend on the vacant site for adsorption; also, it can form a multilayer. The IP values of C and K_{diff} were within reasonable agreement with each other for non-linear regression. The observation drawn from these results is that non-linear regression can be applied as an indicator for best kinetic fit compared to linear regression, which can be misleading due to its unreliability.

4.18 Adsorption of fixed-bed column

This chapter presents the breakthrough curves constituting the removing Fe and Mn from groundwater using the fixed-packed bed tri-medium adsorption treatment process. The Fe and Mn levels before and after adsorption were used to evaluate how efficient the integrated approach was.

4.19 Breakthrough and Desorption curves

The primary objective of breakthrough curves and desorption mechanism in the adsorption application process for this experiment was to assess the rate at which the influent concentration is in equilibrium with the effluent concentration (Polakovic et al., 2005). This technique contributes to adsorption's key factors: adsorbate equilibrium capacity (the detainment of adsorbate on the adsorbent) and the rate of desorption/saturation of the adsorbent (Malik et al., 2018). Performing this analysis aids not only in evaluating the adsorbent efficiency of the column but contributes to the selection of adequately designed system for industrial application, especially in water treatment(Himanshu Patel, 2019).

4.19.1 Iron (Fe)

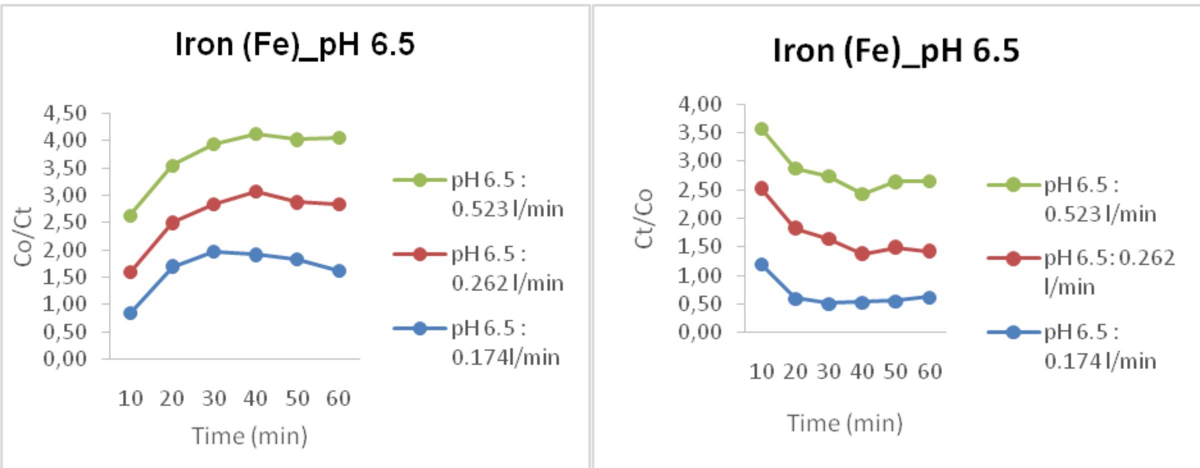

Figure 4. 814a: Breakthrough curve at pH 6.5 (Fe) & 4b: Desorption rate at pH 6.5 (Fe)

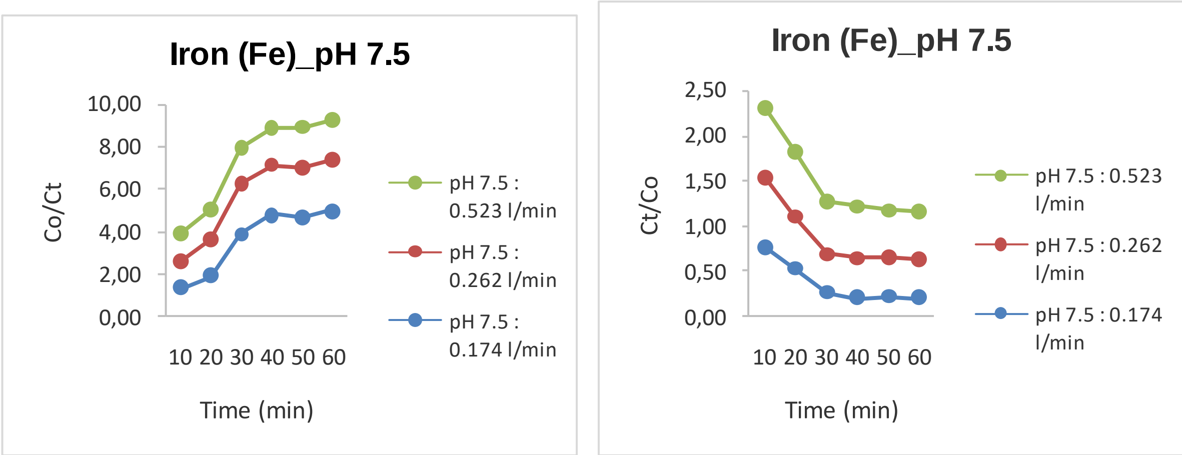

Figure 4. 824c: Breakthrough curve at pH 7.5 (Fe) & 4d: Desorption rate at pH 7.5 (Fe)

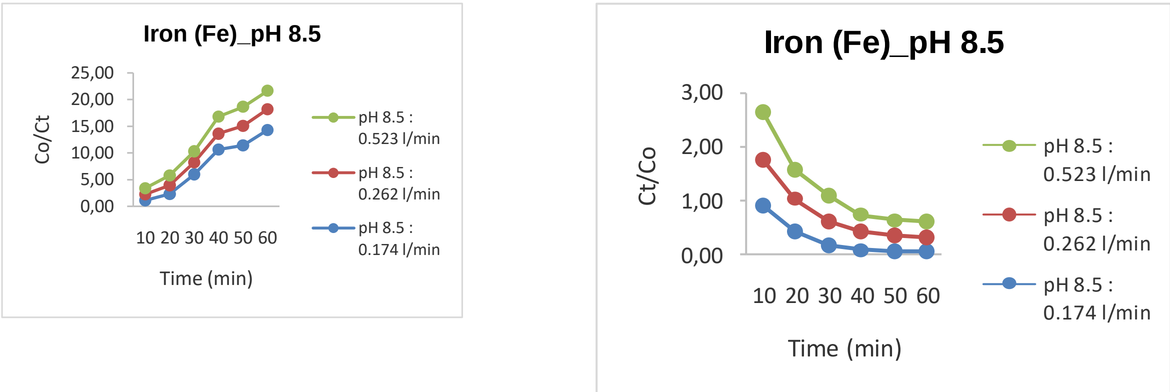

Figure 4. 83 4e: Breakthrough curve at pH 8.5 (Fe) &4f: Desorption rate at pH 8.5 (Fe)

The breakthrough curves for Iron (Fe) were analyzed at pH 6.5, 7.5 & 8.5, flow rates 0.174, 0.262 & 0.523 and contact times of 10, 30 & 60 min, as illustrated in Figures 4a, 4c & 4e, while the saturation graphs are presented by Figure 4b, 4d & 4f. According to H. Patel (2021), when a fixed bed column reaches the saturation point, the shape of a breakthrough curve exhibits' S', demonstrating the steps followed by an influent slowly entering the fixed bed column until it saturates it to reach an equivalent concentration on the effluent. However, figure 4a shown above is contrary to this study. The results presented in Figure 4a indicate that during the runs, the system reached the saturation point in a short period, which resulted in minimum Fe adsorption. This observation is seconded by figure 4b, where the saturation point was noticed at 20 minutes with no more adsorbate uptake. This is due to the pH of 6.5, which is classified as acidic with high hydronium ions in the solution. This positive hydronium ion increases the electrostatic repulsion force between an adsorbent and adsorbate, resulting in less Iron adsorption (Himanshu Patel, 2019)**.** The exhibit of this repulsion is the -10% Fe removal that was observed at pH 6.5 and flow rate 0.523l/min.

Aligning to the expected results of the breakthrough curves is figure 4c & 4e. The results in this graph followed the mass transfer zone (MTZ) and primary sorption zone (PSZ) & exhibited the "s" shape. The breakthrough curve was satisfactorily expressed at pH 7.5 & 8.5, flow rate 0.174, 0262 & 0.523 l/min. This result describes that the above conditions suit the column by complying with the MTZ that the effluent concentration saturates the upper strata of the column by being adsorbed on the vacant sites of the bed before it passes to the next level of the column, as illustrated by MTZ hierarchy in figure 2-6 in the literature. The Iron removal of 93% confirms the vacant site available at pH 8.5 and flow rate 0.174l/min in figure 4e, which is results of more alkaline pH that has neutralized the hydronium ions and increased the interaction between the adsorbate-adsorbent. Even though figure 4d & 4f shows the saturation at 30 minutes, however the column has more adsorption sites as compared to figure 4b.

4.19.2 Manganese (Mn)

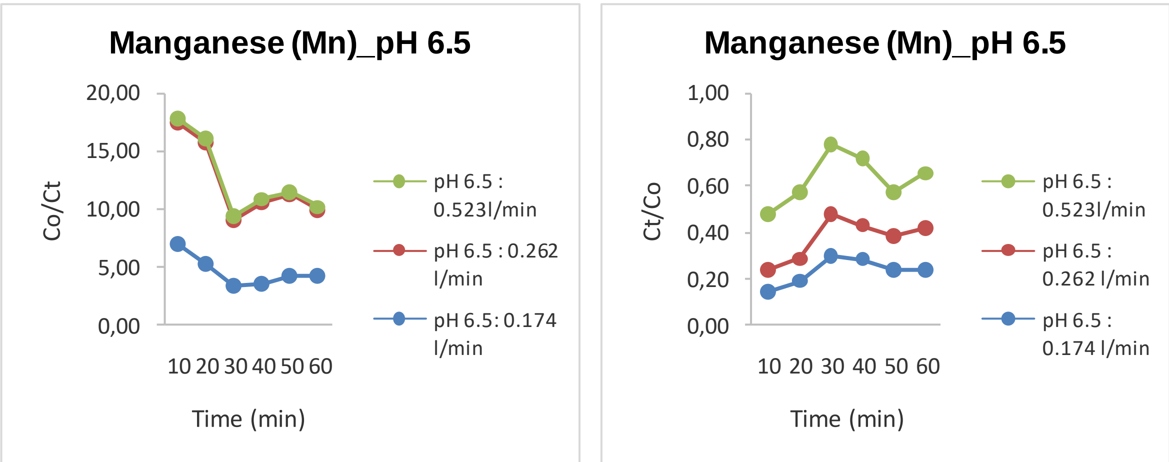

Figure 4.844g: Breakthrough curve at pH 6.5 (Mn) & 4h: Desorption rate at pH 6.5 (Mn)

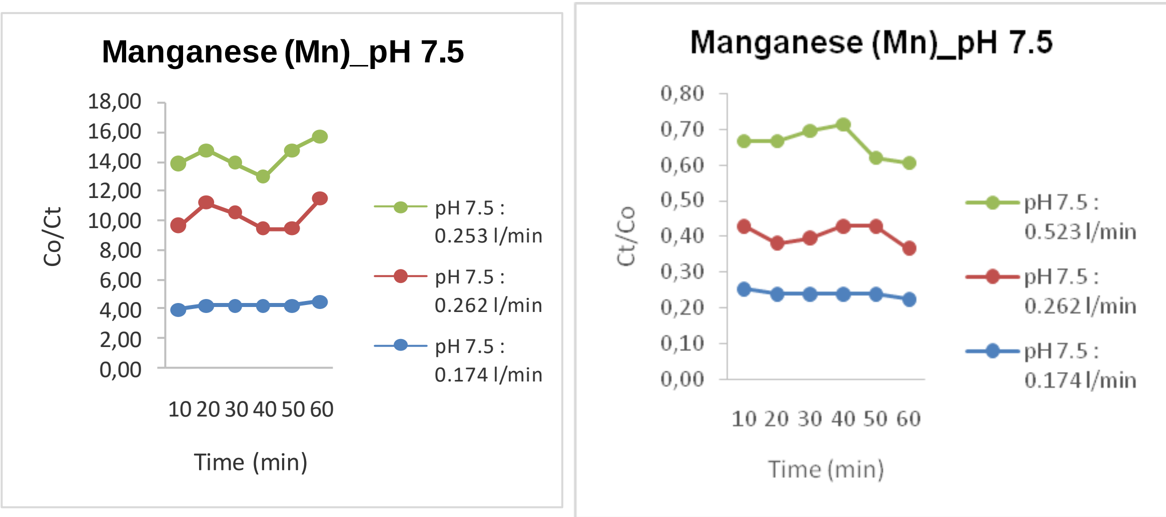

Figure 4.85:4i: Breakthrough curve at pH 7.5 (Mn) & 4j: Desorption rate at pH 7.5 (Mn)

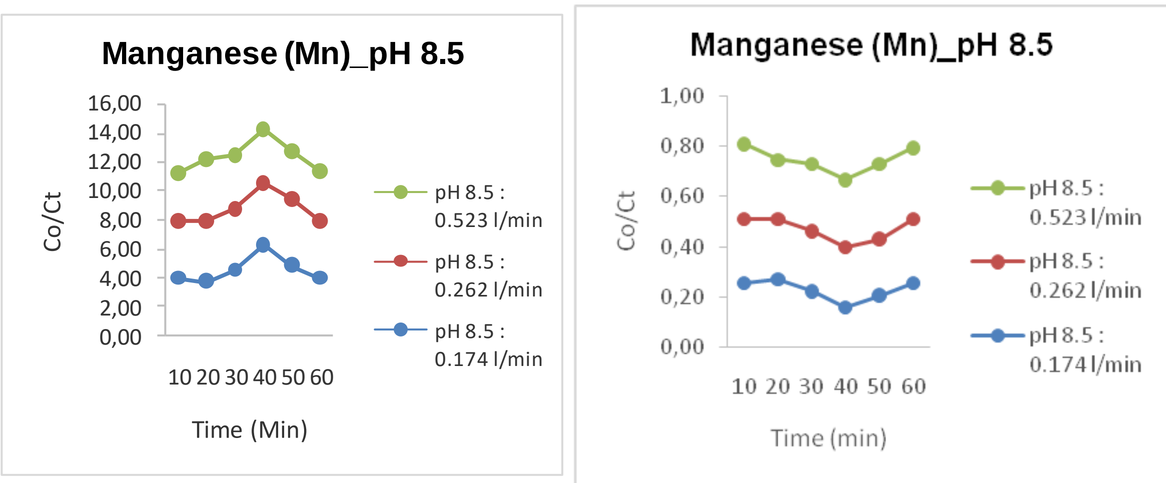

Figure 4. 864k: Breakthrough curve at pH 8.5 (Mn) &4l: Desorption rate at pH 8.5 (Mn)

The manganese breakthrough adsorption curve presented in Figures 4g, 4i, & 4k and saturation curves in Figures 4h, 4j &4l show an expected outcome of the manganese adsorption from the system. As seen in Figures 4g,4i & 4k, the 'S' shape of the breakthrough curve is horizontal, which illustrates that the removal of manganese was achieved by the fixed bed column (Malik et al., 2018). The high removal efficiency of manganese confirms these observations throughout the adsorption of manganese by the system. The saturation presented by Figures 4h, 4j & 4l also shows the vertical shape distribution of manganese removal due to the system being saturated at a high percentage removal efficiency. The contributing factor to the high-efficiency removal of this parameter is due to the manganese compounds forming part of an oxidizing agent when reacting with an oxidant (Sarkar et al., 2018).Even though the system worked effectively on manganese removal, the concentration did not reach 0.1mg/l as required by SANS: 241 water drinking standards. This hindering might be caused a decrease in bed vacant sites as the media reaches saturation point (Flintsch, 2012).

4.19.3 Effect of adsorbent bed height on breakthrough curve

The bed height is vital in the contact time of the adsorbent and the adsorbate. The fixed bed column in this experiment was packed with three mediums: polystyrene beads, glass media and ion exchange resin. These mediums were divided into three-bed heights according to the size of the column in which they were packed. However, the adsorption of an adsorbate to the adsorbent was not quantified per media in the queue; it was done collectively for the entire system because the column volume was small. Quantifying the adsorbent-adsorbate per media would have yielded insignificant results since the contact time between the specific media and the solution might have been minimal. According to Omitola et al. (2022), bed height is empirically to increase the breakthrough of the solution and increase adsorption by having more vacant sites in the media. As illustrated by iron (Fe) and manganese (Mn) figures above, Fe removal was less than Mn adsorbed. The bed high might have a detrimental effect on this observation since it can be seen that even at 60 minutes, no more iron was removed by the column, which implies that the column was saturated (Himanshu Patel, 2019)**.** It can be concluded that the higher the bed height, the more vacant sites for adsorption, the higher the bed exhaustion rate, and the better the operation (Omitola et al., 2022)**.**

4.19.4Effect of flow rate on breakthrough curve

This experiment was performed at various flow rates of 0.174 l/min, 0.262 l/min & 0.523 l/min. The flow rate signifies the rate at which the adsorbate is adsorbed onto the surface of the fixed bed and also might attribute to the adsorption/ desorption of an adsorbate (Polakovic et al., 2005). Fe's 93% removal efficiency was observed at 0.174l/min flow rate, and 93% Mn was noticed at 0.262l/min. With the lowest adsorption efficiency for both metals detected at 0.523 l/min, the highest flow rate of the experiment was Fe (-33%) and Mn (77%). Due to the residence time, the high flow rate in this research did not yield the positive removal of both metal ions. This less adsorption might also result fromthe adsorbed Iron and Manganese desorption at a higher flow rate, consequently increasing the metal irons concentration in the effluent and resulting in earlier breakthrough time (Flintsch, 2012; H. Patel, 2021).

4.20 Fixed Bed Mathematical models

4.20.1 Iron (Fe)

Table 4:26 Iron (Fe) Fixed Bed Modelling constants

Iron (Fe)									
RUNS	1	2	3	4	5	6	7	8	9
pH	6.5			7.5			8.5		
Flow rate (l/min)	0,174 (l/min)	0,262 (l/min)	0,523 (l/min)	0,174 (l/min)	0,262 (l/min)	0,523 (l/min)	0,174 (l/min)	0,262 (l/min)	0,523 (l/min)
Thomas Constants									
q_{eq} (mg/g)	-0.0016	-	-	-0.011	-0.005	0.037	-0.027	-0.021	-0.020
K_{TH} (L/mg/min)	0.0019	-	-	-0.003	-0.001	-0.001	-0.002	-0.001	-0.002
R^2	0.11	-	-	0.78	0.65	0.87	0.80	0.87	0.78
Adam-Bohartz									
N_o (mg/g)	-27.351	-4.061	-2.264	1.614	10.033	7.344	0.495	0.623	26.478
K_{AB} (L/mg/min)	0.001	-0.005	0.002	-0.010	-0.003	-0.003	-0.020	-0.010	-0.004
R^2	0.33	0.87	0.71	0.82	0.69	0.90	0.90	0.96	0.89
Yoon Nelson									
K_{YN} (min^{-1})	0.0039	-	-	-0.006	-0.012	-0.019	-0.005	-0.037	-0.005
τ (min)	19.98	-	-	140.00	-24.58	-58.99	335.69	-26.81	83.30
R^2	0.11	--	-	0.848	0.73	0.93	0.85	0.91	0.93

4.20.2 Manganese (Mn)

Table 4:27 Manganese (Mn) fixed bed modelling constants

Iron (Fe)									
RUNS	1	2	3	4	5	6	7	8	9
pH	6.5			7.5			8.5		
Flow rate (l/min)	0,174 (l/min)	0,262 (l/min)	0,523 (l/min)	0,174 (l/min)	0,262 (l/min)	0,523 (l/min)	0,174 (l/min)	0,262 (l/min)	0,523 (l/min)
Thomas Constant									
q_{eq} (mg/g)	0.039	0.024	-0.014	-0.056	0.091	-0.014	-0.037	0.179	0.047
K_{TH} (L/mg/min)	0.001	0.006	-0.005	-0.001	0.001	-0.005	-0.001	0.000	0.003
R^2	0.36	0.60	0.15	0.71	5.00E-05	0.15	0.10	0.04	0.06
Adam-Bohartz									
N_o (mg/g)	-48.133	-24.225	26.478	78.889	-103.240	26.478	51.565	-255.514	-65.795
K_{AB} (L/mg/min)	0.0010	0.0049	-0.0039	-0.0101	0.0009	-0.0039	-0.0009	0.0003	0.0023
R^2	0.37	0.60	0.15	0.71	7.00E-05	0.16	0.10	0.04	0.06
Yoon Nelson									
K_{YN} (min^{-1})	0.003	0.012	-0.011	-0.002	0.002	-0.011	-0.003	0.001	0.006
τ (min)	-479.982	-192.673	56.767	692.887	-741.004	56.767	450.426	-1466.910	-191.219
R^2	0.36	0.60	0.15	0.71	5.00E-05	0.15	0.10	0.04	0.06

4.21 Modelling of fixed bed column data

Mathematical models were developed to investigate the appraisal efficiency and capabilities for operating a fixed bed column. The commonly deployed models for this experiment were Thomas Model, Adams & Bohart and Yoon-Nelson Model (Dima et al., 2020).

4.21.1 Thomas model

This model depicts the early stage of the adsorption process, where the adsorption forces are more active (Malik et al., 2018). The experimental data were linearly fitted by plotting $\ln[C_o/C_t - 1]$ against t in this model to determine the model constant q_{eq} (adsorption capacity) and K_{TH} (the rate constant), which depicts whether the experimental data fit the model or rejects it. As shown by table 4.26 above, the value of q_{eq} is harmful to both Iron and Manganese removal from run 1 to run 7; this explains why this model doesn't fit the data for this experiment.

4.21.2 Adams-Bohart

The model stresses that the adsorption rate is more dependent on the exposed & available sides of the adsorbent and adsorbate concentration (Apiratikul & Chu, 2021). The assessment of this model was performed by determining the equilibrium capacity N_o (mg/g) and K_{AB} (L/mg/min) rate constant from the intercept and slope of ln(Ct/Co) against time (t) (Himanshu Patel, 2019). The results shown in table 4.26 for Fe adsorption from run 1-3 the negative values of the adsorption capacity were notices N_o (-27.351, -4.061 & -2.261 mg/g) and run 1, 2,5,8, 9 for Mn demonstrated by table 4.27 this value describes the high concentration of Iron and Manganese in the solution than on the adsorbate. It is due to the low pH of 6.5 and high flow rates in these runs, where the pH contributed to more positive hydronium ions in the system that caused repulsion between the adsorbate and adsorbent. The flow rate contributed to the low retention time of the solution for extended contact time (Dima et al., 2020). However, from the pH of 7.5-8.5, high adsorption capacities were observed from run 4-7 for Fe at N_o of (1.614, 10.033, 7.344, 0.495, 0.623 & 26.478 mg/g) and Mn at No of (26.478, 78.889, 26.478 & 51.565 mg/g) for run 3, 4, 6 & 7 respectively. The observed increase in adsorption capacity results from high pH, which neutralizes the system and creates more interaction between adsorbent and adsorbate, increasing the bed's vacant sides for more adsorption (Inglezakis & Fyrillas, 2017). It can be concluded that the Adam-Bohart Model fits the data experiment for Iron and Manganese removal at the given conditions of the investigation. The R2 value in the 0.33-0.96 indicates better applicability than all models.

4.21.3 Yoon-Nelson

The model is based on the assumption that the probable rate of decrease in the adsorption of each adsorbate is proportional to the probability of the adsorbate adsorption and the adsorbate breakthrough on the adsorbent (Malik et al., 2018)**.** The linearized form of this model was determined to form plotting ln (C_t/C_o-C_t), where the intercept and slope were utilized to determine K_{YN} (min^{-1}) rate constant and τ the time required for 50% adsorbate breakthrough (min). In table 4.26, Fe & the adsorbate breakthrough point time at running 5, 6, 7 & 9 were observed to be harmful. In table 4.27 Mn, at runs 1, 2, 5, 8 &9, these results imply that the breakthrough point in this experiment was reached early. However, this observation doesn't conform to the literature for this model. It can be concluded that this model does not fit the experimental data.

CHAPTER 5

Optimization using Surface Response Methodology (RSM)

5. Optimization using response surface methodology

5.1 Introduction

Design of experiments plays a vital role in several spheres of science and industry. It is utilized to conduct and execute experiments by predicting and understanding the system behaviour based on measuring one or more responses. For this reason, the experiments need to be planned, designed and the results analyzed. One of the most applied experiment design method for system optimization is the response surface methodology (RSM). It's widely used as a mathematical and statistical tool for analyzing and process modeling in instances where response is affected by the variables (Durakovic, 2017). We are applying it to this research to predict the response of Iron (Fe) and Manganese (Mn) removal and optimize the process to achieve the desired outcome.

5.2 Adsorption performance for Iron (Fe) and Manganese (Mn) removal predicted using RSM

One of the primary response surface methodologies is the Box-Behnken design. It's a design with one centre point, in which each factor centre is tested on three levels. The three factors investigated include, pH ranges from 6.5 to 8.5, flow rate from 0.174l/min to 0.523l/min and contact time from 10 to 60 minutes. The response surface methodology was used to determine the independent variables' interactions. Analysis of Variance (ANOVA) was used to test the difference between means for statistical significance and evaluate the fitted model's validity. In which statistical model was fitted by considering the experimental data as quadratic, the correlation coefficient presented by R^2, the adjusted determination coefficient as (Adj-R^2) and the adequate precision was to check the adequacies of the model. The model is adequate if P value<0.05, lack of fit if P value >0.05, R^2>0.9 and adequate precision>4 (Antoy, 2014).

5.3 Design matrix for Iron (Fe)

The Box-Behnken design (BBD) design matrix with a total number of 27 experiments was conducted as presented by Table 5-1. Three factors were conducted pH, flow rate and contact time in run order and output data for BBD.

Table 5 -1: Box-Behnken Design output results for Iron (Fe) removal

Run	Factors			Iron(Fe) Removal %	
	A:pH	B:Flow Rate (l/min)	C:Contact Time (min)	Actual Value	Predicted Value
1	8.5	0.174	10	10%	39%
2	8.5	0.174	60	93%	84%
3	7.5	0.523	10	24%	10%
4	8.5	0.523	30	52%	52%
5	7.5	0.262	30	58%	53%
6	6.5	0.174	30	49%	25%
7	6.5	0.523	60	-22%	9%
8	8.5	0.262	30	55%	57%
9	6.5	0.262	10	-33%	-32%
10	8.5	0.174	30	83%	77%
11	8.5	0.523	60	71%	59%
12	6.5	0.523	10	-5%	-37%
13	8.5	0.262	60	74%	64%
14	6.5	0.174	60	38%	33%
15	7.5	0.174	10	24%	34%
16	7.5	0.523	30	41%	48%
17	6.5	0.262	60	19%	13%
18	7.5	0.174	30	74%	72%
19	7.5	0.174	60	80%	80%
20	7.5	0.262	10	22%	15%
21	7.5	0.523	60	47%	55%
22	7.5	0.262	60	58%	60%
23	8.5	0.262	10	14%	19%
24	8.5	0.523	10	12%	14%
25	6.5	0.523	30	-9%	1%
26	6.5	0.174	10	-19%	-12%
27	6.5	0.262	30	-13%	6%

The results of the experimental output and predicted values of Iron removal for the 27 run experiments are presented in Table 5-1, where the results clearly illustrate that a maximum Iron removal of 93.0% was attained with experiment 2, at pH 8.5, flow rate 0.174 l/min and contact time of 60 minute. A notable fair agreement of the results was reached when the R^2 predicted was in close correlation with an experimental R^2.

Table 5- 2: ANOVA Iron Analysis

Analysis of Variance Table [Partial sum of squares – Type III]					
Source	**Sum of Squares**	**df**	**Mean Square**	**F-value**	**p-value**
Model	12.46	6	2.08	19.54	< 0.0001
A-pH	6.41	2	3.2	30.13	< 0.0001
B-Flow Rate	1.35	2	0.6738	6.34	0.0074
C-Contact Time	4.71	2	2.36	22.16	< 0.0001
Residual	2.13	20	0.1063	-	-
Cor Total	14.59	26	-	**R^2**	0.8543
Std. Dev.	0.3261	-	-	**Adjusted R^2**	0.8106
Mean	1.4	-	-	**Predicted R^2**	0.7344
Coefficient of Varience %	23.24	-	-	**Adeq Precision**	153,197

Analysis of Variance (ANOVA) was used to test the difference between means for statistical significance and to evaluate the validity of the fitted model Table 5-2

Iron removal % $=+1.40+0.6870\ A^1-0.007A^2-0.3107B^1+0.1059B^2+0.5837C^1-0.2130C^2$

Equation 5-1: Iron Removal %

The Model F-value of 19.54 implies the model is significant. There is only a 0.01% chance that an F-value this large could occur due to noise. P-values less than 0.0500 indicate model terms are significant. In this case all the model terms are significant. The Predicted R^2 of 0.7344 is in reasonable agreement with the Adjusted R^2 of 0.8106; the difference is less than 0.2. Adeq Precision measures the signal-to-noise ratio. A ratio greater than 4 is desirable. The ratio of 15.320 indicates an adequate signal. This model can be used to navigate the design space

5.4 Iron (Fe) Model Validation

An appropriate approximation validation of the model was developed, and fitted to approximate the actual system accuracy. Three various types of model were investigated for diagnostics: the normal, residual and predicted vs. experimental plot

5.4.1 Actual vs Predicted Values for Iron

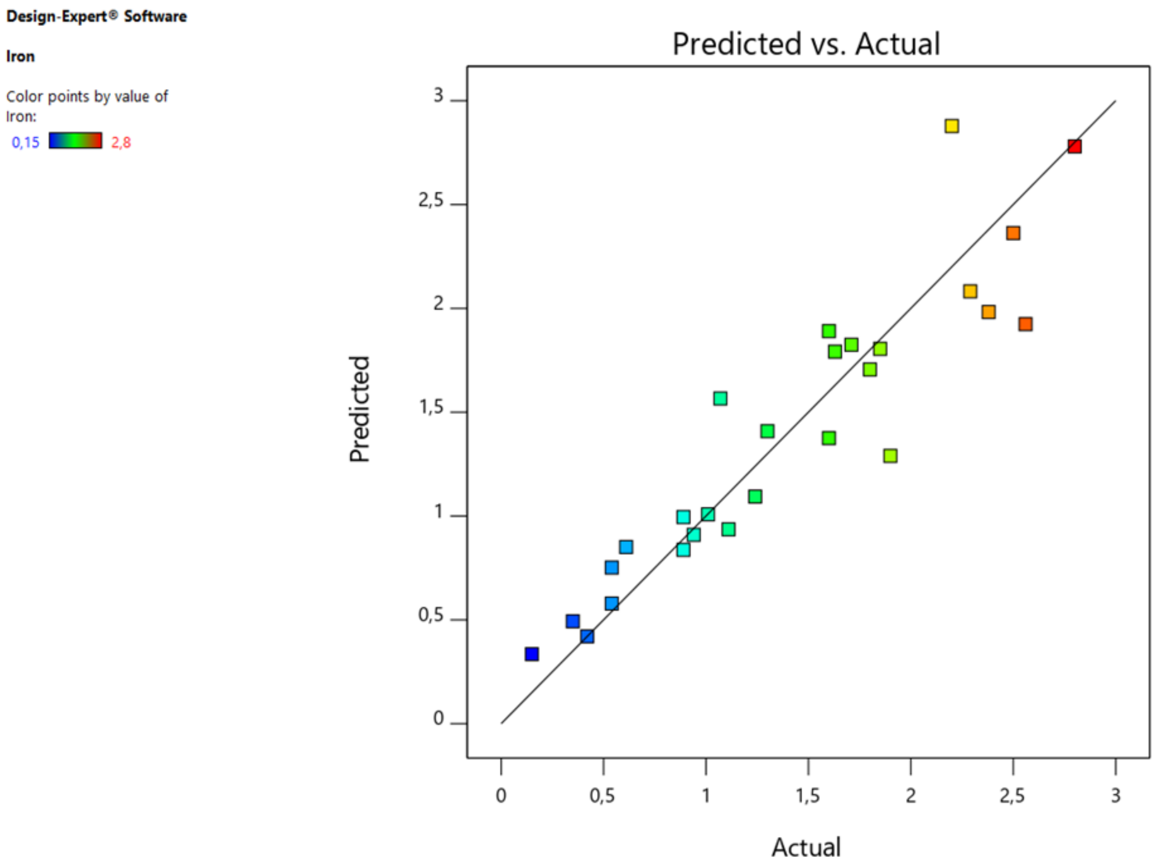

Figure 5- 1: Actual vs Predicted Values for Iron

The Actual vs. predicted models represented by Figure 5.1 is validated by the predicted value points that are close to the experimental values of Iron, as illustrated above the values are not far apart from one another, that confirm the model validity.

5.4.2 Normal probability plot of residuals Iron

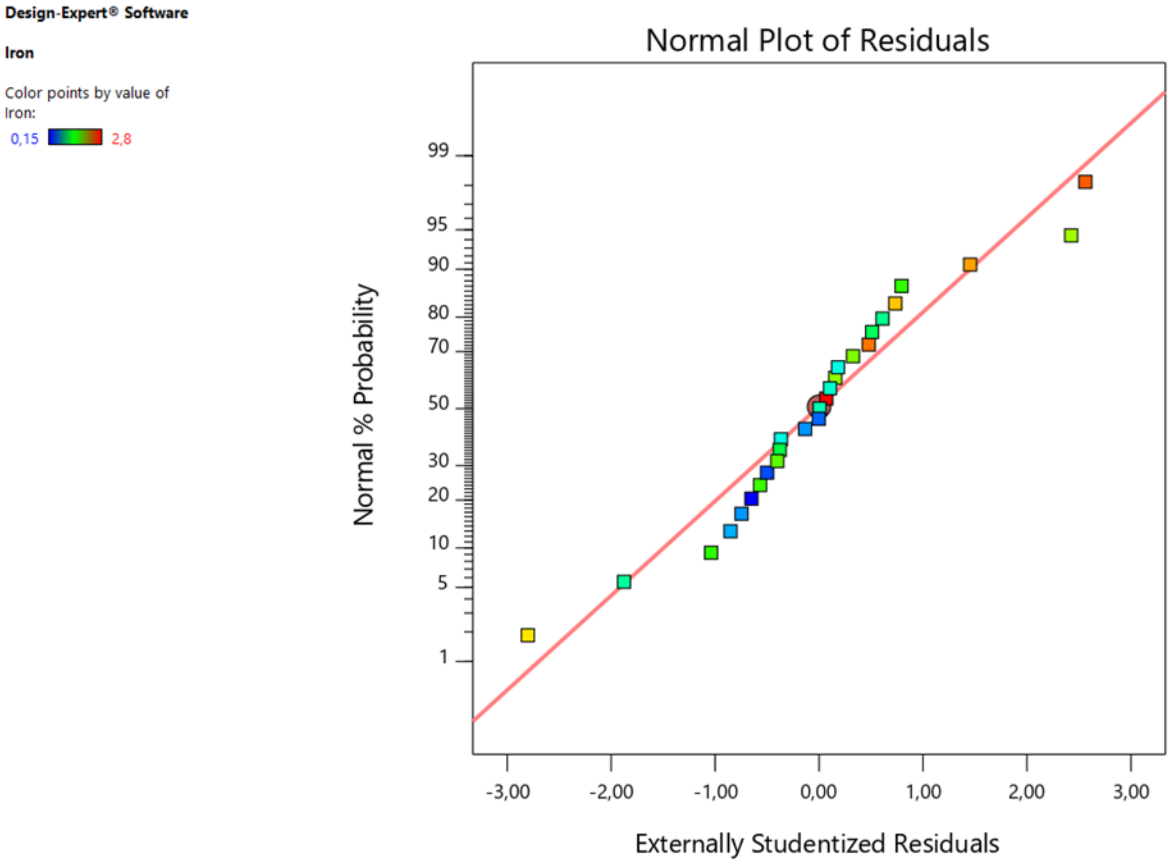

Figure 5 2: Normal probability plot of residuals Iron

The data normality can be evaluated by plotting the normal probability graph with the residuals as seen in Figure 5.2. This plot is a technique that graphically determines the proximity of data distribution. If the plot points are reasonably close to the straight line it can be surmised that the data is normally distributed. It is noticeable on Figure 5.2 that the normal probability plot the points are closely aligned, suggesting normal distribution. The linear fit validates the normality of the data.

5.4.3: Residual vs Predicted Iron

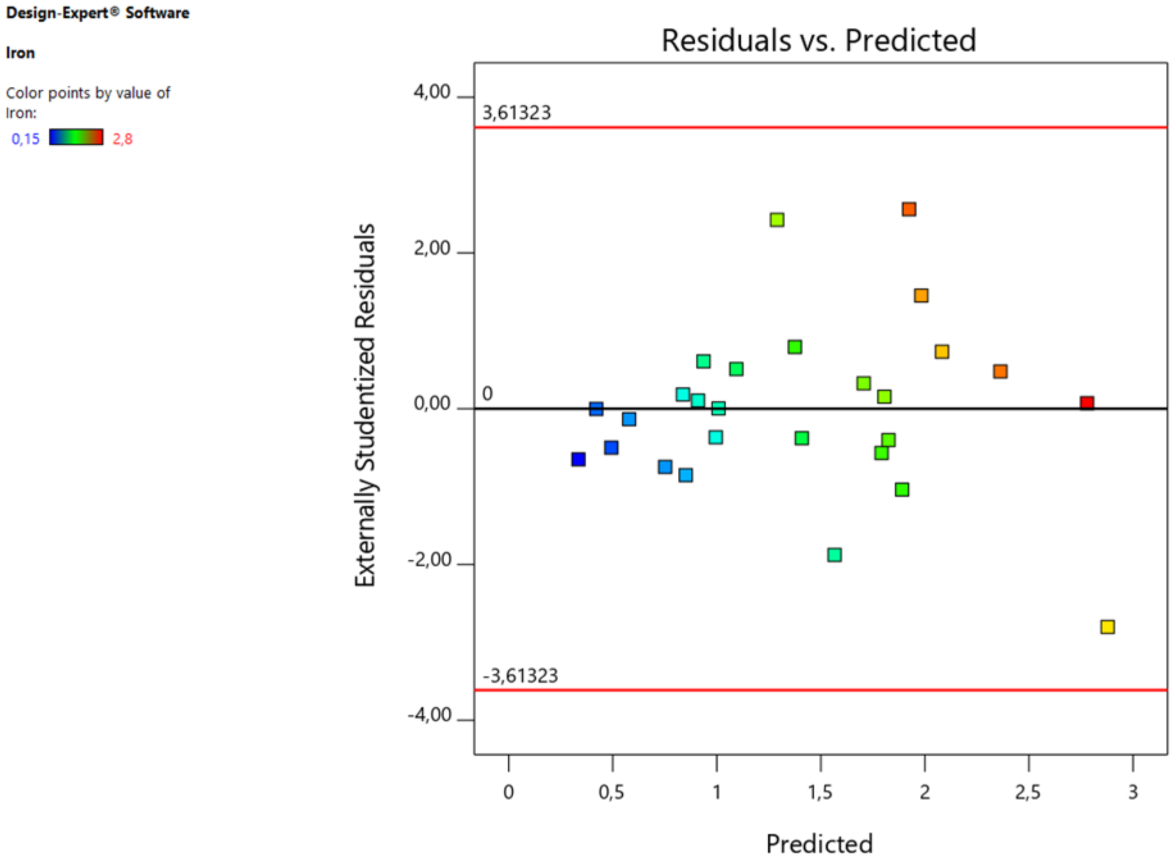

Figure 5 3: Residual vs Predicted Iron

The residuals vs. predicted graph for the Iron data can be seen in figure 5-3. According to Roman, (2021)an indication that the model is correct is that there is no obvious pattern or structure shown by the residuals. From figure 5-3 it can be seen that it is in accordance with the statement made by the author as the points are all scattered randomly.

5.4.4: 3-D Contour plot Iron removal average performance

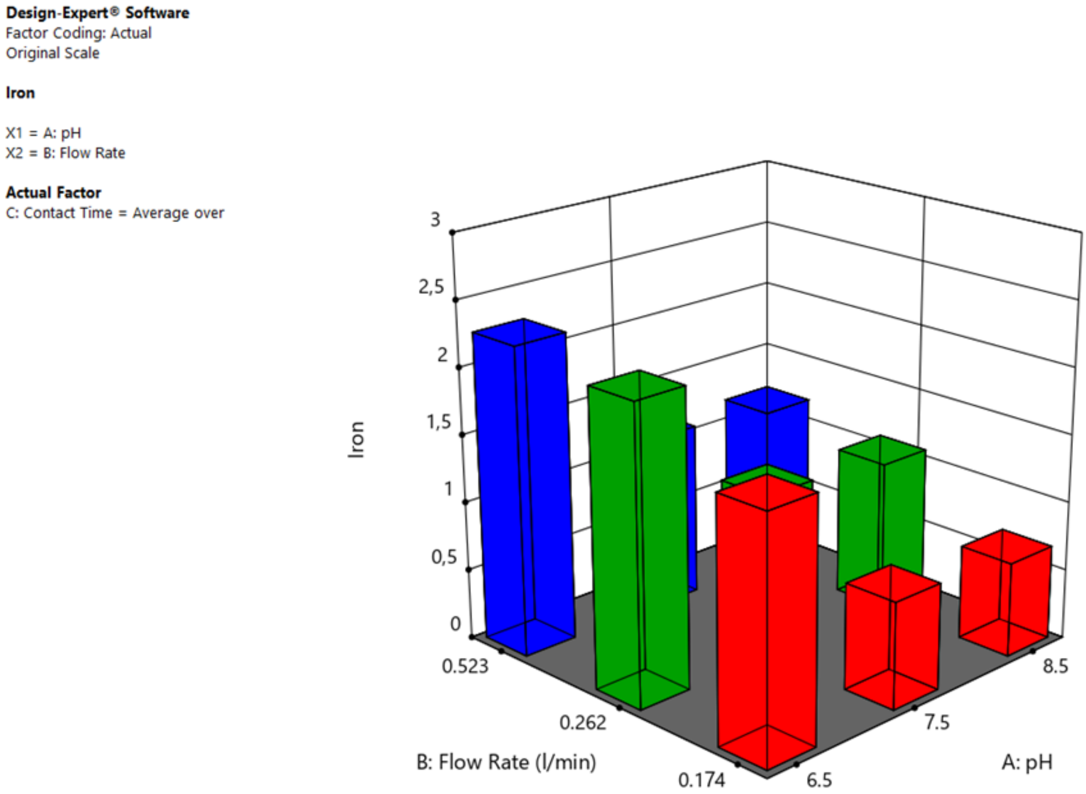

Figure 5 4: 3-D Contour plot Iron removal average performance

Figure 5-4 shows the contour and 3D graphs for the factor's pH and flow rate, with the Iron concentration kept constant, so that the relationship between factors A and B can be assessed. It can be seen from the graphs that the pH value of 8.5 and the low flow rate of 0.174l/min are yielding the optimal Iron removal efficiencies. Both these parameters seem to play a vital role for the removal of iron, this is due to the high alkalinity in the water that allows more negative ions where iron can be attracted to, as compared to high iron adsorption rejection at the pH of 6.5 and flow rate 0.523 l/min, also illustrated on Figure 5-4 above.

5.4.5 Iron removal Box Model

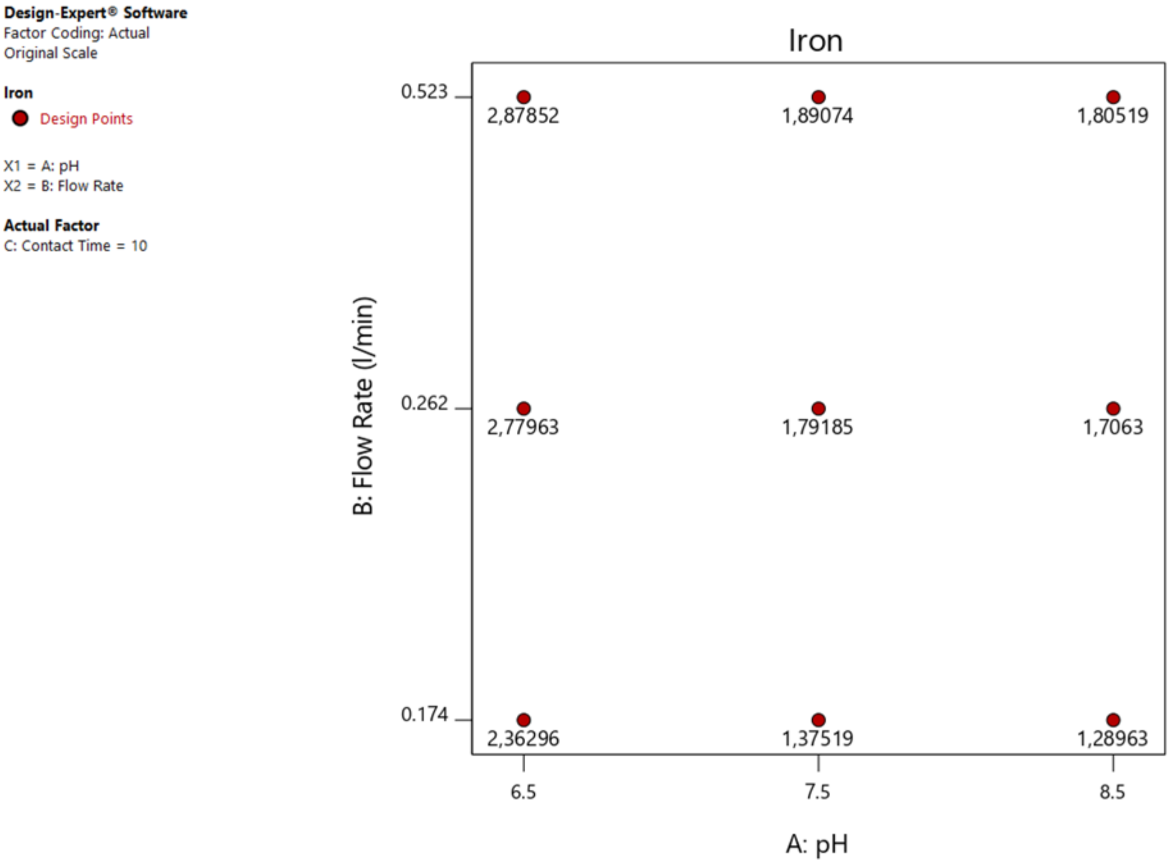

Figure 5 5: Iron Box model

Figure 5-5 shows the box generated by the Design Expert software for the removal of Iron for the factors pH and flow rate. The box model indicates that the main contributing factor for Iron removal is pH, and then flow rate second. As notice on the above Figure 5-5 pH of 8.5 has best results as compared to other pH values.

Table 5 3: Box-Behnken Design output results for Manganese (Mn) removal

Run	Factors			Manganese(Mn) Removal %	
	A:pH	B:Flow Rate (l/min)	C:Contact Time (min)	Actual Value	Predicted Value
1	8.5	0.174	10	80%	79%
2	8.5	0.174	60	80%	79%
3	7.5	0.523	10	77%	78%
4	8.5	0.523	30	79%	78%
5	7.5	0.262	30	88%	86%
6	6.5	0.174	30	77%	79%
7	6.5	0.523	60	81%	80%
8	8.5	0.262	30	81%	85%
9	6.5	0.262	10	93%	91%
10	8.5	0.174	30	83%	81%
11	8.5	0.523	60	78%	76%
12	6.5	0.523	10	81%	85%
13	8.5	0.262	60	80%	83%
14	6.5	0.174	60	81%	83%
15	7.5	0.174	10	80%	81%
16	7.5	0.523	30	79%	80%
17	6.5	0.262	60	86%	87%
18	7.5	0.174	30	81%	82%
19	7.5	0.174	60	83%	84%
20	7.5	0.262	10	86%	85%
21	7.5	0.523	60	83%	82%
22	7.5	0.262	60	89%	88%
23	8.5	0.262	10	80%	83%
24	8.5	0.523	10	77%	76%
25	6.5	0.523	30	77%	77%
26	6.5	0.174	10	89%	87%
27	6.5	0.262	30	86%	83%

The results of the experimental output and predicted values of Manganese removal for the 27 run experiments are presented in Table 5-3, where the results clearly illustrate that a maximum Manganese removal of 93.0% was attained with experiment 9, at pH 6.5, flow rate 0.262 l/min and contact time of 10 minute. A notable fair agreement of the results was reached when the R^2 predicted was in close correlation with an experimental R^2.

Table 5- 4: ANOVA Manganese Analysis

Analysis of Variance Table [Partial sum of squares – Type II]					
Source	**Sum of Squares**	**df**	**Mean Square**	**F-value**	**p-value**
Model	0.2788	10	0.0279	7.66	0.0002
A-pH	0.0496	2	0.0248	6.82	0.0072
B-Flow Rate	0.1441	2	0.0721	19.81	< 0.0001
C-Contact Time	0.008	2	0.004	1.09	0.3586
AC	0.0771	4	0.0193	5.3	0.0065
Residual	0.0582	16	0.0036		
Cor Total	0.337	26		**R^2**	0.8273
Std. Dev.	0.0603			**Adjusted R^2**	0.7193
Mean	0.4837			**Predicted R^2**	0.5081
Coefficient of Varience %	12.47			**Adeq Precision**	105,914

Analysis of Variance (ANOVA) was used to test the difference between means for statistical significance and to evaluate the validity of the fitted model Table 5-4

Manganese Removal%=$+0.4837-0.0393A^1-0.0204A^2+0.119B^1-0.0948B^2-0.0148C^1+$

$0.0241C^2-0.0963A^1C^1+0.0615A^2C^1+0.0748A^1C^2-0.0207A^2C^2$

Equation 5-2: Manganese removal %

The Model F-value of 7.66 implies the model significance and that only 0.02% chance that an F-value this large could occur due to noise**.** P-values less than 0.0500 indicate model terms are significant for this experiment pH (A) and flow rate (B) are significant model terms. Their P values are less than 0.0500. The Predicted R^2 of 0.5081 is not as close to the Adjusted R^2 of 0.7193 as one might typically expect; i.e. the difference is more than 0.2. This may indicate a large block effect or a possible problem with the model and/or data. Adeq Precision measures the signal to noise ratio. A ratio greater than 4 is desirable. The ratio of 10.591 indicates an adequate signal. This model can be used to navigate the design space.

5.5 Manganese (Mn) Model Validation

5.5.1. Actual vs. Predicted Values for Manganese

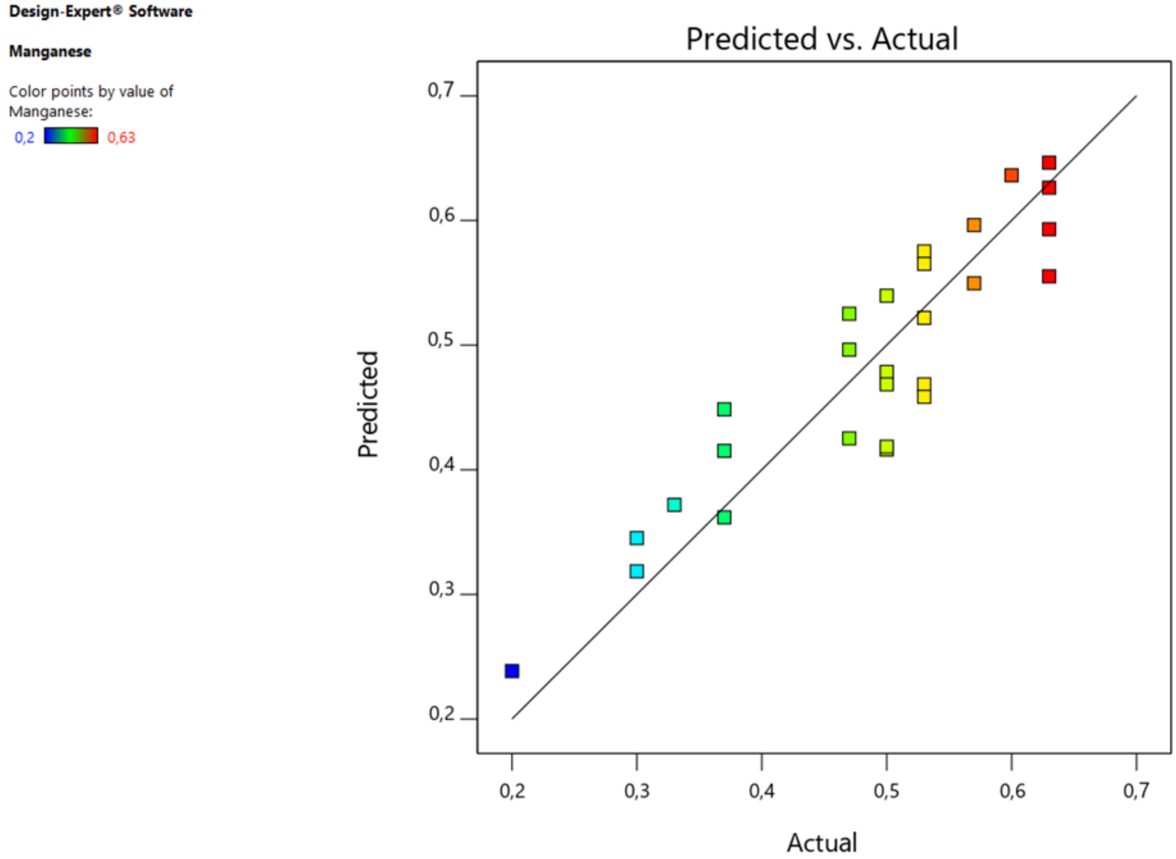

Figure 5 6: Actual vs. Predicted Values for Manganese

The Actual vs. predicted models represented by Figure 5.1 is validated by the predicted value points that are close to the experimental values of Manganese, as illustrated above the values are not far apart from one another, that confirm the model validity.

5.5.2. Normal plot of residuals Manganese

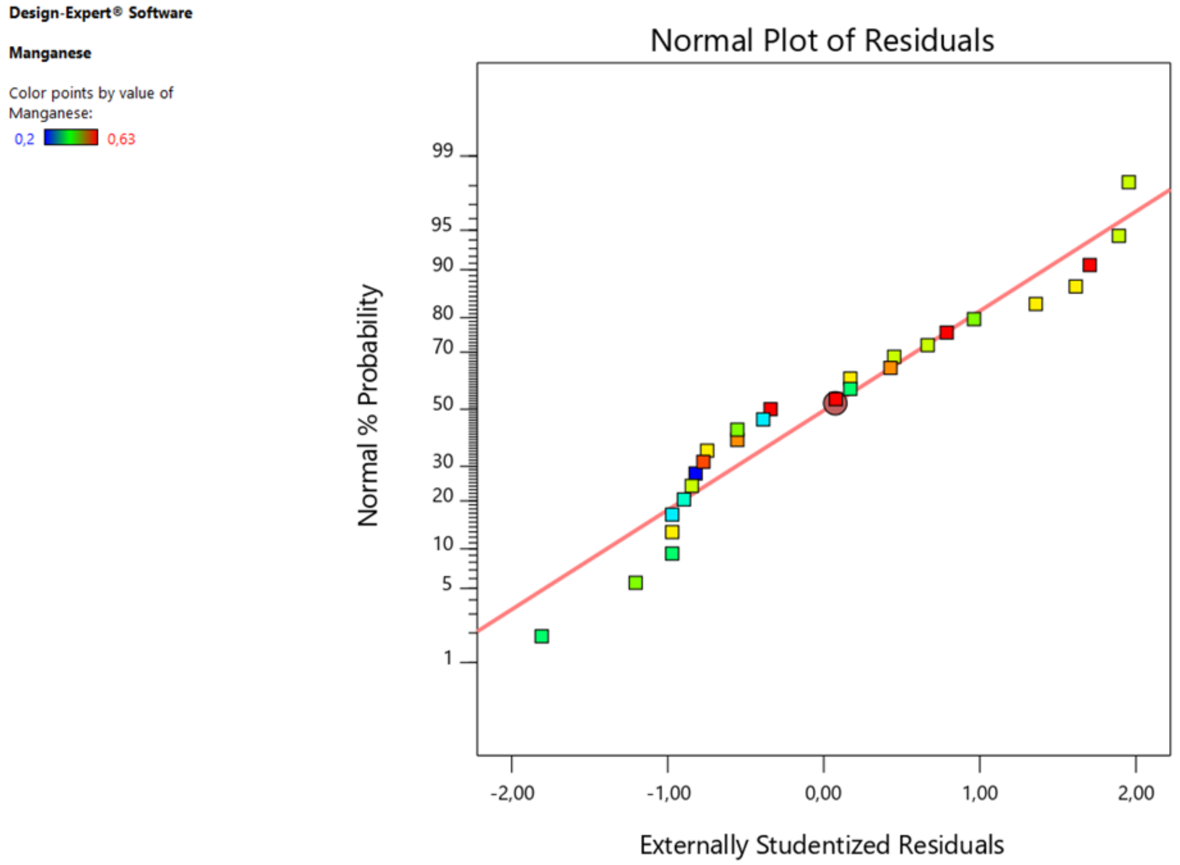

Figure 5 7: Normal plot of residuals Manganese

The data normality can be evaluated by plotting the normal probability graph with the residuals as seen in Figure 5.2. This plot is a technique that graphically determines the proximity of data distribution (Antoy, 2014). If the plot points are reasonably close to the straight line it can be surmised that the data is normally distributed. It is noticeable on Figure 5.2 that the normal probability plot the points are closely aligned, suggesting normal distribution. The linear fit validates the normality of the data for Manganese removal.

5.5.3. Residual vs. Predicted Manganese

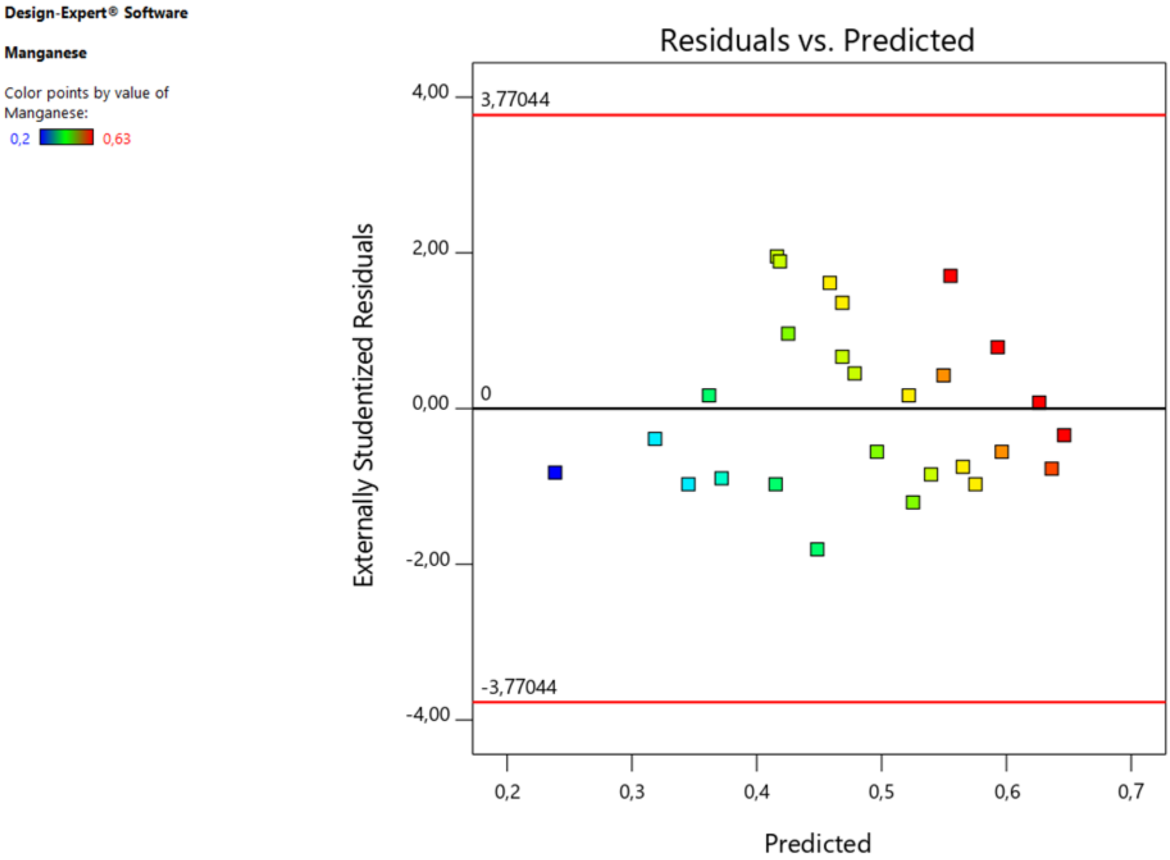

Figure 5 8: Residual vs. Predicted Manganese

The residuals vs. predicted graph for the Manganese data can be seen in figure 5-3. According to Roman, (2021) an indication that the model is correct is that there is no obvious pattern or structure shown by the residuals. From figure 5-3 it can be seen that it is in accordance with the statement made by the author as the points are all scattered randomly.

5.5.4. 3-D Contour plot Manganese removal average performance

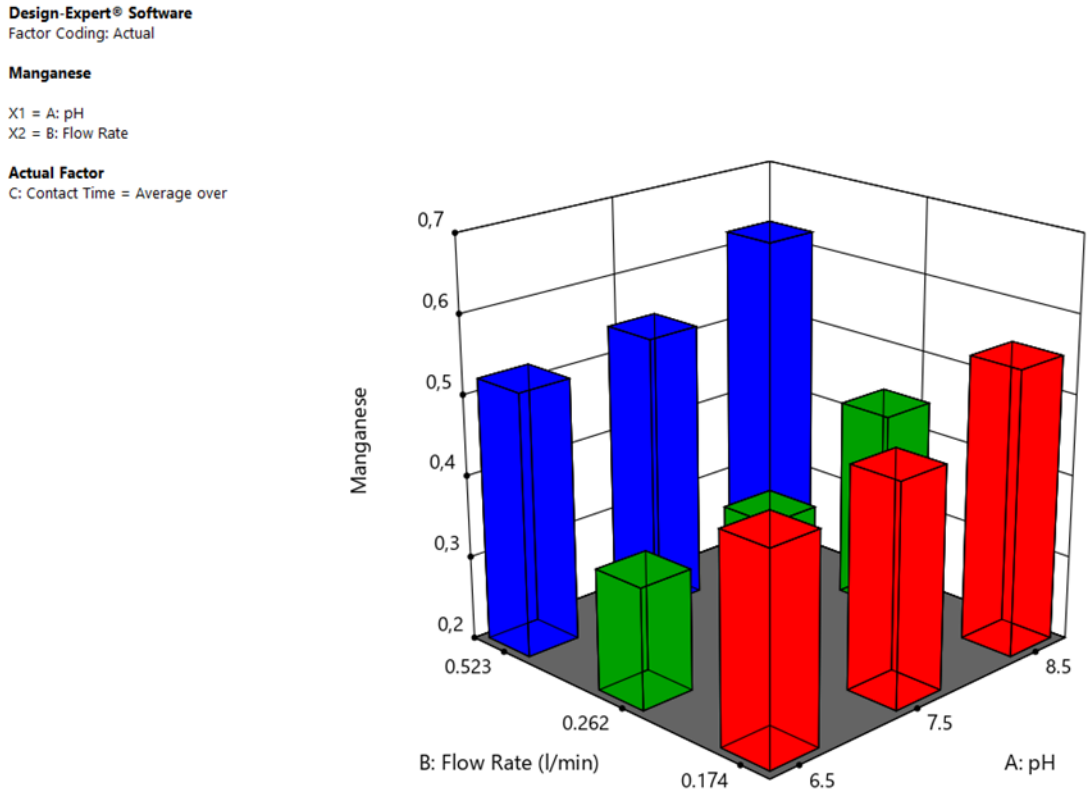

Figure 5 9: 3-D Contour plot Manganese removal average performance

Figure 5-4 shows the contour and 3D graphs for the factor's pH and flow rate, with the Manganese concentration kept constant, so that the relationship between factors A and B can be assessed. It can be seen from the graphs that pH values of 6.5 and the medium flow rate of 0.262l/min are yielding the optimal Iron removal efficiencies. Both these parameters seem to play a vital role for the removal of Manganese. Manganese showed high removal efficiencies due to Manganese oxygen tolerant, for the oxidising agents injected into the system to enhance oxidation (Vries et al., 2017).

5.5.5. Manganese Box Model

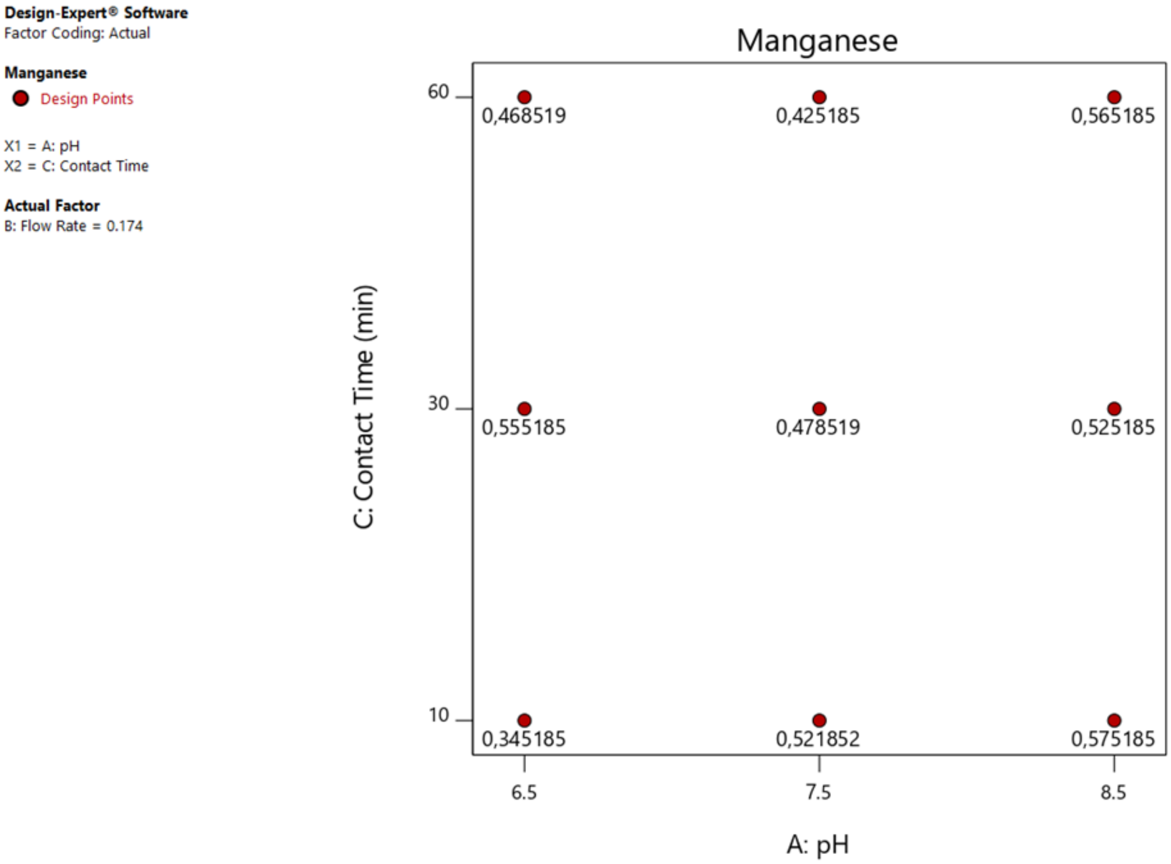

Figure 5 10: Manganese Box model

Figure 5-5 shows the box generated by the Design Expert software for the removal of Manganese for the factors pH and contact time. The box model indicates that the main contributing factor for Manganese removal is pH, and then contacts time second. As notice on the above Figure 5-5 pH of 6.5 has best results as compared to other pH values.

CHAPTER6

Conclusion

&

Recommendations

6. Conclusion and recommendation

6.1 Conclusion

The integrated treatment process used in this study consisted of two steps, chemical dosage (oxidation) and adsorption. The favourable conditions for removing Iron (Fe) and Manganese (Mn) from groundwater were investigated in various medium-packed bed columns.

The chemical dosage was applied to enhance the removal of Fe and Mn from groundwater by oxidation. The adsorption process was investigated to determine the effects of pH, flow rate and dosage on removing Fe and Mn in sixty minutes. The isotherms and kinetics models were then applied to describe the adsorption data.

The FTIR was used to determine the functional group on the mediums, Glass Media, Polystyrene Beads and ion exchange resin; the FTIR results indicated that the medium contains bonds favourable for Fe and Mn adsorption.

The highest average removal of Fe and Mn were 71% and 89% in sixty minutes, respectively. However, the best removal of Fe and Mn was 93% at these conditions of pH: 8.5, flow rate: 0.174l/min and dosage: 1.67ml/min for Fe at 50 minutes and pH: 6.5, flow rate: 2.52l/min and dosage: 0.262ml/min for Mn at 20 minutes. Fe was more pH and flow rate dependent of all three operating conditions than Mn, and Mn was more oxidation rate dependent. From these results, it can be said the adsorption of Fe best occurs at high pH and low flow rate, which results in extended contact time, and Mn occurs at high oxidant dosing.

The adsorption mechanism is observed to be governed by pseudo-second-order reaction kinetics and follows the Freundlich Isotherms closely for the removal of iron and manganese. The Mathematical model Adams & Bohart Model illustrated high adsorption capacities compared to Yoon Nelson and Thomas's model.

6.2 Recommendation

Future researchers should investigate specifically the low pH effect of removing iron from groundwater—the manganese groundwater compound's capability to enhance manganese removal from the solution. The oxidation effectiveness of oxygen is produced from the reaction of sodium hypochlorite and hydrogen peroxide. Lastly, to investigate the acceptable sizes of glass, polystyrene beads and ion exchange media in one column to remove iron and manganese to determine if the medium size affects these metal adsorption.

References

7. References

A.O, D. (2012). Langmuir, Freundlich, Temkin and Dubinin–Radushkevich Isotherms Studies of Equilibrium Sorption of Zn 2+ Unto Phosphoric Acid Modified Rice Husk. *IOSR Journal of Applied Chemistry*, *3*(1), 38–45. https://doi.org/10.9790/5736-0313845

Africa, S. (2018). *WWF-SA Addressing food-related health challenges in South Africa : Is there appetite for collaboration ?*

Ahmad, M. (2012). Iron and Manganese removal from groundwater Iron and manganese removal from groundwater. *DUO Research Archieve*, *10852/1254*(University of Oslo).

Antoy, J. (2014). Design of Experiments for Engineers and Scientists: Second Edition. *Design of Experiments for Engineers and Scientists: Second Edition*, *July*, 1–672. https://doi.org/10.1016/C2012-0-03558-2

Apiratikul, R., & Chu, K. H. (2021). Improved fixed bed models for correlating asymmetric adsorption breakthrough curves. *Journal of Water Process Engineering*, *40*(April). https://doi.org/10.1016/j.jwpe.2020.101810

Arun Yadav,Abhijit Sonje,Priyanka Mathur,Amrish Chandra, D. A. J. and C. P. (2012). Detailed Study of Ground Water , Contamination Sources & Approches To Clean Ground Water. *International Journal of Comprehensive Pharmacy*, *02*(02), 1–5.

Aziz, M., & Kasongo, G. (2019). Scaling prevention of thin film composite polyamide Reverse Osmosis membranes by Zn ions [Article]. *Desalination*, *464*, 76–83. https://doi.org/10.1016/j.desal.2019.04.021

Babu, J. R. (2015). Assessment of Groundwater Pollution in Parts of Guntur District Using Remote Sensing & GIS Assessment of Groundwater Pollution in Parts of Guntur District Using. *Researchgate.Net*, *04*(July 2011), 1024–1030. https://www.researchgate.net/profile/John_Babu_M/publication/267252045_Assessment_of_Groundwater_Pollution_in_Parts_of_Guntur_District_Using_Remote_Sensing_GIS/links/55c58de208aebc967df38db9.pdf

Baharudin, F., Mohd Tadza, M. Y., Mohd Imran, S. N., & Jani, J. (2018). Removal of Iron and Manganese in Groundwater using Natural Biosorbent. *IOP Conference Series: Earth and Environmental Science*, *140*(1). https://doi.org/10.1088/1755-1315/140/1/012046

Barloková, D., & Ilavský, J. (2010). Removal of iron and manganese from water using filtration by natural materials. *Polish Journal of Environmental Studies*, *19*(6), 1117–

1122.

Bekri-Abbes, I., Bayoudh, S., Baklouti, M., Papon, E., & LeClercq, D. (2006). Converting waste polystyrene into adsorbent: Optimisation of reaction parameters and properties. *Progress in Rubber, Plastics and Recycling Technology*, *22*(3), 179–193. https://doi.org/10.1177/147776060602200303

Botai, C. M., Botai, J. O., & Adeola, A. M. (2018). Spatial distribution of temporal precipitation contrasts in South Africa. *South African Journal of Science*, *114*(7–8). https://doi.org/10.17159/sajs.2018/20170391

Boyraz, U. (2012). *An Investigation on Ground Water Flow Incorporating Surface / Ground Water Interactions Surface / Ground Water Interactions*. *June*, 1–11.

By, P., & Ahmed Mohamed Atta, E. (2007). *Iron and manganese rremoval technologies*. *1*, 1–15. https://s3.amazonaws.com/academia.edu.documents/33928884/Iron_and_Manganese_Removal.pdf?AWSAccessKeyId=AKIAIWOWYYGZ2Y53UL3A&Expires=1528288159&Signature=j0ZdzNlUcgPBLUQwnGDSjDcPLVA%3D&response-content-disposition=inline%3B filename%3DIron_and_Manganese_Re

Camargo, F., Leucas, H. De, & Ladeira, A. C. (n.d.). *Sorption / Oxidation of Manganese in Aqueous System*. *60*, 1–7.

Chandler, J. (1989). Iron and manganese. *Water Well Journal*, *43*(3), 40–42. https://doi.org/10.1201/9780203491454.ch10

Cheng, Y., Huang, T., Liu, C., & Zhang, S. (2019). Effects of dissolved oxygen on the start-up of manganese oxides filter for catalytic oxidative removal of manganese from groundwater. *Chemical Engineering Journal*, *371*(February), 88–95. https://doi.org/10.1016/j.cej.2019.03.252

Cheshire, J. (2022). Making the invisible visible. In *Significance* (Vol. 19, Issue 3). https://doi.org/10.1111/1740-9713.01654

Dalai, C., Jha, R., & Desai, V. R. (2015). Rice Husk and Sugarcane Baggase Based Activated Carbon for Iron and Manganese Removal. *Aquatic Procedia*, *4*(Icwrcoe), 1126–1133. https://doi.org/10.1016/j.aqpro.2015.02.143

Dashtban Kenari, S. L., & Barbeau, B. (2016). Understanding ultrafiltration fouling of ceramic and polymeric membranes caused by oxidized iron and manganese in water treatment. *Journal of Membrane Science*, *516*(June), 1–12.

https://doi.org/10.1016/j.memsci.2016.06.003

De Munari, A., & Schäfer, A. I. (2010). Impact of speciation on removal of manganese and organic matter by nanofiltration. *Journal of Water Supply: Research and Technology - AQUA*, *59*(2–3), 152–163. https://doi.org/10.2166/aqua.2010.067

Deng, Y., Englehardt, J. D., Abdul-Aziz, S., Bataille, T., Cueto, J., De Leon, O., Wright, M. E., Gardinali, P., Narayanan, A., Polar, J., & Tomoyuki, S. (2013). Ambient iron-mediated aeration (IMA) for water reuse. *Water Research*, *47*(2), 850–858. https://doi.org/10.1016/j.watres.2012.11.005

Diaz-Alarcón, J. A., Alfonso-Pérez, M. P., Vergara-Gómez, I., Díaz-Lagos, M., & Martínez-Ovalle, S. A. (2019). Removal of iron and manganese in groundwater through magnetotactic bacteria. *Journal of Environmental Management*, *249*(June), 109381. https://doi.org/10.1016/j.jenvman.2019.109381

Dima, J. B., Ferrari, M., & Zaritzky, N. (2020). Mathematical Modeling of Fixed-Bed Columns Adsorption: Hexavalent Chromium onto Chitosan Flakes. *Industrial and Engineering Chemistry Research*, *59*(34), 15378–15386. https://doi.org/10.1021/acs.iecr.0c02004

Division, S. S. (2011). *SANS 241-1 : 2011 SOUTH AFRICAN NATIONAL STANDARD Drinking water Part 1 : Microbiological , physical , aesthetic*.

du Toit, W., Holland, M., Weidemann, R., & Botha, F. (2012). Can groundwater be successfully implemented as a bulk water resource within rural Limpopo Province? analysis based on GRIP datasets. *Water SA*, *38*(3), 391–398. https://doi.org/10.4314/wsa.v38i3.4

EPA. (2007). Healthy Drinking Waters. *Report*, 1–4.

Espinoza Márquez, E., Soto Zarazúa, G. M., & Pérez Bueno, J. de J. (2020). Prospects for the Use of Electrooxidation and Electrocoagulation Techniques for Membrane Filtration of Irrigation Water. *Environmental Processes*, 391–420. https://doi.org/10.1007/s40710-020-00439-2

Ferreira, A. S., Mota, A. A., Oliveira, A. M., Rodrigues, F. I. L., Pacífico, S. N., Da Silva, J. E., Abagaro, B. T. O., Saraiva, G. D., De Castro, A. J. R., Teixeira, R. N. P., & Sousa Neto, V. O. (2019). Equilibrium and kinetic modelling of adsorption: Evaluating the performance of adsorbent in softening water for irrigation and animal consumption. *Revista Virtual de Quimica*, *11*(6), 1752–1766. https://doi.org/10.21577/1984-6835.20190123

File, W. W. (2018). *WWF Wednesday Water File Getting To Grips With Groundwater*. *January*, 5–7.

Flintsch, G. W. (2012). *S Urface C Haracteristics*. *October*.

Ghosh, G. C., Khan, M. J. H., Chakraborty, T. K., Zaman, S., Kabir, A. H. M. E., & Tanaka, H. (2020). Human health risk assessment of elevated and variable iron and manganese intake with arsenic-safe groundwater in Jashore, Bangladesh. *Scientific Reports*, *10*(1). https://doi.org/10.1038/s41598-020-62187-5

Goher, M. E., Hassan, A. M., Abdel-Moniem, I. A., Fahmy, A. H., Abdo, M. H., & El-sayed, S. M. (2015). Removal of aluminum, iron and manganese ions from industrial wastes using granular activated carbon and Amberlite IR-120H. *Egyptian Journal of Aquatic Research*, *41*(2), 155–164. https://doi.org/10.1016/j.ejar.2015.04.002

Goodwill, J. E. (2015). *ScholarWorks @ UMass Amherst Evaluation of Ferrate Preoxidation for Drinking Water Treatment Submitted to the Graduate School of the*. *November*.

Govorova, Z., Semenovykh, V., & Medvedeva, V. (2019). Compact groundwater treatment units. *IOP Conference Series: Materials Science and Engineering*, *687*(4). https://doi.org/10.1088/1757-899X/687/4/044025

Hameed, S. (2019). Removal of Iron and Manganese from Ground Water by Different Techniques. *Journal of Research on the Lepidoptera*, *50*(4), 458–468. https://doi.org/10.36872/lepi/v50i4/201110

Imaging, M. R., View, M., Effects, S., & Edition, S. (2016). *Iron oxide*.

Indah, S., & Helard, D. (2017). Evaluation of Iron and Manganese-coated Pumice from Sungai Pasak, West Sumatera, Indonesia for the Removal of Fe (II) and Mn (II) from Aqueous Solutions. *Procedia Environmental Sciences*, *37*, 556–563. https://doi.org/10.1016/j.proenv.2017.03.042

Inglezakis, V. J., & Fyrillas, M. M. (2017). Adsorption fixed beds modeling revisited: Generalized solutions for S-shaped isotherms. *Chemical Engineering Communications*, *204*(11), 1299–1317. https://doi.org/10.1080/00986445.2017.1364240

Ioannou, A., Paschalidis, C., Doula, M., Paschalidis, C., & Doula, M. (1994). The sorption isotherms of potassium. *Communications in Soil Science and Plant Analysis*, *25*(9–10), 1373–1386. https://doi.org/10.1080/00103629409369121

Isaeva, M., & Castro, N. M. (2011). Water Treatment for the Removal of Iron and Manganese. *Bachelors Degree Project*. http://www.divaportal.org/smash/get/diva2:460329/FULLTEXT01

Iserhien-Emekeme, R., Ofomola, M. O., Bawallah, M., & Anomohanran, O. (2017). Lithological identification and underground water conditions in Jeddo using geophysical and geochemical methods. *Hydrology*, *4*(3). https://doi.org/10.3390/hydrology4030042

Jestinos Mzezewa. (2010). *Characterisation of rainfall at a semi-arid ecotope in the Limpopo Province (South Africa) and its implications for sustainable crop production*. *36*(1). http://www.wrc.org.za

Khadse, G. K., Patni, P. M., & Labhasetwar, P. K. (2015). Removal of iron and manganese from drinking water supply. *Sustainable Water Resources Management*, *1*(2), 157–165. https://doi.org/10.1007/s40899-015-0017-4

KRISHNAIAH, K., & SHAHABUDEEN, P. (2012). *Applied Design of Experiments and Taguchi Methods* (Issue June). https://books.google.com/books?id=hju9JYVhfV8C&pgis=1

Kumar, R., & Raj, H. (2018). Threat and Mitigation of Ground Water Contamination in India. *Acta Scientific Nutritional Health*, *2*(8), 29–31.

Kumari, R., Khan, M. A., Mahto, M., Qaiyum, M. A., Mohanta, J., Dey, B., & Dey, S. (2020). Dewaxed Honeycomb as an Economic and Sustainable Scavenger for Malachite Green from Water. *ACS Omega*, *5*(31), 19548–19556. https://doi.org/10.1021/acsomega.0c02011

Kwakye-Awuah, B., Sefa-Ntiri, B., Von-Kiti, E., Nkrumah, I., & Williams, C. (2019). Adsorptive removal of iron and manganese from groundwater samples in Ghana by zeolite y synthesized from bauxite and kaolin. *Water (Switzerland)*, *11*(9). https://doi.org/10.3390/w11091912

Lazar, L., Bandrabur, B., Tataru-f, R., Drobot, M., Bulgariu, L., & Gutt, G. (2014). *Ftir Analysis of Ion Exchange Resins With Application*. *13*(9), 2145–2152.

Li, C., Wang, S., Du, X., Cheng, X., Fu, M., Hou, N., & Li, D. (2016). Immobilization of iron- and manganese-oxidizing bacteria with a biofilm-forming bacterium for the effective removal of iron and manganese from groundwater. *Bioresource Technology*, *220*, 76–84. https://doi.org/10.1016/j.biortech.2016.08.020

Liu, X., Liu, W., Liu, L., Tang, Q., Liu, J., & Yang, H. (2021). Environmental flow requirements largely reshape global surface water scarcity assessment. *Environmental Research Letters*, *16*(10). https://doi.org/10.1088/1748-9326/ac27cb

M. Hamzaoui, , B. Bestani, N. B. (2018). The use of linear and nonlinear methods for adsorption isotherm optimization of basic green 4-dye onto sawdust-based activated carbon. *Journal of Material and Environmental Sciences*, *9*(4), 1110–1118.

M, P. M. P., M, S. M. B., & Kavya, S. (2016). Greywater Reuse: A sustainable solution for Water Crisis in Bengaluru City, Karnataka, India. *International Journal of Research in Chemical, Metallurgical and Civil Engineering*, *3*(1), 1–4. https://doi.org/10.15242/ijrcmce.iae0316411

Malik, D. S., Jain, C. K., & Yadav, A. K. (2018). Heavy Metal Removal by Fixed-Bed Column – A Review. *ChemBioEng Reviews*, *5*(3), 173–179. https://doi.org/10.1002/cben.201700018

Manahan , Stanley E. " ENVIRONMENTAL SCIENCE, TECHNOLOGY, AND CHEMISTRY ". (n.d.).

Mohd Remy Rozainy, M. A. Z., Jamil, R., & Adlan, M. N. (2015). A review of removal iron and manganese by using cascade aeration systems. *Jurnal Teknologi*, *74*(11), 69–76. https://doi.org/10.11113/jt.v74.4875

Molari, M., Janssen, F., Janssen, F., Vonnahme, T. R., Vonnahme, T. R., Wenzhöfer, F., Wenzhöfer, F., Boetius, A., & Boetius, A. (2020). The contribution of microbial communities in polymetallic nodules to the diversity of the deep-sea microbiome of the Peru Basin (4130-4198m depth). *Biogeosciences*, *17*(12), 3203–3222. https://doi.org/10.5194/bg-17-3203-2020

Mota, E. A., Felestrino, É. B., Leão, V. A., & Guerra-Sá, R. (2020). Manganese (II) removal from aqueous solutions by Cladosporium halotolerans and Hypocrea jecorina. *Biotechnology Reports*, *25*. https://doi.org/10.1016/j.btre.2020.e00431

Naik, P. K. (2015). *Remediation of Arsenic Contamination in Groundwater*. *June*, 1–14.

Nalbantcilar, M. T., & Pinarkara, D. (2015). Impact of industry on ground water contamination: A case study in Konya city, Turkey. *Global Nest Journal*, *17*(4), 796–815. https://doi.org/10.30955/gnj.001635

Ojovan, M. I., & Lee, W. E. (2005). Immobilisation of Radioactive Wastes in Glass. *An Introduction to Nuclear Waste Immobilisation*, 213–249. https://doi.org/10.1016/b978-008044462-8/50019-3

Omitola, O. B., Abonyi, M. N., Akpomie, K. G., & Dawodu, F. A. (2022). Adams - Bohart , Yoon - Nelson , and Thomas modeling of the fix - bed continuous column adsorption of amoxicillin onto silver nanoparticle - maize leaf composite. *Applied Water Science*, *12*(5), 1–9. https://doi.org/10.1007/s13201-022-01624-4

Orlov, Valerii, Martynov, S., & Kunytskiy, S. (2016). Energy saving in water treatment technologies with polystyrene foam filters. *Journal of Water and Land Development*, *31*(1), 119–122. https://doi.org/10.1515/jwld-2016-0042

Orlov, Valeriy, Safonyk, A., Martynov, S., & Kunytskyi, S. (2016). Simulation the process of iron removal the underground water by polystyrene foam filters. *International Journal of Pure and Applied Mathematics*, *109*(4), 881–888. https://doi.org/10.12732/ijpam.v109i4.11

Osuagwu, J. C., Nwakwasi, N. L., & Nwachukwu, A. N. (2018). Iron removal in waste water using expanded polystyrene as an artificial media. *Nigerian Journal of Technology*, *37*(3), 841. https://doi.org/10.4314/njt.v37i3.38

Ozturk, G., & Silah, H. (2020). Adsorptive Removal of Remazol Brilliant Blue R from Water by Using a Macroporous Polystyrene Resin: Isotherm and Kinetic Studies. *Environmental Processes*, 479–492. https://doi.org/10.1007/s40710-020-00429-4

Palmucci, W., Rusi, S., & Di Curzio, D. (2016). Mobilisation processes responsible for iron and manganese contamination of groundwater in Central Adriatic Italy. *Environmental Science and Pollution Research*, *23*(12), 11790–11805. https://doi.org/10.1007/s11356-016-6371-4

Patel, H. (2021). Comparison of batch and fixed bed column adsorption: a critical review. *International Journal of Environmental Science and Technology*, *June*. https://doi.org/10.1007/s13762-021-03492-y

Patel, Himanshu. (2019). Fixed-bed column adsorption study: a comprehensive review. *Applied Water Science*, *9*(3), 1–17. https://doi.org/10.1007/s13201-019-0927-7

Piccin, J. S., Dotto, G. L., & Pinto, L. A. A. (2011). Adsorption isotherms and thermochemical data of FDandC RED N° 40 Binding by chitosan. *Brazilian Journal of Chemical Engineering*, *28*(2), 295–304. https://doi.org/10.1590/S0104-66322011000200014

Polakovic, M., Gorner, T., Villiéras, F., De Donato, P., & Bersillon, J. L. (2005). Kinetics of salicylic acid adsorption on activated carbon. *Langmuir*, *21*(7), 2988–2996. https://doi.org/10.1021/la047143+

Prasad, N. (2011). *GROUND WATER RECHARGE Some of the authors of this publication are also working on these related projects: Improvements in Drinking Water Supply in*

Drought Prone Thrithala Panchayat With People's Participation " funded by DST, New Delhi View project Landslides in the Western Ghats-A Case Study View project N B Narasimha Prasad Centre for Water Resources Development and Management. https://doi.org/10.13140/RG.2.2.21142.55367

Rivera, A. (2017). The state of ground water in Canada. *Ground Water Canada*, *January*. https://www.groundwatercanada.com/education/the-state-of-ground-water-what-we-know-and-dont-know-about-ground-water-in-canada-3584

Robey, K. (2014). *A feasibility study of in-situ iron removal in the Atlantis Primary Aquifer, Western Cape Province, South Africa*. *August*, 1–175.

Roccaro, P., Barone, C., Mancini, G., & Vagliasindi, F. G. A. (2007). Removal of manganese from water supplies intended for human consumption: a case study. *Desalination*, *210*(1–3), 205–214. https://doi.org/10.1016/j.desal.2006.05.045

Roman, F. (2021a). *The treatment of carwash wastewater using an integrated chemical coagulation and adsorption process*. *July*.

Roman, F. (2021b). *The treatment of carwash wastewater using an integrated chemical coagulation and adsorption process*. *June*.

Saeidi, N., & Parvini, M. (2015). Accuracy of Dubinin-Astakov and Dubinin-Raduchkevic Adsorption Isotherm Models in Evaluating Micropore Volume of Bontonite. *Periodica Polytechnica Chemical Engineering*, *60*(2), 123–129. https://doi.org/10.3311/ppch.8374

Said, K. A. M., Ismail, N. Z., Jama'in, R. L., Alipah, N. A. M., Sutan, N. M., Gadung, G. G., Baini, R., & Zauzi, N. S. A. (2018). Application of freundlich and Temkin isotherm to study the removal of Pb(II) via adsorption on activated carbon equipped polysulfone membrane. *International Journal of Engineering and Technology(UAE)*, *7*(3.18 Special Issue 18), 91–93. https://doi.org/10.14419/ijet.v7i3.18.16683

Salem, M. G., El-Awady, M. H., & Amin, E. (2012). Enhanced removal of dissolved iron and manganese from nonconventional water resources in delta district, Egypt. *Energy Procedia*, *18*, 983–993. https://doi.org/10.1016/j.egypro.2012.05.113

Sanderson, M. R., & Frey, R. S. (2015). Structural impediments to sustainable groundwater management in the High Plains Aquifer of western Kansas. *Agriculture and Human Values*, *32*(3), 401–417. https://doi.org/10.1007/s10460-014-9567-6

SANS. (2015). South African National Standard (SANS). *Drinking Water for SANS*, *241*, 1–2. https://vinlab.com/wp-content/uploads/2016/10/SANS-241-2015.pdf

Sarkar, S., Poulose, S., Sahoo, P. K., & Joseph, J. (2018). Flexible and stretchable guided-mode resonant optical sensor: single-step fabrication on a surface engineered polydimethylsiloxane substrate. *OSA Continuum*, *1*(4), 1277. https://doi.org/10.1364/osac.1.001277

Scher, C. A., & Caputo, D. L. (2014). A Forensic Approach to Solve a Ground Water Contamination Problem. *Proceedings of the Water Environment Federation*, *2006*(11), 1800–1810. https://doi.org/10.2175/193864706783750015

Schöntag, J. M., Pizzolatti, B. S., Jangada, V. H., de Souza, F. H., & Sens, M. L. (2015). Water quality produced by polystyrene granules as a media filter on rapid filters. *Journal of Water Process Engineering*, *5*, 118–126. https://doi.org/10.1016/j.jwpe.2015.02.001

Services, H. (2002). Toxicological Profile for 2-Hexanone. *ATSDR's Toxicological Profiles*, *September*. https://doi.org/10.1201/9781420061888_ch4

Sharifi, S., Hosseini, M., Mirzaei, A., & Salmani Oskuloo, A. (2015). Catalytic Decomposition of Hydrogen Peroxide in the Presence of Synthesized Iron-Manganese oxide Nanocomposites via Different Methods. *International Journal of Nanoscience and Nanotechnology*, *11*(4), 233–240.

Sharma, S. K. (2001). Adsorptive iron removal from groundwater. *Intemational Institute for Infrastructural, Hydraulic and Environmental Engineering*, *Master the*, 39–41.

Sheet, S. D. (2018). *Crushed Glass Filter Media*. *May*, 1–4.

Talaat, H. A., Ghaly, M. Y., Kamel, E. M., Ahmed, E. M., & Awad, A. M. (2010). Simultaneous Removal of Iron and Manganese from Ground Water by Combined Photo-Electrochemical Method. *Journal of American Science*, *6*(12), 1–12. http://www.sciencepub.net/nature

Tekerlekopoulou, A. G., Vasiliadou, I. A., & Vayenas, D. V. (2006). Physico-chemical and biological iron removal from potable water. *Biochemical Engineering Journal*, *31*(1), 74–83. https://doi.org/10.1016/j.bej.2006.05.020

Tredoux, G., Cavé, L., & Engelbrecht, P. (2004). Groundwater pollution: Are we monitoring appropriate parameters? *Water SA*, *30*(5), 662–667. https://doi.org/10.4314/wsa.v30i5.5180

Turp, S. M., Turp, A., Ekinci, N., Ozdemir, S., & Yetilmezsoy, K. (2022). *IMPROVED METHYLENE BLUE BIOSORPTION ONTO GREEN ALGAE : Ulva IMPROVED*

METHYLENE BLUE BIOSORPTION ONTO GREEN ALGAE : Ulva Lactuca. *January*.

Vries, D., Bertelkamp, C., Schoonenberg Kegel, F., Hofs, B., Dusseldorp, J., Bruins, J. H., de Vet, W., & van den Akker, B. (2017). Iron and manganese removal: Recent advances in modelling treatment efficiency by rapid sand filtration. *Water Research*, *109*(March 2019), 35–45. https://doi.org/10.1016/j.watres.2016.11.032

Water Resource. (2020). The Water Wheel. *The Water Wheel January/February 2020*, 1–4.

World Health Organization. (2011). Manganese in Drinking-water. *Manganese in Drinking-Water. Background Document for Development of WHO Guidelines for Drinking Water Quality*, 1–21.

CHAPTER 7

APPENDICES

Appendix A: Iron and Manganese Data for determining system equilibrium

Table 7A 1: Trial Run for Iron and manganese at pH 6.5

Flow Rate 0.174l/min & 1.67ml/min dosing rate		
pH of 6.5 at 100 minutes run		
Time (min)	Iron (mg/l)	Manganese (mg/l)
0	2.1	2.7
10	2.50	0.30
20	1.24	0.67
30	1.07	0.63
40	1.10	0.40
50	1.15	0.57
60	1.3	0.50
70	1.27	0.57
80	1.27	0.50
90	1.24	0.60
100	1.25	0.47

Table 7A. 2:Trial Run for Iron and manganese at pH 7.5

Flow Rate 0.174l/min & 1.67ml/min dosing rate		
pH of 7.5 at 100 minutes run	Iron	Manganese
Time (min)	(mg/l)	(mg/l)
0	2.1	2.7
10	1.60	0.53
20	1.11	0.50
30	0.54	0.50
40	0.40	0.47
50	0.45	0.53
60	0.42	0.47
70	0.4	0.50
80	0.44	0.50
90	0.4	0.53
100	0.36	0.50

Table 7A 3: Trial Run for Iron and manganese at pH 8.5

Flow Rate 0.174l/min & 1.67ml/min dosing rate		
pH of 8.5 at 2 hour 30 minutes run		
Time (min)	Iron (mg/l)	Manganese (mg/l)
0	2.1	2.7
10	1.90	0.53
20	0.91	0.47
30	0.35	0.50
40	0.20	0.53
50	0.18	0.50
60	0.15	0.53
70	0.14	0.47
80	0.14	0.43
90	0.12	0.47
100	0.16	0.47
110	0.13	0.47
120	0.13	0.40
130	0.14	0.40
140	0.14	0.43
150	0.13	0.47

Appendix B: Raw data and percentage removal

Table 7B. 1: Best conditions for the removal of iron and manganese

Parameter	pH	Flow rate	Oxidation rate	Time	Removal
		(l/min)	(ml/min)	(min)	%
Iron (Fe)	8.5	0.174	1.67	20	93
Manganese (Mn)	6.5	2.62	0.252	60	93

Table 7B. 2: Raw data for Iron

Iron (mg/l)									
Time (min)	**6.5**			**7.5**			**8.5**		
	0,174 (l/min)	**0,262 (l/min)**	**0,523 (l/min)**	**0,174 (l/min)**	**0,262 (l/min)**	**0,523 (l/min)**	**0,174 (l/min)**	**0,262 (l/min)**	**0,523 (l/min)**
	1,67 (ml/min)	**2,52(ml/min)**	**5,0 (ml/min)**	**1,67 (ml/min)**	**2,52(ml/min)**	**5,0 (ml/min)**	**1,67 (ml/min)**	**2,52(ml/min)**	**5,0 (ml/min)**
10	2.50	2.80	2.20	1.60	1.63	1.60	1.90	1.8	1.85
20	1.24	2.60	2.20	1.11	1.20	1.50	0.91	1.28	1.14
30	1.07	2.38	2.29	0.54	0.89	1.24	0.35	0.94	1.01
40	1.10	1.80	2.20	0.44	0.90	1.20	0.20	0.71	0.66
50	1.15	2.00	2.40	0.45	0.90	1.10	0.18	0.58	0.58
60	1.30	1.71	2.56	0.42	0.89	1.11	0.15	0.54	0.61

Average	1.39	2.22	2.31	0.76	1.07	1.29	0.61	0.98	0.97
Experiment Runs	**1**	**2**	**3**	**4**	**5**	**6**	**7**	**8**	**9**

Table 7B 3: Data for Iron removal %

Iron (mg/l) % (Removal)									
Time	**6.5**			**7.5**			**8.5**		
	0,174 (l/min)	**0,262 (l/min)**	**0,523 (l/min)**	**0,174 (l/min)**	**0,262 (l/min)**	**0,523 (l/min)**	**0,174 (l/min)**	**0,262 (l/min)**	**0,523 (l/min)**
(min)	**1,67 (ml/min)**	**2,52(ml/min)**	**5,0 (ml/min)**	**1,67 (ml/min)**	**2,52(ml/min)**	**5,0 (ml/min)**	**1,67 (ml/min)**	**2,52(ml/min)**	**5,0 (ml/min)**
10	-19%	-33%	-5%	24%	22%	24%	10%	14%	12%
20	41%	-24%	-5%	47%	43%	29%	57%	39%	46%
30	49%	-13%	-9%	74%	58%	41%	83%	55%	52%
40	48%	14%	-5%	79%	57%	43%	91%	66%	69%
50	45%	5%	-14%	79%	57%	48%	91%	72%	72%
60	38%	19%	-22%	80%	58%	47%	93%	74%	71%
Average	34%	-5%	-10%	64%	49%	38%	71%	54%	54%
Experiment Runs	**1**	**2**	**3**	**4**	**5**	**6**	**7**	**8**	**9**

Table 7B 4: Manganese Raw data

Manganese (mg/l)									
Time (min)	**6.5**			**7.5**			**8.5**		
	0,174 (l/min)	**0,262 (l/min)**	**0,523 (l/min)**	**0,174 (l/min)**	**0,262 (l/min)**	**0,523 (l/min)**	**0,174 (l/min)**	**0,262 (l/min)**	**0,523 (l/min)**
	1,67 (ml/min)	**2,52(ml/min)**	**5,0 (ml/min)**	**1,67 (ml/min)**	**2,52(ml/min)**	**5,0 (ml/min)**	**1,67 (ml/min)**	**2,52(ml/min)**	**5,0 (ml/min)**
10	0.30	0.20	0.50	0.53	0.37	0.50	0.53	0.53	0.63
20	0.40	0.20	0.60	0.50	0.30	0.60	0.57	0.50	0.50
30	0.63	0.37	0.63	0.50	0.33	0.63	0.47	0.50	0.57
40	0.60	0.30	0.60	0.50	0.40	0.60	0.33	0.50	0.57
50	0.50	0.30	0.40	0.50	0.40	0.40	0.43	0.47	0.63
60	0.50	0.37	0.50	0.47	0.30	0.50	0.53	0.53	0.60
Average	0.49	0.29	0.54	0.50	0.35	0.54	0.48	0.51	0.58
Experiment run	1	2	3	4	5	6	7	8	9

Table 7B 5: Data for Manganese removal %

Manganese (mg/l) % (Removal)									
Time	6.5			7.5			8.5		
	0,174 (l/min)	0,262 (l/min)	0,523 (l/min)	0,174 (l/min)	0,262 (l/min)	0,523 (l/min)	0,174 (l/min)	0,262 (l/min)	0,523 (l/min)
(min)	**1,67 (ml/min)**	**2,52(ml/min)**	**5,0 (ml/min)**	**1,67 (ml/min)**	**2,52(ml/min)**	**5,0 (ml/min)**	**1,67 (ml/min)**	**2,52(ml/min)**	**5,0 (ml/min)**
10	89%	93%	81%	80%	86%	81%	80%	80%	77%
20	85%	93%	78%	81%	89%	78%	79%	81%	81%
30	77%	86%	77%	81%	88%	77%	83%	81%	79%
40	78%	89%	78%	81%	85%	78%	88%	81%	79%
50	81%	89%	85%	81%	85%	85%	84%	83%	77%
60	81%	86%	81%	83%	89%	81%	80%	80%	78%
Average	82%	89%	80%	81%	87%	80%	82%	81%	78%
Experiment run	1	2	3	4	5	6	7	8	9

Appendix C: FTIR Fuctional Groups

Table 7C 1: FTIR fuctional Groups

Functional group/assignment	Wavenumber (cm^{-1})
1. Saturated Aliphatic (alkene/alkyl)	
a) Methyl (−CH3)	
Methyl C-H asym./sym. Stretch	2970–2950/2880–2860
Methyl C-H asym./sym. Bend	1470–1430/1380–1370
gem-Dimethyl or ‘‘iso’’- (doublet)	1385–1380/1370–1365
Trimethyl or ‘‘tert-butyl’’ (multiplet)	1395–1385/1365
b) Methylene (>CH2)	
Methylene C-H asym./sym. Stretch	2935–2915/2865–2845
Methylene C-H bend	1485–1445
Methylene —(CH2)n— rocking (n ≥ 3)	750–720
Cyclohexane ring vibrations	1055–1000/1005–925
c) Methyne (>CH−)	
Methyne C-H stretch	2900–2880
Methyne C-H bend	1350–1330
Skeletal C-C vibrations	1300–700
d) Special methyl (−CH3) frequencies	
Methoxy, methyl ether O-CH3, C-H stretch	2850–2815
Methylamino, N-CH3, C-H stretch	2820–2780
2. Olefinic (alkene)	
Alkenyl C=C stretch	1680–1620
Aryl-substituted C=C	1625
Conjugated C=C	1600

Terminal (vinyl) C-H stretch	3095–3075
	3040–3010
Pendant (vinylidene) C-H stretch	3095–3075
Medial, cis- or trans-C-H stretch	3040–3010
Vinyl C-H in-plane bend	1420–1410
Vinylidene C-H in-plane bend	1310–1290
Vinyl C-H out-of-plane bend	995–985 + 915–890
Vinylidene C-H out-of-plane bend	895–885
trans-C-H out-of-plane bend	970–960
cis-C-H out-of-plane bend	700 (broad)
3. Aromatic ring (aryl)	
C=C-C Aromatic ring stretch	1615–1580
	1510–1450
Aromatic C-H stretch	3130–3070
Aromatic C-H in-plane bend	1225–950 (several)
Aromatic C-H out-of-plane bend	900–670 (several)
C-H Monosubstitution (phenyl)	770–730 + 710–690
C-H 1,2-Disubstitution (ortho)	770–735
C-H 1,3-Disubstitution (meta)	810–750 + 900–860
C-H 1,4-Disubstitution (para)	860–800
Aromatic combination bands	2000–1660 (several)
4. Acetylenic(alkyne)	
C≡C Terminal alkyne (monosubstituted)	2140–2100
C≡C Medial alkyne (disubstituted)	2260–2190
Alkyne C-H stretch	3320–3310
Alkyne C-H bend	680–610
Alkyne C-H bend	630 (typical)
5. Aliphatic organohalogen compound	
Aliphatic fluoro compounds, C-F stretch	1150–1000
Aliphatic chloro compounds, C-Cl stretch	800–700
Aliphatic bromo compounds, C-Br stretch	700–600
Aliphatic iodo compounds, C-I stretch	600–500

6. Alcohol and hydroxy compound	
Hydroxy group, H-bonded OH stretch	3570–3200 (broad)
Normal ‘‘polymeric’’ OH stretch	3400–3200
Dimeric OH stretch	3550–3450
Internally bonded OH stretch	3570–3540
Nonbonded hydroxy group, OH stretch	3645–3600 (narrow)
Primary alcohol, OH stretch	3645–3630
Secondary alcohol, OH stretch	3635–3620
Tertiary alcohol, OH stretch	3620–3540
Phenols, OH stretch	3640–3530
Primary or secondary, OH in-plane bend	1350–1260
Phenol or tertiary alcohol, OH bend	1410–1310
Alcohol, OH out-of-plane bend	720–590
Primary alcohol, C-O stretch	~1050
Secondary alcohol, C-O stretch	~1100
Tertiary alcohol, C-O stretch	~1150
Phenol, C-O stretch	1200
7. Ether and oxy compound	
Methoxy, C-H stretch (CH3-O-)	2820–2810
Alkyl-substituted ether, C-O stretch	1150–1050
Cyclic ethers, large rings, C-O stretch	1140–1070
Aromatic ethers, aryl -O stretch	1270–1230
Epoxy and oxirane rings	~1250 + 890–800
Peroxides, C-O-O- stretch	890–8201)
8. Ether and oxy compound	
Methoxy, C-H stretch (CH3-O-)	2820–2810
Alkyl-substituted ether, C-O stretch	1150–1050
Cyclic ethers, large rings, C-O stretch	1140–1070
Aromatic ethers, aryl -O stretch	1270–1230
Epoxy and oxirane rings	~1250 + 890–800)
Peroxides, C-O-O- stretch	890–820)
9.Carbonyl compound	
Carboxylate (carboxylic acid salt)	1610–1550/1420–1300

Amide	1680–1630
Quinone or conjugated ketone	1690–1675/(1650–1600)
Carboxylic acid	1725–1700
Ketone	1725–1705
Aldehyde	1740–1725/(2800–2700)
Ester	1750–1725
Six-membered ring lactone	1735
Alkyl carbonate	1760–1740
Acid (acyl) halide	1815–1770
Aryl carbonate	1820–1775
Five-membered ring anhydride	1870–1820/1800–1775
Transition metal carbonyls	2100–1800
10.Nitrogen multiple and cumulated double bond compound	
Aliphatic cyanide/nitrile	2280–2240
Aromatic cyanide/nitrile	2240–2220
Cyanate (-OCN and C-OCN stretch)	2260–2240/1190–1080
Isocyanate (-N=C=O asym. stretch)	2276–2240
Thiocyanate (-SCN)	2175–2140
Isothiocyanate (-NCS)	2150–1990
Open-chain imino (-C=N-)	1690–1590
Open-chain azo (-N=N-)	1630–1575
a) Nitrogen-oxy compounds	
Aliphatic nitro compounds	
Organic nitrates	1640–1620/1285–1270
Aromatic nitro compounds	1555–1485/1355–1320
b) Phosphorus-oxy compounds	
Organic phosphates (P=O stretch)	1350–1250
Aliphatic phosphates (P-O-C stretch)	1050–990

Aromatic phosphates (P-O-C stretch)	1240–1190/995–850
c) Sulfur-oxy compounds	
Dialkyl/aryl sulfones	1335–1300/1170–1135
Organic sulfates	1420–1370/1200–1180
Sulfonates	1365–1340/1200–1100
d) Silicon-oxy compounds	
Organic siloxane or silicone (Si-O-Si)	1095–1075/1055–1020
Organic siloxane or silicone (Si-O-C)	1110–1080
11.Thiols and thio-substituted compounds	
Thiols (S-H stretch)	2600–2550
Thiol or thioether, CH2-S-(C-S stretch)	710–685
Thioethers, CH3-S-(C-S stretch)	660–630
Aryl thioethers, ø-S (C-S stretch)	715–670
Disulfides (C-S stretch)	705–570
Disulfides (S-S stretch)	620–600
Aryl disulfides (S-S stretch)	500–430
Polysulfides (S-S stretch)	500–470
12.Common inorganic ions	
Carbonate ion	1490–1410/880–860
Sulfate ion	1130–1080/680–610
Nitrate ion	1380–1350/840–815
Phosphate ion	1100–1000
Ammonium ion	3300–3030/1430–1390
Cyanide ion, thiocyanate ion, and related ions	2200–2000
Silicate ion	1100–900

Table 7C 2: FTIR sample data for polystyrene Beads

Date	Tuesday, June 28 2022
Sample	Polystyrene beads.ASC
Wavelength	**Transmittence**
cm^{-1}	**% T**
4000	94.733
3999	94.734
3998	94.735
3997	94.736
3996	94.744
3995	94.754
3994	94.761
3993	94.761
3992	94.758
3991	94.754
3990	94.754
3989	94.755
3988	94.756
3987	94.753
3986	94.748
3985	94.742
3984	94.739
3983	94.741
3982	94.747
3981	94.753
3980	94.757
3979	94.758
3978	94.757
3977	94.753
3976	94.747
3975	94.741
3974	94.738
3973	94.742
3972	94.751
3971	94.759
3970	94.763
3969	94.760
3968	94.753
3967	94.746
3966	94.739
3965	94.735

3964	94.734
3963	94.735
3962	94.739
3961	94.745
3960	94.751
3959	94.757
3958	94.761
3957	94.766
3956	94.773
3955	94.781
3954	94.788
3953	94.791
3952	94.789
3951	94.781
3950	94.772
3949	94.764
3948	94.760
3947	94.759
3946	94.759
3945	94.759
3944	94.758
3943	94.757
3942	94.756
3941	94.756
3940	94.756
3939	94.754
3938	94.752
3937	94.753
3936	94.758
3935	94.768
3934	94.778
3933	94.783
3932	94.785
3931	94.785
3930	94.786
3929	94.787
3928	94.784
3927	94.779
3926	94.774
3925	94.774
3924	94.780
3923	94.789
3922	94.795
3921	94.791
3920	94.778

3919	94.762
3918	94.752
3917	94.754
3916	94.766
3915	94.783
3914	94.800
3913	94.814
3912	94.824
3911	94.829
3910	94.832
3909	94.833
3908	94.835
3907	94.836
3906	94.836
3905	94.834
3904	94.830
3903	94.825
3902	94.818
3901	94.808
3900	94.796
3899	94.784
3898	94.775
3897	94.769
3896	94.767
3895	94.772
3894	94.784
3893	94.802
3892	94.820
3891	94.836
3890	94.848
3889	94.854
3888	94.852
3887	94.843
3886	94.831
3885	94.821
3884	94.813
3883	94.803
3882	94.786
3881	94.771
3880	94.770
3879	94.789
3878	94.818
3877	94.840
3876	94.846
3875	94.841

3874	94.836
3873	94.840
3872	94.850
3871	94.858
3870	94.863
3869	94.869
3868	94.877
3867	94.880
3866	94.874
3865	94.858
3864	94.841
3863	94.830
3862	94.826
3861	94.825
3860	94.826
3859	94.835
3858	94.859
3857	94.902
3856	94.953
3855	94.987
3854	94.987
3853	94.973
3852	94.967
3851	94.956
3850	94.923
3849	94.879
3848	94.845
3847	94.834
3846	94.841
3845	94.855
3844	94.867
3843	94.877
3842	94.888
3841	94.901
3840	94.911
3839	94.915
3838	94.912
3837	94.907
3836	94.906
3835	94.904
3834	94.900
3833	94.894
3832	94.890
3831	94.888
3830	94.884

3829	94.876
3828	94.863
3827	94.853
3826	94.857
3825	94.873
3824	94.895
3823	94.907
3822	94.904
3821	94.900
3820	94.911
3819	94.934
3818	94.948
3817	94.941
3816	94.920
3815	94.900
3814	94.888
3813	94.879
3812	94.870
3811	94.868
3810	94.879
3809	94.898
3808	94.915
3807	94.926
3806	94.941
3805	94.962
3804	94.978
3803	94.978
3802	94.959
3801	94.939
3800	94.932
3799	94.932
3798	94.923
3797	94.903
3796	94.883
3795	94.874
3794	94.877
3793	94.884
3792	94.887
3791	94.884
3790	94.880
3789	94.876
3788	94.875
3787	94.876
3786	94.878
3785	94.881

3784	94.886
3783	94.891
3782	94.894
3781	94.892
3780	94.886
3779	94.881
3778	94.884
3777	94.894
3776	94.906
3775	94.919
3774	94.930
3773	94.941
3772	94.947
3771	94.946
3770	94.939
3769	94.934
3768	94.933
3767	94.933
3766	94.932
3765	94.934
3764	94.941
3763	94.951
3762	94.957
3761	94.952
3760	94.939
3759	94.930
3758	94.932
3757	94.945
3756	94.966
3755	94.992
3754	95.025
3753	95.057
3752	95.078
3751	95.080
3750	95.074
3749	95.071
3748	95.069
3747	95.063
3746	95.046
3745	95.019
3744	94.995
3743	94.991
3742	94.995
3741	94.990
3740	94.975

3739	94.962
3738	94.954
3737	94.947
3736	94.940
3735	94.937
3734	94.942
3733	94.949
3732	94.956
3731	94.962
3730	94.969
3729	94.973
3728	94.971
3727	94.960
3726	94.944
3725	94.932
3724	94.929
3723	94.937
3722	94.951
3721	94.965
3720	94.976
3719	94.980
3718	94.983
3717	94.987
3716	94.998
3715	95.012
3714	95.024
3713	95.026
3712	95.019
3711	95.013
3710	95.015
3709	95.020
3708	95.022
3707	95.019
3706	95.016
3705	95.013
3704	95.007
3703	94.996
3702	94.984
3701	94.974
3700	94.966
3699	94.958
3698	94.951
3697	94.951
3696	94.959
3695	94.977

3694	95.001
3693	95.027
3692	95.050
3691	95.069
3690	95.079
3689	95.080
3688	95.075
3687	95.068
3686	95.056
3685	95.041
3684	95.028
3683	95.019
3682	95.015
3681	95.017
3680	95.026
3679	95.044
3678	95.067
3677	95.083
3676	95.084
3675	95.082
3674	95.088
3673	95.094
3672	95.088
3671	95.069
3670	95.046
3669	95.034
3668	95.034
3667	95.036
3666	95.033
3665	95.030
3664	95.032
3663	95.043
3662	95.058
3661	95.071
3660	95.078
3659	95.077
3658	95.069
3657	95.060
3656	95.059
3655	95.069
3654	95.085
3653	95.096
3652	95.095
3651	95.080
3650	95.056

3649	95.037
3648	95.031
3647	95.032
3646	95.030
3645	95.021
3644	95.008
3643	94.999
3642	94.998
3641	95.005
3640	95.015
3639	95.023
3638	95.028
3637	95.034
3636	95.039
3635	95.043
3634	95.050
3633	95.066
3632	95.090
3631	95.113
3630	95.116
3629	95.098
3628	95.078
3627	95.070
3626	95.063
3625	95.049
3624	95.036
3623	95.032
3622	95.039
3621	95.050
3620	95.054
3619	95.051
3618	95.048
3617	95.047
3616	95.046
3615	95.042
3614	95.037
3613	95.032
3612	95.030
3611	95.029
3610	95.029
3609	95.030
3608	95.034
3607	95.045
3606	95.062
3605	95.076

3604	95.081
3603	95.072
3602	95.053
3601	95.033
3600	95.022
3599	95.021
3598	95.027
3597	95.032
3596	95.033
3595	95.033
3594	95.035
3593	95.041
3592	95.047
3591	95.049
3590	95.045
3589	95.036
3588	95.025
3587	95.018
3586	95.016
3585	95.016
3584	95.012
3583	95.006
3582	95.001
3581	95.001
3580	95.007
3579	95.018
3578	95.031
3577	95.041
3576	95.047
3575	95.050
3574	95.054
3573	95.059
3572	95.065
3571	95.065
3570	95.056
3569	95.036
3568	95.010
3567	94.993
3566	94.995
3565	95.012
3564	95.032
3563	95.045
3562	95.052
3561	95.054
3560	95.056

3559	95.059
3558	95.064
3557	95.069
3556	95.073
3555	95.071
3554	95.064
3553	95.055
3552	95.049
3551	95.052
3550	95.063
3549	95.074
3548	95.080
3547	95.080
3546	95.080
3545	95.083
3544	95.089
3543	95.093
3542	95.096
3541	95.100
3540	95.105
3539	95.111
3538	95.114
3537	95.112
3536	95.107
3535	95.101
3534	95.095
3533	95.088
3532	95.079
3531	95.072
3530	95.069
3529	95.071
3528	95.075
3527	95.078
3526	95.077
3525	95.074
3524	95.068
3523	95.059
3522	95.052
3521	95.049
3520	95.051
3519	95.059
3518	95.069
3517	95.079
3516	95.088
3515	95.096

3514	95.103
3513	95.106
3512	95.105
3511	95.102
3510	95.100
3509	95.098
3508	95.095
3507	95.088
3506	95.078
3505	95.071
3504	95.068
3503	95.071
3502	95.080
3501	95.090
3500	95.098
3499	95.101
3498	95.100
3497	95.098
3496	95.097
3495	95.096
3494	95.094
3493	95.089
3492	95.081
3491	95.072
3490	95.067
3489	95.065
3488	95.067
3487	95.071
3486	95.076
3485	95.081
3484	95.087
3483	95.093
3482	95.100
3481	95.105
3480	95.110
3479	95.117
3478	95.127
3477	95.138
3476	95.148
3475	95.154
3474	95.155
3473	95.153
3472	95.150
3471	95.147
3470	95.144

3469	95.140
3468	95.136
3467	95.131
3466	95.126
3465	95.119
3464	95.112
3463	95.104
3462	95.097
3461	95.095
3460	95.096
3459	95.104
3458	95.116
3457	95.130
3456	95.141
3455	95.144
3454	95.139
3453	95.129
3452	95.119
3451	95.115
3450	95.118
3449	95.126
3448	95.135
3447	95.141
3446	95.145
3445	95.148
3444	95.150
3443	95.148
3442	95.143
3441	95.139
3440	95.137
3439	95.138
3438	95.141
3437	95.144
3436	95.148
3435	95.154
3434	95.164
3433	95.177
3432	95.188
3431	95.191
3430	95.186
3429	95.174
3428	95.158
3427	95.142
3426	95.130
3425	95.125

3424	95.127
3423	95.132
3422	95.137
3421	95.143
3420	95.152
3419	95.161
3418	95.168
3417	95.168
3416	95.163
3415	95.156
3414	95.154
3413	95.158
3412	95.163
3411	95.163
3410	95.156
3409	95.145
3408	95.134
3407	95.130
3406	95.132
3405	95.137
3404	95.142
3403	95.147
3402	95.153
3401	95.160
3400	95.163
3399	95.162
3398	95.158
3397	95.154
3396	95.153
3395	95.155
3394	95.158
3393	95.160
3392	95.158
3391	95.154
3390	95.147
3389	95.142
3388	95.137
3387	95.134
3386	95.134
3385	95.136
3384	95.141
3383	95.149
3382	95.159
3381	95.167
3380	95.170

3379	95.167
3378	95.159
3377	95.148
3376	95.138
3375	95.132
3374	95.132
3373	95.136
3372	95.142
3371	95.148
3370	95.155
3369	95.164
3368	95.170
3367	95.172
3366	95.168
3365	95.164
3364	95.163
3363	95.166
3362	95.171
3361	95.172
3360	95.166
3359	95.156
3358	95.146
3357	95.143
3356	95.147
3355	95.154
3354	95.158
3353	95.158
3352	95.154
3351	95.150
3350	95.149
3349	95.149
3348	95.148
3347	95.146
3346	95.142
3345	95.141
3344	95.143
3343	95.151
3342	95.161
3341	95.172
3340	95.181
3339	95.185
3338	95.183
3337	95.173
3336	95.161
3335	95.151

3334	95.145
3333	95.141
3332	95.135
3331	95.127
3330	95.120
3329	95.118
3328	95.122
3327	95.129
3326	95.135
3325	95.135
3324	95.129
3323	95.119
3322	95.110
3321	95.106
3320	95.106
3319	95.109
3318	95.115
3317	95.122
3316	95.126
3315	95.125
3314	95.123
3313	95.124
3312	95.130
3311	95.140
3310	95.149
3309	95.155
3308	95.154
3307	95.150
3306	95.143
3305	95.137
3304	95.132
3303	95.129
3302	95.127
3301	95.125
3300	95.124
3299	95.124
3298	95.129
3297	95.134
3296	95.139
3295	95.140
3294	95.138
3293	95.135
3292	95.133
3291	95.135
3290	95.145

3289	95.159
3288	95.171
3287	95.173
3286	95.167
3285	95.159
3284	95.155
3283	95.156
3282	95.161
3281	95.162
3280	95.157
3279	95.150
3278	95.146
3277	95.150
3276	95.159
3275	95.170
3274	95.182
3273	95.192
3272	95.197
3271	95.197
3270	95.194
3269	95.191
3268	95.187
3267	95.183
3266	95.179
3265	95.180
3264	95.188
3263	95.199
3262	95.206
3261	95.201
3260	95.185
3259	95.168
3258	95.159
3257	95.158
3256	95.163
3255	95.170
3254	95.177
3253	95.183
3252	95.187
3251	95.189
3250	95.190
3249	95.193
3248	95.194
3247	95.194
3246	95.192
3245	95.191

3244	95.190
3243	95.190
3242	95.192
3241	95.195
3240	95.198
3239	95.197
3238	95.192
3237	95.185
3236	95.180
3235	95.180
3234	95.185
3233	95.190
3232	95.192
3231	95.192
3230	95.196
3229	95.203
3228	95.211
3227	95.216
3226	95.217
3225	95.218
3224	95.221
3223	95.226
3222	95.234
3221	95.242
3220	95.249
3219	95.251
3218	95.249
3217	95.244
3216	95.237
3215	95.232
3214	95.229
3213	95.229
3212	95.231
3211	95.233
3210	95.237
3209	95.242
3208	95.247
3207	95.248
3206	95.246
3205	95.244
3204	95.241
3203	95.239
3202	95.240
3201	95.246
3200	95.258

3199	95.272
3198	95.283
3197	95.291
3196	95.295
3195	95.297
3194	95.298
3193	95.301
3192	95.303
3191	95.307
3190	95.311
3189	95.317
3188	95.324
3187	95.330
3186	95.335
3185	95.339
3184	95.343
3183	95.347
3182	95.353
3181	95.362
3180	95.373
3179	95.382
3178	95.385
3177	95.383
3176	95.379
3175	95.376
3174	95.374
3173	95.374
3172	95.376
3171	95.378
3170	95.380
3169	95.382
3168	95.385
3167	95.388
3166	95.391
3165	95.391
3164	95.390
3163	95.387
3162	95.386
3161	95.387
3160	95.392
3159	95.398
3158	95.405
3157	95.409
3156	95.411
3155	95.416

3154	95.422
3153	95.429
3152	95.434
3151	95.438
3150	95.442
3149	95.447
3148	95.454
3147	95.461
3146	95.467
3145	95.468
3144	95.466
3143	95.462
3142	95.458
3141	95.459
3140	95.468
3139	95.484
3138	95.500
3137	95.508
3136	95.503
3135	95.489
3134	95.477
3133	95.473
3132	95.478
3131	95.487
3130	95.495
3129	95.497
3128	95.495
3127	95.495
3126	95.501
3125	95.516
3124	95.532
3123	95.540
3122	95.539
3121	95.530
3120	95.521
3119	95.519
3118	95.523
3117	95.528
3116	95.526
3115	95.511
3114	95.489
3113	95.466
3112	95.449
3111	95.437
3110	95.427

3109	95.413
3108	95.389
3107	95.357
3106	95.322
3105	95.292
3104	95.273
3103	95.265
3102	95.268
3101	95.277
3100	95.289
3099	95.301
3098	95.313
3097	95.322
3096	95.327
3095	95.326
3094	95.317
3093	95.301
3092	95.275
3091	95.235
3090	95.176
3089	95.097
3088	95.000
3087	94.894
3086	94.786
3085	94.688
3084	94.609
3083	94.563
3082	94.555
3081	94.581
3080	94.631
3079	94.689
3078	94.746
3077	94.795
3076	94.836
3075	94.872
3074	94.898
3073	94.910
3072	94.904
3071	94.882
3070	94.845
3069	94.794
3068	94.725
3067	94.639
3066	94.539
3065	94.431

3064	94.319
3063	94.211
3062	94.120
3061	94.057
3060	94.026
3059	94.031
3058	94.071
3057	94.142
3056	94.233
3055	94.328
3054	94.418
3053	94.503
3052	94.585
3051	94.668
3050	94.745
3049	94.811
3048	94.861
3047	94.895
3046	94.915
3045	94.925
3044	94.928
3043	94.922
3042	94.907
3041	94.878
3040	94.835
3039	94.778
3038	94.707
3037	94.619
3036	94.504
3035	94.353
3034	94.164
3033	93.938
3032	93.682
3031	93.406
3030	93.122
3029	92.848
3028	92.602
3027	92.406
3026	92.284
3025	92.255
3024	92.325
3023	92.483
3022	92.712
3021	92.987
3020	93.281

3019	93.566
3018	93.821
3017	94.038
3016	94.219
3015	94.371
3014	94.500
3013	94.605
3012	94.687
3011	94.746
3010	94.782
3009	94.799
3008	94.801
3007	94.793
3006	94.778
3005	94.756
3004	94.728
3003	94.702
3002	94.686
3001	94.689
3000	94.711
2999	94.747
2998	94.794
2997	94.847
2996	94.905
2995	94.964
2994	95.022
2993	95.072
2992	95.113
2991	95.141
2990	95.157
2989	95.163
2988	95.166
2987	95.170
2986	95.182
2985	95.198
2984	95.215
2983	95.226
2982	95.229
2981	95.227
2980	95.223
2979	95.220
2978	95.221
2977	95.223
2976	95.222
2975	95.216

2974	95.206
2973	95.193
2972	95.175
2971	95.154
2970	95.130
2969	95.102
2968	95.066
2967	95.023
2966	94.978
2965	94.936
2964	94.898
2963	94.861
2962	94.818
2961	94.768
2960	94.710
2959	94.650
2958	94.592
2957	94.539
2956	94.493
2955	94.452
2954	94.418
2953	94.390
2952	94.365
2951	94.339
2950	94.308
2949	94.269
2948	94.221
2947	94.164
2946	94.096
2945	94.013
2944	93.911
2943	93.790
2942	93.652
2941	93.499
2940	93.330
2939	93.146
2938	92.947
2937	92.736
2936	92.514
2935	92.282
2934	92.041
2933	91.787
2932	91.520
2931	91.244
2930	90.966

2929	90.691
2928	90.421
2927	90.152
2926	89.884
2925	89.616
2924	89.343
2923	89.055
2922	88.744
2921	88.411
2920	88.078
2919	87.788
2918	87.601
2917	87.577
2916	87.747
2915	88.099
2914	88.574
2913	89.095
2912	89.596
2911	90.037
2910	90.409
2909	90.718
2908	90.980
2907	91.208
2906	91.414
2905	91.602
2904	91.774
2903	91.934
2902	92.086
2901	92.229
2900	92.365
2899	92.492
2898	92.614
2897	92.731
2896	92.844
2895	92.952
2894	93.052
2893	93.141
2892	93.219
2891	93.289
2890	93.353
2889	93.416
2888	93.480
2887	93.543
2886	93.602
2885	93.656

2884	93.707
2883	93.758
2882	93.809
2881	93.858
2880	93.904
2879	93.945
2878	93.980
2877	94.009
2876	94.033
2875	94.054
2874	94.074
2873	94.093
2872	94.112
2871	94.133
2870	94.154
2869	94.165
2868	94.160
2867	94.139
2866	94.109
2865	94.071
2864	94.021
2863	93.954
2862	93.868
2861	93.766
2860	93.651
2859	93.520
2858	93.371
2857	93.197
2856	92.992
2855	92.749
2854	92.466
2853	92.143
2852	91.801
2851	91.489
2850	91.272
2849	91.208
2848	91.319
2847	91.582
2846	91.941
2845	92.333
2844	92.710
2843	93.047
2842	93.338
2841	93.589
2840	93.805

2839	93.989
2838	94.144
2837	94.275
2836	94.390
2835	94.491
2834	94.579
2833	94.653
2832	94.715
2831	94.769
2830	94.818
2829	94.860
2828	94.894
2827	94.920
2826	94.944
2825	94.969
2824	94.994
2823	95.015
2822	95.030
2821	95.040
2820	95.047
2819	95.056
2818	95.068
2817	95.081
2816	95.094
2815	95.106
2814	95.119
2813	95.131
2812	95.139
2811	95.142
2810	95.145
2809	95.151
2808	95.160
2807	95.170
2806	95.180
2805	95.191
2804	95.203
2803	95.213
2802	95.221
2801	95.226
2800	95.231
2799	95.235
2798	95.240
2797	95.248
2796	95.259
2795	95.270

2794	95.278
2793	95.282
2792	95.284
2791	95.287
2790	95.288
2789	95.287
2788	95.285
2787	95.286
2786	95.292
2785	95.302
2784	95.313
2783	95.323
2782	95.330
2781	95.334
2780	95.336
2779	95.338
2778	95.339
2777	95.339
2776	95.337
2775	95.336
2774	95.340
2773	95.349
2772	95.361
2771	95.374
2770	95.386
2769	95.394
2768	95.397
2767	95.396
2766	95.395
2765	95.395
2764	95.397
2763	95.401
2762	95.406
2761	95.410
2760	95.412
2759	95.411
2758	95.407
2757	95.406
2756	95.407
2755	95.413
2754	95.421
2753	95.428
2752	95.434
2751	95.438
2750	95.444

2749	95.451
2748	95.457
2747	95.459
2746	95.461
2745	95.464
2744	95.466
2743	95.465
2742	95.461
2741	95.456
2740	95.452
2739	95.451
2738	95.453
2737	95.457
2736	95.458
2735	95.456
2734	95.451
2733	95.449
2732	95.452
2731	95.461
2730	95.472
2729	95.483
2728	95.487
2727	95.484
2726	95.478
2725	95.472
2724	95.472
2723	95.477
2722	95.485
2721	95.489
2720	95.489
2719	95.486
2718	95.486
2717	95.488
2716	95.489
2715	95.488
2714	95.488
2713	95.491
2712	95.497
2711	95.503
2710	95.505
2709	95.503
2708	95.500
2707	95.500
2706	95.503
2705	95.508

2704	95.512
2703	95.514
2702	95.517
2701	95.521
2700	95.525
2699	95.526
2698	95.525
2697	95.521
2696	95.518
2695	95.517
2694	95.518
2693	95.521
2692	95.524
2691	95.526
2690	95.527
2689	95.526
2688	95.524
2687	95.524
2686	95.526
2685	95.529
2684	95.530
2683	95.530
2682	95.532
2681	95.537
2680	95.541
2679	95.545
2678	95.548
2677	95.552
2676	95.556
2675	95.556
2674	95.552
2673	95.544
2672	95.538
2671	95.536
2670	95.540
2669	95.550
2668	95.561
2667	95.570
2666	95.574
2665	95.574
2664	95.572
2663	95.568
2662	95.567
2661	95.567
2660	95.568

2659	95.568
2658	95.565
2657	95.557
2656	95.545
2655	95.536
2654	95.533
2653	95.535
2652	95.540
2651	95.544
2650	95.550
2649	95.562
2648	95.577
2647	95.587
2646	95.587
2645	95.579
2644	95.569
2643	95.565
2642	95.567
2641	95.571
2640	95.576
2639	95.583
2638	95.592
2637	95.595
2636	95.590
2635	95.580
2634	95.574
2633	95.578
2632	95.589
2631	95.599
2630	95.604
2629	95.606
2628	95.608
2627	95.613
2626	95.621
2625	95.629
2624	95.632
2623	95.629
2622	95.622
2621	95.618
2620	95.618
2619	95.624
2618	95.633
2617	95.641
2616	95.648
2615	95.656

2614	95.666
2613	95.679
2612	95.690
2611	95.694
2610	95.688
2609	95.675
2608	95.662
2607	95.654
2606	95.655
2605	95.660
2604	95.664
2603	95.667
2602	95.669
2601	95.674
2600	95.681
2599	95.687
2598	95.690
2597	95.691
2596	95.690
2595	95.688
2594	95.685
2593	95.683
2592	95.681
2591	95.681
2590	95.684
2589	95.692
2588	95.706
2587	95.721
2586	95.730
2585	95.729
2584	95.720
2583	95.710
2582	95.704
2581	95.700
2580	95.697
2579	95.697
2578	95.703
2577	95.712
2576	95.724
2575	95.734
2574	95.741
2573	95.741
2572	95.736
2571	95.732
2570	95.739

2569	95.758
2568	95.780
2567	95.797
2566	95.804
2565	95.799
2564	95.789
2563	95.779
2562	95.772
2561	95.766
2560	95.761
2559	95.758
2558	95.759
2557	95.766
2556	95.775
2555	95.784
2554	95.792
2553	95.798
2552	95.799
2551	95.798
2550	95.797
2549	95.794
2548	95.793
2547	95.796
2546	95.808
2545	95.821
2544	95.828
2543	95.821
2542	95.807
2541	95.794
2540	95.786
2539	95.785
2538	95.790
2537	95.799
2536	95.811
2535	95.820
2534	95.823
2533	95.821
2532	95.813
2531	95.805
2530	95.802
2529	95.807
2528	95.818
2527	95.831
2526	95.842
2525	95.850

2524	95.850
2523	95.846
2522	95.840
2521	95.836
2520	95.834
2519	95.832
2518	95.832
2517	95.840
2516	95.856
2515	95.873
2514	95.882
2513	95.878
2512	95.861
2511	95.841
2510	95.827
2509	95.826
2508	95.838
2507	95.856
2506	95.869
2505	95.871
2504	95.863
2503	95.855
2502	95.854
2501	95.860
2500	95.868
2499	95.873
2498	95.873
2497	95.871
2496	95.867
2495	95.865
2494	95.868
2493	95.874
2492	95.878
2491	95.878
2490	95.870
2489	95.859
2488	95.850
2487	95.848
2486	95.854
2485	95.866
2484	95.878
2483	95.885
2482	95.887
2481	95.882
2480	95.871

2479	95.859
2478	95.852
2477	95.852
2476	95.858
2475	95.867
2474	95.876
2473	95.882
2472	95.887
2471	95.894
2470	95.904
2469	95.915
2468	95.924
2467	95.936
2466	95.950
2465	95.959
2464	95.956
2463	95.940
2462	95.924
2461	95.915
2460	95.920
2459	95.933
2458	95.948
2457	95.955
2456	95.949
2455	95.936
2454	95.926
2453	95.924
2452	95.925
2451	95.922
2450	95.917
2449	95.913
2448	95.918
2447	95.932
2446	95.949
2445	95.963
2444	95.969
2443	95.968
2442	95.966
2441	95.964
2440	95.962
2439	95.959
2438	95.957
2437	95.957
2436	95.958
2435	95.957

2434	95.956
2433	95.954
2432	95.954
2431	95.958
2430	95.964
2429	95.969
2428	95.972
2427	95.977
2426	95.989
2425	96.005
2424	96.018
2423	96.021
2422	96.016
2421	96.007
2420	96.002
2419	96.003
2418	96.009
2417	96.010
2416	96.003
2415	95.993
2414	95.992
2413	96.003
2412	96.019
2411	96.031
2410	96.035
2409	96.032
2408	96.027
2407	96.026
2406	96.029
2405	96.031
2404	96.031
2403	96.031
2402	96.036
2401	96.044
2400	96.049
2399	96.045
2398	96.036
2397	96.023
2396	96.011
2395	96.002
2394	95.999
2393	96.001
2392	96.007
2391	96.016
2390	96.024

2389	96.026
2388	96.017
2387	96.002
2386	95.988
2385	95.980
2384	95.974
2383	95.969
2382	95.961
2381	95.952
2380	95.943
2379	95.936
2378	95.936
2377	95.942
2376	95.949
2375	95.953
2374	95.954
2373	95.958
2372	95.965
2371	95.973
2370	95.976
2369	95.966
2368	95.944
2367	95.918
2366	95.899
2365	95.890
2364	95.891
2363	95.897
2362	95.906
2361	95.913
2360	95.915
2359	95.914
2358	95.913
2357	95.914
2356	95.915
2355	95.913
2354	95.906
2353	95.896
2352	95.889
2351	95.890
2350	95.896
2349	95.899
2348	95.894
2347	95.884
2346	95.876
2345	95.874

2344	95.878
2343	95.885
2342	95.894
2341	95.904
2340	95.910
2339	95.908
2338	95.897
2337	95.882
2336	95.868
2335	95.860
2334	95.858
2333	95.863
2332	95.872
2331	95.883
2330	95.894
2329	95.896
2328	95.885
2327	95.861
2326	95.839
2325	95.827
2324	95.828
2323	95.838
2322	95.857
2321	95.880
2320	95.904
2319	95.921
2318	95.928
2317	95.926
2316	95.917
2315	95.906
2314	95.895
2313	95.882
2312	95.872
2311	95.876
2310	95.897
2309	95.925
2308	95.944
2307	95.949
2306	95.947
2305	95.949
2304	95.957
2303	95.964
2302	95.970
2301	95.973
2300	95.979

2299	95.987
2298	95.996
2297	96.001
2296	95.998
2295	95.990
2294	95.983
2293	95.976
2292	95.965
2291	95.953
2290	95.945
2289	95.946
2288	95.949
2287	95.955
2286	95.970
2285	96.001
2284	96.039
2283	96.066
2282	96.075
2281	96.071
2280	96.062
2279	96.057
2278	96.056
2277	96.057
2276	96.056
2275	96.056
2274	96.062
2273	96.072
2272	96.083
2271	96.095
2270	96.112
2269	96.128
2268	96.128
2267	96.108
2266	96.082
2265	96.068
2264	96.070
2263	96.078
2262	96.087
2261	96.090
2260	96.081
2259	96.055
2258	96.024
2257	96.012
2256	96.029
2255	96.068

2254	96.110
2253	96.139
2252	96.144
2251	96.133
2250	96.125
2249	96.138
2248	96.164
2247	96.181
2246	96.170
2245	96.129
2244	96.078
2243	96.041
2242	96.036
2241	96.067
2240	96.116
2239	96.153
2238	96.159
2237	96.139
2236	96.123
2235	96.132
2234	96.170
2233	96.215
2232	96.244
2231	96.246
2230	96.222
2229	96.184
2228	96.146
2227	96.125
2226	96.130
2225	96.151
2224	96.173
2223	96.189
2222	96.202
2221	96.220
2220	96.242
2219	96.256
2218	96.249
2217	96.220
2216	96.193
2215	96.200
2214	96.249
2213	96.309
2212	96.335
2211	96.307
2210	96.244

2209	96.177
2208	96.128
2207	96.111
2206	96.124
2205	96.156
2204	96.183
2203	96.190
2202	96.180
2201	96.166
2200	96.162
2199	96.173
2198	96.199
2197	96.221
2196	96.226
2195	96.210
2194	96.183
2193	96.150
2192	96.119
2191	96.109
2190	96.139
2189	96.197
2188	96.251
2187	96.282
2186	96.302
2185	96.326
2184	96.347
2183	96.346
2182	96.326
2181	96.300
2180	96.273
2179	96.249
2178	96.238
2177	96.245
2176	96.256
2175	96.251
2174	96.227
2173	96.201
2172	96.188
2171	96.189
2170	96.196
2169	96.205
2168	96.211
2167	96.204
2166	96.175
2165	96.127

2164	96.079
2163	96.062
2162	96.096
2161	96.188
2160	96.330
2159	96.500
2158	96.649
2157	96.711
2156	96.661
2155	96.548
2154	96.451
2153	96.417
2152	96.426
2151	96.432
2150	96.421
2149	96.418
2148	96.447
2147	96.498
2146	96.529
2145	96.517
2144	96.481
2143	96.461
2142	96.473
2141	96.500
2140	96.515
2139	96.512
2138	96.494
2137	96.465
2136	96.427
2135	96.394
2134	96.389
2133	96.415
2132	96.455
2131	96.488
2130	96.498
2129	96.486
2128	96.464
2127	96.447
2126	96.438
2125	96.428
2124	96.404
2123	96.369
2122	96.336
2121	96.318
2120	96.310

2119	96.306
2118	96.305
2117	96.308
2116	96.312
2115	96.315
2114	96.319
2113	96.327
2112	96.343
2111	96.364
2110	96.385
2109	96.396
2108	96.397
2107	96.391
2106	96.389
2105	96.394
2104	96.399
2103	96.396
2102	96.390
2101	96.387
2100	96.394
2099	96.408
2098	96.421
2097	96.423
2096	96.403
2095	96.365
2094	96.321
2093	96.290
2092	96.281
2091	96.290
2090	96.305
2089	96.319
2088	96.334
2087	96.350
2086	96.368
2085	96.382
2084	96.389
2083	96.390
2082	96.384
2081	96.367
2080	96.344
2079	96.323
2078	96.307
2077	96.291
2076	96.275
2075	96.273

2074	96.291
2073	96.319
2072	96.340
2071	96.357
2070	96.380
2069	96.413
2068	96.439
2067	96.446
2066	96.435
2065	96.414
2064	96.388
2063	96.367
2062	96.365
2061	96.385
2060	96.416
2059	96.446
2058	96.468
2057	96.482
2056	96.483
2055	96.469
2054	96.440
2053	96.401
2052	96.362
2051	96.334
2050	96.328
2049	96.346
2048	96.382
2047	96.429
2046	96.476
2045	96.509
2044	96.526
2043	96.542
2042	96.569
2041	96.591
2040	96.580
2039	96.527
2038	96.458
2037	96.399
2036	96.367
2035	96.373
2034	96.428
2033	96.522
2032	96.610
2031	96.653
2030	96.648

2029	96.620
2028	96.584
2027	96.538
2026	96.476
2025	96.415
2024	96.380
2023	96.388
2022	96.431
2021	96.485
2020	96.527
2019	96.549
2018	96.550
2017	96.528
2016	96.487
2015	96.441
2014	96.405
2013	96.381
2012	96.364
2011	96.357
2010	96.373
2009	96.415
2008	96.465
2007	96.503
2006	96.520
2005	96.521
2004	96.517
2003	96.520
2002	96.536
2001	96.561
2000	96.576
1999	96.558
1998	96.505
1997	96.437
1996	96.390
1995	96.389
1994	96.427
1993	96.473
1992	96.487
1991	96.453
1990	96.387
1989	96.331
1988	96.322
1987	96.362
1986	96.417
1985	96.443

1984	96.425
1983	96.382
1982	96.335
1981	96.296
1980	96.280
1979	96.311
1978	96.391
1977	96.480
1976	96.533
1975	96.540
1974	96.520
1973	96.482
1972	96.429
1971	96.373
1970	96.333
1969	96.316
1968	96.319
1967	96.339
1966	96.374
1965	96.406
1964	96.418
1963	96.412
1962	96.410
1961	96.417
1960	96.417
1959	96.389
1958	96.331
1957	96.258
1956	96.189
1955	96.140
1954	96.115
1953	96.110
1952	96.113
1951	96.120
1950	96.123
1949	96.113
1948	96.080
1947	96.031
1946	95.989
1945	95.975
1944	95.993
1943	96.025
1942	96.049
1941	96.055
1940	96.049

1939	96.052
1938	96.078
1937	96.127
1936	96.185
1935	96.234
1934	96.265
1933	96.284
1932	96.307
1931	96.339
1930	96.373
1929	96.394
1928	96.405
1927	96.415
1926	96.426
1925	96.430
1924	96.428
1923	96.434
1922	96.454
1921	96.471
1920	96.468
1919	96.446
1918	96.423
1917	96.415
1916	96.417
1915	96.422
1914	96.424
1913	96.427
1912	96.436
1911	96.457
1910	96.488
1909	96.515
1908	96.524
1907	96.516
1906	96.506
1905	96.504
1904	96.505
1903	96.502
1902	96.492
1901	96.478
1900	96.468
1899	96.465
1898	96.468
1897	96.472
1896	96.473
1895	96.464

1894	96.444
1893	96.415
1892	96.384
1891	96.357
1890	96.338
1889	96.324
1888	96.310
1887	96.294
1886	96.280
1885	96.268
1884	96.255
1883	96.241
1882	96.224
1881	96.207
1880	96.193
1879	96.190
1878	96.196
1877	96.204
1876	96.205
1875	96.198
1874	96.191
1873	96.188
1872	96.189
1871	96.187
1870	96.185
1869	96.191
1868	96.210
1867	96.232
1866	96.245
1865	96.249
1864	96.253
1863	96.263
1862	96.278
1861	96.292
1860	96.304
1859	96.321
1858	96.348
1857	96.381
1856	96.410
1855	96.431
1854	96.446
1853	96.459
1852	96.470
1851	96.479
1850	96.479

1849	96.472
1848	96.464
1847	96.466
1846	96.480
1845	96.496
1844	96.506
1843	96.509
1842	96.510
1841	96.511
1840	96.509
1839	96.505
1838	96.502
1837	96.504
1836	96.507
1835	96.510
1834	96.516
1833	96.523
1832	96.526
1831	96.521
1830	96.513
1829	96.504
1828	96.489
1827	96.465
1826	96.437
1825	96.410
1824	96.389
1823	96.374
1822	96.365
1821	96.364
1820	96.370
1819	96.379
1818	96.385
1817	96.380
1816	96.364
1815	96.341
1814	96.315
1813	96.288
1812	96.266
1811	96.248
1810	96.229
1809	96.205
1808	96.180
1807	96.159
1806	96.144
1805	96.130

1804	96.116
1803	96.103
1802	96.099
1801	96.110
1800	96.131
1799	96.151
1798	96.164
1797	96.169
1796	96.176
1795	96.193
1794	96.218
1793	96.243
1792	96.266
1791	96.289
1790	96.313
1789	96.336
1788	96.356
1787	96.372
1786	96.389
1785	96.407
1784	96.421
1783	96.429
1782	96.432
1781	96.433
1780	96.431
1779	96.426
1778	96.423
1777	96.426
1776	96.439
1775	96.457
1774	96.469
1773	96.470
1772	96.458
1771	96.439
1770	96.417
1769	96.396
1768	96.381
1767	96.378
1766	96.384
1765	96.389
1764	96.384
1763	96.368
1762	96.345
1761	96.321
1760	96.293

1759	96.265
1758	96.239
1757	96.215
1756	96.188
1755	96.154
1754	96.109
1753	96.047
1752	95.966
1751	95.883
1750	95.819
1749	95.777
1748	95.739
1747	95.692
1746	95.633
1745	95.567
1744	95.501
1743	95.441
1742	95.385
1741	95.326
1740	95.268
1739	95.235
1738	95.243
1737	95.281
1736	95.331
1735	95.363
1734	95.349
1733	95.281
1732	95.184
1731	95.108
1730	95.097
1729	95.176
1728	95.334
1727	95.526
1726	95.708
1725	95.851
1724	95.951
1723	96.021
1722	96.073
1721	96.115
1720	96.146
1719	96.167
1718	96.180
1717	96.192
1716	96.212
1715	96.241

1714	96.274
1713	96.300
1712	96.314
1711	96.320
1710	96.324
1709	96.331
1708	96.343
1707	96.362
1706	96.384
1705	96.405
1704	96.421
1703	96.431
1702	96.434
1701	96.424
1700	96.415
1699	96.414
1698	96.412
1697	96.411
1696	96.413
1695	96.415
1694	96.413
1693	96.410
1692	96.407
1691	96.402
1690	96.400
1689	96.406
1688	96.415
1687	96.418
1686	96.404
1685	96.376
1684	96.360
1683	96.365
1682	96.368
1681	96.371
1680	96.379
1679	96.387
1678	96.391
1677	96.385
1676	96.367
1675	96.351
1674	96.347
1673	96.354
1672	96.367
1671	96.380
1670	96.390

1669	96.392
1668	96.382
1667	96.365
1666	96.354
1665	96.353
1664	96.361
1663	96.376
1662	96.394
1661	96.409
1660	96.418
1659	96.424
1658	96.432
1657	96.444
1656	96.457
1655	96.463
1654	96.463
1653	96.481
1652	96.508
1651	96.511
1650	96.514
1649	96.514
1648	96.504
1647	96.497
1646	96.506
1645	96.516
1644	96.525
1643	96.541
1642	96.561
1641	96.575
1640	96.578
1639	96.575
1638	96.572
1637	96.574
1636	96.583
1635	96.593
1634	96.591
1633	96.581
1632	96.575
1631	96.574
1630	96.573
1629	96.571
1628	96.568
1627	96.562
1626	96.554
1625	96.546

1624	96.541
1623	96.540
1622	96.534
1621	96.521
1620	96.507
1619	96.500
1618	96.497
1617	96.492
1616	96.476
1615	96.446
1614	96.408
1613	96.360
1612	96.291
1611	96.190
1610	96.047
1609	95.848
1608	95.574
1607	95.217
1606	94.791
1605	94.318
1604	93.837
1603	93.416
1602	93.140
1601	93.064
1600	93.188
1599	93.474
1598	93.853
1597	94.250
1596	94.607
1595	94.905
1594	95.146
1593	95.339
1592	95.494
1591	95.617
1590	95.705
1589	95.749
1588	95.735
1587	95.662
1586	95.543
1585	95.410
1584	95.307
1583	95.281
1582	95.355
1581	95.507
1580	95.685

1579	95.846
1578	95.975
1577	96.078
1576	96.163
1575	96.229
1574	96.277
1573	96.315
1572	96.343
1571	96.361
1570	96.380
1569	96.406
1568	96.425
1567	96.431
1566	96.433
1565	96.440
1564	96.451
1563	96.459
1562	96.459
1561	96.448
1560	96.410
1559	96.365
1558	96.343
1557	96.313
1556	96.272
1555	96.224
1554	96.171
1553	96.114
1552	96.047
1551	95.958
1550	95.843
1549	95.707
1548	95.549
1547	95.353
1546	95.103
1545	94.793
1544	94.436
1543	94.049
1542	93.639
1541	93.226
1540	92.914
1539	92.838
1538	92.981
1537	93.256
1536	93.608
1535	94.023

1534	94.486
1533	94.920
1532	95.243
1531	95.458
1530	95.615
1529	95.743
1528	95.848
1527	95.938
1526	96.020
1525	96.097
1524	96.166
1523	96.228
1522	96.287
1521	96.337
1520	96.369
1519	96.386
1518	96.400
1517	96.413
1516	96.423
1515	96.428
1514	96.429
1513	96.424
1512	96.414
1511	96.409
1510	96.414
1509	96.418
1508	96.415
1507	96.416
1506	96.417
1505	96.385
1504	96.327
1503	96.254
1502	96.152
1501	95.980
1500	95.682
1499	95.164
1498	94.254
1497	92.772
1496	90.825
1495	88.895
1494	87.475
1493	86.823
1492	87.035
1491	88.073
1490	89.623

1489	91.169
1488	92.376
1487	93.241
1486	93.872
1485	94.348
1484	94.717
1483	95.012
1482	95.242
1481	95.406
1480	95.516
1479	95.593
1478	95.639
1477	95.644
1476	95.607
1475	95.532
1474	95.422
1473	95.292
1472	95.186
1471	95.131
1470	95.101
1469	95.067
1468	95.018
1467	94.962
1466	94.900
1465	94.839
1464	94.799
1463	94.787
1462	94.777
1461	94.733
1460	94.609
1459	94.300
1458	93.548
1457	92.130
1456	90.321
1455	88.654
1454	87.352
1453	86.492
1452	86.204
1451	86.520
1450	87.260
1449	88.158
1448	89.019
1447	89.745
1446	90.341
1445	90.864

1444	91.366
1443	91.850
1442	92.290
1441	92.669
1440	92.994
1439	93.286
1438	93.578
1437	93.894
1436	94.220
1435	94.505
1434	94.734
1433	94.931
1432	95.108
1431	95.265
1430	95.400
1429	95.514
1428	95.605
1427	95.673
1426	95.723
1425	95.762
1424	95.797
1423	95.825
1422	95.846
1421	95.855
1420	95.849
1419	95.840
1418	95.847
1417	95.872
1416	95.907
1415	95.941
1414	95.972
1413	96.002
1412	96.032
1411	96.059
1410	96.085
1409	96.111
1408	96.131
1407	96.142
1406	96.138
1405	96.117
1404	96.073
1403	96.002
1402	95.904
1401	95.776
1400	95.630

1399	95.503
1398	95.436
1397	95.437
1396	95.483
1395	95.545
1394	95.600
1393	95.637
1392	95.656
1391	95.661
1390	95.652
1389	95.627
1388	95.588
1387	95.543
1386	95.502
1385	95.464
1384	95.423
1383	95.374
1382	95.315
1381	95.251
1380	95.181
1379	95.111
1378	95.047
1377	94.994
1376	94.952
1375	94.917
1374	94.894
1373	94.884
1372	94.887
1371	94.898
1370	94.910
1369	94.921
1368	94.930
1367	94.938
1366	94.946
1365	94.954
1364	94.963
1363	94.981
1362	95.015
1361	95.062
1360	95.113
1359	95.157
1358	95.195
1357	95.227
1356	95.256
1355	95.281

1354	95.299
1353	95.306
1352	95.307
1351	95.308
1350	95.316
1349	95.334
1348	95.357
1347	95.379
1346	95.402
1345	95.430
1344	95.463
1343	95.495
1342	95.519
1341	95.533
1340	95.542
1339	95.550
1338	95.559
1337	95.565
1336	95.562
1335	95.548
1334	95.520
1333	95.478
1332	95.428
1331	95.382
1330	95.353
1329	95.347
1328	95.356
1327	95.374
1326	95.394
1325	95.414
1324	95.431
1323	95.447
1322	95.461
1321	95.473
1320	95.481
1319	95.481
1318	95.474
1317	95.461
1316	95.441
1315	95.419
1314	95.397
1313	95.382
1312	95.376
1311	95.379
1310	95.385

1309	95.394
1308	95.406
1307	95.427
1306	95.458
1305	95.498
1304	95.540
1303	95.581
1302	95.620
1301	95.659
1300	95.694
1299	95.721
1298	95.738
1297	95.744
1296	95.743
1295	95.745
1294	95.753
1293	95.765
1292	95.776
1291	95.780
1290	95.778
1289	95.777
1288	95.780
1287	95.787
1286	95.797
1285	95.806
1284	95.814
1283	95.819
1282	95.820
1281	95.815
1280	95.810
1279	95.812
1278	95.823
1277	95.835
1276	95.842
1275	95.844
1274	95.849
1273	95.859
1272	95.870
1271	95.878
1270	95.881
1269	95.881
1268	95.881
1267	95.887
1266	95.901
1265	95.922

1264	95.944
1263	95.965
1262	95.986
1261	96.005
1260	96.018
1259	96.022
1258	96.014
1257	96.004
1256	95.999
1255	96.007
1254	96.024
1253	96.042
1252	96.054
1251	96.057
1250	96.052
1249	96.042
1248	96.031
1247	96.025
1246	96.029
1245	96.041
1244	96.056
1243	96.070
1242	96.082
1241	96.090
1240	96.091
1239	96.086
1238	96.077
1237	96.069
1236	96.065
1235	96.067
1234	96.074
1233	96.083
1232	96.092
1231	96.099
1230	96.100
1229	96.097
1228	96.092
1227	96.091
1226	96.095
1225	96.097
1224	96.090
1223	96.071
1222	96.048
1221	96.030
1220	96.026

1219	96.034
1218	96.046
1217	96.052
1216	96.046
1215	96.038
1214	96.038
1213	96.049
1212	96.062
1211	96.068
1210	96.062
1209	96.044
1208	96.018
1207	95.989
1206	95.958
1205	95.920
1204	95.873
1203	95.816
1202	95.752
1201	95.682
1200	95.604
1199	95.523
1198	95.450
1197	95.396
1196	95.369
1195	95.367
1194	95.385
1193	95.411
1192	95.440
1191	95.462
1190	95.468
1189	95.447
1188	95.393
1187	95.306
1186	95.179
1185	95.010
1184	94.806
1183	94.603
1182	94.449
1181	94.387
1180	94.430
1179	94.562
1178	94.747
1177	94.946
1176	95.130
1175	95.285

1174	95.406
1173	95.494
1172	95.557
1171	95.604
1170	95.641
1169	95.671
1168	95.694
1167	95.710
1166	95.719
1165	95.720
1164	95.709
1163	95.683
1162	95.637
1161	95.565
1160	95.462
1159	95.328
1158	95.175
1157	95.023
1156	94.899
1155	94.831
1154	94.839
1153	94.927
1152	95.078
1151	95.260
1150	95.438
1149	95.590
1148	95.711
1147	95.805
1146	95.877
1145	95.935
1144	95.990
1143	96.052
1142	96.119
1141	96.181
1140	96.230
1139	96.268
1138	96.301
1137	96.329
1136	96.353
1135	96.375
1134	96.394
1133	96.410
1132	96.420
1131	96.426
1130	96.430

1129	96.427
1128	96.412
1127	96.389
1126	96.361
1125	96.330
1124	96.296
1123	96.259
1122	96.221
1121	96.186
1120	96.152
1119	96.115
1118	96.076
1117	96.036
1116	96.000
1115	95.972
1114	95.951
1113	95.936
1112	95.924
1111	95.915
1110	95.906
1109	95.896
1108	95.891
1107	95.897
1106	95.914
1105	95.935
1104	95.954
1103	95.973
1102	95.988
1101	95.994
1100	95.992
1099	95.989
1098	95.991
1097	95.993
1096	95.995
1095	96.001
1094	96.016
1093	96.035
1092	96.048
1091	96.048
1090	96.034
1089	96.012
1088	95.985
1087	95.960
1086	95.934
1085	95.901

1084	95.854
1083	95.798
1082	95.739
1081	95.680
1080	95.621
1079	95.560
1078	95.488
1077	95.391
1076	95.265
1075	95.121
1074	94.975
1073	94.836
1072	94.712
1071	94.613
1070	94.545
1069	94.513
1068	94.516
1067	94.554
1066	94.623
1065	94.712
1064	94.810
1063	94.913
1062	95.022
1061	95.134
1060	95.241
1059	95.338
1058	95.422
1057	95.498
1056	95.570
1055	95.638
1054	95.694
1053	95.731
1052	95.746
1051	95.745
1050	95.734
1049	95.724
1048	95.727
1047	95.752
1046	95.802
1045	95.868
1044	95.939
1043	96.003
1042	96.041
1041	96.042
1040	96.006

1039	95.938
1038	95.830
1037	95.656
1036	95.390
1035	95.021
1034	94.558
1033	94.031
1032	93.493
1031	93.009
1030	92.632
1029	92.399
1028	92.337
1027	92.459
1026	92.736
1025	93.100
1024	93.475
1023	93.815
1022	94.103
1021	94.338
1020	94.530
1019	94.695
1018	94.848
1017	94.988
1016	95.110
1015	95.217
1014	95.315
1013	95.407
1012	95.489
1011	95.557
1010	95.604
1009	95.624
1008	95.617
1007	95.590
1006	95.548
1005	95.502
1004	95.469
1003	95.479
1002	95.548
1001	95.663
1000	95.795
999	95.919
998	96.016
997	96.079
996	96.107
995	96.113

994	96.114
993	96.118
992	96.125
991	96.131
990	96.131
989	96.115
988	96.081
987	96.034
986	95.983
985	95.936
984	95.893
983	95.857
982	95.831
981	95.814
980	95.807
979	95.815
978	95.839
977	95.879
976	95.929
975	95.983
974	96.029
973	96.052
972	96.043
971	96.008
970	95.954
969	95.891
968	95.824
967	95.762
966	95.712
965	95.678
964	95.667
963	95.688
962	95.746
961	95.830
960	95.924
959	96.014
958	96.091
957	96.146
956	96.180
955	96.201
954	96.218
953	96.230
952	96.231
951	96.217
950	96.188

949	96.143
948	96.087
947	96.035
946	96.001
945	95.981
944	95.969
943	95.965
942	95.980
941	96.021
940	96.083
939	96.151
938	96.218
937	96.281
936	96.341
935	96.396
934	96.445
933	96.489
932	96.533
931	96.575
930	96.605
929	96.614
928	96.604
927	96.587
926	96.568
925	96.544
924	96.515
923	96.489
922	96.467
921	96.438
920	96.387
919	96.315
918	96.231
917	96.135
916	96.019
915	95.869
914	95.676
913	95.439
912	95.175
911	94.912
910	94.676
909	94.478
908	94.328
907	94.244
906	94.243
905	94.327

904	94.482
903	94.691
902	94.936
901	95.198
900	95.457
899	95.698
898	95.908
897	96.079
896	96.215
895	96.327
894	96.426
893	96.510
892	96.576
891	96.625
890	96.660
889	96.685
888	96.706
887	96.736
886	96.779
885	96.824
884	96.855
883	96.869
882	96.875
881	96.878
880	96.877
879	96.871
878	96.865
877	96.863
876	96.867
875	96.878
874	96.897
873	96.921
872	96.946
871	96.967
870	96.980
869	96.981
868	96.977
867	96.980
866	96.991
865	97.003
864	97.007
863	97.008
862	97.013
861	97.024
860	97.032

859	97.031
858	97.014
857	96.987
856	96.961
855	96.947
854	96.940
853	96.919
852	96.871
851	96.804
850	96.730
849	96.649
848	96.556
847	96.447
846	96.334
845	96.230
844	96.149
843	96.101
842	96.091
841	96.110
840	96.155
839	96.229
838	96.331
837	96.450
836	96.570
835	96.682
834	96.783
833	96.874
832	96.957
831	97.024
830	97.068
829	97.087
828	97.094
827	97.110
826	97.138
825	97.160
824	97.171
823	97.177
822	97.188
821	97.198
820	97.197
819	97.187
818	97.173
817	97.159
816	97.148
815	97.147

814	97.155
813	97.163
812	97.161
811	97.150
810	97.139
809	97.132
808	97.129
807	97.129
806	97.127
805	97.120
804	97.108
803	97.096
802	97.082
801	97.060
800	97.031
799	97.004
798	96.983
797	96.963
796	96.934
795	96.892
794	96.829
793	96.742
792	96.643
791	96.552
790	96.475
789	96.388
788	96.274
787	96.144
786	96.017
785	95.894
784	95.761
783	95.604
782	95.420
781	95.200
780	94.936
779	94.628
778	94.273
777	93.870
776	93.421
775	92.934
774	92.414
773	91.844
772	91.214
771	90.531
770	89.813

769	89.075
768	88.332
767	87.613
766	86.934
765	86.281
764	85.627
763	84.961
762	84.287
761	83.616
760	82.965
759	82.374
758	81.895
757	81.567
756	81.399
755	81.375
754	81.456
753	81.589
752	81.722
751	81.827
750	81.905
749	81.993
748	82.160
747	82.490
746	83.049
745	83.857
744	84.880
743	86.036
742	87.210
741	88.308
740	89.289
739	90.165
738	90.964
737	91.704
736	92.397
735	93.050
734	93.660
733	94.205
732	94.666
731	95.039
730	95.336
729	95.571
728	95.756
727	95.894
726	95.977
725	95.997

724	95.969
723	95.934
722	95.930
721	95.964
720	96.021
719	96.081
718	96.120
717	96.120
716	96.066
715	95.948
714	95.741
713	95.401
712	94.876
711	94.105
710	93.007
709	91.484
708	89.464
707	86.929
706	83.893
705	80.385
704	76.444
703	72.125
702	67.494
701	62.636
700	57.670
699	52.775
698	48.287
697	44.839
696	43.333
695	44.584
694	48.820
693	55.393
692	62.960
691	70.113
690	75.991
689	80.410
688	83.594
687	85.874
686	87.527
685	88.749
684	89.672
683	90.388
682	90.970
681	91.462
680	91.874

679	92.209
678	92.479
677	92.707
676	92.907
675	93.081
674	93.237
673	93.383
672	93.526
671	93.678
670	93.854
669	94.054
668	94.269
667	94.441
666	94.534
665	94.604
664	94.699
663	94.808
662	94.907
661	94.982
660	95.048
659	95.126
658	95.226
657	95.338
656	95.441
655	95.528
654	95.615
653	95.713
652	95.811
651	95.884
650	95.921
649	95.936
648	95.950
647	95.977
646	96.015
645	96.051
644	96.074
643	96.081
642	96.076
641	96.062
640	96.041
639	96.013
638	95.975
637	95.919
636	95.839
635	95.747

634	95.663
633	95.601
632	95.560
631	95.528
630	95.491
629	95.440
628	95.384
627	95.336
626	95.304
625	95.274
624	95.234
623	95.186
622	95.154
621	95.158
620	95.206
619	95.294
618	95.402
617	95.502
616	95.574
615	95.618
614	95.643
613	95.664
612	95.686
611	95.712
610	95.746
609	95.785
608	95.818
607	95.830
606	95.813
605	95.783
604	95.768
603	95.776
602	95.791
601	95.789
600	95.768
599	95.742
598	95.721
597	95.697
596	95.660
595	95.604
594	95.525
593	95.429
592	95.337
591	95.274
590	95.242

589	95.222
588	95.200
587	95.179
586	95.160
585	95.131
584	95.071
583	94.969
582	94.827
581	94.670
580	94.531
579	94.422
578	94.317
577	94.176
576	93.999
575	93.823
574	93.670
573	93.515
572	93.321
571	93.087
570	92.837
569	92.596
568	92.378
567	92.188
566	92.019
565	91.858
564	91.693
563	91.519
562	91.328
561	91.127
560	90.939
559	90.777
558	90.608
557	90.391
556	90.145
555	89.928
554	89.758
553	89.581
552	89.347
551	89.058
550	88.737
549	88.381
548	87.979
547	87.536
546	87.060
545	86.555

544	86.052
543	85.598
542	85.207
541	84.858
540	84.573
539	84.443
538	84.546
537	84.878
536	85.401
535	86.082
534	86.871
533	87.689
532	88.488
531	89.267
530	90.014
529	90.682
528	91.253
527	91.755
526	92.211
525	92.606
524	92.942
523	93.254
522	93.566
521	93.861
520	94.119
519	94.340
518	94.528
517	94.683
516	94.822
515	94.965
514	95.095
513	95.174
512	95.209
511	95.259
510	95.355
509	95.477
508	95.599
507	95.722
506	95.833
505	95.893
504	95.889
503	95.859
502	95.846
501	95.858
500	95.903

499	96.001
498	96.132
497	96.218
496	96.216
495	96.180
494	96.187
493	96.231
492	96.244
491	96.211
490	96.198
489	96.284
488	96.472
487	96.685
486	96.809
485	96.774
484	96.618
483	96.463
482	96.400
481	96.429
480	96.505
479	96.591
478	96.660
477	96.692
476	96.693
475	96.690
474	96.687
473	96.661
472	96.628
471	96.646
470	96.729
469	96.832
468	96.924
467	97.022
466	97.120
465	97.154
464	97.080
463	96.934
462	96.790
461	96.679
460	96.617
459	96.640
458	96.760
457	96.895
456	96.950
455	96.923

454	96.853
453	96.744
452	96.601
451	96.488
450	96.481
449	96.613
448	96.857
447	97.139
446	97.349
445	97.395
444	97.263
443	97.024
442	96.775
441	96.599
440	96.550
439	96.623
438	96.725
437	96.740
436	96.683
435	96.702
434	96.866
433	97.055
432	97.118
431	97.052
430	96.978
429	96.981
428	97.055
427	97.148
426	97.191
425	97.147
424	97.070
423	97.090
422	97.231
421	97.341
420	97.224
419	96.901
418	96.661
417	96.657
416	96.761
415	96.846
414	96.886
413	96.886
412	96.832
411	96.706
410	96.559

409	96.549
408	96.819
407	97.299
406	97.654
405	97.587
404	97.158
403	96.700
402	96.441
401	96.380
400	96.533

Appendix D: Sample Calculations

Pollutant removal percentage

% Iron and Manganese removal was calculated:

$$\%\,Iron\ removal = \frac{initial - final}{initial} X\ 10$$

$$\%\,Iron\ removal = \frac{2.1 - 0.15}{2.1}\ X\ 100$$

$$\%\,Iron\ removal = 93\%$$

Adsorption Capacity

$$Q_e = \frac{C_o - C_e}{m} X\ v$$

$$Q_e = \frac{2.1 - 0.15}{4555.68}\ X\ 5.23$$

$$Q_e = 0.0022 mg/g$$

$$\text{oxidation dosing rate (ORD)} = \frac{\text{oxidation flow rate (l/min)}}{\text{oxidation flow rate}\left(\frac{l}{\text{min}}\right) + \text{solutionflow rate (l/min)}}$$

$$\text{ODR} = \frac{0.00167}{0.00167 + 0.174}$$

$$\text{ODR} = 0.95$$

Langmuir Isotherm

$$\frac{1}{q_e} = \frac{1}{Q_m} + \frac{1}{bQ_m C_e}$$

b and q_m were determined from the linearized form of equation 2.2 as shown above, Where the slope of the equation is $1/qm$ and the intercept is $1/bqm$

The equation of the linearized plot of the Langmuir isotherm was then used to calculate the variables

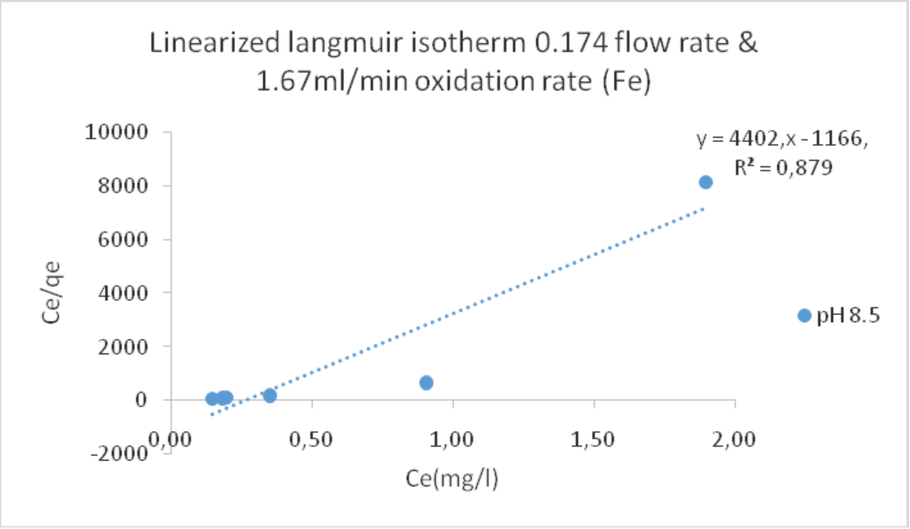

Y=4402.4x-1166.8

$$4402.4 = \frac{1}{q_m}$$

q_m = 0.00023 mg/g

$$-1166.8 = \frac{1}{q_m b}$$

b = -3.773

RL was calculated using equation

$$R_L = \frac{1}{1 + bC_o}$$

$$R_L = \frac{1}{1 + (-3.772\ X\ 2.1)}$$

R_L= - 0.144

Freundlich Isotherm

The linear form of the Freundlich isotherm, Equation below, was used to plot log qe versus Ce. This allowed for the determination of the constant Kf and exponent 1/n.

$$\ln q_e = \ln K_F + \frac{1}{n} \ln C_e$$

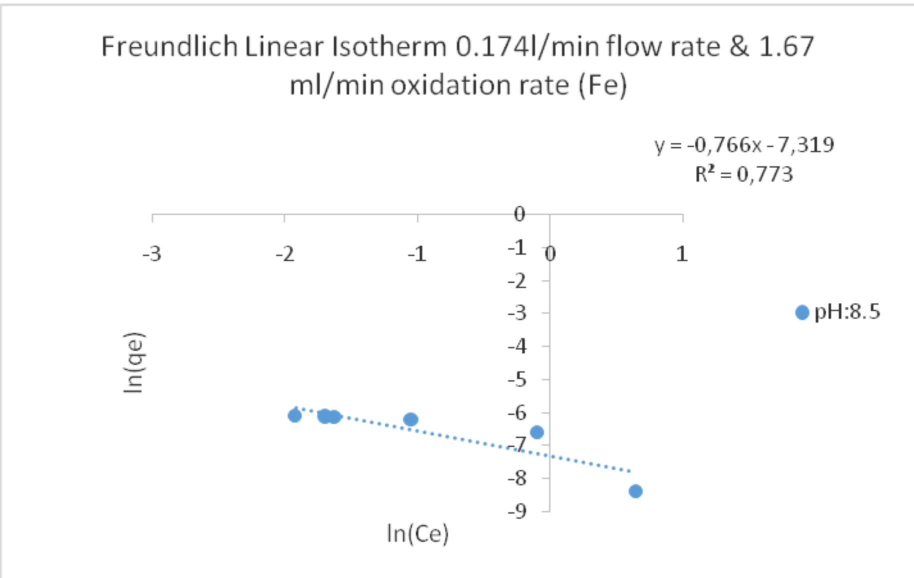

Y= -0.7663x -7.3196

-0.7663=1/n

n = -1.305

ln (K) = -7.3196

K= 0.00066

Temkin Isotherm

Equation below was used to fit data to the Temkin isotherm

$$q_e = \frac{RT}{b} lnK_T + \frac{RT}{b} lnC_e$$

The linear form this equation allows for the values of K_T and b to be deduced by plotting In (Ce) versus q_e

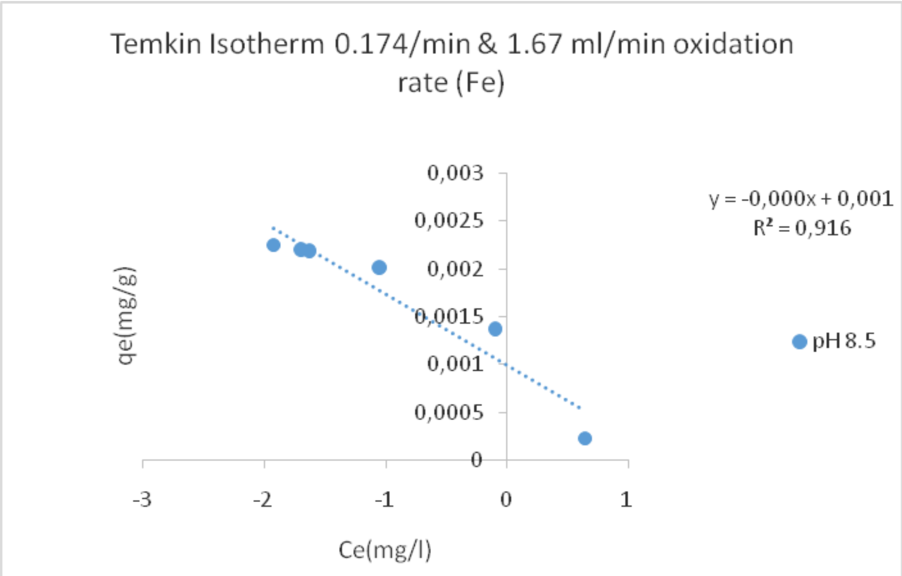

K_T = (-0.0007/0.001)

K_T = 0.496

b = -0.0007

Dubinin–Radushkevich Isotherm

Equation below was used to fit data to the Dubinin-Raduschkevich isotherm

$$\varepsilon = RTln\left(1 + \frac{1}{C_e}\right)$$

The Polanyi potential (Ɛ) (J/mol) was calculated with below equation

$$E = \frac{1}{\sqrt{2\beta}}$$

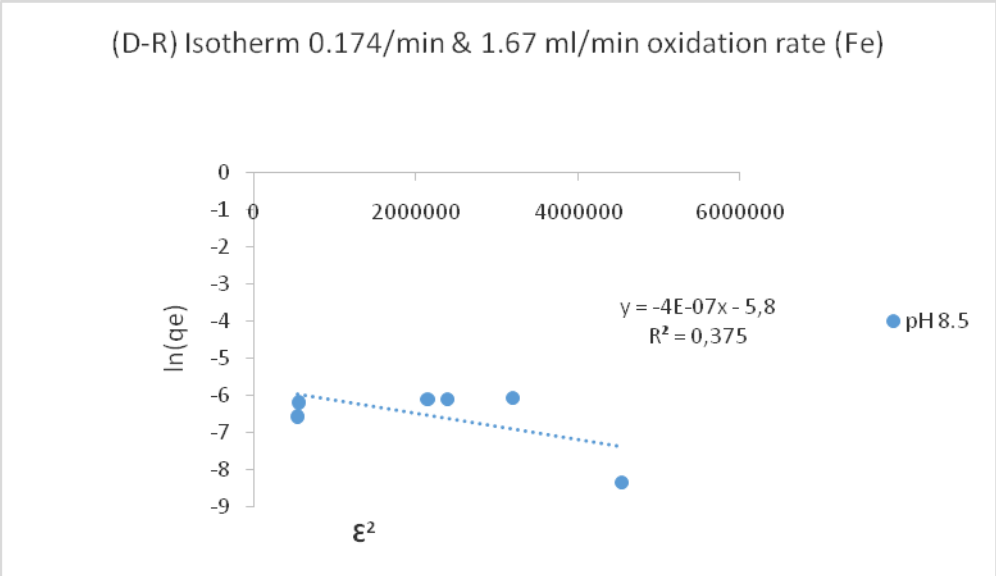

Y=-4E-07x -5.8

Ln (q_m) =-5.8

q_m=0.0003

B = -4E-0.7

Pseudo First Order (PFO)

The data was fitted to first order kinetics model using the following equation

$$\ln(q_e - q_t) = lnq_e - k_1 t$$

The following equation was used to plot log (qe-qt) versus time. From slope and intercept, k1 and qe calculated was found

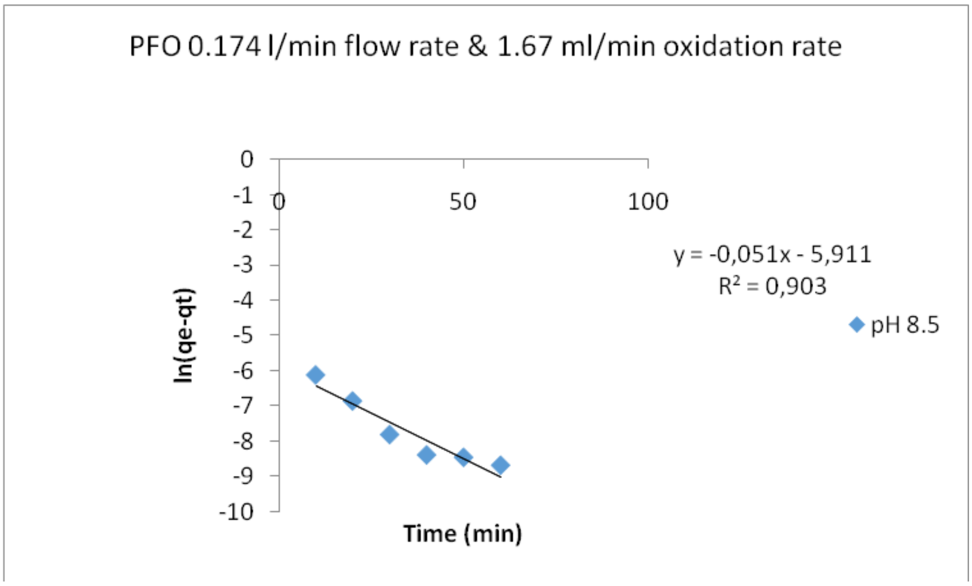

$q_e = 10^{-5.911}$

$q_e = 1.227 \times 10^{-06}$

$K_1 = 2.303 \times 0.0519$

$K_1 = 0.119$

Pseudo Second Order (PSO)

The following equation was used to fit the data to second order kinetics:

$$\frac{t}{q_t} = \frac{1}{k_2 q_e^2} + \frac{t}{q_e}$$

The following equation was used to plot t/qt versus time. From slope and intercept, k_2 and qe calculated was found

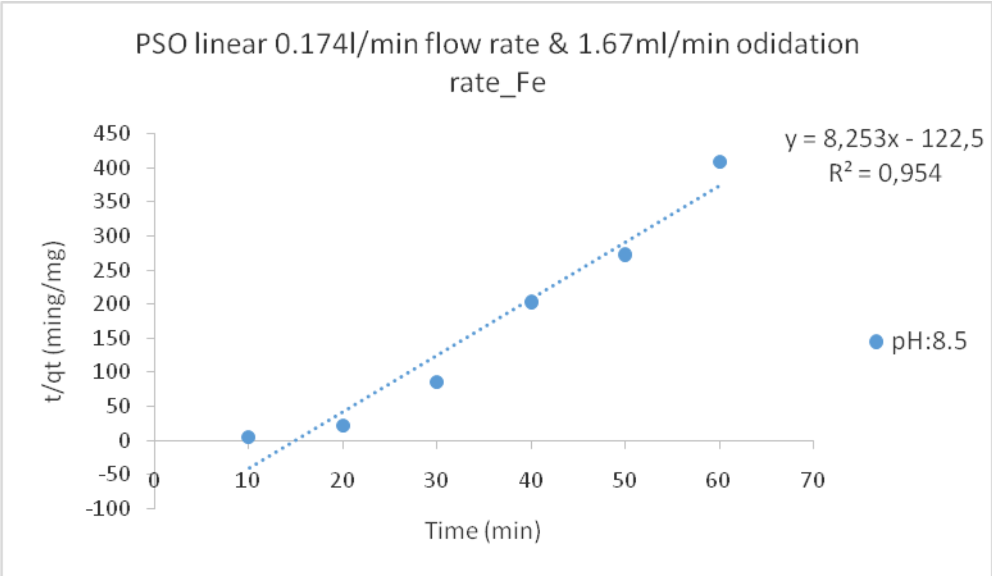

$$q_e = \frac{1}{slope}$$

q_e=1/8.2536

q_e=0.121

$$K_2 = \frac{1}{slope\ q_e^2}$$

$$K_2 = \frac{1}{-122.5\ x\ 0.121^2}$$

K_2 = -0.558

Intra particle diffusion model (IP)

The following equation was used to fit the data

$$q_t = k_d t^{0.5} + C$$

A plot of qt versus t0.5 was plotted and used to determine the values of Kid and C

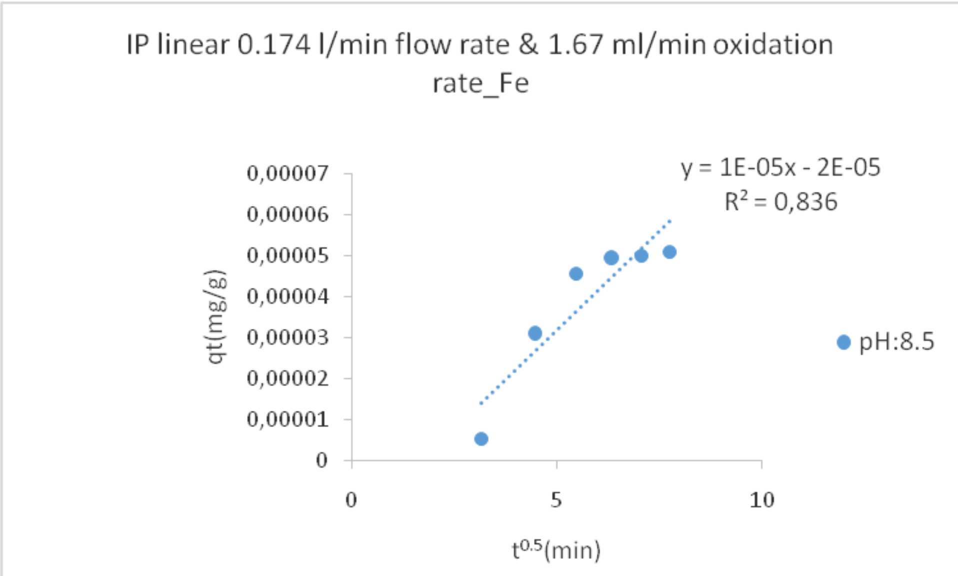

$K_d = 1x10^{-05}$

$C = 2 \times 10^{-5}$

The Elovich Kinetic

The following equation was used to fit the data

$$\frac{dq_t}{d_t} = a\ exp^{\beta q_t}$$

The plot of qt vs t determines the adsorption nature.

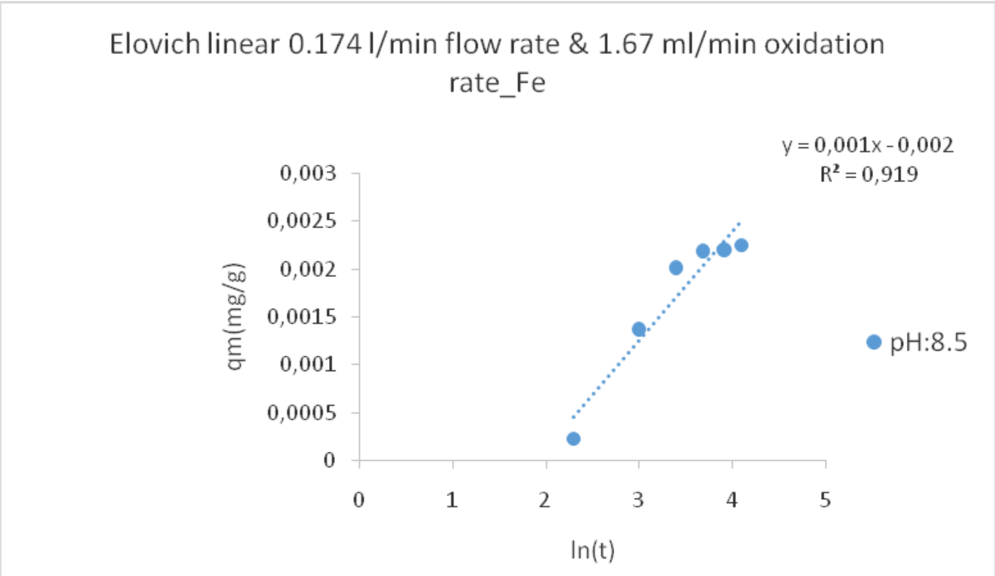

$$\alpha = \frac{1}{0.0011}$$

α=1340.16

$$\beta = \exp\left(\alpha C - ln\alpha\right)$$

β= exp ((1340.16 x 0.0022) –ln1340.16))

β= 7.392 x 10^{-5}

Appendix E: Sample Preparation and analytical procedures

Iron and Manganese concentration determination procedure

The iron and manganese samples were all tested using HANNA high-range HI97721C and HI97709C, respectively. The procedure followed was that given in the instruction guide provided by HANNA.

pH

The pH was read off the pH meters when the probe of the EC meter was placed inside the feed or the treated samples.

Oxidation dosing rate

A manual valve controlled it, and a small volumetric cylinder measured the dosage to determine the accurate dosage per influent flow rate.